PFC/RR-86-17

DOE/ET-51013-189
UC20D

Conceptual Design of a Commercial Tokamak Reactor using Resistive Magnets

Rene J. Leclaire, Jr.*

June 1986

Plasma Fusion Center
Massachusetts Institute of Technology
Cambridge, Massachusetts 02139 USA

*present address: Los Alamos National Laboratory
(S-4), Los Alamos, NM 87544

CONCEPTUAL DESIGN OF A COMMERCIAL TOKAMAK REACTOR USING RESISTIVE MAGNETS

by

RENE JOSEPH LECLAIRE JR.

B.S., M.S., University of Lowell
1980

M.S., Nucl. E., Massachusetts Institute of Technology
1984

Submitted to the Department of
Nuclear Engineering
in Partial Fulfillment of the
Requirements for the Degree of

DOCTOR OF SCIENCE

at the

MASSACHUSETTS INSTITUTE OF TECHNOLOGY
JUNE 1986

Signature of Author
Department of Nuclear Engineering
May 2,1986

Certified by
Daniel R. Cohn
Thesis Supervisor

Accepted by
Allen F. Henry
Chairman, Departmental Graduate Committee

CONCEPTUAL DESIGN OF A COMMERCIAL TOKAMAK REACTOR USING RESISTIVE MAGNETS

by

RENE JOSEPH LECLAIRE JR.

Submitted to the Department of Nuclear Engineering
on MAY 2, 1986 in Partial Fulfillment of the
Requirements for the Degree of DOCTOR OF SCIENCE

ABSTRACT

The potential of resistive magnet tokamaks as commercial electricity producing power plants is investigated. Parametric studies indicate that attractive design space exists for these reactors at relatively low field ($2.5 - 4.5$ T), moderate wall loading ($3 - 4$ MW/m^2) and medium to large net electric outputs (> 600 MW$_e$). High toroidal beta ($20 - 25$ %) possible in the second regime of plasma stability [1] may provide advantages of reduced recirculating power and plasma current but moderate beta reactors ($6 - 10$ %) remain attractive.

The cost of the increased recirculating power of resistive magnets in comparison with superconducting magnets may be offset by cost savings from reduced shielding requirements and simpler technology. In addition, the possibility of incorporating readily demountable toroidal field coils in resistive magnet tokamaks combined with the reduced complexity of these designs could lead to significantly improved availability over current fusion power plant concepts.

A conceptual design for the Resistive magnet Commercial Tokamak Reactor (RCTR) is presented. The layout of the nuclear island is driven by compatibility requirements of the demounting capability with structural and blanket design considerations. The nuclear island is fully demountable with access to all components within the toroidal field coils possible via simple vertical lifts. The blanket system, segmented for vertical removal, uses a self-cooled liquid lithium breeder/coolant with vanadium structure and an HT-9 reflector. The first wall is also lithium cooled with a vanadium structure but is constructed in a single, pre-tested unit for assembly and periodic replacement. Ohmic and equilibrium field coils are located within the bore of the toroidal field coil for improved performance.

Thesis Supervisor: Dr. Daniel R. Cohn

Title: Senior Scientist, Plasma Fusion Center

ACKNOWLEDGEMENTS

I would like to take this opportunity to acknowledge a number of individuals who helped make this work possible. First, I wish to thank my advisor, Dr. Daniel R. Cohn, for his guidance and support throughout my time at MIT. I am also indebted to Dr. Leslie Bromberg who taught me much of what I know about system studies.

My thanks also go to the remaining members of my thesis committee, Professor Jeff Freidberg, Professor Mujid Kazimi and Professor John Meyer for taking the time to read and comment on this work. I have also had the pleasure of interacting with a number of staff and faculty members during the course of the thesis. In particular, I would like to acknowledge the efforts of Dr. Emmanuel Bobrov, Professor Jeff Freidberg, Professor Mujid Kazimi, Dr. Robert Potok, Dr. John Williams and Dr. Ted Yang.

I was fortunate to have the services of Nikolai Diatchenko for the drafting of the engineering drawings of the conceptual design. Anatole Chernomordik did an outstanding job on the trimetric view of the RCTR concept. My wife, Cathy, did an excellent job on the remaining figures in the thesis.

Finally, I would like to dedicate this thesis to my wife and family. This is as much their work as mine.

Contents

List of Figures

List of Tables

Chapter 1

Introduction

1.1 Motivation

One of the most important questions facing the fusion community today concerns the attractiveness of tokamaks as commercial electricity producing reactors. Critics claim that tokamak geometry and components are too complex, its cost too high and that required maintenance on these devices will be either difficult or impossible. Indeed, a major effort is underway to identify innovations which may significantly improve the tokamak concept as a commercial power producer [2]. The objective of this thesis is to explore the potential of tokamaks using resistive magnets as commercial electricity producing reactors. This alternative to superconducting magnet designs combined with other innovations or extrapolations in engineering and physics may provide the fusion community with a significantly more attractive tokamak concept than STARFIRE [3], the most recent vision of the commercial fusion future.

Until recently, resistive magnet tokamaks had only been considered as experimental devices [4], ignition machines [5] or as commercial devices in largely non-electricity producing applications such as the production of copious neutrons and process heat [6,7]. These machines are generally characterized by compact size, high power density and high magnetic field. These characteristics are ideal for such near term applications when low cost and high performance are the primary concerns. The major drawback of resistive magnets, high dissipated power due to joule heating in the conductor, can largely be overlooked in these types of applications.

However, many consider commercial electricity producing applications inappropriate for resistive magnets due to the relatively large recirculating power requirements. We will show that high field, high wall loading and large recirculating power need not characterized these designs and identify attractive options for resistive magnet tokamaks. Low toroidal field more naturally characterizes commercial resistive magnet tokamaks because the minimum dissipated power in the toroidal field (TF) coils is desired. Recirculating power can be further reduced through design by minimizing the distance between the plasma and the TF coil, maximizing the conductor filling fraction, and placing the poloidal field (PF) coils within the bore of the TF coil.

The concepts presented herein for the Resistive magnet Commercial Tokamak Reactor (RCTR) will explore the advantages of resistive magnets such as reduced complexity and demountability (dismantling of the TF coil) as well as incorporate other innovations such as high beta possible with plasmas operating in the so-called second region of stability [1]. We will attempt to optimize the concept, taking into account all major systems and give special attention to some of the major components, developments in which could lead to a significantly improved reactor concept.

1.2 Resistive versus Superconducting Magnets

The major disadvantage of resistive or normal magnets in comparison to superconducting magnets is the relatively large dissipated power associated with them. The refrigeration power required to maintain the superconducting environment of $\approx$ 4 K in a superconducting magnet is generally considerably less than the joule losses in a normal magnet. This is an important consideration for commercial electricity producing reactors since a larger recirculating power requirement means that less power is available for sale off site. However, we will show that the resistive power of the magnets can be minimized in a number of ways and that recirculating power does not fundamentally limit the use of resistive magnet tokamaks in pure fusion (electricity production only) applications. In addition, resistive magnets offer a number of advantages in comparison to the superconducting variety in the areas of durability, complexity and maintenance.

Resistive magnets in commercial applications tend to operate at relatively low stresses because the build of the magnet is made large to minimize the current density and dissipated power. Thus, operation in both the steady state and pulsed modes is not a problem from the point of view of approaching the yield stress or endurance limit, respectively, for the materials of interest. For superconducting magnets, the low ductility at operating temperature implies a large structure to decrease stresses in the pulsed mode. In steady state mode, superconducting magnets generally operate at higher stress because of smaller magnet builds and higher peak magnetic fields. In addition, the power required to drive steady state current is typically similar to that required by the TF coils in a resistive magnet device.

Normal magnets require less shielding than the superconducting variety and thus can be more compact. This can lead to lower costs and higher system power density in the resistive device for the same wall loading. Resistive magnets are less sensitive to neutron streaming and are more tolerant to local hot spots. They are also less sensitive to changing magnetic fields.

Resistive magnets are generally less complex than superconducting magnets, consisting basically of sheets of copper with no requirements for a cryogenic environment. This can lead to a more reliable and available system and perhaps to a lower overall cost. These factors are particularly important in light of the fact that many of the weaknesses of present commercial tokamak designs are associated with either cost or reliability and availability.

A major advantage associated with resistive coils is the possibility of taking apart or demounting the coils with relatively simple designs. Concepts have been proposed for demountable superconducting coils but are not being considered presently in major tokamak studies due to complexities involved with the large number of filaments and the cryogenic environment. In contrast, joints in resistive coils are already being used in a number of devices [8,9] and are being considered even in compact, high field applications [10].

Demountability of the TF coils offers significant advantages to tokamak design. Readily demountable coils may facilitate maintenance with a resulting increase in availability. Furthermore, demountable coils allow the use of various coils inside the TF coil including equilibrium field (EF), ohmic field (OH) and bean shaping coils (for possible high beta application). Placing coils within the TF coil can significantly reduce the resistive power of EF coils, increase the attractiveness of the use of a magnetic divertor, reduce the overturning moment

Net Electric Power, MW_e	1200
Wall Loading, MW/m^2	3
Toroidal Beta, %	24
Major Radius, m	7.5
Aspect Ratio	5
Field on Axis, T	2.4
Plasma Current, MA	4.7
Nuclear Island Weight, ktonnes	14.2
Thermal Power, MW	3380
TF Dissipated Power, MW_e	108
Total Recirculating Power, MW_e	228
Direct Cost, $M	2065
Capital Cost, $M	3680
Cost of Electricity, mills/kW·hr	45.4
Recirc. Power Fraction	0.16
Mass Utilization, T/MW_{th}	4.2
Eng. Power Density, MW_{th}/m^3	1.2

Table 1.1: RCTR Illustrative Case

on the TF and allow the achievement of higher elongations.

Thus, despite relatively high recirculating power, resistive magnets may offer significant advantages over superconductors in commercial electricity producing applications from the points of view of complexity, maintenance and cost.

1.3 Resistive Magnet Commercial Tokamak Reactor (RCTR)

Parametric and systems analysis of tokamaks using resistive magnets have identified a number of attractive options for RCTR. Major parameters characterizing an illustrative case for these devices is shown in table 1.1. A trimetric view of the RCTR concept is shown in figure 1.1. The case shown assumes operation in the second regime of plasma stability. Discussed in more detail in chapter five, the second regime requires careful control of the plasma pressure profiles and operation at high aspect ratio but may provide access to very high beta. The aspect ratio of five and choices of net electric power output, $P_{net,e} = 1200$ MW_e, and wall loading of $P_{wall} = 3$ MW/m^2 leads to a major radius of 7.5 m. $\beta = 24\%$ is achieved assuming operation in the second stable region.

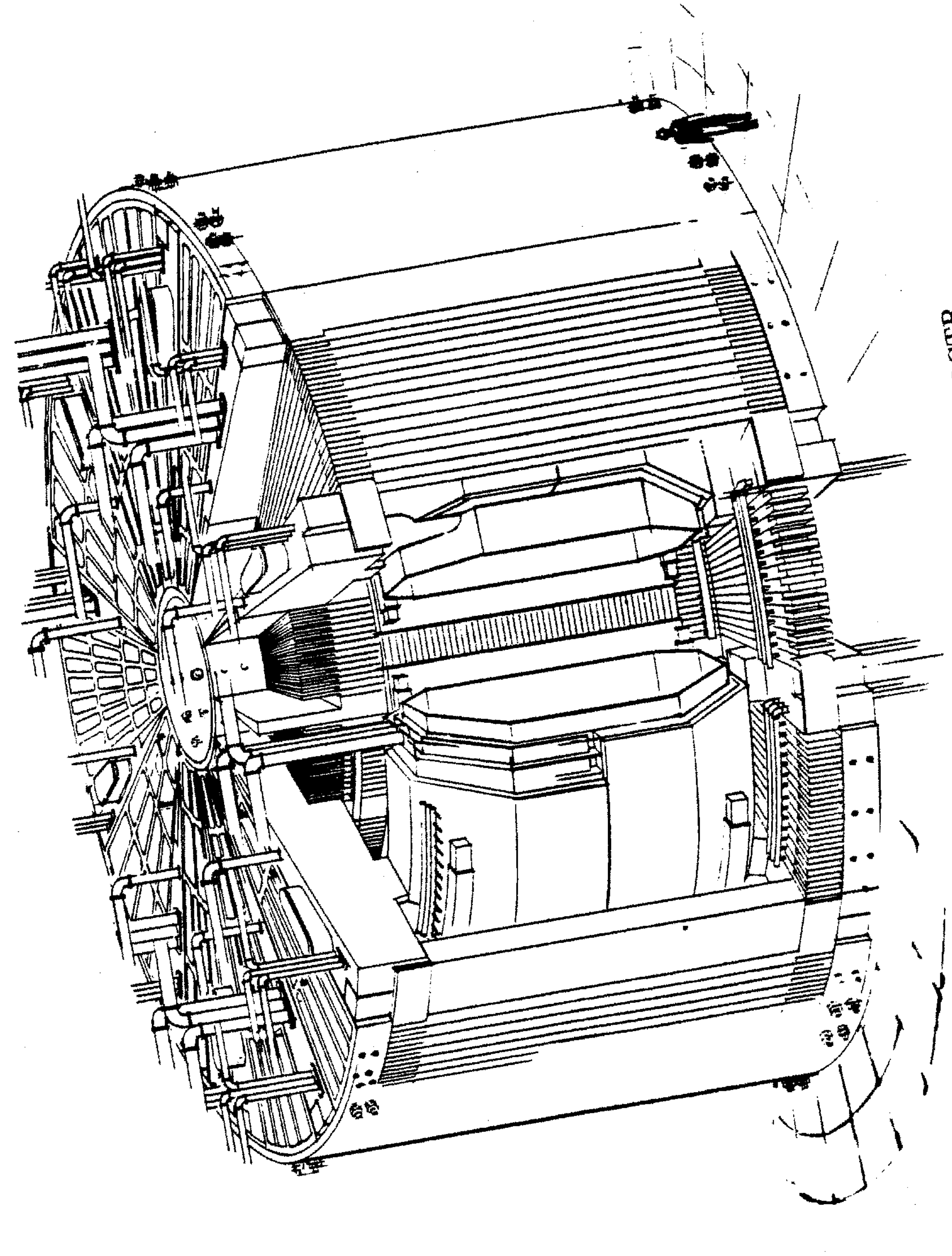

Figure 1.1: Trimetric View of RCTR

The high beta results in a very modest magnetic field on the axis of the plasma of 2.4 T. As a result of the use of second stability at high aspect ratio, the plasma current is also modest at 4.7 MA. Very long pulses driven by an OH coil internal to the TF coil are possible. The design of table 1.1 is capable of six hour pulses although pulses approaching one day in length are possible with similar machines.

The TF coil is optimized for lowest cost by trading off weight against dissipated power. The power required by the TF coil is 108 MW. Combining the power requirements for blanket pumping, balance of plant and other auxiliaries, the total auxiliary power requirement is 228 MW. This is comparable to the recirculating power requirements of STARFIRE, including the power needed to drive the steady state RF current. All magnet coils are constructed of copper and insulated with polyimides. Ceramic insulation may be used in areas of highest radiation dose. The coils are cooled with helium flowing through channels formed during their casting.

The weight of the nuclear island (all components within the TF boundary including the TF and external support structure) is 14.2 ktonnes including 8.6 ktonnes for the coils. This compares quite favorably with STARFIRE (≈ 26 ktonnes) because of the compact nature of the nuclear island. Also, shielding is not required between the plasma and the coils and the TF coils serve as an effective biological shield.

Two figures of merit, engineering power density (EPD) and mass utilization factor (MU) are also shown in table 1.1 where:

$$EPD = \frac{\text{Total MW}_{th}}{\text{Volume enclosed by the TF coils}} \tag{1.1}$$

and

$$MU = \frac{\text{Weight of nuclear island}}{\text{Total MW}_{th}}. \tag{1.2}$$

The high engineering power density (1.2 versus 0.3 for STARFIRE) and favorable mass utilization (4.2 versus 6.7 for STARFIRE) shown illustrate an asset for resistive magnet designs; the capability for high system power density at moderate wall loading and the compactness of the nuclear island (leading to lower weight and cost).

An engineering drawing of the plan view of RCTR is shown in figure 1.2. The TF coil is of frame type and is demountable with lap joints in each of the four corners. The inboard leg of the toroidal field coil is unusually large to minimize the resistive power. Note that the demountability allows placement of the ohmic and equilibrium field coils inside the TF bore. The cooling channel arrangement is also shown.

The blanket is a self-cooled liquid lithium design using a vanadium structure and a ferritic steel (HT-9) reflector. A separate shield is not necessary. The blanket is divided into twelve sections toroidally and is divided along the midplane, allowing the blanket sectors to be removed independently of the first wall. The lithium coolant enters through vertical ports and flows poloidally at moderate velocity to minimize the MHD pressure drop.

Lithium flows toroidally in the vanadium first wall at relatively high velocity (≈ 1 m/s) to provide the required cooling at acceptable pressure drops. The first wall is designed as a single piece which can be removed as such when necessary to avoid the breaking of vacuum during assembly and repair operations. The use of a self-pumped first wall or limiter [11] is envisioned for impurity control.

External structures are designed to support the in-plane vertical bursting forces on the TF coils and the overturning forces created by the interaction of the poloidal field and toroidal current. This structure consists of inner and outer steel cylinders tied together by twelve steel flanges separating the TF coil packs. Wedge shaped steel caps sit above the coil packs and are secured to both inner and outer cylinders with a number of steel plugs. These structures are shown in a top view in figure 1.3. The vertical forces are transferred from the steel caps to the cylinders by the steel plugs. The overturning forces are taken by the continuous structure formed by the steel caps, flanges and inner and outer cylinders.

The nuclear island is designed with maintenance as a major priority. All components are removable with simple vertical lifts without the need for breaking of welds and with as few bolts as possible. Assembly of the nuclear island is illustrated in figures 3.9 through 3.14 of chapter 3 (after page 84). The lower sections of the TF coils and wedges are assembled first on top of the lower cap and around the inner torque cylinder. This is followed by the placement of the inner leg section of the TF and wedges and the insertion of the OH coils. Then

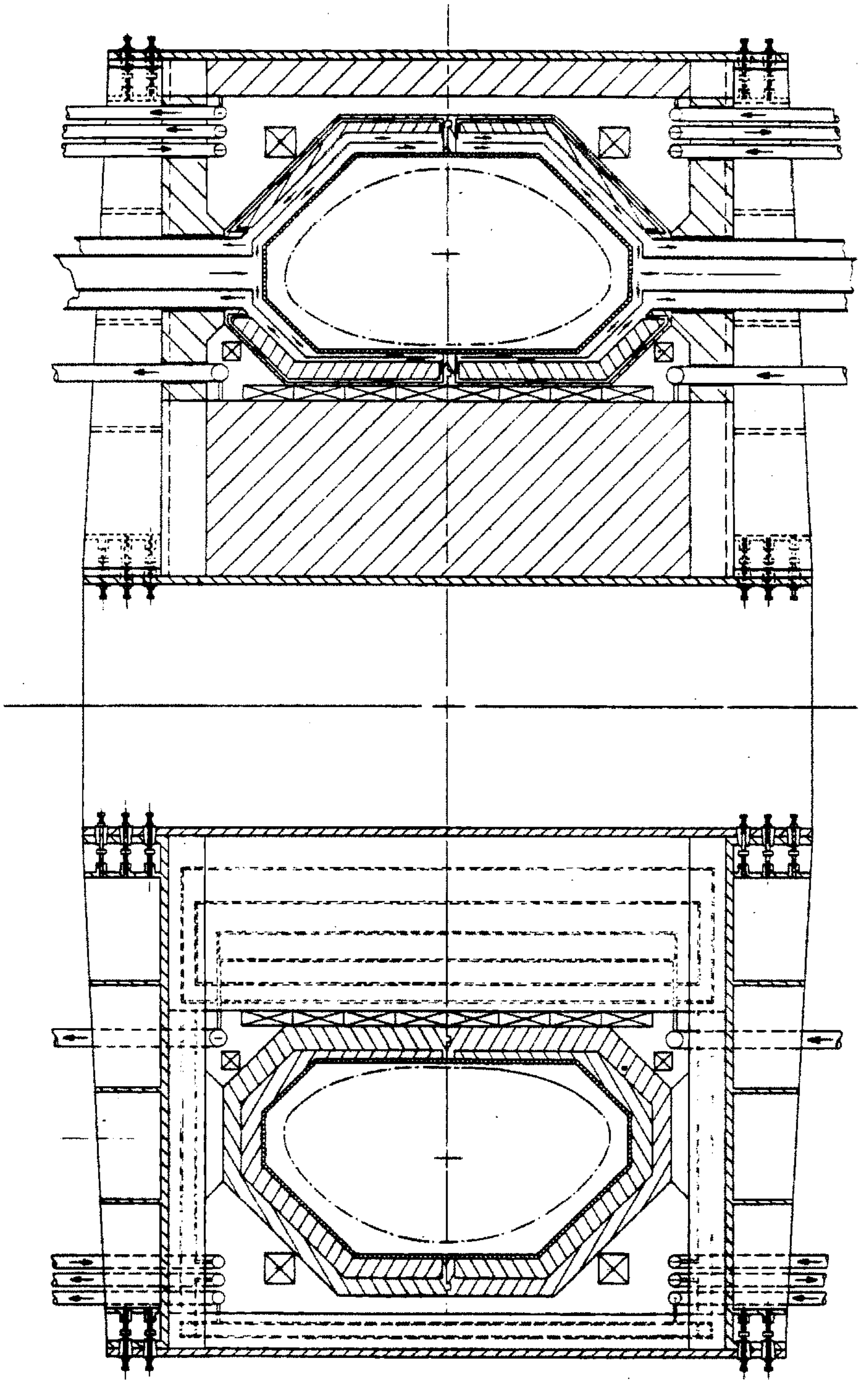

Figure 1.2: Plan View of RCTR Concept

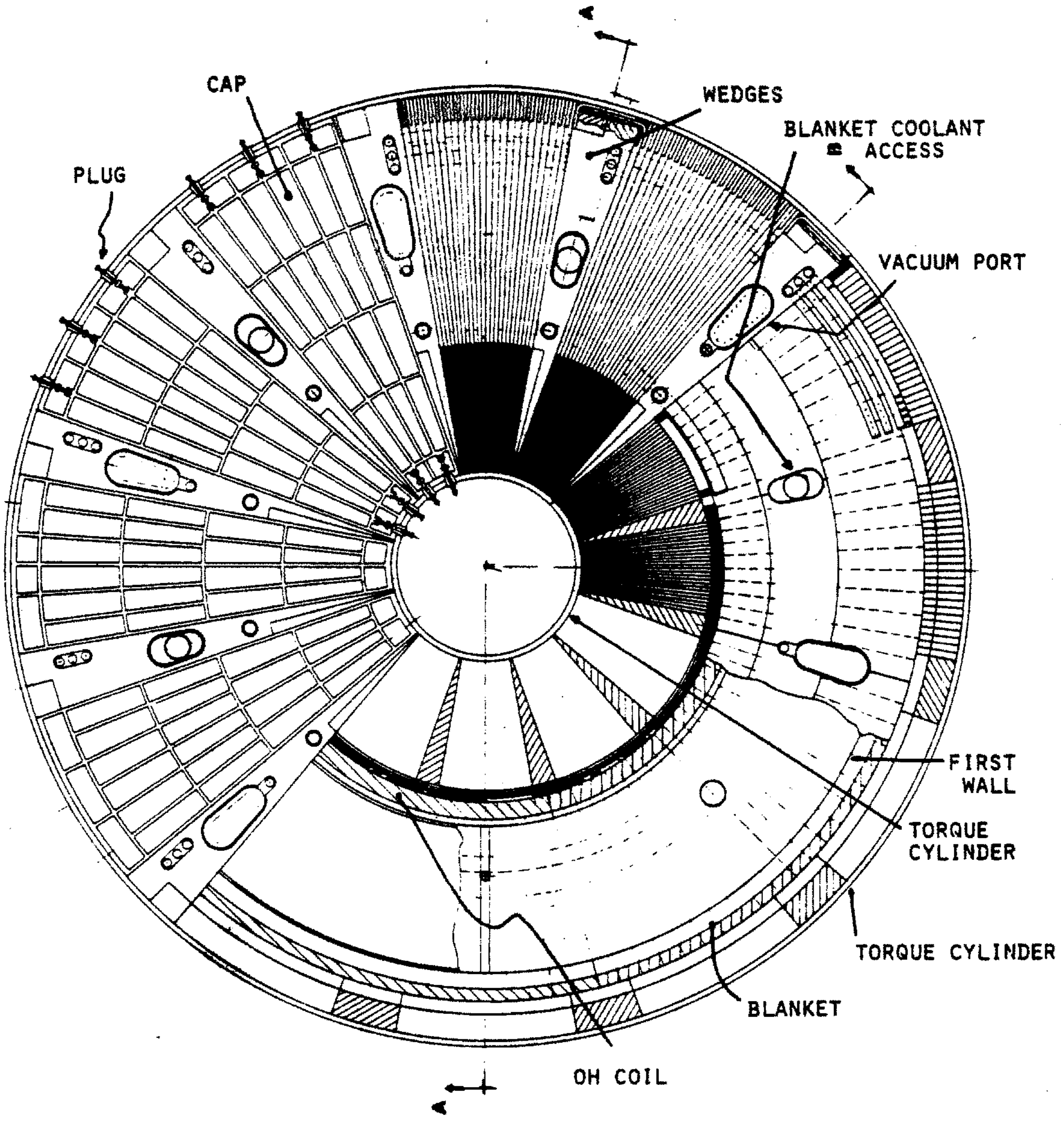

Figure 1.3: Top View of RCTR Concept

the blanket sectors can be lowered in followed by the first wall which is inserted as a single piece (already vacuum-tested). With the upper blanket sectors in place, the outer sections of the TF coil and wedges are inserted. The outer torque cylinder then drops in around the entire assembly. Final assembly takes place with the insertion of the upper TF coil and wedge sections followed by the upper caps and plugs.

Repair and replacement of components takes place in the reverse of the order shown in the diagrams. Note that sections of the TF coil and blanket can be removed with the removal of a single section of plugs and cap but removal of the first wall and other toroidally continuous structures requires removal of the entire top structure. Some repairs may be possible through the six vertical ports penetrating to the vacuum chamber.

Several viable options have been identified for RCTR although the basic design for the coils, blanket/first wall and maintenance scheme remains common to all. These options include low beta designs in the event operation in the second stability regime does not prove practical, the use of aluminum TF coils, and operation at relatively low wall loading (≈ 1 MW/m^2).

1.4 Outline of the Thesis

Exploring parameter space to identify the most attractive options for commercial electricity producing reactors using resistive magnets was a major emphasis of the thesis. Chapter two describes a code developed to make this exploration and details the results and conclusions of each of the tradeoffs made. The next two chapters discuss systems aspects and engineering for some of the components which are of key importance in the design. Chapter three covers maintenance, detailing the design for the demountable TF coils. Chapter four discusses the blanket and first wall design. In Chapter five, the issue of beta limits in tokamak design is explored. The impact of the uncertainty in beta on reactor design is evaluated and recommendations are made for the sensible use of present scalings in reactor design codes. Finally, in chapter six, results, conclusions and recommendations for further work are presented.

Chapter 2

Parametric Studies

2.1 Introduction

The case presented in chapter one characterizing an illustrative concept for RCTR is just one of an infinite variety of designs possible. The purpose of this chapter is to present the methodology used to find the most attractive concepts given the starting point we have selected. The starting point is a tokamak design using resistive magnets because we perceive that such a concept may have unique characteristics which could lead to an improved commercial fusion reactor. We wish also to emphasize the issues of complexity, maintenance and cost since these are perceived as areas of importance to the eventual realization of commercial fusion. Given this starting point, parameters such as power output, magnetic field, major radius and many others must be selected self-consistently to arrive at the best possible illustrative concepts which then form the basis for more detailed analysis.

A partial list of the parameters of interest characterizing an electricity producing tokamak using resistive magnets is shown in table 2.1. General comments on the approach used to reduce these unknowns to a manageable number in a manner leading to the identification of illustrative concepts for RCTR are made in section 2.2. This approach is incorporated into a zero dimensional computer code which is discussed in section 2.3. Section 2.4 summarizes the results of the parametric trade-offs. The choice of illustrative designs is discussed in section 2.5. Finally, chapter two is summarized in section 2.6.

Parameter	Units	Symbol
Net Electric Power	MW_e	$P_{net,e}$
Neutron Wall Loading	MW/m^2	P_w
Major Radius	m	R
Minor Radius	m	a
Aspect Ratio	—	A
Elongation	—	k
Toroidal Beta	—	β
Weight, Nuclear Island	Tonnes	W
Magnetic Field on Axis	Tesla	B_0
Plasma Current	Amperes	I_p
Fusion Power	Megawatts (MW)	P_f
Total Thermal Power	MW	P_{th}
TF Coil Dissipated Power	MW_e	P_{TF}
Total Auxiliary Requirement	MW_e	P_r
Burntime (Pulse Length)	Hours	τ_b
Capital Cost	Billions ($\$B$)	C
Cost of Electricity	mills/kW·hr	COE
Magnet Coil Stress	MPa	σ
Stored Energy	Joules (GJ)	E_s

Table 2.1: Parameters Characterizing Resistive Tokamaks

2.2 Approach to Parametric Surveys

There are almost as many ways to approach the parametric studies as there are parameters to be studied. The philosophy used here is to reduce the number of major inputs to a minimum and look at the sensitivity of the results to these inputs. These major input parameters were selected to be as well characterized as possible in the sense that their allowable or desirable range of values is well known and/or set by external constraints such as engineering limits. Additional comments describing 'major' input parameters and the approach used to select them will emerge naturally as each input and its impact on the trade-offs is discussed.

Fusion power, P_f, and neutron wall loading, P_w, were considered from the beginning as possible inputs for the parametric analysis because they each form a good basis of comparison for different reactors and reactor concepts and their range of values is relatively well characterized. Fusion power represents the fundamental desirable outcome of building a fusion device while wall loading is a fundamental driver of the size, cost and feasibility of the machine. The thermal power requirements of present day power reactors and the engineering constraints on first wall lifetime help to characterize these parameters with considerations outside their impact on the parametric trade-offs.

In addition, the specification of fusion power and wall loading significantly reduces the number of unknowns in the problem because their ratio is only a function of geometry. Specifically;

$$\frac{P_f}{P_w} = 5\pi^2 aR\sqrt{\frac{1+k^2}{2}} \tag{2.1}$$

where a is the minor radius, R the major radius and k is the elongation. We choose to treat elongation as an input (and explore the sensitivity of the results to this choice) so that this ratio is only a function of a and R.

However, fusion power can be a deceiving basis of comparison with resistive magnet tokamaks because of the potentially large recirculating power requirements. Thus, the net electric power output, $P_{net,e}$, of the fusion plant (the useful power output after accounting for recirculating power requirements) is a superior basis of comparison and a better choice for an input parameter. $P_{net,e}$ can be written as:

$$P_{net,e} = \eta_{th} M P_f - P_r \tag{2.2}$$

where η_{th} is the thermal conversion efficiency, M is blanket energy multiplication and P_r is the total recirculating power requirement including magnets, coolant pumping and other auxiliaries.

For a given choice of blanket design, M and η_{th} are well characterized. However, we have introduced an additional unknown in P_r which cannot be determined before the geometry of the device is known. Therefore, a guess for the recirculating power is made which leads to the determination of a reactor geometry (in a manner described below). Once the geometry is known, the recirculating power for that specific geometry can be determined and the net electric power found. The guess is then modified in an iterative process until the desired $P_{net,e}$ is obtained.

Next, we choose to treat aspect ratio (A $= \frac{R}{a}$) as an input parameter. This choice is also a powerful lever in reducing the unknowns and is surprisingly well characterized for these designs. For reactors operating in the second regime of plasma stability, high aspect ratios of 5 to 6 are required for stability while early parametric studies showed that low aspect ratio (about 3) was desirable for reactors in the first stability regime. This will be discussed in greater detail in section 2.4. The choices of P_w, $P_{net,e}$, k, and A now determine the minor and major radius of the device uniquely.

The final major input choice is the beta scaling desired. For operation in the second regime of stability, maximum beta may be set by plasma equilibrium limits. Empirical and theoretical limits exist for maximum beta in the first region of plasma stability. These limits will be presented in more detail in chapter 5 but they are generally found as a function of elongation, aspect ratio, plasma triangularity and plasma safety factor. Thus, for reasonable choices of plasma triangularity and safety factor, beta is determined and the rest of the parameters characterizing the tokamak fall into place.

Magnetic field on the axis of the plasma, B_0, is now determined from expressions for either fusion power or wall loading. This determines the required plasma current and ohmic system requirements. Then the toroidal field coil is determined based on an optimization of weight and cost to be discussed in the next section. Finally, the remainder of the system's characteristics can be determined including stored energies, EF requirements, stresses, weights and costs.

The methodology can be represented as a progression from the plasma axis outwards. Choices of wall loading, net electric power, aspect ratio and beta scaling essentially determine the plasma requirements and geometry which then determine the OH and EF requirements. Adding requirements for the blanket design then determines the bore of the TF coil. Finally, the TF coil is optimized and the remaining characteristics of the device are evaluated.

2.3 The Parametric Code

The methodology of section 2.2 has been incorporated into a computer code *RTPAC* written in the MACSYMA programming language. The code evolved from a parametric code written by L. Bromberg [12] to investigate resistive magnet ignition devices. However, the optimization and characterization of a commercial device is quite different from that of an ignition machine and the codes are left with relatively little in common. A listing of the code is included in Appendix A.

MACSYMA is a very interactive programming language within a symbolic program written in LISP. It is quite similar to FORTRAN in most respects although more powerful and much more interactive in nature. Details on how MACSYMA can be interpreted and converted to FORTRAN are contained in Appendix A.

A list of the major inputs required by *RTPAC* is shown in Table 2.2. Also indicated in table 2.2 are the determining factors for these inputs. Note that the choice of most of the inputs does not narrow the focus of the parametric study but are the result of external constraints and choices. For instance, the choice of a blanket option (with neutronics and other analysis of that option) determine blanket energy multiplication, thermal efficiency, and the dimensions of the blanket/shield/first wall regions.

A flow diagram for *RTPAC* is shown in Figure 2.1. The first step of the calculation is to find the average toroidal beta consistent with the choice of beta scaling. In the second stability region of plasma stability, the maximum beta is set by MHD equilibrium limits [14] while experimental [15] and theoretical [16]

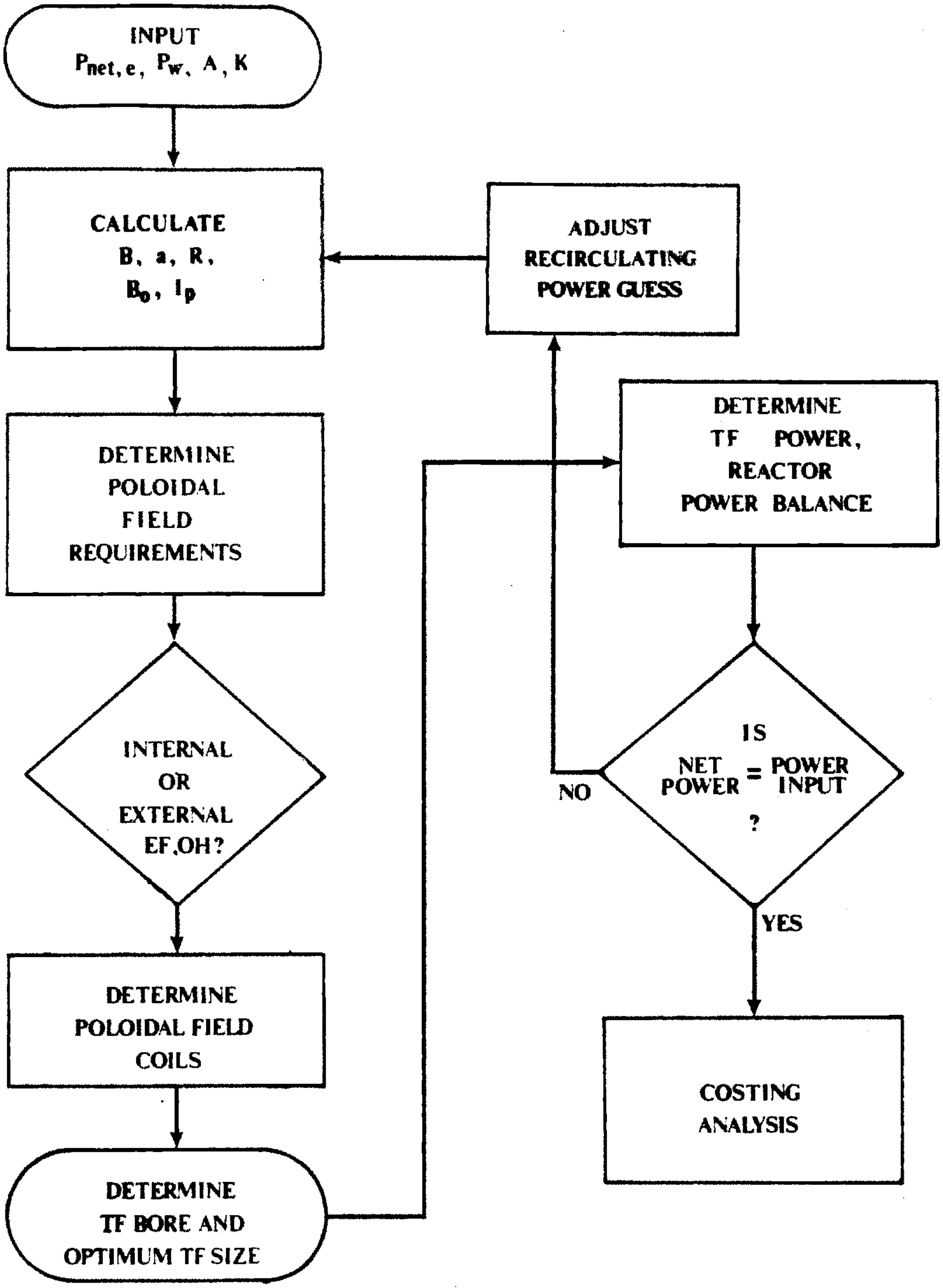

Figure 2.1: Flow Diagram for Parametric Code RTPAC

Input	Determination
net electric power	sensitivity study
wall loading	sensitivity study
aspect ratio	sensitivity study
elongation	sensitivity study
beta	scaling law
plasma safety factor	MHD theory
blanket multiplication	neutronics
tritium breeding	neutronics
blanket thicknesses	blanket analysis
burntime	sensitivity study
material properties	material data base
material unit costs	costing literature
availability	sensitivity study
cost factors	TPSS [13] guidelines

Table 2.2: Major Inputs Required for RTPAC

formulations exist for beta limits in the first stability region. More detail on accessible beta regimes is contained in chapter five. The code assumes operation at ninety percent of the maximum volume average beta indicated by the selected scaling.

Choices for net electric power, wall loading, aspect ratio, and elongation combined with a guess for the recirculating power then determine the fusion power and the major and minor radii. Then from the expression for wall loading;

$$P_w = \frac{2}{5} C \beta^2 {B_o}^4 a \sqrt{\frac{1+k^2}{2k^2}} \tag{2.3}$$

the magnetic field on the axis of the plasma can be determined. C is a constant depending on the plasma temperature and profiles which is calculated assuming the plasma is ignited and operation at the maximum of the fusion power density versus temperature (C) is desired. However, for typical RCTR parameters, operation at the maximum in C results in a violation the Murakami limit on average density [17]:

$$n_{max} = 1.5 \frac{B_o}{R_o q^*} \times 10^{20} \tag{2.4}$$

where all units are in MKS and q^* is as defined below. The difference is about a factor of two for moderate beta devices which could be compensated for by the uncertainty in the limit itself (which may improve for auxiliary and alpha heated plasmas [18]) and/or by a moderate increase in magnetic field to make up for operation at the higher temperature (and lower C) demanded by the Murakami limit. With high beta devices the difference could be closer to a factor of $5 - 10$ and Murakami could possibly represent a more fundamental limit.

The plasma current, I_p, can be determined from an expression for the plasma safety factor, q^* [14];

$$q^* = \frac{5a^2 B_o}{2RI_p} k. \tag{2.5}$$

Next, the ohmic system can be evaluated. The analysis for ohmic and equilibrium field system requirements is similar to the development used in Bromberg's code [12] with options added to allow placement internal to the toroidal field coil and to extend the results to higher elongations. The resistive volt second requirement is calculated for relatively impurity free plasmas and including finite aspect ratio corrections [19]. Plasma burntime is treated as an input. Inductive volt second requirements for the EF system are found using a numerical fit to the results of a series of large-scale plasma equilibrium code runs (see below). An allowance is also made for start-up volt-second requirements.

Once the requirements are determined, the ohmic coil can be sized using a stress constraint and the placement of the coil with respect to the TF coil. With the plasma geometry determined and a reasonable plasma scrape-off distance selected, an allowance for blanket, first wall, and reflector/shield components (see chapter 4) defines the inner edge of the ohmic coil if it is internal to the TF coil. The code also allows for an ohmic coil external to the TF bore and the use of RF current drive or RF assisted start-up. However, this investigation emphasizes the OH driven current option with the OH placed inside the TF bore.

Since the plasma chamber, blanket envelope and OH coil have been determined, the inner bore of the TF coil is now defined. The total TF current required is determined by;

$$B_o = \frac{\mu_o I_t}{2\pi R} \tag{2.6}$$

where μ_o is the permeability of free space. However, the build (width) of the TF coil still needs to be found. Typically, this is done by imposing a stress constraint and operating at some maximum allowable stress at the inboard leg.

However, this is inappropriate in light of the importance of the dissipated power of the TF coil in an electricity producing device. Therefore, we optimize the TF coil with dissipated power and weight rather than high performance in mind.

The optimization is done for a frame-type rather than a bitter (circular or oval) coil because of demountability constraints discussed in chapter 3. The widths of the inner, outer and horizontal legs of the coil are varied independently using an algorithm which attempts to minimize the cost of the coil as a function of its weight and dissipated power. The inner leg of the TF coil is optimized simply for minimum dissipated power because this region of low cross-section is the site of a relatively large fraction of the dissipated power and a relatively small fraction of the weight and cost. The code allows the inner leg to grow in size until a further increase in bulk no longer results in an appreciable decrease in dissipated power.

In order to find the dimensions of the remaining TF legs, it is first necessary to find the volume and dissipated power for a frame coil. These are straightforward calculations for this simple geometry with the results:

$$\begin{aligned} V \; = \; & 4\pi f_o \Delta_o R_t (R_h + \Delta_t) + 2\pi f_i {R_a}^2 (2f' - f'^2)(R_h + \Delta_t) \\ & + 4\pi f_o \Delta_t R_t (R_b - R_t) + 2\pi ({R_t}^2 - {R_a}^2) \Delta_t f_i \end{aligned} \tag{2.7}$$

$$\begin{aligned} P_{tf} \; = \; & \frac{4\pi P_0 (R_h + \Delta_t)}{R_t \Delta_o f_o} + \frac{8\pi P_0 (R_h + \Delta_t)}{{R_a}^2 (2f' - f'^2) f_i} \\ & + \frac{4\pi P_0 (R_b - R_t)}{R_t \Delta_o f_o} + \frac{4\pi P_0 \log(\frac{R_t}{R_a})}{\Delta_t f_i} \end{aligned} \tag{2.8}$$

$$P_0 = 2\pi \eta_r \frac{{R_0}^2 {B_0}^2}{{\mu_o}^2} \tag{2.9}$$

where f_o and f_i are the volumetric fractions of copper in the outer and inner sections, respectively, $f' = \frac{\Delta_i}{R_a}$, η_r is the resistivity of the conductor, B_0 is the magnetic field at the axis of the plasma and the remaining geometrical parameters are as defined in figure 2.2.

The TF coil is sized for minimum cost assuming that the cost of electricity can be written in the form:

$$\frac{COE}{COE_0} = \alpha_1 \frac{P_{tf}}{P_{tf0}} + \alpha_2 \frac{V}{V_0} \tag{2.10}$$

where COE_0, P_{tf0} and V_0 are normalizations and the alphas are constants. This function is minimized by taking partial derivatives with respect to the widths of the horizontal and outer TF legs, Δ_t and Δ_o. For the simplified case where the contributions from the inner leg and the corners are neglected, the result for the widths at minimal cost of electricity is:

$$(\Delta_o)_{min} = \frac{\alpha_1 V_0 P_0}{\alpha_2 P_0 R_t^{\,2} f_o^{\,2}} \tag{2.11}$$

$$(\Delta_t)_{min} = \frac{\frac{2P_0(R_b - R_t)}{R_t f_o} + \frac{2P_0 log(\frac{R_t}{R_a})}{f_i}}{2f_o R_t(R_b - R_t) + (R_t^{\,2} - R_a^{\,2})f_i} \tag{2.12}$$

The constants α_1 and α_2 are determined by fitting equation 2.10 to the results of a series of parametrics which find the cost of electricity as a function of variations in the resistive power and weight of the TF coils.

A routine is also included to estimate the equilibrium field (EF) system. Usually, this type of calculation is quite involved and makes use of a large plasma equilibrium code such as NQX [20]. Here we make use of a routine utilized in previous MIT studies [21] which uses a numerical fit to the results of a series of NQX equilibrium calculations. This method, although approximate and limited in scope, is useful for parametric studies. Given geometry, plasma safety factor and toroidal field, the routines yields estimates for the inductive volt second contribution of the EF system and the currents in four (two above and below the midplane) EF coils.

At this point, all major systems have been determined and the code calculates the remaining characteristics of the device. Stresses in the coils and support structure are found using the results of section 3.5. The reactor power balance includes recirculating requirements for the TF, OH and EF coils, pumping power for the blanket and TF cooling systems and power requirements of the balance of plant. Stored energy for the coil systems and figures of merit such as engineering power density, recirculating power fraction and mass utilization are also calculated. Evaluation of the weight of the nuclear island includes an accounting of all major systems and an allowance for structural components.

The capital cost and cost of electricity of the device including balance of plant are calculated according to guidelines set up for commercial reactor investigations [13]. The fusion plant is split into seven major accounts for the calculation of plant direct cost: the cost of equipment, engineering and labor. These accounts, listed in table 2.3, contain cost evaluations of the major plant systems scaled with factors such as weight and thermal power from other reactor studies.

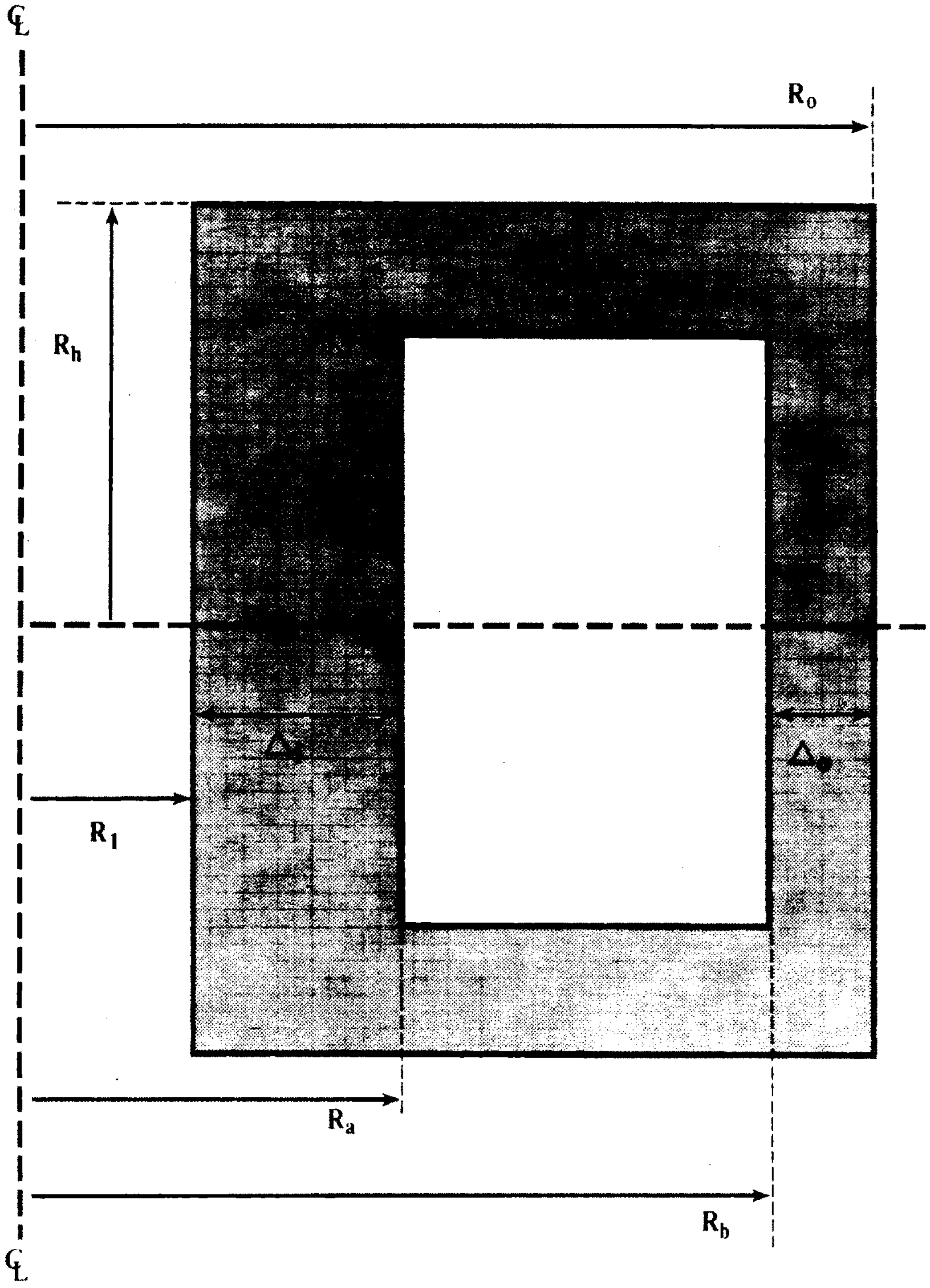

Figure 2.2: RCTR Coil Geometry

#	Account
20	Land and Land Rights
21	Structures and Site Facilities
22	Reactor Plant Equipment
23	Turbine Plant Equipment
24	Electric Plant Equipment
25	Miscellaneous Plant Equipment
26	Heat Rejection System

Table 2.3: Major Cost Accounts

The total constructed cost, including allowances for indirect costs and contingency costs, is calculated using guidelines set up during the Tokamak Power System Studies (TPSS) series [2]. The constructed cost (or overnight constructed cost) is the instantaneous cost of the fusion plant. The capital cost (C) is calculated taking into account inflation and other financial parameters and represents the cost of the plant over the time in which it is constructed. The financial parameters are reduced to a plant cost factor which is applied to the constructed cost depending on construction time, inflation rate and escalation.

The final cost component to be calculated is the cost of electricity (COE). This represents the yearly cost of running and paying off the fusion plant. The definition used in this study is:

$$COE = \frac{LAFCR \cdot C + (AOC + AFC) \cdot LN}{0.00876 \cdot P_{net,e} \cdot A_v} \tag{2.13}$$

where LAFCR is the levelized annual fixed charge rate, AOC is the annual operating cost including replacement parts, LN is the levelizing factor, AFC is the annual fuel cost and A_v is the plant availability. LAFCR and LN are cost factors applied to capital and annual costs to account for interest and inflation. These, as well as the plant cost factors, have been compiled in reference [13]. The operating cost is determined in *RTPAC* based on the materials used in the blanket, first wall, and ohmic systems and their lifetimes. An option is included in the code to account for possible degradation of availability with increasing wall loading. Costs are also compiled for a multiplexed plant (see section 2.4.4). The costing routine is presented in greater detail in appendix B.

The final step in the code is to use the calculated value of dissipated power for the TF coil plus allowances for other plant auxiliaries to determine the net electric power of the plant. If this does not match the $P_{net,e}$ input, the recirculating power guess is adjusted accordingly and the entire routine runs iteratively until the desired $P_{net,e}$ is attained.

RTPAC can be run in a number of modes. It can be used to converge a single case or to run a series of parametric scans as a function of one of the inputs. Output is available in tabular and graphical form.

2.4 Trade-off Studies

RTPAC has been used to run a great many parametric scans to identify the most attractive illustrative cases for RCTR. While the code solves for the various components of the tokamak plant self-consistently and tries to optimize its configuration to some extent, the results are sensitive to the required inputs; mainly $P_{net,e}$, P_w, S, A and the choice of beta scaling. However, these inputs have been chosen for their usefulness as bases of comparison.

The choice of beta scaling represents a selection between first and second stability plasma performance; that is, the benefits possible with higher betas possibly attainable in the second regime can be evaluated. In addition, the magnitude of the beta attainable is varied representing, for instance, the usefulness of higher triangularity in first stability or operation at lower safety factor in second stability.

Neither elongation nor aspect ratio can be chosen clearly from external considerations except in the case of the use of the second stability regime where high aspect ratio is a requirement and elongations greater than 2 may not be possible. However, clear trends will emerge from the trade-offs for these two parameters due to fundamental restraints on resistive magnet tokamak design and the beta limits themselves. Optimum values exist which are valid over a wide range of parameter space.

Net electric output and wall loading are also parameters whose values cannot be determined a priori. Although clear trends will emerge for the selection of these parameters, no clear consensus exists in the fusion community on the importance of the factors constraining $P_{net,e}$ and P_w. Specifically, smaller net electric outputs lead to lower capital investments but a higher cost of electricity. This is complicated by the relative inaccuracy of present estimates for these cost factors. In the case of wall loading, the trade-off of larger plant size at low wall loading versus increased risk and maintenance problems at high wall loading is not well characterized at this stage of fusion development.

However, an important strength of $P_{net,e}$ and P_w as input parameters is that they are important bases of comparison for different machines and different concepts. It seems unwise to compare two commercial fusion devices with significantly different net electric power outputs and/or wall loads. Such comparisons should be made on the basis of equal power delivered to the customer and equal risk from a wall loading standpoint since wall loading carries important (and yet relatively poorly understood) materials and maintenance constraints with it.

In the following subsections, trade-offs for each of the major inputs will be discussed. The trade-offs include scans through a relatively wide range of the input parameter in question as well as repetition of these scans for various values of the remaining inputs. The trade-offs for high beta (second stability regime) and moderate beta (first stability regime) devices are discussed separately. The last subsection discusses other trade-offs dealing with plasma burntime, thermal efficiency and the relative costs of resistive magnet and superconducting magnet tokamaks.

2.4.1 High Beta Cases

High beta reactors are characterized by relatively large major radius (high aspect ratio), low plasma current, and low field (see chapter five for possible exceptions). The low field and large size lead to relatively low dissipated power in the TF coils with a low recirculating power requirement as a result. In fact, the recirculating power requirements of an ohmically driven resistive magnet tokamak can be comparable to those of a superconducting device using steady state RF driven current.

Wall Loading

The results of a wall loading scan for an aspect ratio of 5, net electric output of 1200 MW_e, elongation of 1.8 and beta of 24% is shown graphically in Figure 2.3. Major radius and nuclear island weight decrease rapidly with increasing wall load between 1 and 3 $\mathrm{MW/m^2}$ and more gradually thereafter due to decreasing wall

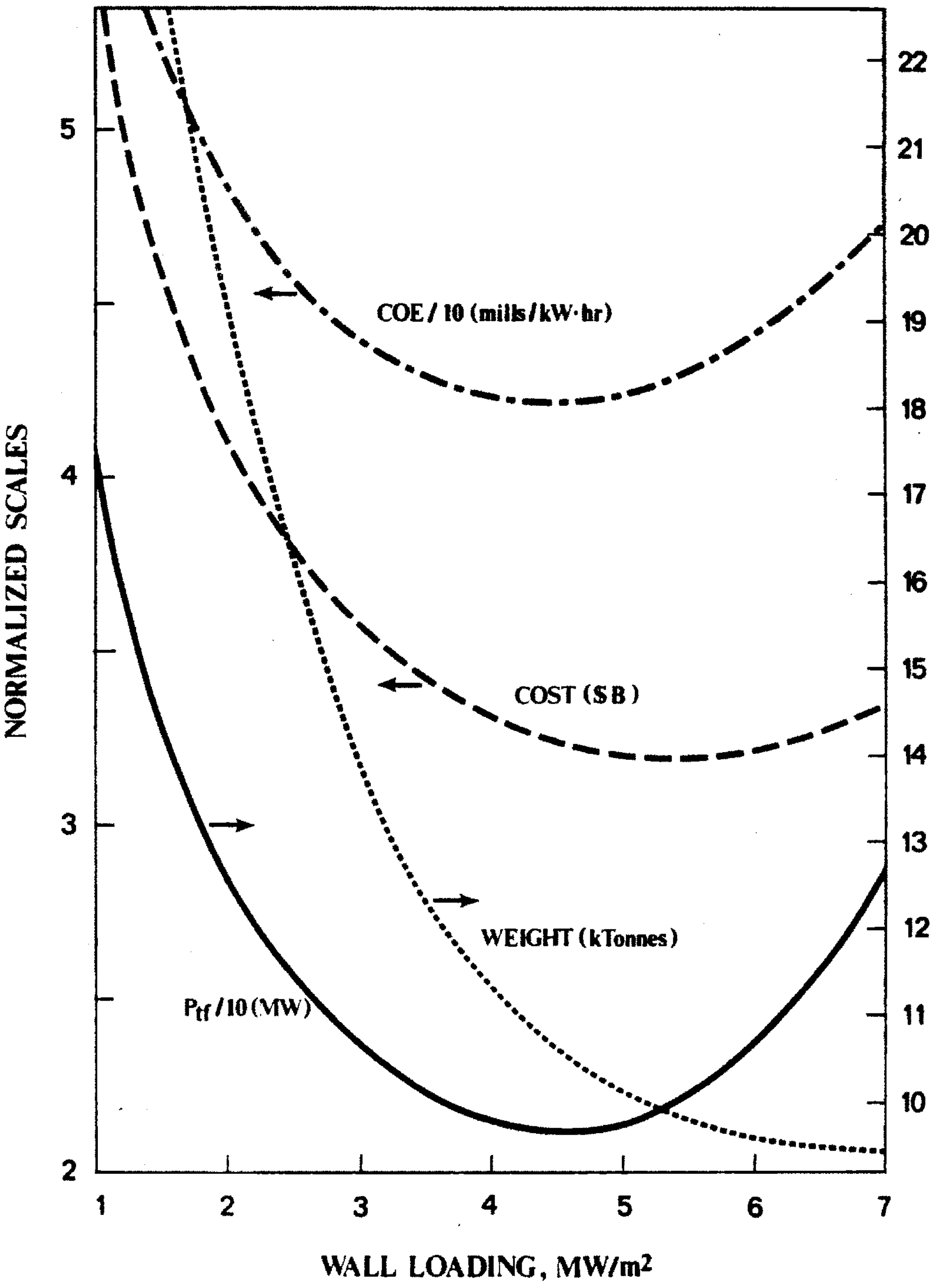

Figure 2.3: Second Stability Wall Load Scan, 1200 MW_e, $\beta = 24\%$, k = 1.8, A = 5

area requirements for constant power. Magnetic field on axis increases gradually with increasing wall loading because comparable fusion power is required in a device which is growing smaller.

Recirculating power requirements decrease rapidly up to ≈ 3 MW/m^2; after which the curves show a minimum. The volume of the TF coil decreases rapidly at first, accounting for the decrease in recirculating power but then the increasing magnetic field takes effect. Eventually, the device becomes small enough that there is insufficient space inboard in the TF coil to keep the current density in the coil low. Both capital cost and cost of electricity track the size and weight of the devices downward. The curves become flat at high wall loads and exhibit a minimum in the case shown. The costs begin to increase eventually due to the increased recirculating power and the increased operating costs from shorter component lifetimes. The COE curve increases more rapidly after the minimum than the capital cost because a mild degradation of availability with increased wall loading has been included in this case. Without the availability degradation, the COE curve would more closely match the capital cost. The recirculating power and cost increases could be moderated to some degree by relaxing the aspect ratio constraint, for example. However, the basic trends of the curves remain unchanged for a wide range of parameter space.

Preferred wall load is in the area of 4 MW/m^2. Most of the benefit for operating at higher wall load (lower size, cost, etc.) is achieved by 4 MW/m^2 while going to even higher wall loading will result in shorter component lifetimes and probably lower reliability and more difficult maintenance (and possibly higher cost). For the latter reasons, it may be attractive to go to lower wall loading (< 4 MW/m^2). However, significant penalties are paid in terms of size, recirculating power and cost for wall loadings less than ≈ 3 MW/m^2.

Net Electric Output

A parametric scan for net electric power outputs between 400 and 1400 MW$_e$ is shown in figure 2.4. The case shown is for a wall loading of 3 MW/m^2, an aspect ratio of 5, and an elongation of 1.8.

Major radius and weight increase almost linearly with increasing net electric power. Plasma current increases moderately as the minor radius increases with larger machine sizes. Since magnetic field remains fairly constant due to its

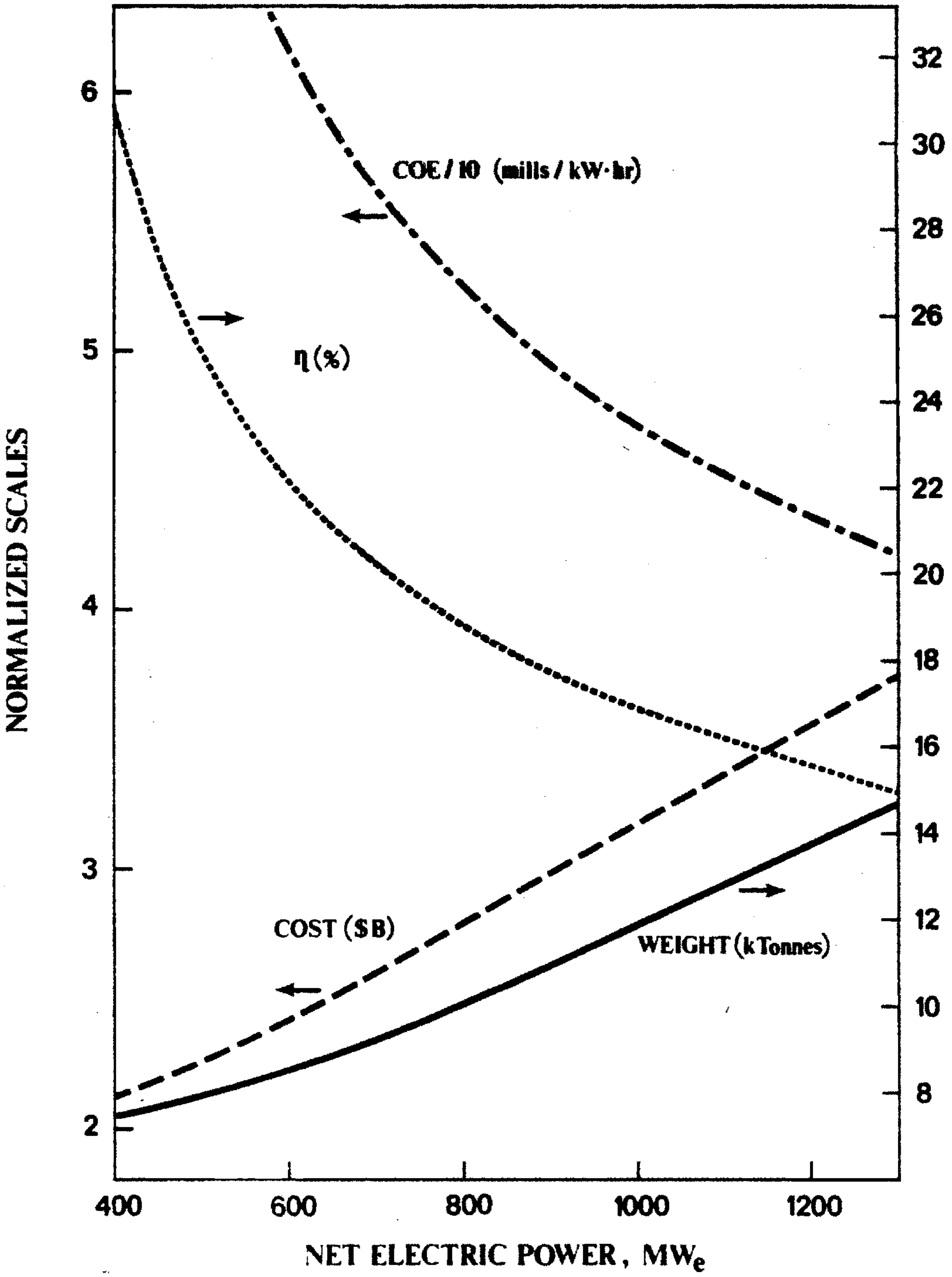

Figure 2.4: Second Stability Net Power Scan, 3 MW/m^2, A = 5, k = 1.8, $\beta = 24\%$

weak dependence on minor radius, the recirculating power slowly tracks the size of the device upwards. However, the recirculating power fraction increases gradually with decreasing net electric power down to about 600 MW_e; after which it increases more rapidly. This rapid increase is due to the fact that as the device gets very small, it produces a small amount of electricity but still requires substantial recirculating power. Capital cost also increases moderately with increasing net electric power as the tokamak continually increases in size to deliver the required power.

However, moving from right to left on the curves, the cost of electricity (COE) increases gradually and then more rapidly with decreasing $P_{net,e}$. Strong economies of scale are evident here; the size (and cost) of the device do not decrease nearly as rapidly as the power delivered does. Thus, the unit cost of delivering a watt of electricity becomes a limiting factor in the construction of small resistive magnet tokamaks.

Tokamaks are typically sized at 1000 to 1200 MW_e. However, reactors in smaller unit sizes require significantly lower investments. The parametrics show that resistive magnet tokamaks can be constructed in smaller (or larger) sizes with cost of electricity as the major limiting factor. High beta versions of RCTR could likely remain attractive in sizes as low as 600 MW_e with moderate penalties in cost of electricity. Versions in even smaller net electric sizes would probably only be attractive as demonstration reactors or in multiplexing applications (see section 2.4.4).

Aspect Ratio

High beta attainable in the second regime of plasma stability requires the use of large aspect ratios in the range of 5 - 6 (see chapter 5). Parametrics on aspect ratio are not warrented because this parameter is dictated by the physics. If second stability were attainable at lower aspect ratio then even higher beta would be required for stability and the device would likely improve further. Otherwise, its seems likely that operation at the lowest aspect ratio resulting in a stable second stability case with present theory is most desirable because this device will be of smallest size. Once high beta is achieved at large aspect ratio, there is little motivation to go to even higher A.

Elongation

The elongation parameter is also restricted by second stability physics. At present, second stability cases have not been found at elongations higher than ≈ 1.8. In fact, the second stability regime is most easily accessed at low elongation [1]. The approach used in this study is to operate at the highest elongation allowed by present theory because the benefits of high beta are attained while the device is at its smallest size.

Beta

The magnitude of beta assumed in the parametrics can be varied by changing the value of the plasma safety factor in the calculation of the beta equilibrium limit which is used to place an upper limit on beta. This variation represents a sensitivity to the uncertainty of achieving a given magnitude of beta in the second stable region. A typical beta scan is shown in figure 2.5. The inputs are $P_{net,e} = 1200$ MW$_e$, $P_w = 3$ MW/m^2, A = 5, and k = 1.8.

With net electric power and wall loading fixed, increasing beta (from right to left in the figures) has only a mildly beneficial effect on major radius and weight. However, the required magnet field diminishes significantly with increasing beta and results in lower recirculating power requirements for the same net electric power. This is the major benefit for RCTR of the higher beta possibly attainable with second stability physics. Low plasma current (typically 5 - 6 MA) can also be a significant advantage.

Mild benefits are attained in cost and cost of electricity with increasing beta above $\beta \approx 15 - 20\%$ due to the moderate reductions in size and weight. In addition, the large economies of scale present have the result that the cost of producing the extra power (required to make up for increased recirculating power requirements at lower beta) is relatively unimportant. However, firm conclusions based on cost considerations are difficult to make since costing methodologies for the components of a fusion device are relatively poorly developed.

The major advantages of high beta operation are low recirculating power and low plasma current. The principle drawbacks are the high aspect ratio required and the uncertainties associated with second stability physics. Betas of 15 -

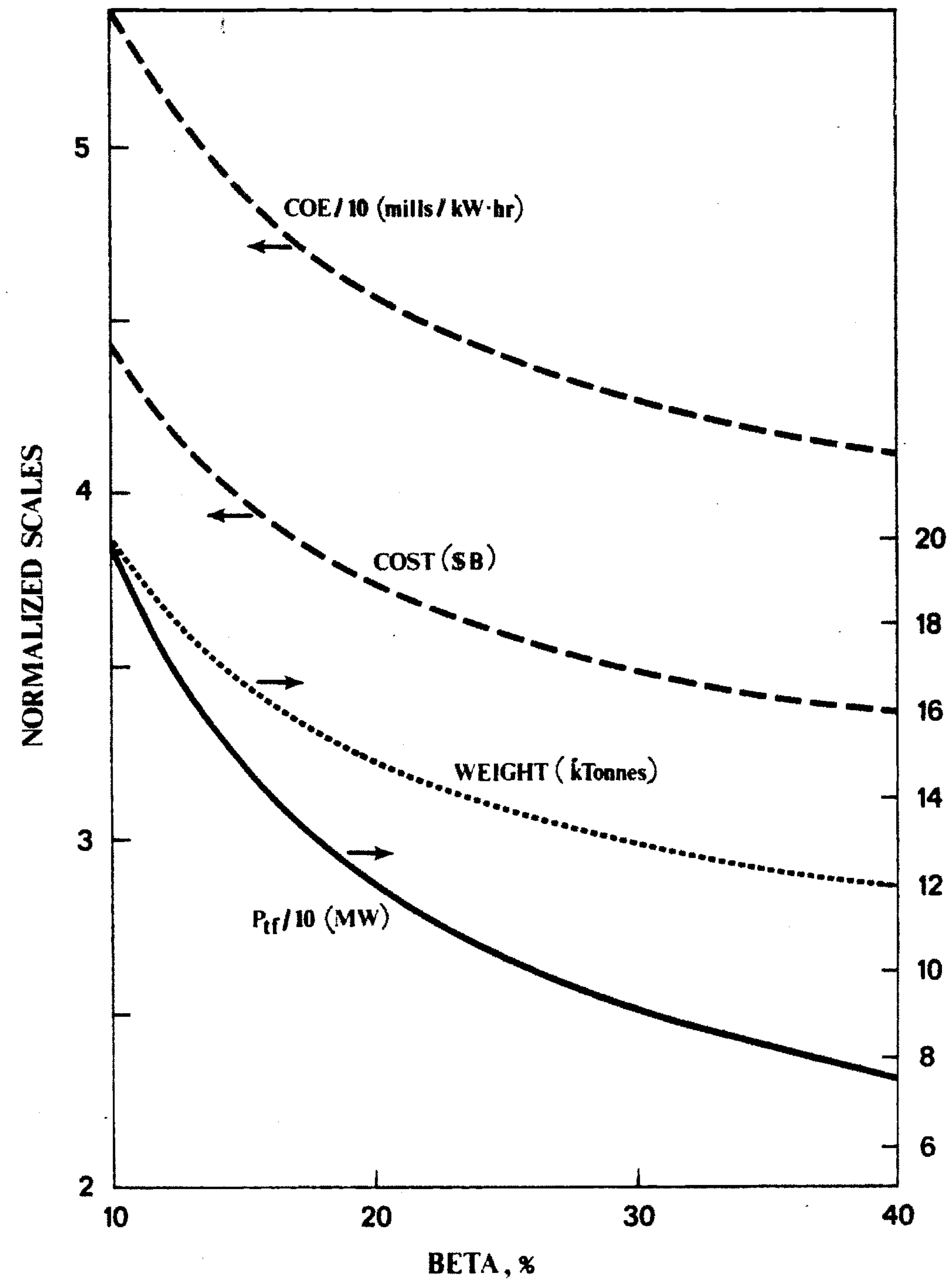

Figure 2.5: Second Stability Beta Scan, 1200 MW_e, 3 MW/m^2, $A = 5$, $k = 1.8$

20 % presently being projected for the second stability regime are high enough to achieve a large share of the benefits associated with high beta operation.

2.4.2 Moderate Beta Reactors

RCTR type devices operating with moderate betas allowed in the first regime of plasma stability are smaller in size (lower aspect ratio) and have higher recirculating powers than high beta versions. However, low beta devices operating typically with 6 - 10 % beta are not subject to the uncertainties of second stability physics (see chapter 5). For the most part, parametrics show the same general behavior in most of the trade-offs as in the high beta case. Differences in behavior will be emphasized in the discussions that follow.

Wall Loading

The results of a wall loading scan for moderate beta reactors is shown in figure 2.6. The cases shown are at $P_{net,e}$ = 1200 MW$_e$, A = 3, k = 1.8, and a beta of 7.3 % using the beta limit scaling obtained from Doublet III (D-III) data [15].

The same trends observed in the high beta cases are evident here. However, the shape of the curves, in particular the minimum in recirculating power, is more pronounced. This behavior is due to the low aspect ratio assumed in the cases. As the wall loading increases, the machines gets so small that the space available to the inboard TF leg is critical. Above 5 - 6 MW/m^2, the recirculating power is rapidly increasing due to small inboard TF magnet builds and the size and magnetic field of the device must increase accordingly to deliver the required net electric output. This effect could be mitigated to some extent by operating at higher aspect ratio (at least for the high wall loading cases) but parametrics show that although the cost increases can be moderated, the larger resulting machine size brings a similar loss of attractiveness relative to the lower wall loading versions.

Optimum wall loadings are in the 3 - 4 MW/m^2 range although these devices can operate at even lower wall loads with less penalty compared to the high beta cases. There is little incentive to operate at wall loadings above this range especially in light of their possible impact on reliability and maintenance. How-

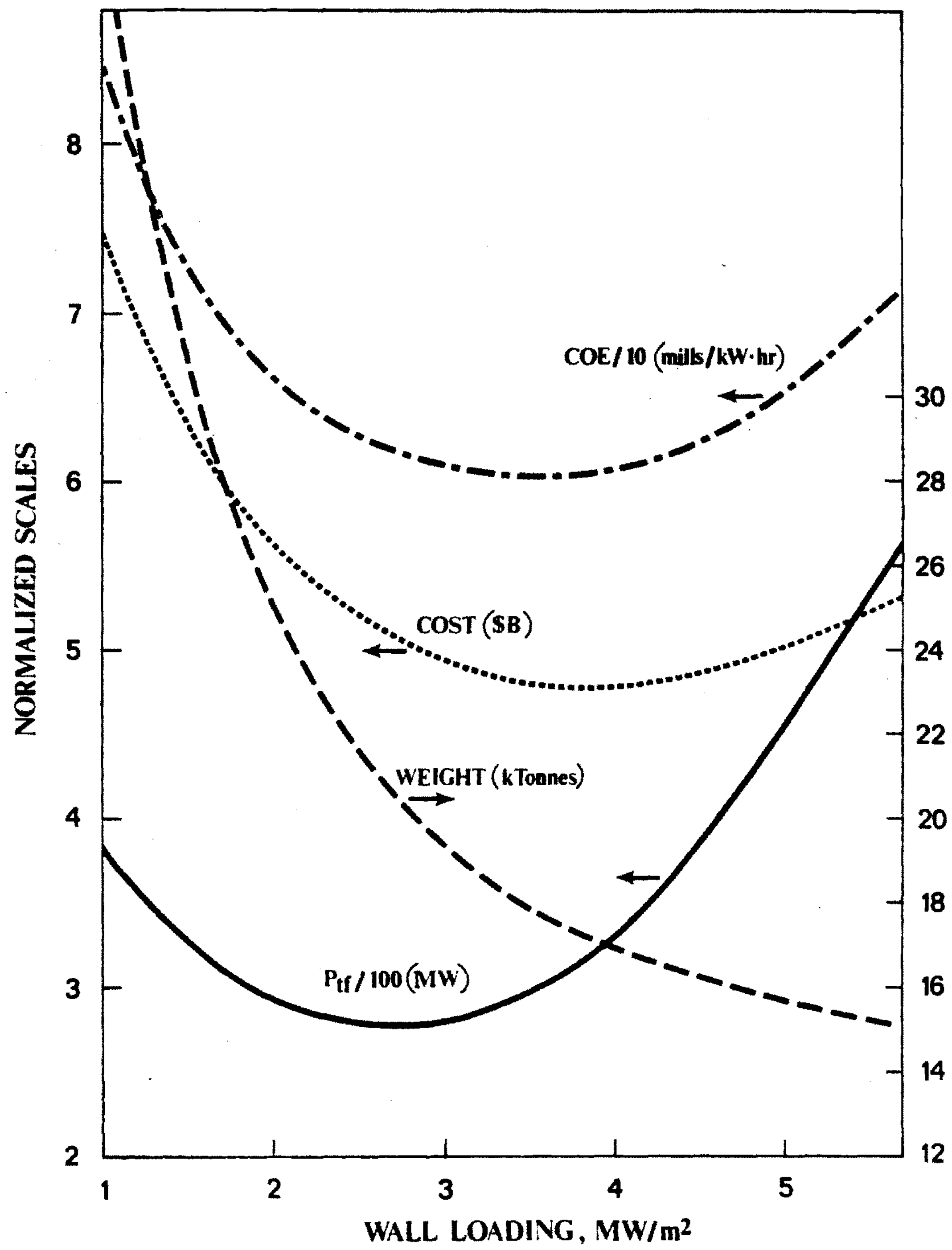

Figure 2.6: First Stability Wall Load Scan, 1200 MW_e, $A = 3$, $k = 1.8$, $\beta = 7.3\%$

ever, operation at wall loadings below this range could be attractive if possible added safety, reliability and maintenance benefits were perceived to outweigh the penalties in size and cost.

Net Electric Output

Again the trends apparent in high beta versions of RCTR are also evident here. $P_{net,e}$ scans for $P_w = 3$ MW/m^2, A = 3 and $\beta = 7.3$ % are shown in figure 2.7. Recirculating power actually exhibits a shallow minimum because the larger area available to the TF coil at high net electric power is competing with the effect of the lower required magnetic fields as machine output is decreased. The result shown is a moderately increasing recirculating power fraction (η) with decreasing $P_{net,e}$ down to about $800 MW_e$. In addition, since the area of the TF coil disappears more rapidly in these low aspect ratio devices, the COE (and η) penalty increases more rapidly as $P_{net,e}$ decreases.

Moderate beta versions of RCTR are thus most attractive at net electric powers above about 800 MW$_e$. Small plant sizes would be even less attractive at higher wall loading due a more rapidly shrinking machine size. Possible benefits of higher aspect ratio are offset by decreasing beta and increased machine size. High beta devices are more attractive in smaller plant sizes.

Aspect Ratio

Moderate aspect ratio devices operating in the first regime of plasma stability are not subject to the aspect ratio constraint of high beta versions. As a result, they tend to be more attractive at lower aspect ratio where the devices are smaller and less costly. Parametric scans for aspect ratio at $P_{net,e} = 1200$ MW$_e$, $P_w = 3$ MW/m^2, k = 1.8, and $\beta = 7.3$ % are shown in figure 2.8.

Two beneficial effects of lower aspect ratio are evident in figure 2.8. The weight and major radius decrease linearly with aspect ratio resulting in lower cost devices. Secondly, beta scalings in the first stability regime vary inversely with aspect ratio which results in lower fields and lower recirculating power with decreasing A.

Note, however, that the curves for cost and recirculating power in figure 2.8 eventually turn up at very low aspect ratio because the inboard leg of the TF coil

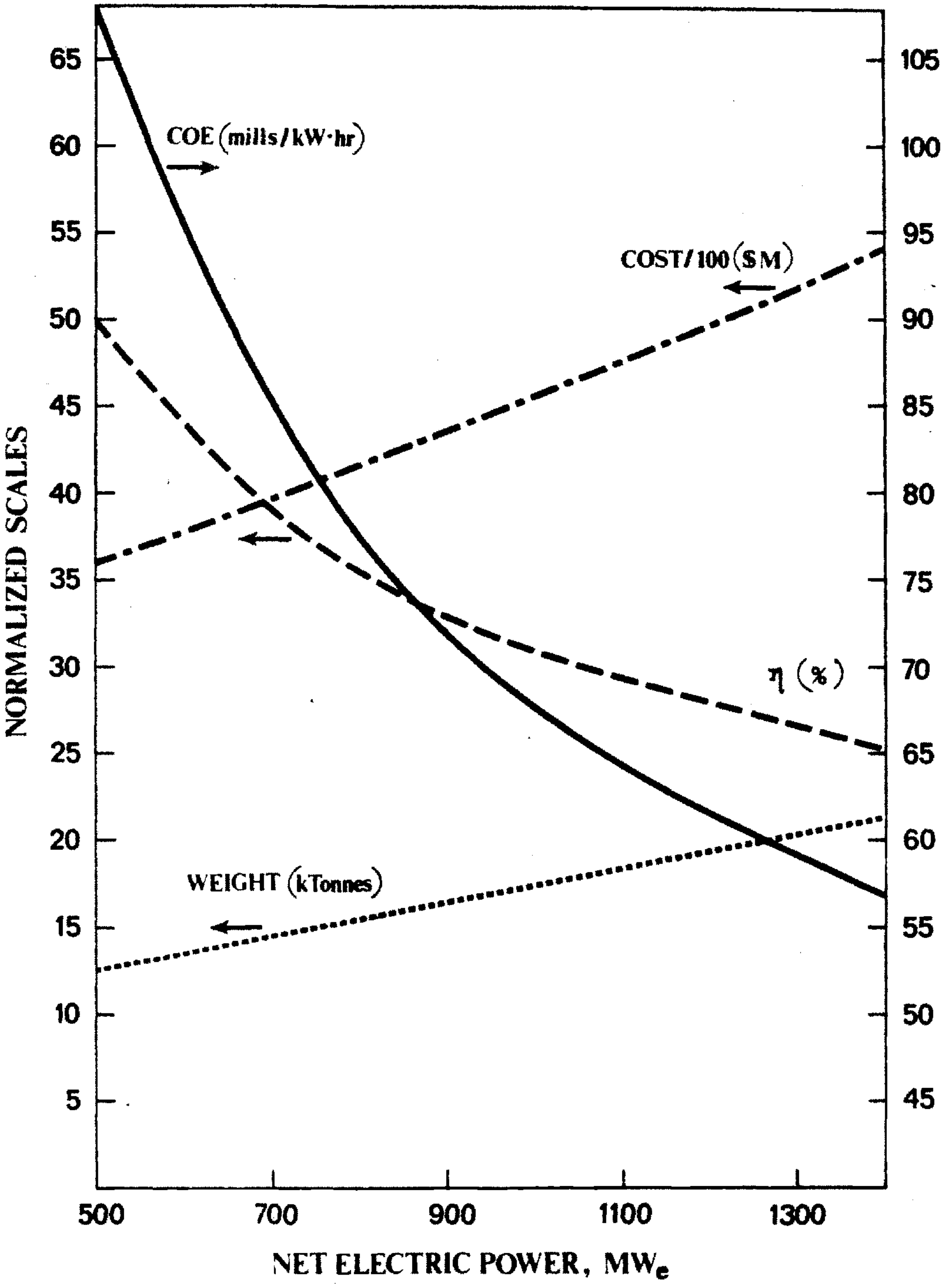

Figure 2.7: First Stability Net Power Scan, 3 MW/m^2, $A = 3$, $k = 1.8$, $\beta = 7.3\%$

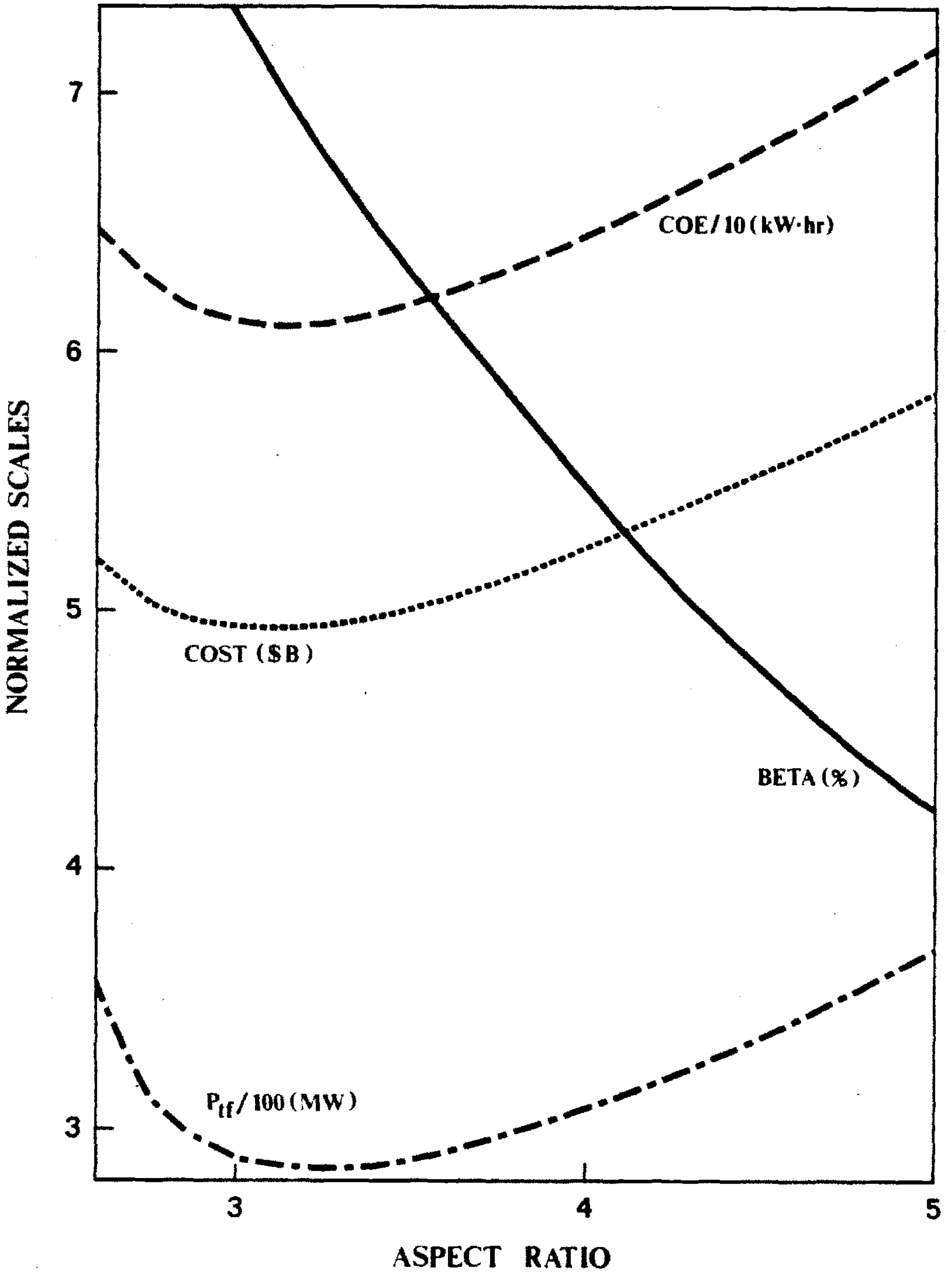

Figure 2.8: First Stability Aspect Ratio Scan, 1200 MW_e, 3 MW/m^2, $\beta = 7.3\%$

is again running out of space. As a result, the current density and recirculating power of the coil and the size of the device are forced to increase.

For a wide range of parameters, the optimum aspect ratio for these devices is 2.8 - 3.3. One possibility for considering operation at higher aspect ratios is the fact that the plasma current required decreases significantly at high aspect ratio. This could result in simpler PF systems and allow the possibility of the use of steady state current drive.

Elongation

Parametric scans versus elongation are shown in figure 2.9. The basic inputs are a wall loading of 3 MW/m^2, net electric power of 1200 MW$_e$, and an aspect ratio of 3. The D-III scaling is still in use.

Higher elongations are now possible with first stability physics. The benefits for increased elongation of smaller size at constant power are evident up to $k \approx 2$. The curves flatten out despite an assumed linear increase of beta with elongation because of a decrease in available space for the TF coil and increased plasma current and poloidal field coil requirements. Parametrics show that at higher wall loading, the recirculating power exhibits a broad minimum in the area of an elongation of 2. The minimum occurs because the machines are getting small enough at higher elongations for the space available at the TF coil to be limiting. In addition the EF system required for the higher elongations is increasingly more complex and increasing in power consumption. The same effect would occur if beta were to saturate eventually with increased elongation. This effect and other uncertainties associated with first stability beta are discussed in more depth in chapter five.

Beta

Beta scalings have a certain degree of uncertainty associated with them even in the first regime of plasma stability because they are untested in reactor regimes. Thus, variations in beta represent the importance of actually achieving the predicted beta values. Such variations also indicate the importance of achieving higher triangularity (for example) if the beta limit does actually improve with increasing triangularity significantly as predicted by some scalings.

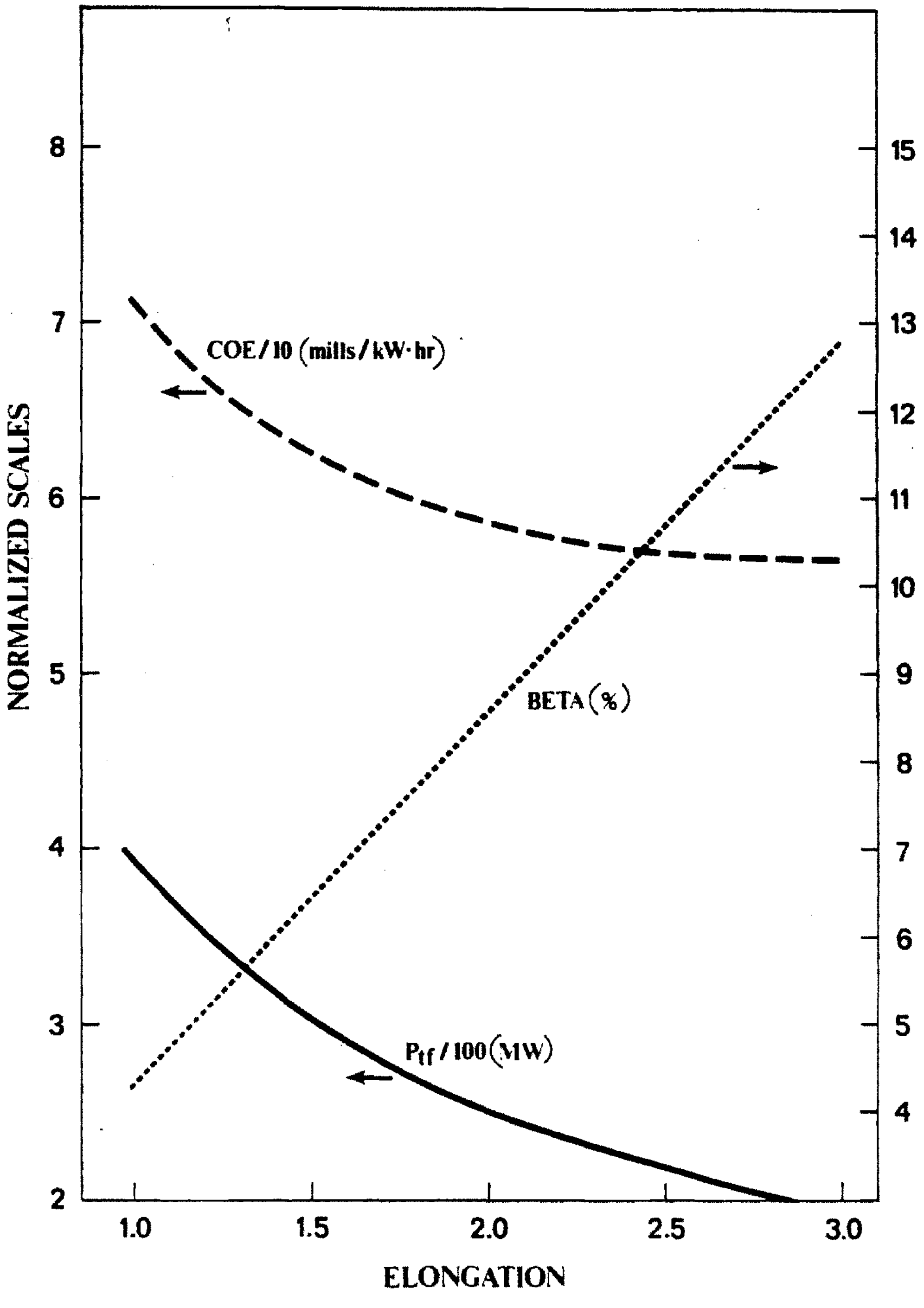

Figure 2.9: First Stability Beta Elongation Scan, 1200 MW_e, 3 MW/m^2, A = 3

Variations in beta for $P_{net,e} = 1200$ MW$_e$, $P_w = 3$ MW/m^2, A = 3, and k = 1.8 are shown in figure 2.10. Similar scalings to the high beta RCTR versions are apparent. Higher beta has a moderately beneficial effect on major radius, weight and cost. It appears desirable to achieve betas above 5 - 6 % where significant savings in recirculating power and cost may be possible. However, above 8 - 10 % there is less incentive to achieve higher beta except to reduce the magnitude of the recirculating power.

2.4.3 Other Trade-offs

Burntime

RCTR devices are capable of relatively long pulses because of the location of the OH coil internal to the TF. The impact of long pulse ohmic driven operation on the characteristics of resistive magnet tokamaks is shown in table 2.4 and table 2.5 for high and moderate beta operation, respectively. All of the cases shown are at 1200 MW$_e$ and 3 MW/m^2.

Using column one (burntime, $\tau_b = 1$ hr) of table 2.4 as reference, it's clear that increasing the pulse length to one day in length has a moderate impact on the device. The high aspect ratio of a high beta device provides a large bore for the ohmic coil which can deliver the required volt-seconds with relatively low peak fields at the coil.

Day long pulses are a bit more difficult to obtain in the low aspect ratio devices of first stability. As shown in table 2.5, however, long pulses are attainable with moderate to large increases in the aspect ratio. Six hour pulses are achieved with moderate increases in size and cost. However, an aspect ratio four with corresponding increases in size and cost is needed for a 12 hour pulse. The situation can be improved significantly with the use of RF assisted start-up [22] as shown in the last column. With the OH coil only required to supply resistive volt seconds for the plasma burn, the twelve hour case with RF start-up shrinks to the size of the three hour pulse length device.

Beta Assumption and Thermal Efficiency

The efficiency for conversion of the thermal energy deposited in the blanket by the fusion neutrons depends significantly on the details of the blanket design.

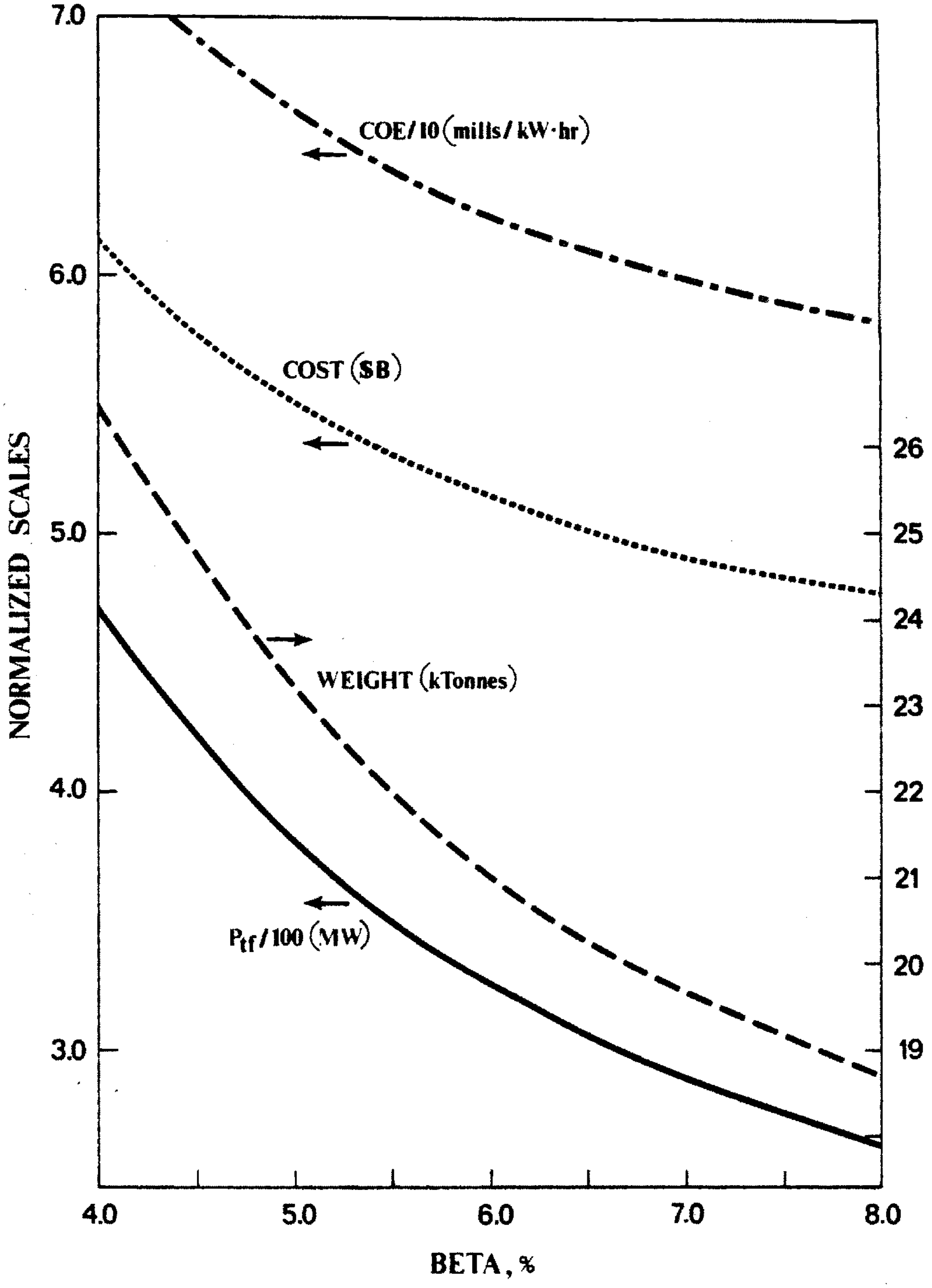

Figure 2.10: First Stability Beta Scan, 1200 MW_e, 3 MW/m^2, $A = 3$, $k = 1.8$

Burntime, hr.	1	6	12	18	24
Major Radius, m	7.52	7.52	7.54	7.57	7.70
Magnetic Field, T	2.4	2.4	2.4	2.4	2.4
Weight, ktonnes	14.2	14.2	15.5	18.1	22.7
Thermal Power, MW_{th}	3376	3381	3396	3428	3533
TF Power, MW	106	108	114	126	166
Auxiliary, MW	225	228	234	248	294
Direct Cost, $M	2038	2065	2130	2252	2495
Capital Cost, $M	3633	3680	3796	4014	4446
Elec. Cost, mills/kW·hr	44.5	44.5	47.6	51.8	59.7
Recirc. Power Frac.	0.16	0.16	0.16	0.17	0.20

Table 2.4: Second Stability vs Burntime, 1200 MW_e, 3 MW/m^2, $k = 1.8$, $\beta = 24\%$

Burntime, hr.	1	3	6	12	12*
Major Radius, m	6.57	6.74	6.95	8.02	6.69
Magnetic Field, T	4.0	4.0	3.9	4.7	4.0
Weight, ktonnes	20.7	24.1	26.8	34.9	23.3
Thermal Power, MW_{th}	3975	4183	4439	4473	4128
TF Power, MW	291	367	439	469	345
Auxiliary, MW	479	565	673	686	541
Direct Cost, $M	2869	3110	3330	3751	3053
Capital Cost, $M	5113	5545	5935	6686	5441
Elec. Cost, mills/kW·hr	63.0	69.5	75.2	85.5	67.9
Recirc. Power Frac.	0.29	0.32	0.36	0.36	0.31

* Using RF assisted start-up

Table 2.5: First Stability vs Burntime, 1200 MW_e, 3 MW/m^2, $k = 1.8$, $\beta = 7.3\%$

Beta Regime	First	Second	First
Efficiency	0.35	0.35	0.45
Major Radius, m	7.34	8.60	6.57
Aspect Ratio	3	5	3
Beta, %	7.3	24	7.3
Field, T	3.9	2.3	4.0
Weight, ktonnes	24.9	17.0	20.7
TF Power, MW	319	124	291
Auxiliary, MW	535	261	479
Direct Cost, $M	3296	2357	2869
Capital Cost, $M	5876	4200	5113
Elec. Cost, mills/kW·hr	72.4	51.2	63.0
Recirc. Power Frac.	0.31	0.18	0.29

Table 2.6: Impact of Improved Thermal Efficiency

The self cooled liquid lithium design with vanadium structure selected for RCTR is capable of thermal efficiencies, η_{th}, as high as 42 - 45 %. This compares to 35 % efficiencies commonly accepted for water cooled systems.

Higher thermal efficiency holds potential benefits for tokamak design because significantly lower fusion power is required for the same net electrical output. The potential of higher η_{th} is exhibited in table 2.6. The table compares moderate and high beta cases with thermal efficiencies of 35 % with a moderate beta case assuming 45 % efficiency. All cases have $P_{net,e}$ = 1200 MW_e, P_w = 3 MW/m^2 and an elongation of 1.8.

Comparing the low efficiency examples, its evident that the high beta case exhibits some advantages over the moderate beta version. Direct cost is lower by about 25 percent due to the lower weight (despite a significantly larger major radius). The major advantages of high beta operation of low recirculating power and low plasma current are evident. However, high beta operation using the second regime of plasma stability has not been firmly established to date. In addition, the lower power densities obtained in plasmas with the flat profiles now being proposed for the stability of high beta operation (see chapter 5) may result in magnetic fields more comparable to those needed in moderate beta designs (for the same net electric output).

Invoking column three we find that some of the same advantages with the high beta assumption can be obtained with the use of a blanket design capable of high thermal efficiency. In fact, nuclear island weight, cost and COE are reduced considerably with respect to the low efficiency case of column one. However, low recirculating power and plasma current are characteristic only of the second stability regime case (column 2).

2.4.4 Multiplexing

Multiplexing refers to the placement of multiple reactors at a single site. It usually refers to the case where the reactors share equipment and structures such as buildings, maintenance and balance of plant components. Sharing of equipment at such a site can result in cost savings and an increase in overall availability because if a single plant fails, it doesn't necessarily hinder the remaining plants from operation.

Other possible advantages of multiplexed plants are shorter construction times and lower costs involved with the initial generation of electricity, more extensive use of factory fabrication with smaller size units and better operational flexibility. Essentially, multiplexing is a method of improving the economy of scale of small reactors; lowering the capital investment with a reduced penalty in the cost of electricity. Its possible that multiplexing could make the inherently large, complex fusion reactor more attractive to the electric utility.

Several studies of fusion reactor multiplexing with the emphasis on superconducting magnet tokamaks are available [23,24]. Here, we apply similar analyses and evaluate multiplexing with resistive magnet tokamaks. The only difference from the analysis of section 2.3 is in the costing of multiple reactors with shared equipment. Multiplexed units are typically 300 – 600 MW_e with 3 to 4 units at a single site.

Cost advantages come about from shorter construction times, higher effective plant availability and the sizing of shared components for the entire plant instead of for a number of small plants which benefits from economies of scale. The details of multiplex cost accounting for each component of the fusion plant are indicated in appendix B with the multiplex accounts suffixed by 'np'.

The results for a typical multiplexed plant are shown in table 2.7. The table compares a multiplexed site consisting of four 350 MW_e reactors with a single 350 MW_e plant and a single 1400 MW_e plant (having the same output as the multiplexed site). In the first column, the single 350 MW_e plant exhibits the

Parameter	**350 MW_e Single Unit**	**1400 MW_e Multiplex**	**1400 MW_e Single Unit**
Net Electric Power, MW_e	350	1400	1400
Wall Loading, MW/m^2	4.3	4.3	4.3
Elongation	1.8	1.8	1.8
Aspect Ratio	5	5	5
Major Radius, m	3.57	3.57	6.84
Nuclear Island Weight, ktonnes	4.6	4.6	12.2
Toroidal Beta, %	24	24	24
Field on Axis, T	3.3	3.3	2.7
Plasma Current, MA	3.5	3.5	4.8
TF Coil Power, MW_e	64	64	105
Total Recirculating, MW_e	138	138	223
Availability	0.70	0.65	0.70
Construction Time, Yrs.	8	6	8
Account 21, $M	124	387	222
Account 22, $M	488	1598	1092
Account 23, $M	104	376	223
Account 24, $M	97	164	151
Account 25, $M	281	810	306
Account 26, $M	16	41	54
Direct Cost, $M	1115	3380	2054
Capital Cost, $ M	1987	5820	3660
COE, mills/kW·hr	91.4	63.5	41.5

Table 2.7: Multiplexing Cost Comparison

qualities of low capital investment but very large cost of electricity. The third column is at the opposite end of the spectrum with the large capital investment and low cost of electricity characteristic of large output (1400 MW_e) single units. The multiplexed plant, shown in the center column, represents an attempt to reduce the capital investment while maintaining a reasonable cost of electricity and a large net electrical output. Indeed, the capital cost of the multiplexed plant is substantially less than four times the single small unit plant cost and the effective cost of electricity of the small unit multiplexed plants is markedly reduced. However, in this case the large single unit plant with the same net electrical output as the multiplexed site still retains a lower C and COE than the multiplex case. Still, there are advantages to multiplexing such as increased operational flexibility which can't be quantified here.

Larger multiplexed plants ($\approx$ 600 MW_e) show an improvement relative to the single plant case but the single plant case always retains some advantage in terms of cost and cost of electricity. Similar studies for superconducting magnet tokamaks [24] found that multiplexed sites could more readily compete with single plants of comparable power output. This result is probably mostly due to a difference in costing and availability assumptions. However, some advantage might be expected for superconducting systems with multiplexing at very low plant sizes because of relatively large recirculating power fractions with resistive magnets.

2.4.5 Resistive Vs. Superconducting Magnet Tokamak Cost Comparison

Until recently, resistive magnets have not been considered seriously for pure fusion (electricity producing) applications due largely to perceptions that the inherently high recirculating power requirements would always lead to less attractive, more costly reactors than those utilizing superconducting magnets. We have shown that recirculating power requirements can be reduced through proper design of the toroidal field coils (low current density and demountability) but recirculating power requirements are still greater than with superconducting magnet applications for low beta reactors and high beta reactors using current drive. In this subsection, we argue that resistive magnet tokamaks should not have constructed costs significantly different from comparable superconducting options. In addition, with comparable constructed costs, RCTR may prove a significantly better option because of possible availability improvements from a simpler concept requiring less repairs and a possibly more maintainable concept using demountable toroidal field coils.

Cost differences between resistive and superconducting magnet tokamaks will probably be in the following major areas:

- magnets
- power supplies
- shielding
- balance of plant

Costs for power supplies and the balance of plant would likely be higher for the resistive case because of larger recirculating power requirements. More power is needed to drive the magnets and the thermal power output required to supply the extra recirculating power requirements is increased. However, because of the large economies of scale in effect with fusion reactors (relatively low incremental cost for a given increase in power output), we expect these costs to be moderate over some range. This is discussed in more detail below.

The cost of shielding for the resistive case is expected to be significantly lower than that for superconductors because of decreased shielding requirements for the more robust resistive coils. The comparative costs for the magnet systems are not as clear. We expect the unit cost of resistive magnets to be less than that for superconductors since they are simpler, require less costly materials and may involve simpler manufacturing techniques. However, resistive magnets could be more massive than their superconducting counterparts depending on the specific design. For example, at low beta resistive magnets can become quite bulky in favor of reduced coil dissipated power. On the other hand, resistive magnets can be made closer fitting to the plasma due to reduced shielding requirements.

Specific cost comparisons are difficult because of the large number of assumptions inherent in any fusion reactor costing analysis. However, we present such a cost comparison in table 2.8, not as proof of the relative costs of superconducting and resistive magnets, but as an illustration of the trade-offs in cost mentioned. The superconducting case shown was taken from reference [24] which included a breakdown of the cost accounts presently in use in commercial tokamak design studies. Both cases deliver 350 MW_e at 4.3 MW/m^2 and are comparably sized devices.

Some differences in cost algorithms is evident from line items such as account 21 and the account designated as 'other' under account 22 which should not be fundamentally different in this type of comparison. Cost savings for the resistive case from smaller blanket and shielding requirements are evident. Heat removal and power supply accounts favor the smaller recirculating power requirements of the superconducting case. The largest difference in accounts occurs in the costing of the magnet systems. According to this comparison, the cost of the magnets systems for the resistive case is well over twice that of the superconducting case. This result is probably very pessimistic for the resistive case because the resistive magnets should not be exceedingly more massive than the superconducting magnets at high beta (24% in this case) and certainly should have a lower unit cost. However, we also would expect a more significant difference favoring the superconducting magnet design in the costing of power supplies than is indicated here.

The total direct costs for the two plants are found to be quite comparable despite the variations in individual accounts. This result in itself does not prove anything about the relative costs of superconducting and resistive magnet tokamaks. However, we find no fundamental reason why resistive magnet tokamaks should require significantly different capital investments than the superconducting variety. Different cost accounts will alternately favor resistive and superconducting magnet designs and the bottom line may fluctuate as much as several hundred million dollars depending on the specific design and various costing assumptions.

For a final remark on the relative costs of resistive and superconducting magnet tokamaks we return to the question of recirculating power. Objections to resistive magnet tokamaks usually center about this requirement and it is useful to try and gain insight into the cost of increased recirculating power. In figure 2.11, the cost of electricity is plotted as a function of recirculating power fraction (η). The figure was generated for reactors with 1200 MW_e, 3 MW/m^2, and 7.3% beta with everything else fixed except the thicknesses of the toroidal field coil.

Parameter	**Superconductor**	**RCTR**
Net Power, MW_e	351	351
Wall Loading, MW/m^2	4.3	4.3
Major Radius, m	3.53	3.57
Aspect Ratio	4	5
Beta, %	25	24
Plasma Current, MA	4.3	3.6
Field, T	3.7	3.2
Burntime, s	5880	5880
TF Power, MW_e	0	65
Aux. Power, MW_e	56	140
Weight, ktonnes	—	4.6
Account 21, $M	152.4	124.4
Account 22, $M	515.6	538.2
— Blanket, $M	21.8	14.8
— Shield, $M	71.7	15.3
— Magnets, $M	64.9	140.8
— Structure, $M	6.4	11.8
— Vacuum, $M	13.3	2.0
— Power Supply, $M	90.2	102.2
— Heat Transport, $M	91.0	104.6
— Cryogenic, $M	4.4	—
— Rad. Waste, $M	3.9	2.8
— Fuel, $M	21.5	28.0
— Other, $M	18.8	59.2
— Control, $M	15.9	33.2
Account 23, $M M	106.4	104.1
Account 24, $M	104.5	97.0
Account 25, $M	18.1	31.1
Account 26, $M	—	16.4
C_{direct}, $M	897	918
C, $M	—	1980
COE, mills/kW·hr	—	80.0

Table 2.8: Cost Comparison of Resistive and Superconducting Tokamaks

The result for the cost of recirculating power shows a broad minimum for η between 25 and 40 %. At η less than 25 %, the cost increases rapidly because the magnets have to become increasing more bulky to achieve lower and lower dissipated powers. Then as the magnets become thinner and the recirculating power fraction increases, the costs from power supplies and the balance of plant (increased P_{th}) start to offset the decreased magnet costs and the curve flattens out and turns over. However, because of the relative size of magnet costs to recirculating power costs and the strong economies of scale, the cost of incurring increased recirculating power requirements does not dominate the overall cost until the recirculating power fraction gets quite high (greater than $\approx 40\%$).

This result supports the contention that large recirculating power need not be a significant cost penalty and should not fundamentally limit resistive magnet tokamaks in pure fusion applications. The result also shows that resistive magnet tokamaks operate best at relatively high recirculating power fractions when in the low beta regime. Although this result, in itself, does not determine the relative costs of superconducting and resistive magnet tokamaks, it suggests that increased capital costs from higher recirculating power requirements might easily be offset by cost savings from decreased shielding and simpler technology with RCTR. On the other hand, possible enhanced availability advantages for RCTR due to simpler design and the use of demountability might not easily be offset by superconducting magnet designs.

2.5 Illustrative Designs

The final step in the parametric analysis is to use the results of the trade-offs to select illustrative designs. These designs are selected to represent the best potential for RCTR and are used as the subject of more detailed analysis. The final objective is to combine detailed analysis of systems which potentially play key roles in the design with illustrative concepts to come up with the most attractive conceptual design possible.

Selecting a single optimized design would be extremely difficult. Even after many parametric trade-offs, there is still too much uncertainty surrounding many aspects of fusion reactor design for unique selections to be made for some of the parameters. For example, its difficult to choose the best wall loading be-

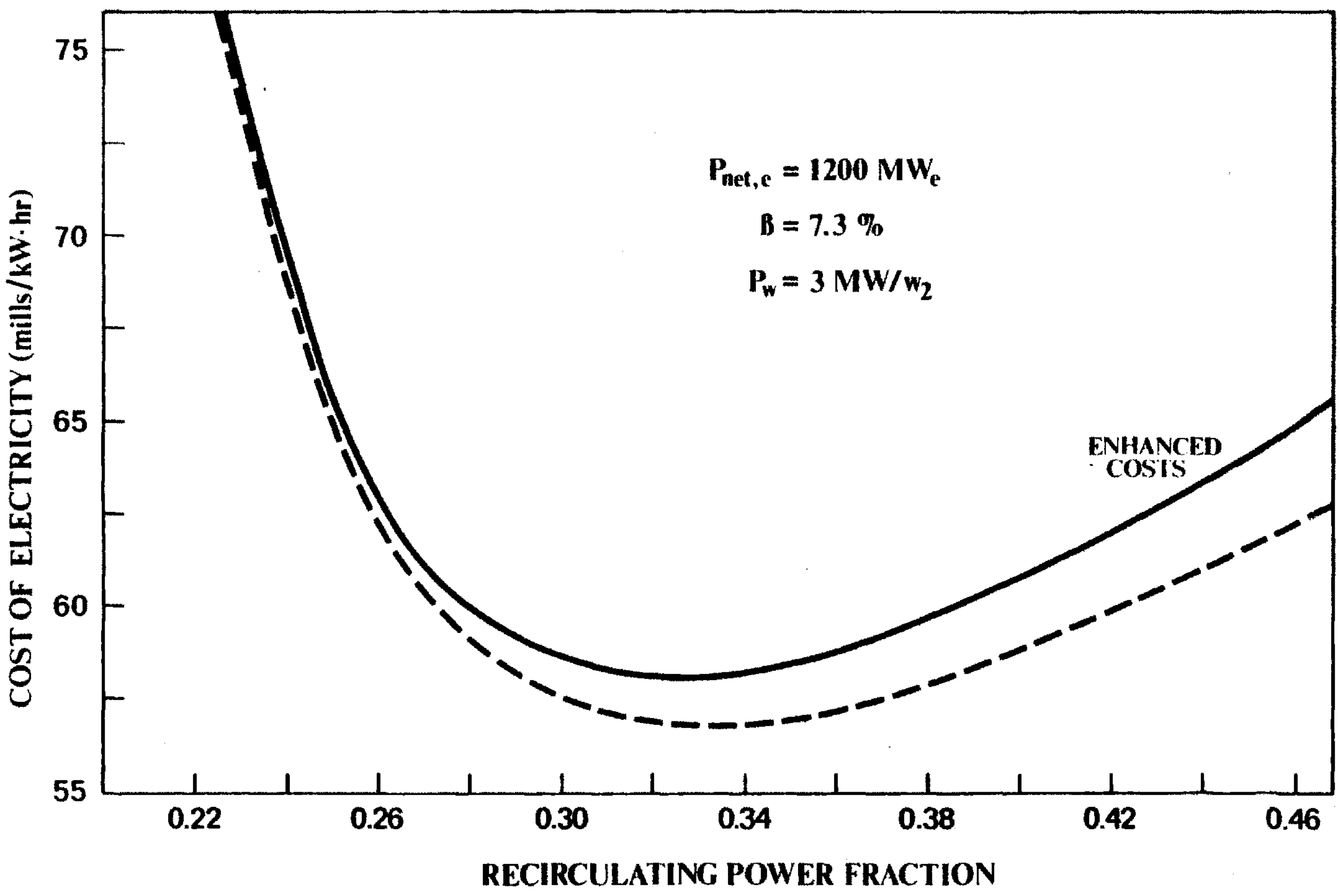

Figure 2.11: Cost of Electricity vs Recirculating Power Fraction

Case	A	B	C	D	E	F
Net Electric Power, MW_e	1200	1200	1200	500	1200	800
Wall Loading, MW/m^2	3	3	3	3	6	1.5
TF Material	Cu	Cu	Al	Cu	Cu	Cu
Beta, %	24	9.6	24	24	24	9.6
Major Radius, m	7.5	6.4	7.9	5.0	5.3	7.9
Aspect Ratio	5	3	5	5	5	3
Magnetic Field, T	2.4	3.5	2.4	2.7	3.1	2.8
Plasma Current, MA	4.7	17.2	4.9	3.5	4.3	16.8
Nuclear Island Weight, ktonnes	14.2	17.8	9.3	8.1	8.4	22.5
Thermal Power, MW	3380	3790	3690	1570	3340	2830
TF Dissipated Power, MW_e	108	225	190	80	108	216
Total Recirculating, MW_e	228	400	355	168	212	400
Direct Costs, $M	2065	2590	1740	1380	1850	2660
Capital Cost, $M	3680	4615	3100	2460	3295	4735
Cost of Electricity, mills/kW·hr	45.4	56.7	38.3	73.9	45.1	80.4
Recirculating Power Fraction	0.16	0.25	0.23	0.25	0.15	0.33

Table 2.9: RCTR Illustrative Concepts

cause of the complex trade-off between greater compactness and higher system power density for high wall loadings and the corresponding increase in risk and engineering difficulty. Indeed, the impact of going to higher wall loads on the cost of the device is relatively poorly understood. However, some intelligent choices for wall loading and other parameters can be made based on the parametrics and consideration of the goals for RCTR and other factors external to the analysis.

This procedure has led to the selection of six illustrative concepts. Each of the concepts, shown in table 2.9, explores a different potential for RCTR depending on separate perceived goals for an attractive commercial tokamak and/or possible future innovations. All of the designs have an internal poloidal field system, a lithium-vanadium blanket/first wall system and demountable toroidal field coils. Each possesses the high engineering power density, good mass utilization and decreased complexity characteristic of resistive magnet tokamaks.

Case A shows the potential of RCTR as a tokamak operating in the second regime of plasma stability. The device has 1200 MW_e and operates at a wall loading of 3 MW/m^2. 1200 MW_e is comparable in size to the large base-load plants in operation today. The wall loading choice is high enough that the device remains fairly compact but low enough that a relatively simple blanket/first wall and impurity control system is possible. High beta of 24 % contributes to a low recirculating power requirement of 228 MW which is comparable to that of a superconducting tokamak using RF driven current. An aspect ratio of 5 leads to the relatively large major radius of 7.5 m but the compact nature of the nuclear island limits the weight to 14.2 ktonnes. The plasma current is comfortably low at 4.7 MA.

If the second stability regime does not prove viable, RCTR can still be attractive with only moderate beta as shown in case B. Again, the net electric power and wall loading are 1200 MW_e and 3 MW/m^2, respectively. Recirculating power requirements (400 MW) and plasma current (17.2 MA) are relatively high but only moderate weight and cost penalties are indicated.

Generally, copper has been considered as the magnet conductor in the analysis. However, despite having twice the resistivity of copper, aluminum can be an attractive alternative to copper. In particular, aluminum has one third the density of copper and becomes far less activated under neutron irradiation. A version of RCTR using aluminum magnets is shown as case C. High beta has been assumed which helps to keep recirculating power requirements to 355 MW. The magnets are bulkier than those of case A (the comparable copper version) but are far less massive and costly. In fact, the total cost predicted for the aluminum magnet case is significantly lower than its comparable copper version.

Case D explores the possibility of using fusion plants in small unit sizes. In case D, 600 MW_e is delivered in a high beta version of RCTR using copper magnets. The cost of electricity is higher than in case A but the capital investment required is significantly reduced. Several of these plants could possibly be combined on a single site in a 'multiplex' arrangement.

The final two cases explore two extremes of physics and engineering feasibility. Case E operates at high wall loading (6 MW/m^2) and high beta (24 %). The high wall loading results in a relatively compact device despite the high aspect ratio required by second stability physics. A cost penalty is not indicated in case E. However, the incremental cost of higher wall loads in terms of replacement and loss of availability is difficult to estimate. In any case, the design of the blanket/first wall and impurity control system is significantly more difficult and uncertain at this level of wall loading.

In contrast, case F is a conservative version of RCTR. The low wall loading of 1.5 MW/m^2 results in a large machine (22 ktonnes) but the first wall may only require replacement once during the lifetime of the plant. Consistent with the conservative theme, only moderate beta (8 %) at low aspect ratio is assumed. This contributes to the relatively large recirculating power (400 MW). A significant cost penalty is also indicated.

Case A is used as the reference case for the more detailed analysis of selected topics discussed in chapters three thru five. However, in most respects, the analysis will be applicable to any of the selected cases presented above.

2.6 Summary

A methodology developed to conduct parametric analyses of resistive magnet tokamaks has been presented. This methodology has been incorporated into a parametric code *RTPAC* which was used to carry out a number of trade-off studies. The results of the parametrics may be summarized as follows:

- High beta reactors (assuming second stability physics)
  - Optimum wall loading is ≈ 4 MW/m^2
  - Reactors with $P_{net,e}$ as low as 600 MW_e remain attractive
  - Pulse lengths as long as one day in length can be achieved
  - Lowest aspect ratio allowed by 2nd stability is desirable
  - Optimum elongation is the highest allowed by 2nd stability (≈ 1.8)
- Low beta reactors

  - Optimum wall loading ≈ 3 - 4 $\mathrm{MW/m^2}$
  - Decreasing $P_{net,e}$ attractive down to ≈ 800 MW_e
  - Pulse lengths of 6 - 12 hours possible
  - Best aspect ratios ≈ 2.8 - 3.3
  - Optimum elongation ≈ 1.8 - 2.0
- High blanket thermal efficiency is an important asset comparable in impact to high beta in many respects
- High beta operation has advantages of low plasma current and low recirculating power and moderate cost advantages
- Aluminum magnets are attractive for their cost and activation advantages despite high dissipated power
- Multiplexing may significantly reduce the cost of small reactors and could make the application of fusion more attractive for the electric utility
- Low beta devices operate best at relatively high recirculating power fractions ($\approx 25 - 40\%$)
- Increased costs due to recirculating power requirements with RCTR relative to superconducting magnet options might easily be offset by cost savings from simpler technology and reduced shielding requirements

The parametric analysis has led to the selection of several illustrative designs. Each illustrative case, summarized in table 2.9, represents an optimized design in the context of a different extrapolated innovation or perception of the most desirable qualities for a fusion reactor.

The following chapters will consider in greater detail some of the systems which could play a key role in the effort to present a more attractive commercial tokamak reactor.

Chapter 3

Demountable Coil System

3.1 Introduction

One of the most attractive aspects of the use of resistive magnets in tokamak design is the possibility for designing the toroidal field coils to be readily demountable. The simple flat plate geometry of bitter type TF coils lends itself relatively easily to the incorporation of joints which segment the coil and make its dismantling possible. With this capability, maintenance of the coil and the components within its bore is facilitated.

A substantial amount of pioneering work on demountable coils for resistive magnets has been done by Jassby [25]. Demountable coils are presently in use in tokamak experiments [8] and have been proposed for use in a TFCX design by Puhn [26]. The present work concerns a demountable concept created for RCTR which offers a maintenance scheme requiring only simple vertical lifts. The concept is integrated with the support structure required to support both the in-plane and out-of-plane forces present and the reference blanket/first wall concept. Such a maintenance scheme is an important asset to this tokamak concept in light of the importance of maintenance and availability in commercial fusion reactor plants.

Section 3.2 outlines some of the important considerations and options which led to the present design. This design is then presented in section 3.3. The assembly and maintenance operations are discussed in section 3.4. Analytical stress calculations were used to size the components of the demountable concept. These are discussed in section 3.5. In section 3.6, the merits of external and internal (to the TF bore) poloidal field coil systems are compared. Internal poloidal field systems are made practical with the use of demountability. Finally, chapter 3 is summarized in section 3.7.

3.2 General Considerations

The major objective of the demountable coil design for RCTR is to provide a means of access to the bore of the toroidal field magnet for maintenance. The design also emphasizes the use of the simplest possible joint design and allows for maximum flexibility in the way the coil is disassembled and the internal components exposed. We demand that OH and EF coils be removable with vertical lifts without the need for cutting or segmentation within the nuclear island. Alternate configurations were investigated in an attempt to minimize the use of bolts and pins and avoid the necessity for the breaking of welds. These requirements are essential for a commercial reactor which cannot afford to be unavailable often or for extended periods. The final requirement is that the maintenance scheme be compatible with support structure and other major components such as the blanket/first wall system.

3.2.1 TF Coil Configuration

A number of options related to the toroidal field coil configuration are available once the choice of resistive coils has been made. The most important of these are related to the coil's demountability.

Both copper and aluminum are viable conductor materials for resistive coils. Copper offers low electrical resistivity and a relatively high yield stress while aluminum is lighter, less costly and becomes significantly less activated under neutron irradiation. Both materials could be applied to a demountable coil. However, aluminum would not be as flexible in applications where the conductor was required to carry loads directly due to its significantly reduced yield stress. This could be less of an issue in high beta applications.

Resistive coils can be constructed in wound or flat plate (Bitter-type) form. Flat plate constructions are simpler and are more useful in high stress applications. High stress capability is not an issue in the concepts considered here but simplicity is highly valued. Most importantly, joint design is significantly more complex in wound designs which consist of many filaments. Additionally, flat plate coils with continuous plates in the throat (inboard side) of the TF coil have a significantly higher fraction of copper than a wound design which lumps coils into discrete units. A higher copper fraction reduces the current density and thus the resistive power in continuous coil sets.

The continuous plate philosophy can be carried to the outboard side of the coil resulting in a close-fitting, nearly toroidally continuous configuration. This configuration maximizes the use of the available volume for copper, allows for the possibility for using the magnet as part of the radiation shield, and could lead to lower port ripple (due to flexibility in the choice of the current path around a port). The alternative configuration is to wedge the coil units only in the throat and lump them into discrete units outboard. This provides more access between coils for pumping, auxiliary heating and diagnostics.

The shape of a TF coil is typically circular or elliptical. Such shapes fit closer to the plasma and are thus more compact than frame-type configurations. In addition, stresses concentrate in the corners of a framed coil causing relatively large local bending. However, it would be difficult to remove components from the TF bore with vertical lifts using rounded coils. Radial replacements requiring segmentation would be necessary. Vertical lifts would be possible with a rounded coil if the joints were located at the midplane of the device but this location is not very accessible. Stress concentration difficulties are not critical with the low field designs presently pursued and can be eliminated in coils which are supported externally.

3.2.2 Joints

The most critical area of a demountable coil is the joint at which the coil is broken for assembly and disassembly. These joints have a number of requirements which include the need to allow current transfer without introducing large local resistance and the need to be supported against magnetic forces. The joint should also be as simple as the demounting scheme allows to promote the availability of the tokamak.

Many varieties of joints for resistive magnets have been proposed. To facilitate the discussion of the various options, we will first classify the joints as sliding or stationary. Then the joints can be further classified according to their shape and how they are supported.

Sliding joints are those which are designed to allow displacements during operation between the two ends of the joint. These joints are generally located at the inboard leg of the TF coil and allow displacements to relieve large stresses in the throat of the magnet caused by the magnetic bursting force on the coil. These forces are then supported instead by external frames. Such joints are useful in compact, high field applications but have not been considered for RCTR.

Stationary joints come in a variety of shapes. The most common types are butt, flanged-butt, lap, scarf, and finger joints. These joint types are depicted in figure 3.1 a - e, respectively.

The butt joint is the simplest of all joint geometries but is one of the toughest to support against magnetic forces and provides a relatively small area for current transfer. These problems are mitigated significantly by the flanged-butt joint. The overlapping area provided in this butt-type joint provides more surface area for contact and for the use of pins or bolts for support.

The lap joint also possesses a relatively simple geometry. In addition, this joint can provide a large area for both current transfer and the location of support components such as pins and bolts. The scarf joint is similar except the leading edge of the joint is tapered instead of rectangular. A finger joint is one of the more complex joint shapes but can provide relatively large surface area in a limited volume.

Joint options can be further classified according to the method of support used to keep the joint in place during operation. Some of the joints and methods of support considered for use with RCTR will be presented in the next section.

The most commonly considered method of support is the use of pins, keys or bolts connecting overlapping areas of flanged butt, lap-type or finger joints. Such joints are already in use on experiments [8,9] but requirements for a large number of inserts may not be consistent with the requirement of commercial devices to be disassembled remotely in a relatively fast and simple manner.

Joints may also be clamped together using external structures, magnetic clamping or hydraulic clamping. Magnetic clamping can be used on inboard lap-type joints, taking advantage of the face compression on the TF plates which results from the inward wedging of the TF coil. The use of hydraulic jacks has also been proposed as a method of providing the necessary clamping. This method is attractive because of the relative ease of assembly and disassembly.

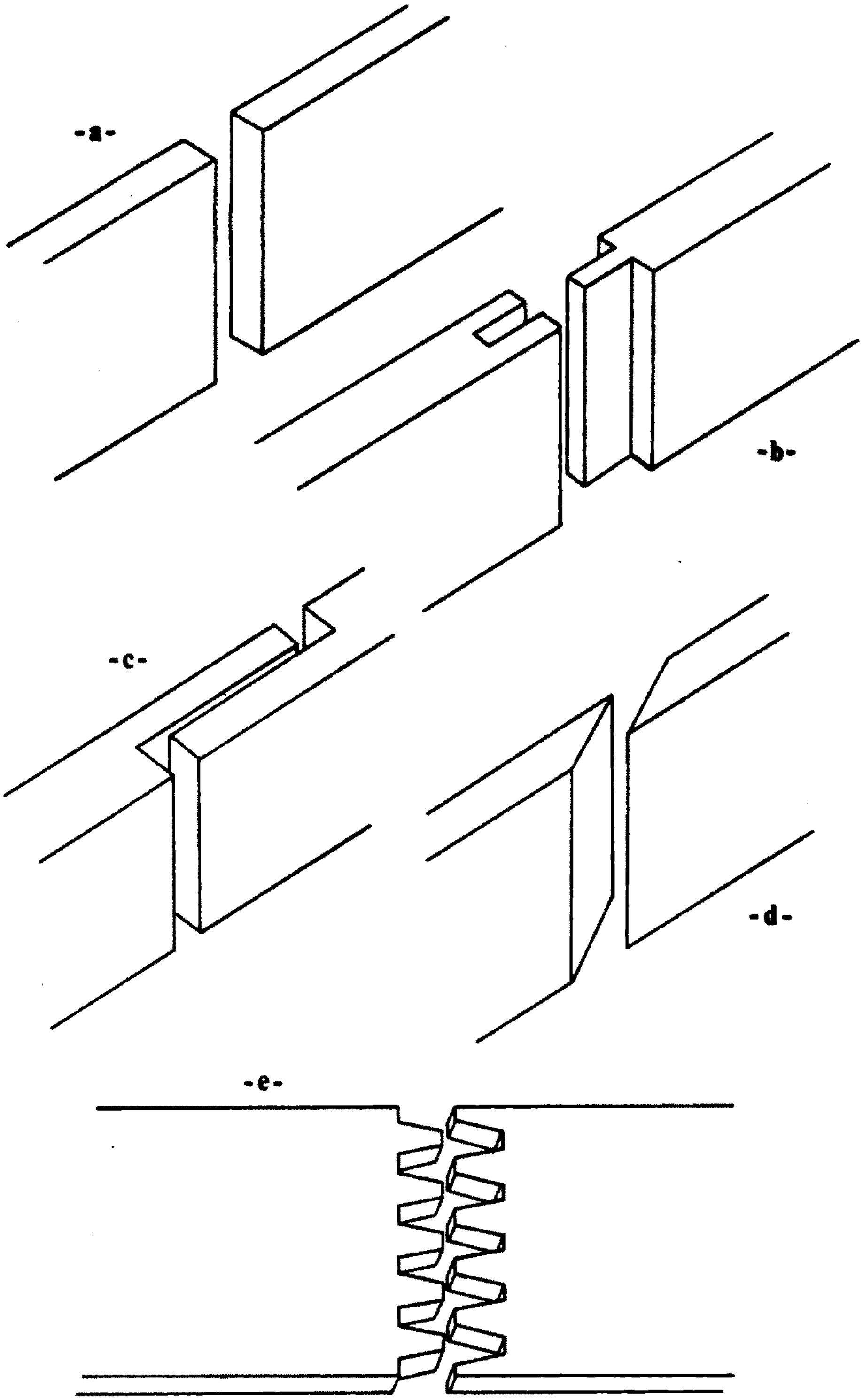

Figure 3.1: Major TF Coil Joint Types

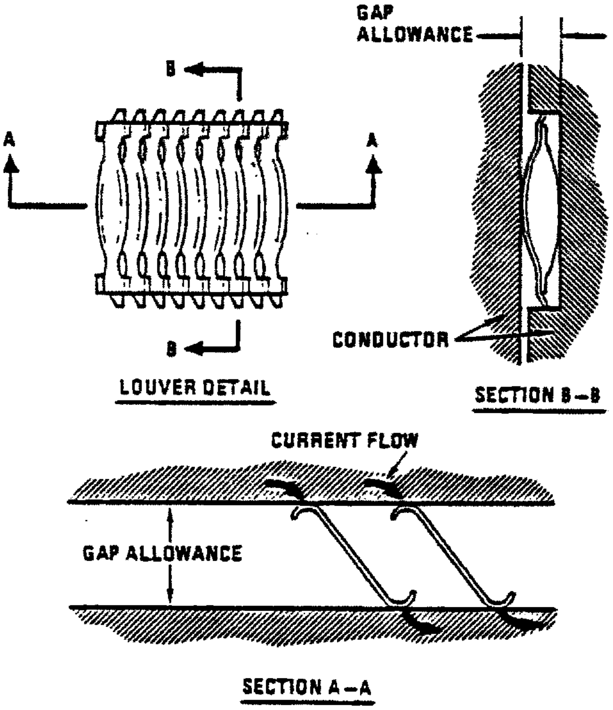

Figure 3.2: MULTILAM Louver Geometry

A major liability of the presence of joints in the TF coil is the resulting break in the current path. The use of springs and MULTILAMS [27] have been proposed as methods of enhancing the current transfer through the joint. Springs require relatively low contact pressure, clearly define the contact area and provide excellent current transfer. However, they are generally more costly and require more machining than MULTILAMS. MULTILAMS (see figure 3.2 taken from reference [27]) are essentially a mesh of louvers much like a venetian blind which provide contact pressure across the gap of the joint. The use of silver coatings with both of these options is recommended to enhance current transfer [4].

3.2.3 TF Coil Support

The choice of TF coil configuration, joint type and support must be reconciled with the need to support the entire TF coil against in-plane and out-of-plane magnetic forces. In the following, various issues relevant to the selection of the demounting concept, taking into account these support requirements as well as the need for simplicity, will be discussed in the context of some of the demounting concepts considered for RCTR.

Most of the development of demountable concepts for RCTR centered on plate-type TF coils using lap joints. Plate-type coils are simple, relatively easy to construct and offer a high fraction of copper in the volume occupied by the coil. In fact, the TF coil can be essentially continuous in the throat and, possibly, in the outboard section of the magnet which helps to lower its power requirements. Plate-type coils are also easily formed into rectangular ('picture frame') coils, making possible the vertical removal of all components within the TF bore. Radial removal of components would be possible with a rounded coil but this would force all components, including the vacuum wall, to be segmented for assembly and disassembly.

The joints in a flat-plate framed coil should occur in the corners of the coil to allow vertical removal of all components with easy access to the joint areas. This consideration led to the selection of lap joints, taking into account their relatively simple shape and the large area provided for both current transfer and support of the magnetic forces trying to open up the coil (see section 3.5). The use of either springs or MULTILAMS with silver coating on the joint surfaces would be adequate for current transfer in the low current density joint designs for RCTR.

A number of concepts have been considered to provide the necessary support against in-plane magnetic loads. These loads essentially attempt to push the sections of the TF coil radially away from the plasma axis.

The first concept uses keys to lock together the horizontal and vertical legs of the TF. Such a keying arrangement is shown in figure 3.3. The keying arrangement could be combined with girth bands to take the outward radial force. The inward radial force is taken by wedging of the coils at the inboard leg. However, the keys will occupy cross-section in the area needed for current transfer through the joint and for cooling, and will significantly increase the complexity of assembly and disassembly.

Perhaps a more desirable approach is to use rings to lock the horizontal and vertical legs together as illustrated in the trimetric view of figure 3.4. Note that the in-plane load is transferred to a region outside the joint area and the

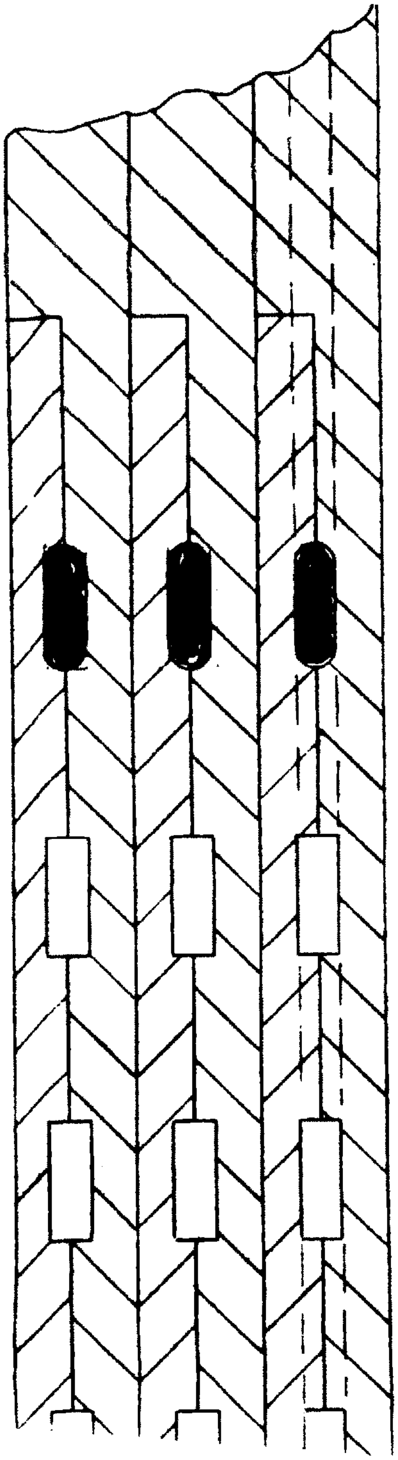

Figure 3.3: Keyed Joint Concept

area available for the locking rings is quite flexible. This would seem to be a relatively simple system to disassemble. However, using the same technique to lock together the outer lap joints could interfere with an outer structure (such as a torque cylinder) required to support the out-of-plane loads on the TF coils.

A third concept, illustrated in figure 3.5, uses caps on the top and bottom of the tokamak which are tied together through the central hole to take the vertical loads. This approach may also be relatively simple to demount. However, the caps and tie rods represent a significant additional investment in materials and machining.

Support of the out-of-plane magnetic loads caused by the interaction of the vertical field and toroidal current depends on whether the coils are discrete or continuous in the outside. If discrete, steel wedges can be inserted between the outer legs of the TF coils as shown in figure 3.6. The wedges are then tied to torque cylinders to resist warping or over-turning of the coil caused by the out-of-plane loads.

Other views of this scheme in use with the locking ring and cap approaches to taking the in-plane forces are shown in figure 3.4 and figure 3.5, respectively. Figure 3.5 shows how the support of the outer joints can be combined with the support of the overturning moment. A steel cylinder flush with the inside edge of the outer TF leg is attached to the wedges between the TF coils which react the over-turning. This is combined with an outer cylinder and a steel band fastened to the wedges on the top and bottom of the device. The result is a capped, double-walled cylinder which reacts the vertical load.

3.2.4 Integration With Other Systems

The demountable design is also driven in a major way by other systems and requirements for the commercial tokamak. These include the blanket and first wall components, and access requirements for cooling, plasma heating and minor repairs.

The blanket and first wall designs were driven by the desirability for components which can be removed readily while avoiding the necessity for breaking of the vacuum boundary within the nuclear island. Requirements for the breaking of vacuum within the nuclear island during assembly and disassembly signifi-

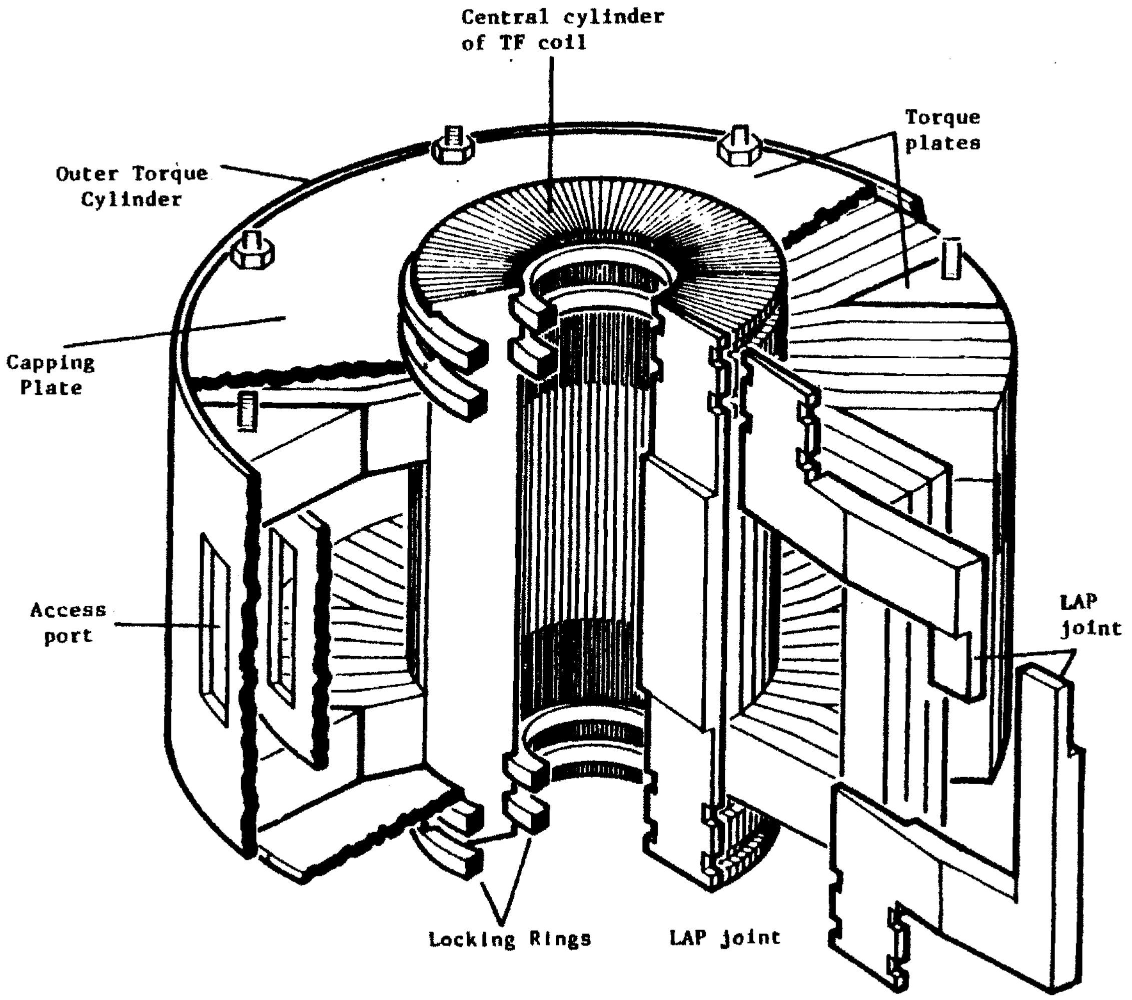

Figure 3.4: Locking Ring Joint Concept

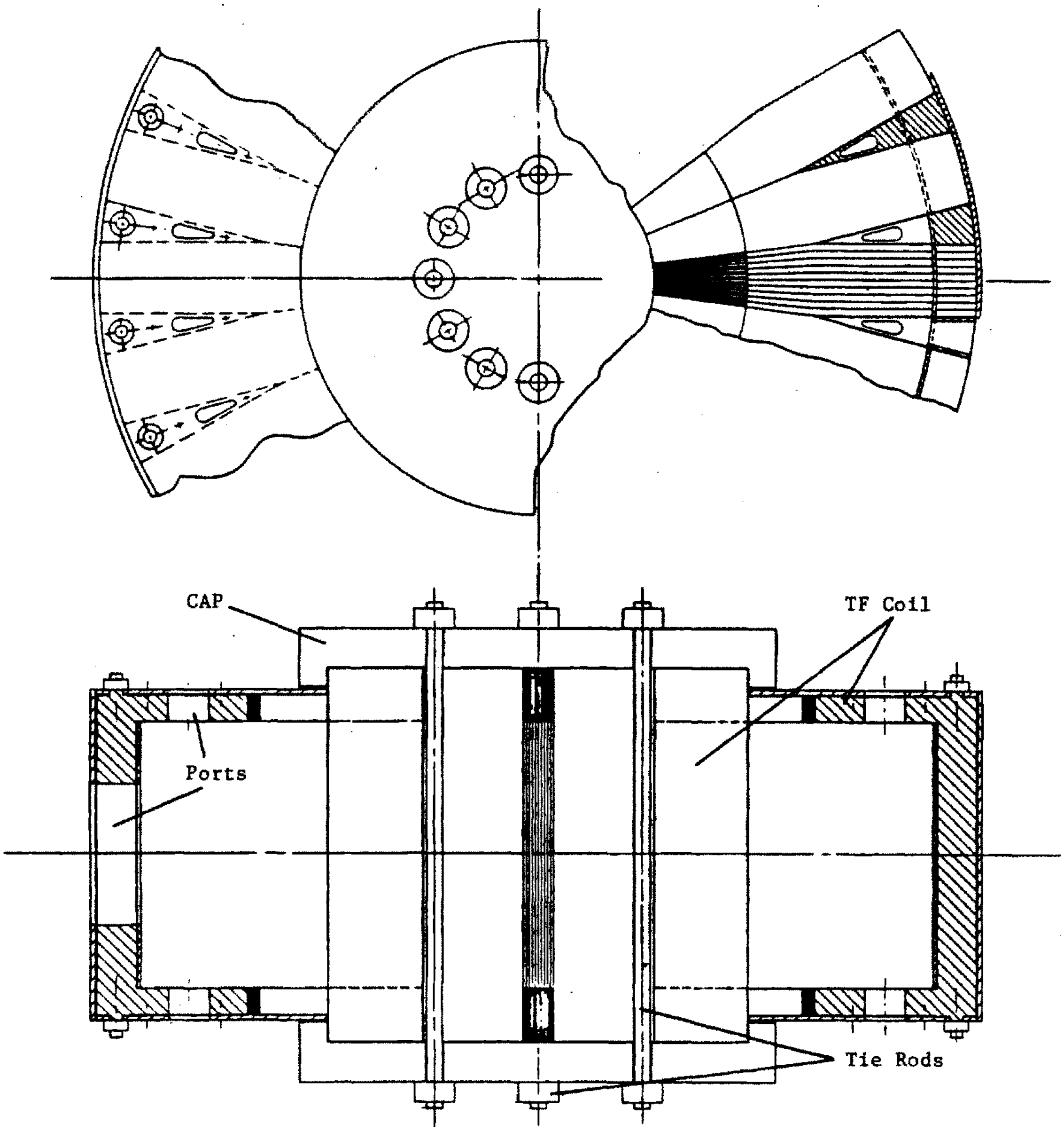

Figure 3.5: Cap Supported Joint Concept

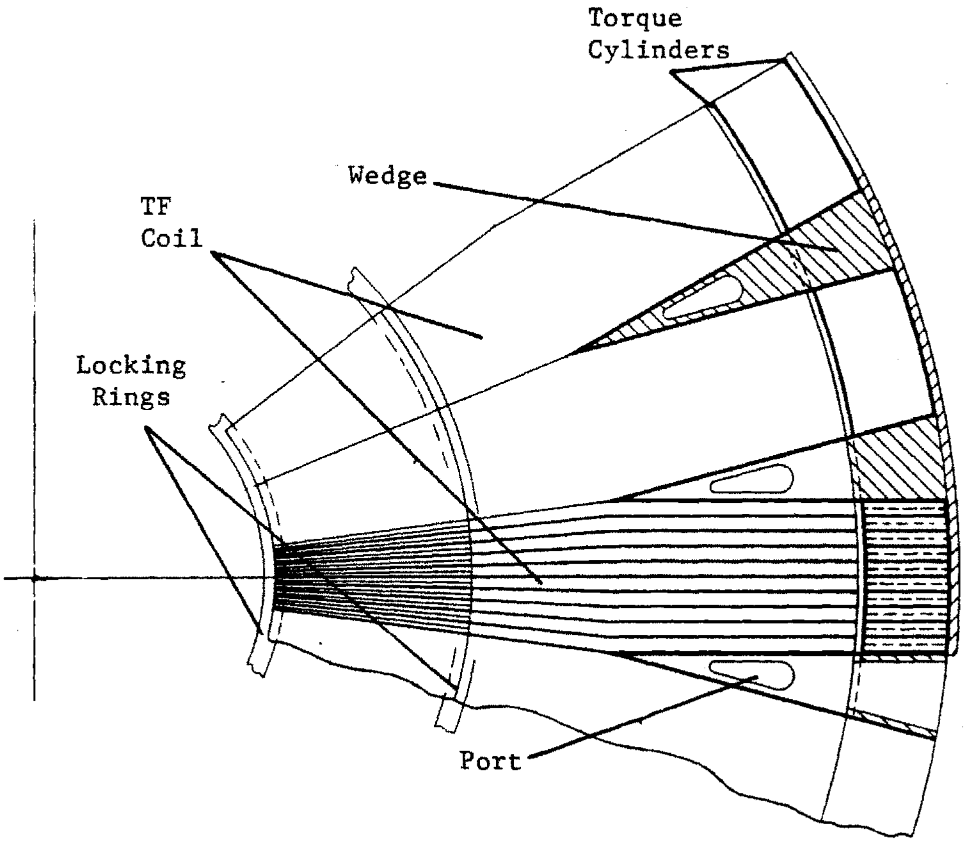

Figure 3.6: Out-of-Plane Support Using Wedges

cantly complicates maintenance with the need for remote cutting and welding, and remote vacuum testing. These operations are likely to be both difficult and time-consuming.

The use of a vacuum boundary (typically the first wall) in a single piece could eliminate the need for welds requiring maintenance and allow pre-testing for vacuum leaks. Such a scheme is unlikely in superconducting tokamaks presently envisioned because demounting of the toroidal field coils would be extremely difficult. Breaking of the vacuum boundary cannot be avoided with poloidally continuous TF coils unless the boundary lies outside that of the coils.

The desire for a single unit vacuum wall prevents the vacuum boundary from being further from the plasma than the furthest toroidally continuous reactor component. Since we wish to have the ability to maintain TF and EF coils, this places the boundary no further from the plasma than the outer (with respect to the plasma) blanket boundary. If the blanket is to be segmented, the vacuum boundary must occur at the first wall and the first wall takes the form of a large vacuum-tight doughnut shell. In addition, the toroidally continuous vacuum wall must be removed and inserted vertically.

The demountable concept may also affect the details of the blanket design. Integrated blanket/first wall systems have been proposed which incorporate the first wall as the first structural wall of the blanket. This may lead to a simpler blanket/first wall system, especially in self-cooled liquid lithium designs. However, if the breaking of the vacuum boundary is to be avoided, the entire blanket/first wall structure must be removed as a single piece. The sheer weight of such systems could be prohibitive.

3.3 Reference Demountable Concept

The considerations outlined in section 3.2 eventually led to the selection and characterization of a reference demountable coil concept for RCTR. The reference concept is based on the parameters of case A from the parametric studies of chapter 2, repeated in table 3.1 for convenience. These parameters were chosen as typical of resistive magnet commercial tokamaks to illustrate the use of the demountable concept.

Net Electric Power, MW_e	1200
Wall Loading, MW/m^2	3
Toroidal Beta, %	24
Major Radius, m	7.5
Aspect Ratio	5
Field on Axis, T	2.4
Plasma Current, MA	4.7
Nuclear Island Weight, ktonnes	14.2
Thermal Power, MW	3380
TF Dissipated Power, MW_e	108
Total Recirculating Power, MW_e	228
Direct Cost, $M	2065
Capital Cost, $M	3680
Cost of Electricity, mills/kW·hr	45.4
Recirc. Power Fraction	0.16
Mass Utilization, T/MW_{th}	4.2
Eng. Power Density, MW_{th}/m^3	1.2

Table 3.1: Base Parameters for Demountable Design

The TF coil is a frame coil constructed from flat plate copper conductor. Aluminum or hybrid copper/aluminum plates would also be viable. The joints, located in each of the four corners, are of lap-type and are externally supported against in-plane and out-of-plane loads. The coils are grouped into twelve bunches which are separated by steel wedges. The bunches consist of twelve TF coils, each carrying 477 kA to provide the field of 2.43 T on the plasma axis.

The copper coil and steel wedge assemblies are enclosed by inner and outer support cylinders. The wedges appear as the spokes of a wheel, keyed into the inner and outer cylinders to support the coils against out-of-plane forces. The cylinders and steel wedges extend above (and below) the height of the TF coils. Steel caps are placed on top of the coils within the pocket formed by this extension and are pinned to the cylinders to support the TF coils against in-plane loads. This assembly is illustrated in the engineering drawings of figure 3.7 (top view) and figure 3.8 (cutaway view).

Vertical access ports are cut into each of the twelve wedge components. Six of these ports provide coolant access to the first wall and blanket assemblies. The remaining six provide direct access to the plasma chamber for vacuum pumping, auxiliary heating and minor repairs. All twelve wedges contain access ports for

TF cooling manifolds. These manifolds are located internal to the TF bore in the four corners of the coil.

Note that no radial access has been identified in this concept. A provision for radial access would require a break in the outer support cylinder to allow vertical removal of the vacuum chamber. Such a break would increase the complexity of the concept due to requirements for support structure at the break and would decrease the structural integrity of the outer cylinder. In addition, the access requirements in a commercial device are relatively modest and may be adequately met in this concept with only vertical access ports.

Some relevant parameters for the demountable concept are shown in table 3.2. The TF coil has very thick inboard legs (2.1 m) and relatively thin outboard and horizontal legs (0.75 m and 0.80 m, respectively) due to the large contribution of dissipated power and relatively small weight contribution inboard. The TF delivers 2.4 T on the plasma axis with a total toroidal current of 91.6 MA which results in a peak field at the coil of 3.5 T. Despite the relatively low magnetic field, the size of this device results in a vertical force (bursting force from the interaction of the TF current and the toroidal field) of 665 MN. However, the large cross-sectional area available to support this force results in an average membrane stress at the midplane (assuming a continuous, unsegmented coil) of just 6.8 MPA (970 psi).

The coil is segmented, however, and the vertical force is transferred through the horizontal TF legs, steel caps and bolts (or plugs) to the support cylinders. The plugs are 25 cm in diameter and number 144 each for the top and bottom supports. Each plug carries an average shear stress of 83 MPA. The cylinder thicknesses required to support both in-plane and out-of-plane forces are 25 cm and 10 cm for the inboard and outboard cylinders, respectively. More detailed information on the stresses is given in section 3.5.

The weights of the TF components are within the capability of present crane technology. For example, the horizontal leg for one of the twelve TF coil bunches weighs approximately 120 tonnes. This is the heaviest TF coil sector but some components within the bore may be heavier depending on the blanket/first wall design.

Current transfer in the joints is facilitated by the low coil current densities and large area available with the lap-type geometry of the joints. Average steady

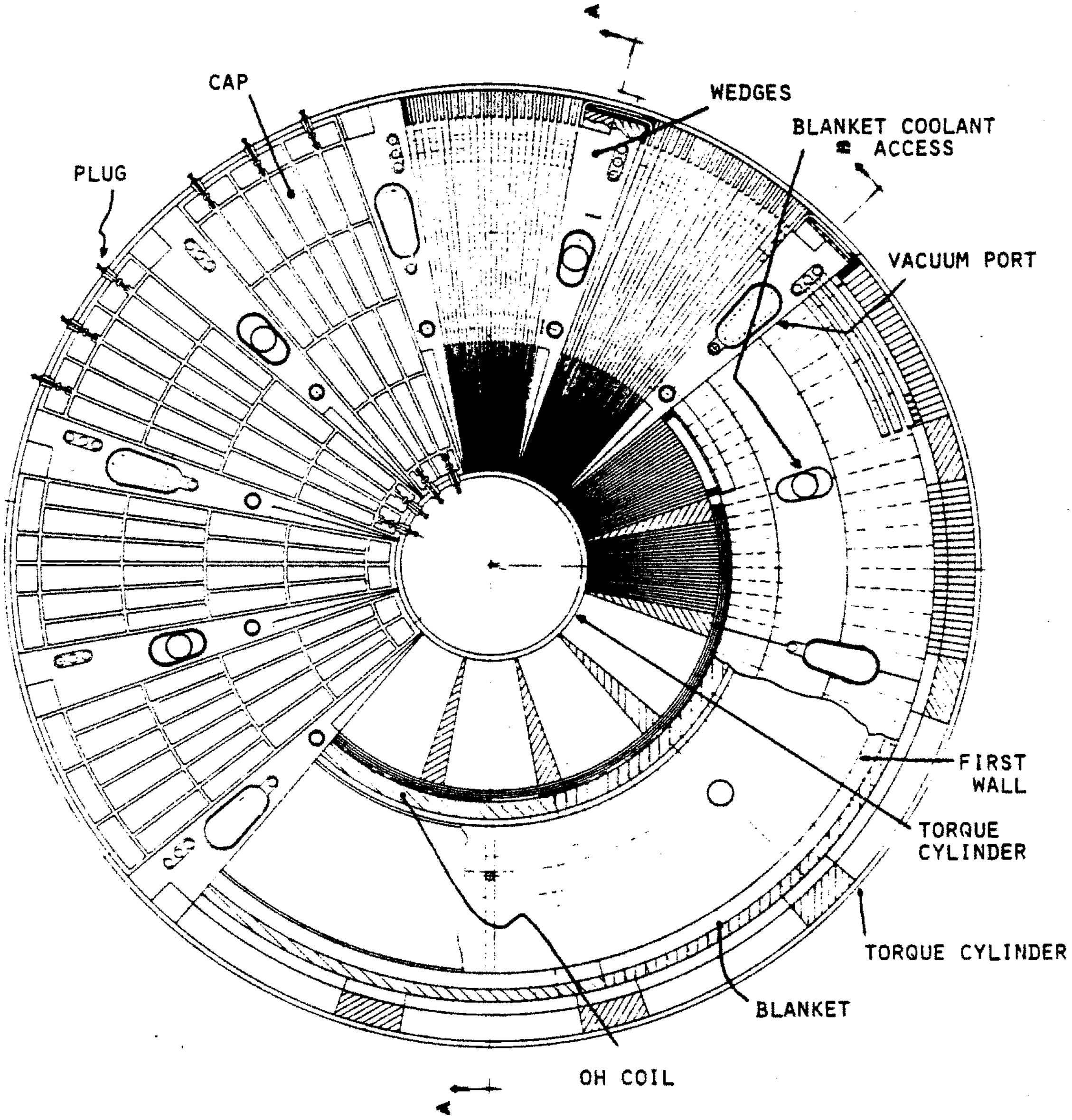

Figure 3.7: Top View of RCTR Nuclear Island

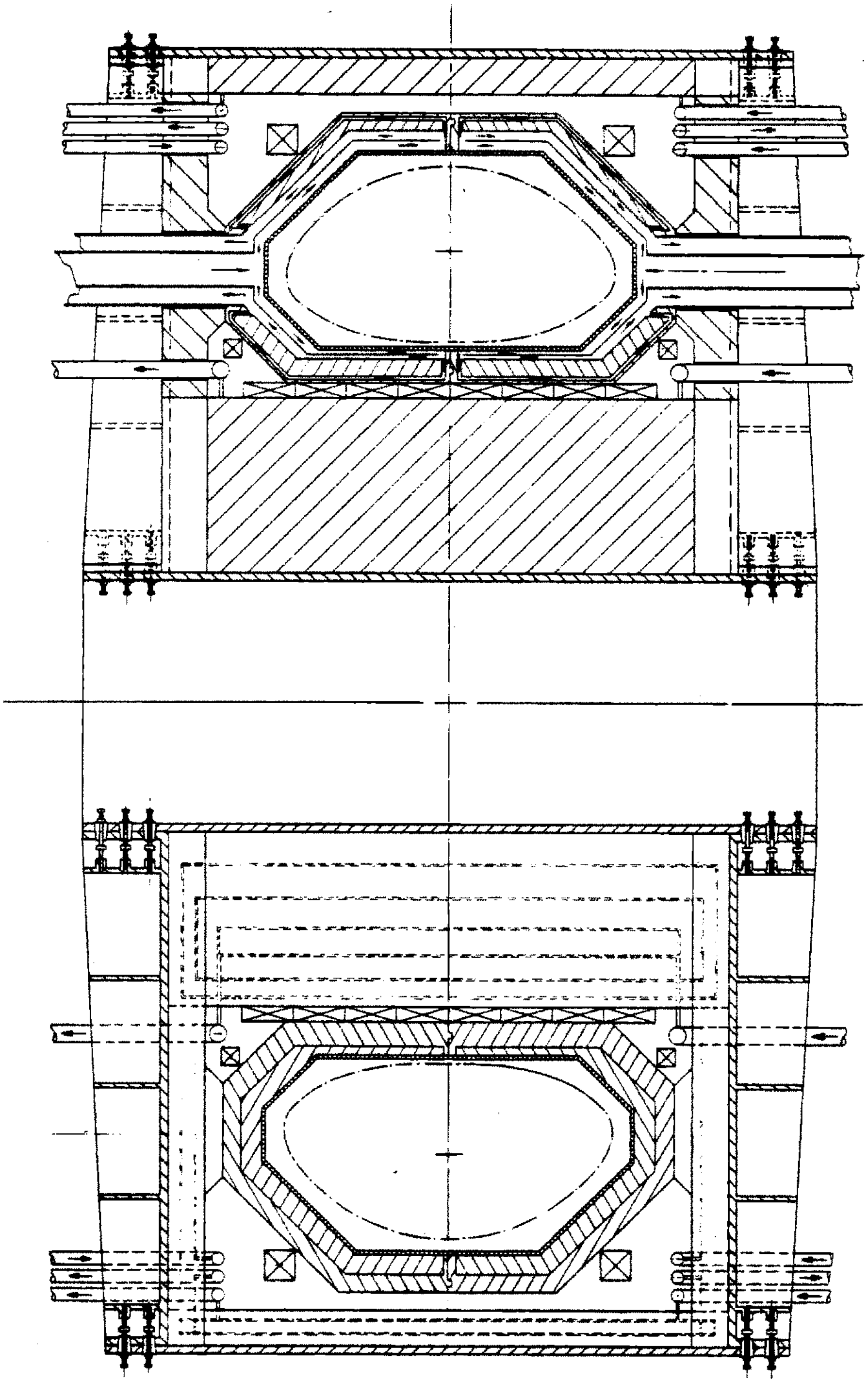

Figure 3.8: Cutaway View of RCTR Nuclear Island

Net Electric Power, MW$_e$	1200
Wall Loading, MW/m^2	3
Toroidal Beta, %	24
Major Radius, m	7.52
Coil Type	Frame
Conductor Material	Copper
Coil Cooling	Helium
Current Per Turn, kA	477
Field On Axis, T	2.43
Peak Field, T	3.51
Inboard Build, m	2.1
Outboard Build, m	0.75
Horizontal Build, m	0.80
Weight, ktonnes	8.6
Number, TF Coils	12
Number of Turns	192
Turns Per Coil	16
Turn Thickness, inboard, cm	9.2 - 13.6

Table 3.2: Demountable Coil Characteristics

state current densities in the inboard and outboard sectors of the TF are only 240 A/cm^2 and 224 A/cm^2, respectively. The area available in the inboard joints is almost 2 m^2 resulting in an average joint current density of 45 A/cm^2. The outer joints have significantly less area available (0.6 m^2) but the current density of 115 A/cm^2 is still within the capability of MULTILAM technology [27].

The toroidal field coils are actively cooled to compensate for both joule and neutron heating. Gaseous helium has been chosen as the reference cooling medium for RCTR. Water cooling is more typical of room temperature resistive magnet designs but water has severe compatibility problems with liquid lithium [28], the coolant/breeder selection for the blanket concept (chapter 4). Helium is also more than adequate for the heat removal task for typical RCTR toroidal field coil current densities. The TF cooling characteristics were determined in this study using a one-dimensional, single phase, compressible flow model computer code developed by Gierszewski [29] for internally cooled resistive magnets. Typical parameters for the illustrative case of table 3.1 are shown in table 3.3.

Net Electric Power, MW_e	1200
Wall Loading, MW/m^2	3
Toroidal Beta, %	24
Cooling medium	Helium
Current Density, Inboard, A/cm^2	240
Joule Heating, MW/m^3	0.06
Neutron Heating, MW/m^3	0.08
Coolant Pressure, MPa	1.5
Mass Flow Rate, kg/s	0.3
Helium Temperature Rise	35
Peak TF Temperature, K	367
Helium Channels per Plate	6
Channel Diameter, cm	1.5 - 3.0
Channel Length, m	8
Exit Velocity, m/s	41.8
Flow Area/Conductor Area, %	5

Table 3.3: Toroidal Field Coil Helium Cooling

3.4 Assembly and Maintenance

A major emphasis has been placed on assembly and maintenance in the development of a nuclear island concept for RCTR. The design of all major components has been driven by the importance of maintenance in commercial tokamak design and the decision to use demountable toroidal field coils. The placement of the equilibrium field coils inside the TF bore (see section 3.6), the blanket/first wall design (chapter 4) and the toroidal field coil design are all subject to maintenance considerations.

Assembly of the RCTR nuclear island is illustrated in figure 3.9 through figure 3.14. In step 1 shown in figure 3.9, the lower steel wedges separated by the lower steel end caps are assembled around the inner support cylinder. The wedges are keyed into the inner cylinder and the end caps are attached to the inner cylinder via steel plugs. The placement of the lower horizontal TF bundles on top of the lower end cap and between the steel wedges is illustrated in step 2. Twelve bunches of 16 one quarter turns of toroidal field coil are assembled in this manner.

The next step involves placement of the inner wedge and TF turns around the inner support cylinder. An inner wedge is dropped into place by matching the two ends of the lap joint from it and the already assembled lower wedge piece and rests up against the inner support cylinder. Insertion of a wedge is followed by the insertion of an inner TF coil bunch in a similar manner. Next, the OH coil (illustrated in step 4 as a solid cylinder) is dropped in around the inner TF/wedge assembly. This is followed by the placement of the lower EF coils. The EF coils are supported from the steel wedges.

In step 5 of figure 3.11, assembly of the lower blanket sectors is illustrated. The blanket is divided along the midplane to allow assembly and removal of the first wall in a single unit. Lower and upper blanket sections are divided into twelve 30 degree sectors. Half of the sectors include cooling ducts for the liquid lithium blanket coolant which are channeled through an equal number of steel wedges. The remaining blanket sectors contain penetrations for the coolant channels of the first wall. Each blanket sector rests on top of protruding areas of the lower steel wedges (visible at previous steps).

The first wall is lowered in next as a single unit. This procedure allows the assembly to be pre-tested for vacuum and coolant integrity before insertion into the nuclear island and avoids the necessity for sealing and breaking of vacuum welds during assembly and maintenance. A similar philosophy could have been applied to the entire blanket/first wall assembly but the weights involved for assembly and maintenance may have been prohibitive (see chapter four). The first wall assembly rests inside the lower blanket assembly. Coolant ducts attached to the first wall fit through penetrations in alternating blanket and steel wedge sectors.

In steps 7 and 8 shown in figure 3.12, the upper blanket and EF coil assemblies are inserted in a complimentary manner to their lower counterparts. Then, in steps 9 and 10 of figure 3.13, the outer section of the nuclear island is assembled. Outer wedge and TF coil sectors are inserted by matching the appropriate lap joints. Then, the outer support cylinder can be dropped in around the entire assembly. The outer support cylinder may not be handled as a single piece due to sheer size and proper fitting constraints. However, the joints required to assemble this component in two or more pieces need not be readily maintainable. At this point, the outer support cylinder can be secured to the lower end caps with steel plugs.

In the final steps, illustrated as steps 11 and 12 in figure 3.14, the upper

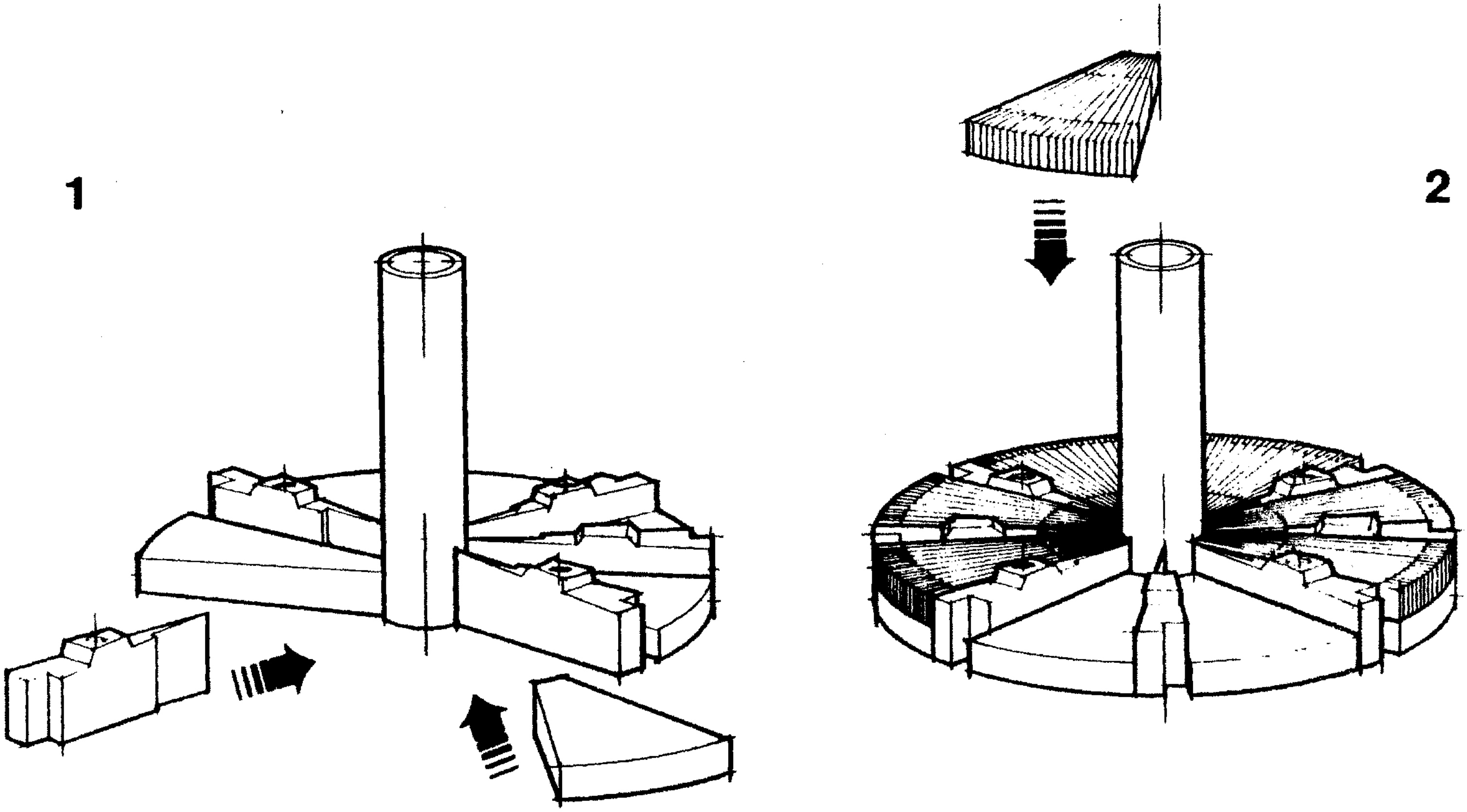

Figure 3.9: Steps 1 and 2 of RCTR Assembly Procedure

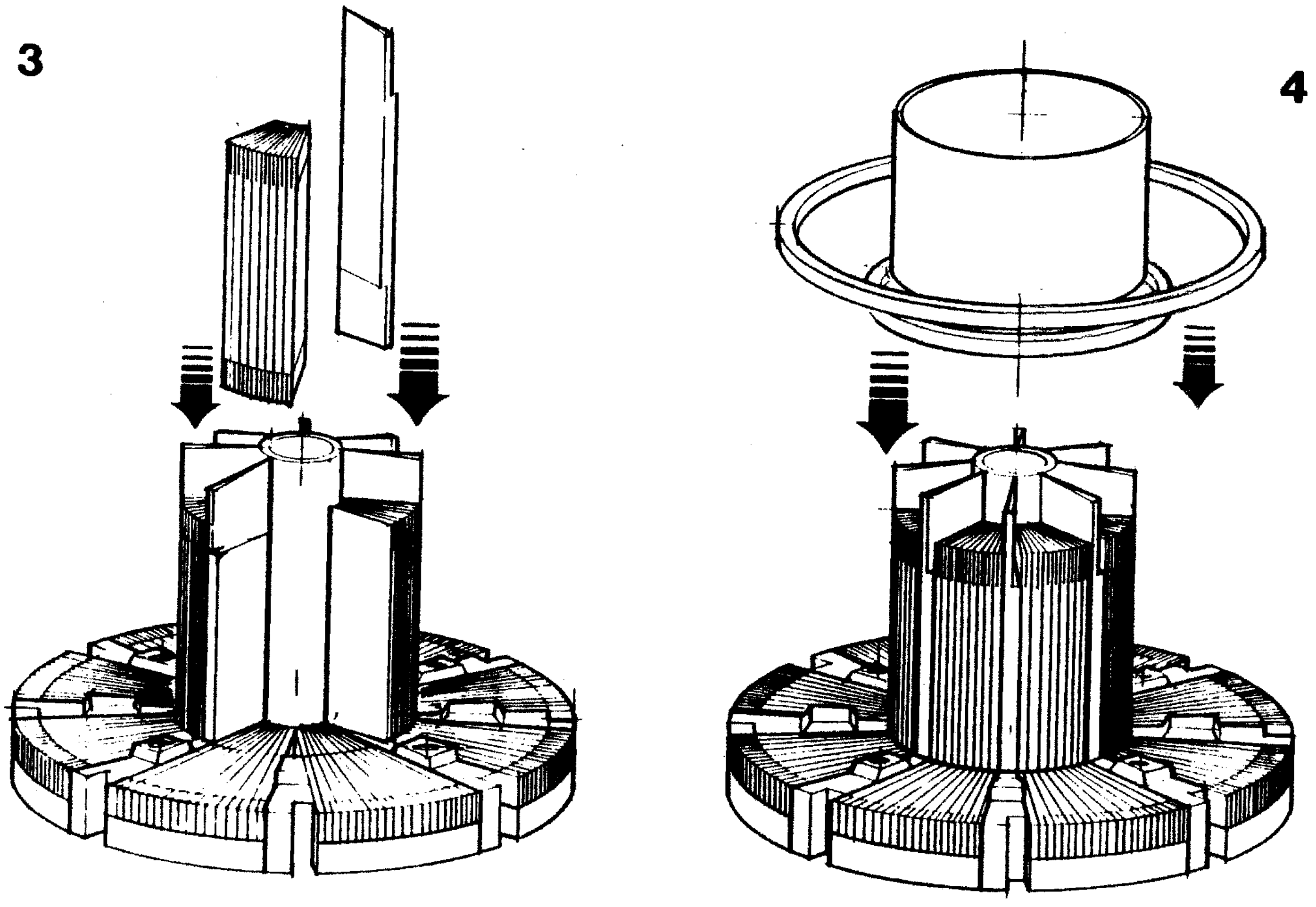

Figure 3.10: Steps 3 and 4 of RCTR Assembly Procedure

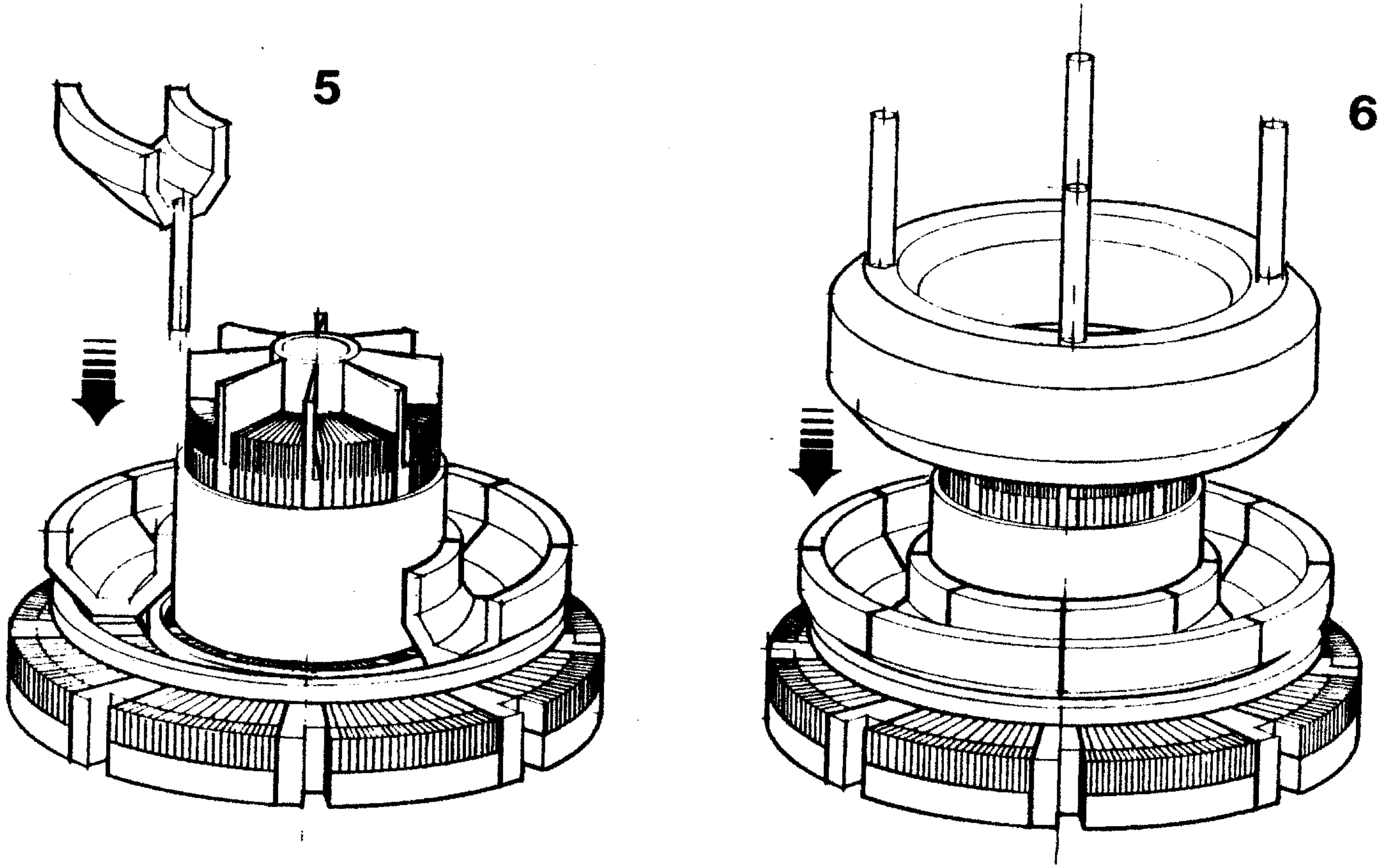

Figure 3.11: Steps 5 and 6 of RCTR Assembly Procedure

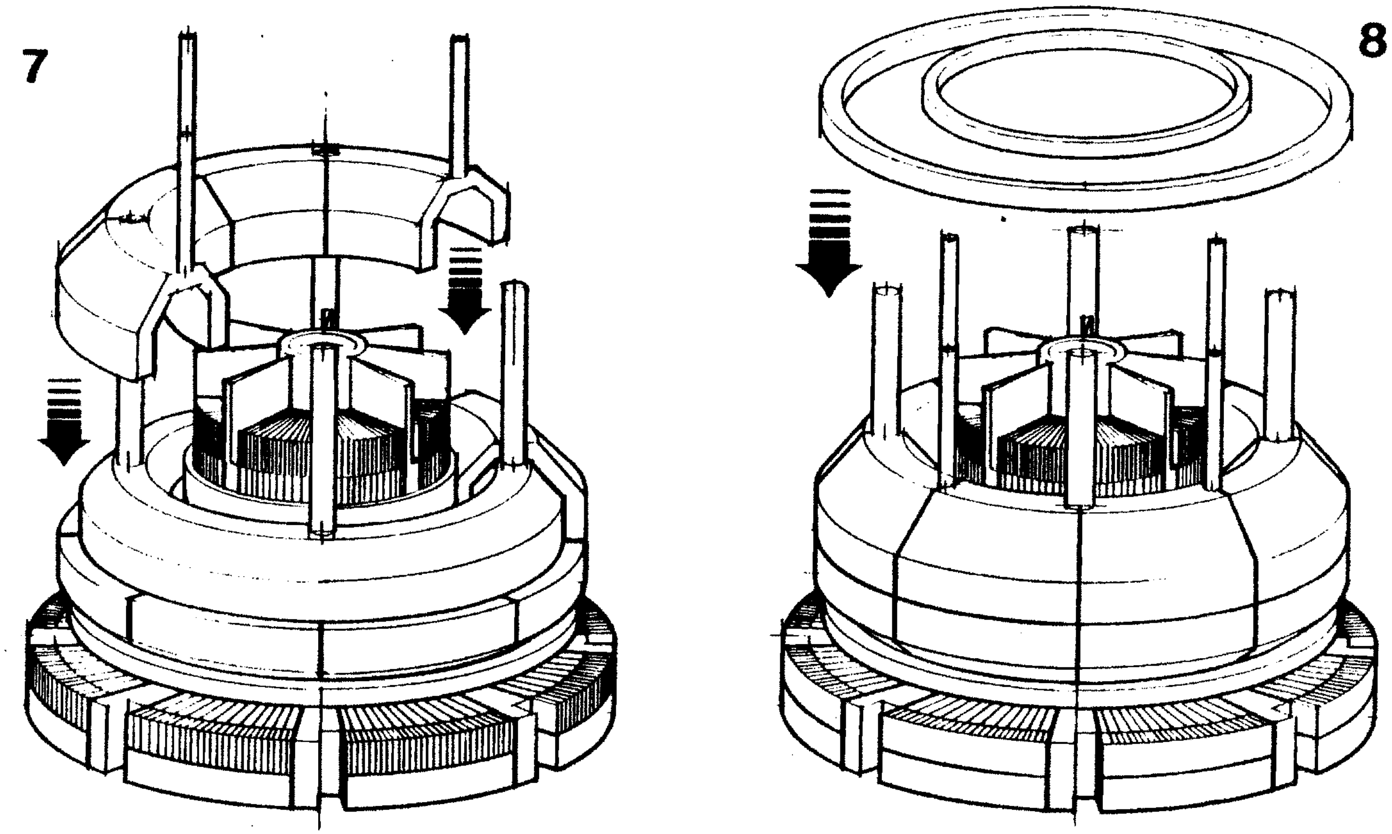

Figure 3.12: Steps 7 and 8 of RCTR Assembly Procedure

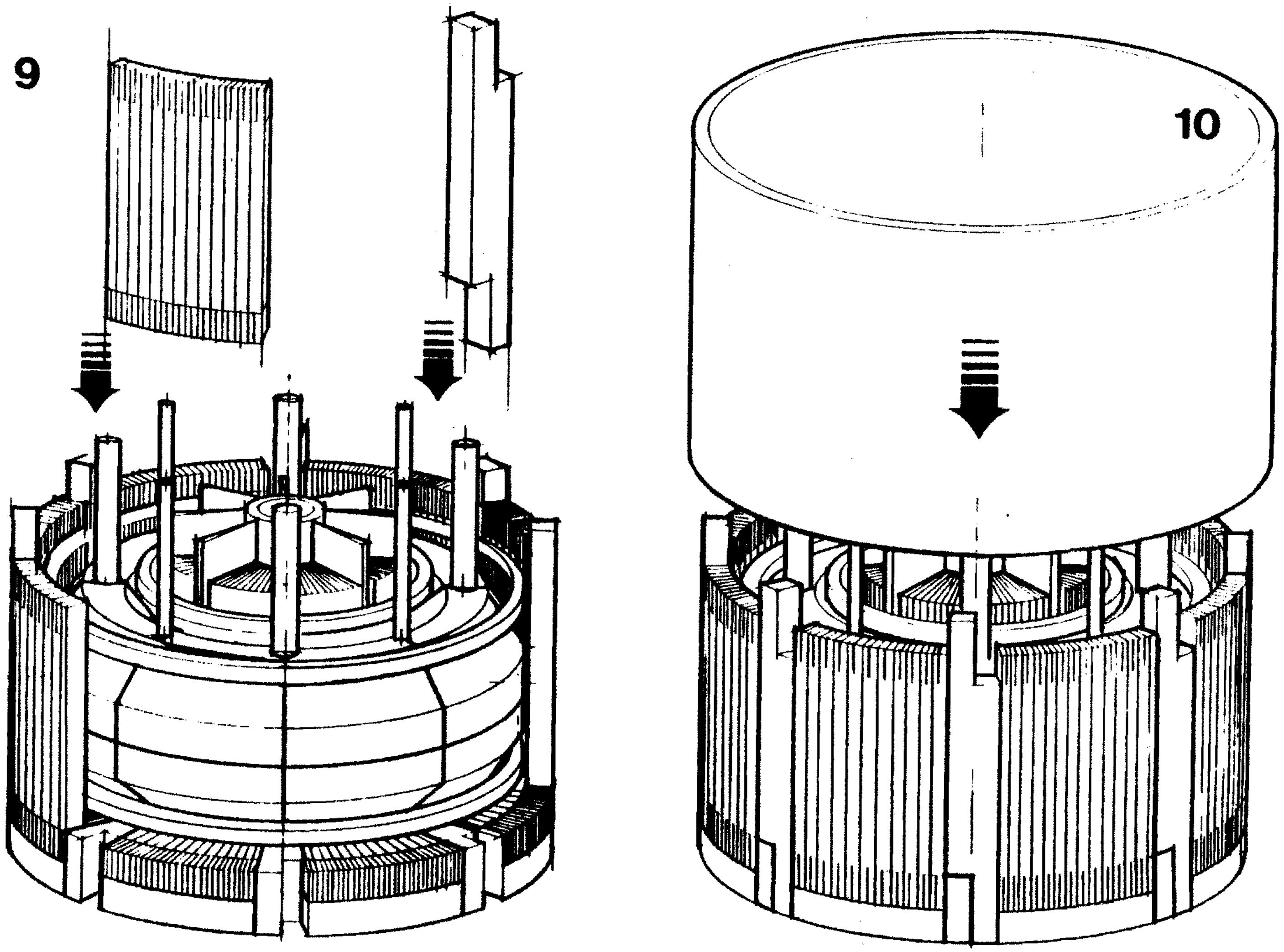

Figure 3.13: Steps 9 and 10 of RCTR Assembly Procedure

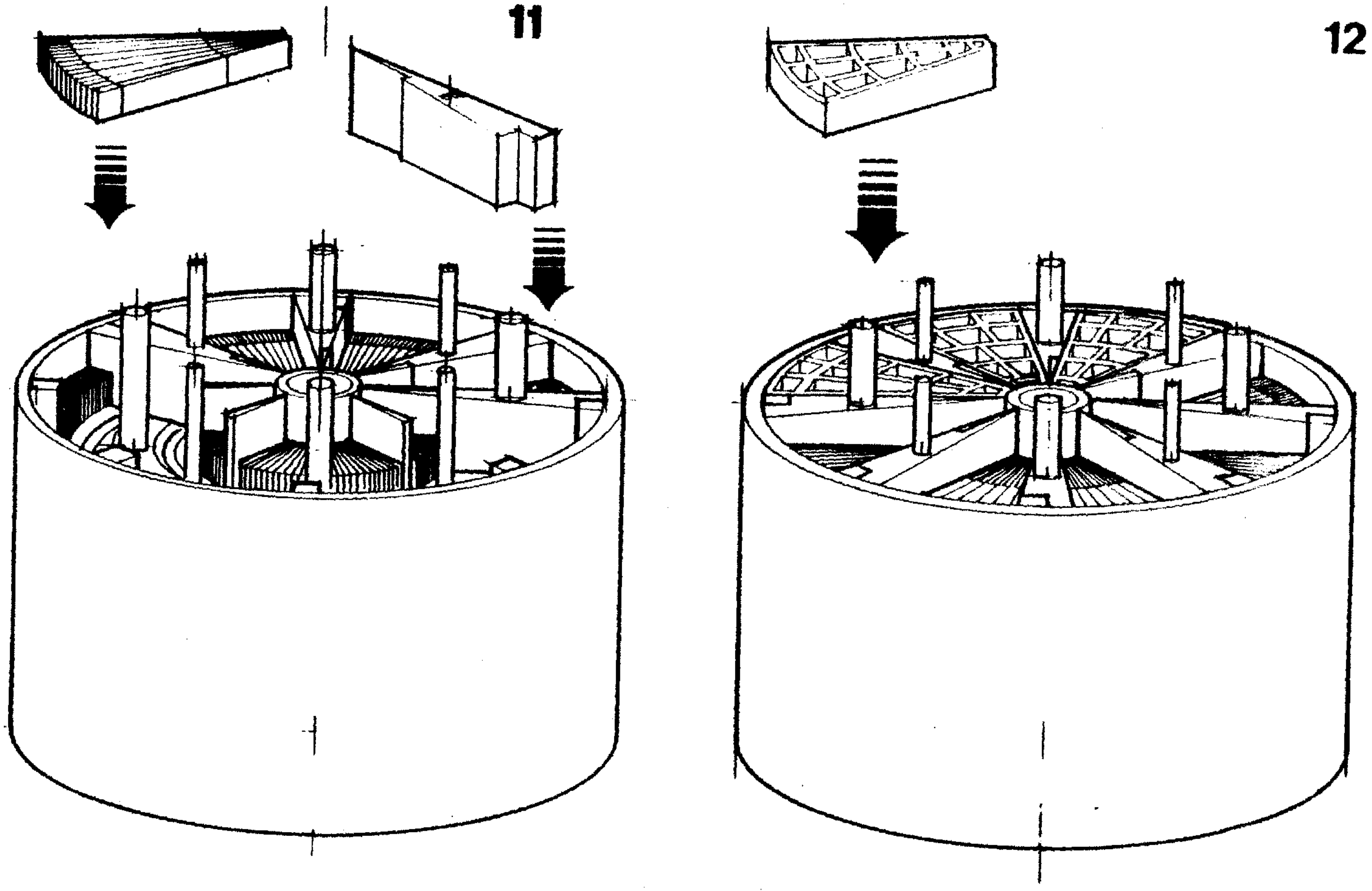

Figure 3.14: Steps 11 and 12 of RCTR Assembly Procedure

sectors of the TF coil and wedges are inserted. Wedges fit over upper cooling channels for both blanket and first wall cooling and are joined at lap joints between the inner and outer vertical wedge pieces already in place. The upper TF bundles fit similarly between vertical sections of the TF coil already assembled. The last step is to drop in the upper end caps between protruding sections of the wedges. These may then be pinned to both the inner and outer support cylinders.

Maintenance of the device is accomplished in reverse order of the above procedure depending on the affected component. It may be possible to accomplish minor repairs through the six ports penetrating to the vacuum chamber. Such repairs could involve the application of spray coatings to the first wall surface or the replacement of tiles at the first wall depending on the impurity control scheme.

Major repairs to non-toroidally continuous structures within the nuclear island and above the device midplane may be made by removing selected sectors of the upper end caps. Such repair or replacement operations could involve upper support components such as wedges and end caps, upper or inner and outer vertical sections of the TF coil, and upper sections of the blanket assembly. Removal of upper blanket sectors in this manner would only be possible if the EF system could be designed such that individual coils would not interfere with the vertical removal of these blanket sectors.

Other major repairs could be accomplished with the removal of the upper end caps. Access to all components within the nuclear island is possible with simple vertical lifts without the need for cutting of components or the breaking of welds.

3.5 TF Coil Stress Analysis

Analytic analysis of the major loads on the TF coil and its associated support structure was performed to characterize the demountable coil concept. Although stresses due to various electromagnetic force reactions are generally not a critical issue in these relatively low field, large size devices, the analysis was useful in characterizing the parametric tradeoffs and sizing various components. Forces and reactions due to both in-plane and out-of-plane interactions are considered.

3.5.1 In-plane Analysis

Loads are generated in the plane of the TF coils due to the interaction of the toroidal current in the TF coil and the resulting toroidal magnetic induction. The force is directed radially outward from the center of the bore of the TF coils. The magnitude of this force can be calculated by integrating the magnetic field pressure over the coils.

Assuming that the magnetic field strength varies inversely with radius within the bore of the coils and linearly with radius outside the bore, the result for the total vertical force generated is:

$$\begin{aligned} F_v &= \frac{B_0^2 R_0^2}{\pi\mu_o}\Big[\ln\Big(\frac{R_b}{R_a}\Big) + \frac{(R_a-R_1)^2}{4R_a^2} + \frac{(R_a-R_1)R_1}{3R_a^2} \\ &\quad + \frac{(R_o-R_b)R_o}{3R_b^2} - \frac{(R_o-R_b)^2}{4R_b^2}\Big] \end{aligned} \tag{3.1}$$

where R_0 is the radius on the axis of the plasma, B_0 is the magnetic field strength at R_0 and the geometrical parameters are as indicated in figure 2.2. The resulting moment on the coils can also be estimated by integrating the product of the magnetic field and the moment arm over the coil. The result is:

$$\begin{aligned} M_v &= \frac{\pi B_0^2 R_0^2}{\mu_o}\Big[(R_b - R_a) + \frac{(R_a-R_1)^3}{5R_a^2} + \frac{(R_a-R_1)R_1^2}{3R_a^2} \\ &\quad + \frac{(R_o-R_b)R_o^2}{3R_b^2} - \frac{(R_o-R_b)^2 R_o}{2R_b^2} \\ &\quad + \frac{(R_a-R_1)^2 R_1}{2R_a^2} + \frac{(R_o-R_b)^3}{5R_b^2}\Big] \end{aligned} \tag{3.2}$$

Similarly, the inward (toward the central axis) radial and outward radial forces, F_i and F_o are:

$$F_i = \pi\frac{B_0^2 R_0^2}{\mu_o R_a}(H - 2\Delta_t) \tag{3.3}$$

$$F_o = \pi\frac{B_0^2 R_0^2}{\mu_o R_b}(H - 2\Delta_t) \tag{3.4}$$

The inwardly directed force F_i is supported by the wedging of the toroidal field coils as they are driven toward the axis of the device. This wedging reaction results in a compressive stress, σ_c, on the face of each of the inboard TF legs.

$$\sigma_c = \frac{B_0^2 R_0^2}{2\mu_o R_a(R_a - R_1)} \tag{3.5}$$

In conventionally designed TF coils (circular or elliptical and without joints) the in-plane forces are reacted in the conductor. These reactions are predominantly tensile stresses with less critical bending components depending on the precise shape of the coil. This loading is typically characterized by the tensile membrane stress, σ_i at the midplane of the inboard leg of the coil where the field is highest and the area available for support is most restricted. σ_i can be written in terms of the total vertical force, F_v and moment M_v as:

$$\sigma_i = \frac{\frac{F_v}{\pi} - \frac{3M_v({R_o}^2 - {R_b}^2)}{2\pi({R_o}^3 - {R_b}^3)}}{({R_a}^2 - {R_1}^2) - \frac{({R_a}^3 - {R_1}^3)({R_o}^2 - {R_b}^2)}{({R_o}^3 - {R_b}^3)}}. \tag{3.6}$$

A similar expression can be written for the midplane tensile stress at the outboard leg of the coil. In addition the tensile stress in the upper and lower TF legs resulting from the outward directed force F_o can be characterized by dividing F_o with a typical conductor cross section available there.

Its important to note that the RCTR toroidal field coils are not conventionally designed in the sense that they are of frame type and incorporate joints which are externally supported. In this type of coil, the reactions to the in-plane bursting force is dominated by bending (bending loads become at least as important as tensile loads). The above force balance analysis is still valid and is useful in parametric surveys to typify the stress state of a given device and in sizing the support cylinders and end plugs. However, the tensile membrane stresses such as σ_i are not important in the RCTR case because the joints are supported externally and the forces are simply transmitted to the external structure without generating tensile loads in the conductor. It is necessary to analyse the coil also as a structural frame to keep track of the shear stresses and deflections expected in an RCTR coil set which *are* reacted in the conductor.

Structural frames appear in many different fields of engineering and a fair amount of literature has been devoted to the subject (see, for example, reference [30]). In fact, Jassby [31] has applied this type of analysis to a frame type toroidal field coil applying a force distribution which varies inversely with radius to the solution by Kleinlogel [32] using rigid frame theory. We have used a simplified version of the expressions in reference [31] taking advantage of the monolith-like nature of the inner legs of the TF. The TF coil system then appears as a series of rectangular frames joined at the inboard leg into a solid core which acts as a continuous elastic support. The result for the moment distribution,

$M_h(x)$ along the horizontal beams is then written as:

$$\begin{aligned} M_h(x) \quad = \quad & \tfrac{\pi {B_0}^2 {R_0}^2 R_a}{\mu_o N}[(1+\tfrac{x}{R_a})\ln(1+\tfrac{x}{R_a}) - \tfrac{x}{h}\{\tfrac{(\lambda+1)S-\lambda T}{(\lambda+2)} \\ & -\tfrac{1}{12(\lambda+2)}(\tfrac{l}{R_a})^2\tfrac{3}{1+\frac{h}{R_a}} + (1+\tfrac{h}{R_a})\ln(1+\tfrac{h}{R_a})\} \\ & +\tfrac{1}{3(\lambda+2)}\{(2\lambda+3\}S - \lambda T - \tfrac{1}{4}(\tfrac{l}{R_a})^2\tfrac{1}{1+\frac{h}{R_a}}\}] \end{aligned} \tag{3.7}$$

where;

$$\lambda = \frac{h}{l}(\frac{I_l}{I_h}) \tag{3.8}$$

$$S = \frac{5}{2} + (\frac{R_a}{h})^2[\frac{h}{R_a}(1+\frac{5}{6}(\frac{h}{R_a})^2) - (1+\frac{h}{R_a})(1+2\frac{h}{R_a})\ln(1+\frac{h}{R_a})] \tag{3.9}$$

$$T = \frac{1}{2} + (\frac{R_a}{h})^2[-\frac{h}{R_a}(1-\frac{2}{3}(\frac{h}{R_a})^2) + (1-(\frac{h}{R_a})^2)\ln(1+\frac{h}{R_a})] \tag{3.10}$$

and the moment is positive for tension on the inside of the coil segment. N is the number of coils in the device, I_h and I_l are the moments of inertia for the horizontal and outer vertical legs, respectively, and h and l are the respective lengths of the horizontal and vertical legs. The distance, x, along the horizontal leg of the coil is measured from R_a. A similar expression can be written for the moment distribution in the vertical legs.

An example of the moment distribution for the horizontal legs using the case of table 3.1 is shown in figure 3.15. The largest bending stresses are found at the ends and in the middle of the coil segment with the highest occurring at the outboard corner. This is typical of frame-type TF coils. The bending stress distribution obtained from;

$$\sigma_b(x) = \frac{M_b(x)\Delta_o}{2\ I_h} \tag{3.11}$$

reveals that the peak bending stress for the distribution in this case is ≈ 56 MPa (8 kpsi) and is well within the capability of high conductivity Copper (yield stress ≈ 320 MPa (45 Kpsi)) or Aluminum (yield stress ≈ 130 MPa (19 kpsi)). This result is typical of the stresses in the outer TF sections and of the relatively low field devices of interest here.

The deflection of the TF legs under the in-plane loading is also of interest and can be calculated by applying the following relation from beam theory [33] to the moment distribution $M_h(x)$ already obtained:

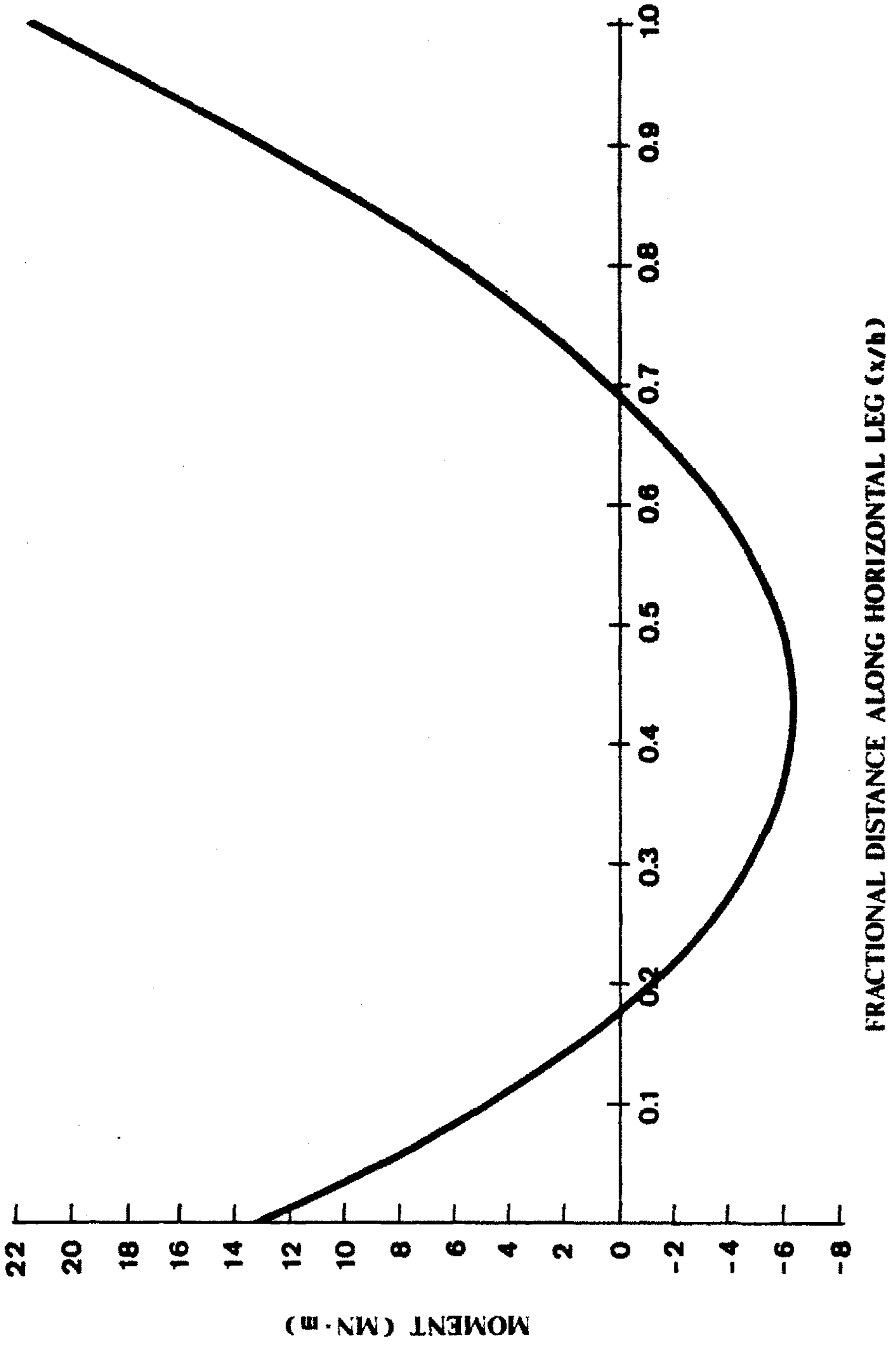

Figure 3.15: Moment Distribution in TF Coil

$$\frac{\partial^2 y}{\partial x^2} = \frac{M_h(x)}{EI_h} \tag{3.12}$$

Before integrating to find the deflection y, the expression for the moment distribution can be simplified by defining

$$A \equiv \frac{\pi {B_0}^2 {R_0}^2 R_a}{\mu_o N}, \tag{3.13}$$

$B \equiv \frac{1}{R_a}$, designating the coefficients multiplying x as C and the remaining terms which do not involve x as D. Then the moment distribution is rewritten as:

$$M_h(x) = A[(1 + Bx)\ln(1 + Bx) + Cx + D]. \tag{3.14}$$

Integrating twice and using the clamped end boundary conditions that the slope of the deflection curve and the deflection are zero at $x = 0$, the deflection distribution is:

$$\begin{aligned} y(x) \;=\; & \tfrac{A}{EI_h}[(\tfrac{Bx^3}{6} + \tfrac{x^2}{2} + \tfrac{x}{2B} + \tfrac{1}{6B^2})\ln(1 + Bx) + \\ & \tfrac{x^3}{6}(C - \tfrac{5B}{6}) + x^2(\tfrac{D}{2} - \tfrac{5}{12}) - \tfrac{x}{6B}]. \end{aligned} \tag{3.15}$$

The deflection distribution generally peaks on the high field side of the center of the horizontal TF leg. For the case illustrated in figure 3.15, the maximum deflection is only ≈ 0.4 mm. Note that this calculation is conservative because it assumes that the entire bending force is taken by the copper with no contribution from the steel end caps above and below.

3.5.2 Out-of-Plane Analysis

The toroidal field coils and supporting structure are also subject to loads transverse to the plane of the coils. These loads are due to the interaction of the vertical field generated by the equilibrium field system and the current in the TF coils. Since the magnitude of the vertical field is roughly proportional to the ratio, I_p/R_0, and the toroidal current is proportional to $R_0 B_0$ then the magnitude of the out-of-plane or overturning force is roughly:

$$F_{out} \; \alpha \; I_p B_0 L \tag{3.16}$$

where L is the length over which the force is acting (radial width of the TF coil). The out-of-plane force acts to twist the coils toroidally in opposite directions at their top and bottom. The twisting is in opposite senses because the direction of the toroidal current (and thus, the overturning) reverses at the top and bottom of the coils.

Generally, finding the shear stresses and deflections due to the overturning is a three dimensional finite element analysis problem due to the complex loading pattern and geometry involved. However, since we require the characterization of a conceptual design rather than the complex analysis of a detailed design and since we expect the overturning reactions to be relatively modest, we have chosen to develop a simpler approach to the solution.

The overturning problem is expected to be relatively modest due to the relatively low fields (and low plasma currents in the case of high beta) involved and the relatively structurally stiff overturning structure incorporated into this design. The overturning structure essentially consists of the steel casing formed by the wedges keyed into the inner and outer support cylinders (the cross-section resembles a spoked wheel). Also, it will be shown in section 3.6 that the overturning moment is significantly reduced with the placement of the EF coils within the bore of the magnet.

The first step in the overturning analysis is to determine the overturning force generated. The simplest approach would be to use a zero-dimensional form similar to the above equation. However, since we also wish to compare the distribution of the overturning force for EF systems internal and external to the TF bore, the same analysis (although more complex than the simplest approach) will be used here.

The EF coil system required for a given device was determined using the MHD equilibrium code NQX [20], available at the National Magnetic Fusion Energy Computing Center. Given geometry and plasma requirements, NQX can be used to determine the required currents in the equilibrium field coils for the first stability regime of plasma stability. Next, this distribution of coils with currents is used to determine the vertical field distribution. A computer code written by Bobrov [34] which finds the magnetic induction at N points in space due to K current carrying filaments was modified to find the vertical field distribution and calculate the resultant average overturning force over the width of the coil. A typical result for a device with $P_\epsilon = 1200 MW_e$, $\beta = 7$ %, $P_w = 4 MW/m^2$, $B_0 = 4.1\ T$ and an internal EF system is shown as the solid line in figure 3.18

The reactions to the out-of-plane forces are now estimated using the result for a cylindrically symmetric shaft subject to torsion loads at each end [35]. The stress can be found from the twisting moment as;

$$\tau_{ot} = \frac{M_{ot} r}{I_z} \tag{3.17}$$

with the angle of twist between the ends:

$$\phi_{ot} = \frac{M_{ot} L}{G I_z}. \tag{3.18}$$

In these relations, M_{ot} is the overturning moment ($= F_{ot} r$), r is the radial distance from the axis of the device to the point of application, L is the height of the shaft (the 'shaft' in this case is the overturning structure), G is the shear modulus of the material and I_z is the polar moment of inertia:

$$I_z = \int r^2 dr. \tag{3.19}$$

The shear stress and angle of twist are calculated by designating the product of the average overturning force and its centroid (determined from the overturning force distribution obtained above) as M_{ot}. The centroid of action for the overturning force is r in this analysis and L is the height of the magnet. Finally, the polar moment of inertia is obtained by integrating over the overturning structure's cross-section. The result is:

$$I_z = (R_o{}^4 - R_1{}^4)(\frac{Np}{4R_1} - \frac{\pi}{2}) + \frac{\pi}{2}[(R_o + t_o)^4 - (R_1 - t_i)^4] \tag{3.20}$$

where N is the number of coils, t_o and t_i are the thicknesses of the outer and inner support cylinders, respectively, and p is the depth (length in the toroidal direction) of the steel flanges at R_1. Note that the analysis assumes that the overturning is reacted only by the steel structure.

Typical overturning moments of a few thousand meganewton-meters result in modest shear stresses ($\approx$ 7 MPa or 1 kpsi) and deflections of $10 - 20$ mm for moderate beta versions of RCTR. These deflections are comparable to those expected from more sophisticated analysis of the high field ignition experiment

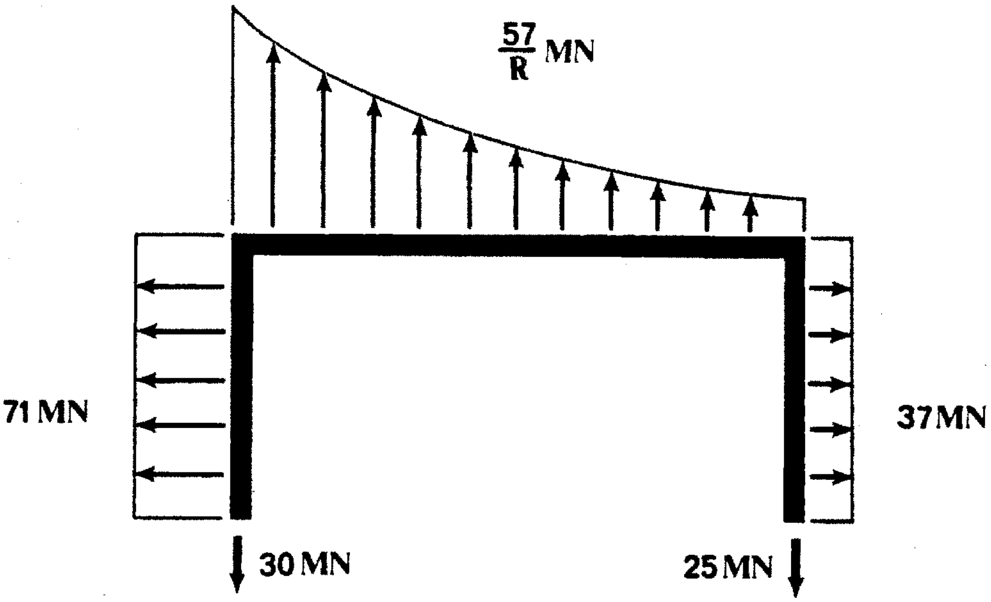

Figure 3.16: In-Plane Forces on the Toroidal Field Coil

LITE [5]. The higher magnetic field of LITE will over-compensate for its lower plasma current in comparison to RCTR and we expect a higher overturning force for LITE. Although the overturning moment will be several times higher for RCTR due to its much larger size, this is compensated for by the increased area available to react the overturning. The overturning reactions are reduced further with high beta versions of RCTR due to their lower plasma currents and lower toroidal fields.

3.5.3 Stress Analysis Results

The results obtained from the stress analysis for the case of table 3.1 are shown in figure 3.16 and table 3.4. Figure 3.16 depicts schematically the in-plane forces on the TF coil. The corresponding reactions are listed in table 3.4 along with the characteristics of the support structure.

Net Electric Power, MW_e	1200
Wall Loading, MW/m^2	3
Toroidal Beta, %	24
Peak Magnetic Field, T	3.51
Total Vertical Force, MN	665
Max. In-Plane Deflection, mm	0.4
Max. In-Plane Shear Stress, MPa	55.9
Number of Plugs	144
Plug Diameter, cm	25
Plug Avg. Shear Stress, MPa	83
Inboard Cylinder Thickness, cm	25
Outboard Cylinder Thickness, cm	10

Table 3.4: RCTR Support Structure

The support structure was sized using guidelines of the ASME Boiler Code Case N-47 [36] for maximum allowable stresses in various components. For example, the steel plugs joining the steel caps and support cylinders experience shear stresses when transferring the vertical in-plane load on the coils to the support cylinders. The shear stress is limited by the code to sixty percent of the maximum allowable stress intensity which is defined as the minimum of $\frac{2}{3}\sigma_y$ and $\frac{1}{3}\sigma_u$. σ_y and σ_u are the yield and ultimate stresses, respectively, of the material in use. Primary membrane stress (such as in the support cylinders) is limited to 100 percent of the maximum stress intensity. Combined stresses (such as the combined vertical and circumferential loads experienced by the outer support cylinder) are evaluated using the Von Mises criterion as prescribed in the code.

The tensile membrane stresses in the inner, outer and horizontal legs are shown for completeness even though these loads are actually transferred to the support structure. The compressive stress at the inboard leg due to wedging is 7.6 MPa (1.1 kpsi) which is sufficient to provide adequate contact pressure between TF turns. The maximum shear stress in the plane of the coil due to bending is 55.9 MPa (8 kpsi). The corresponding maximum deflection is 0.4 mm.

The required inner cylinder thickness of 25 cm is driven by the need to support both the vertical and inward radial forces. The outer cylinder thickness of 10 cm is driven largely by the support requirement for the outward radial force of 37 MN/coil. Requirements for the support of the vertical force do not have a major impact here in comparison to the outward radial force requirements.

Transferring the vertical load in shear requires the use of 144 steel plugs of 25 cm diameter assuming the entire load is carried there. The plugs are arranged in three rows of 24 at the inner cylinder and two rows of 36 at the outer cylinder. The design could be facilitated with the use of a higher strength material requiring smaller and/or fewer plugs.

3.6 Internal vs External Poloidal Field Coils

An important option for a demountable coil system is the possibility allowed for placing the ohmic and equilibrium coils within the magnet bore. Placing the ohmic coil inside the TF bore can significantly increase deliverable volt-seconds to the plasma and/or decrease its peak magnetic field and resistive dissipation. Internal EF coils can be smaller and require less current for the same equilibrium in comparison to external coils. In addition, if a pushing coil (coil used to shape the plasma) is required to achieve high beta with bean-shaped plasmas, placement of this coil within the bore of the TF may greatly facilitate its design.

To illustrate and quantify the importance of these points, a comparison of external and internal PF systems has been done for a low beta version of RCTR with $P_e = 1200$ MW$_e$, $\beta = 7$ %, $P_w = 4$ MW/m^2, and $B_0 = 4.1$ T. The relative positions of the PF systems internal and external to the TF coil are shown in figure 3.17. Note that the currents required for the internal EF set (2.5/3.0 MA) are significantly lower than those required for external coils (9.7/4.7 MA). For EF coil sets with comparable current density, the dissipated power is cut in half (181 versus 88 MW). The internal OH coils can deliver the same volt-seconds as the external set at reduced peak field (8.4 versus 13.2 T) and reduced dissipated power (51 versus 82 MW).

The overturning force due to the interaction of the EF and TF systems was compared using the procedure outlined in the previous section. The result is shown in figure 3.18. The average overturning force per TF plate is significantly improved with internal coils. The local vertical field required to create the vertical field needed at the plasma is lower for internal coils resulting in a lower average overturning force. Equally important, the closer fitting internal

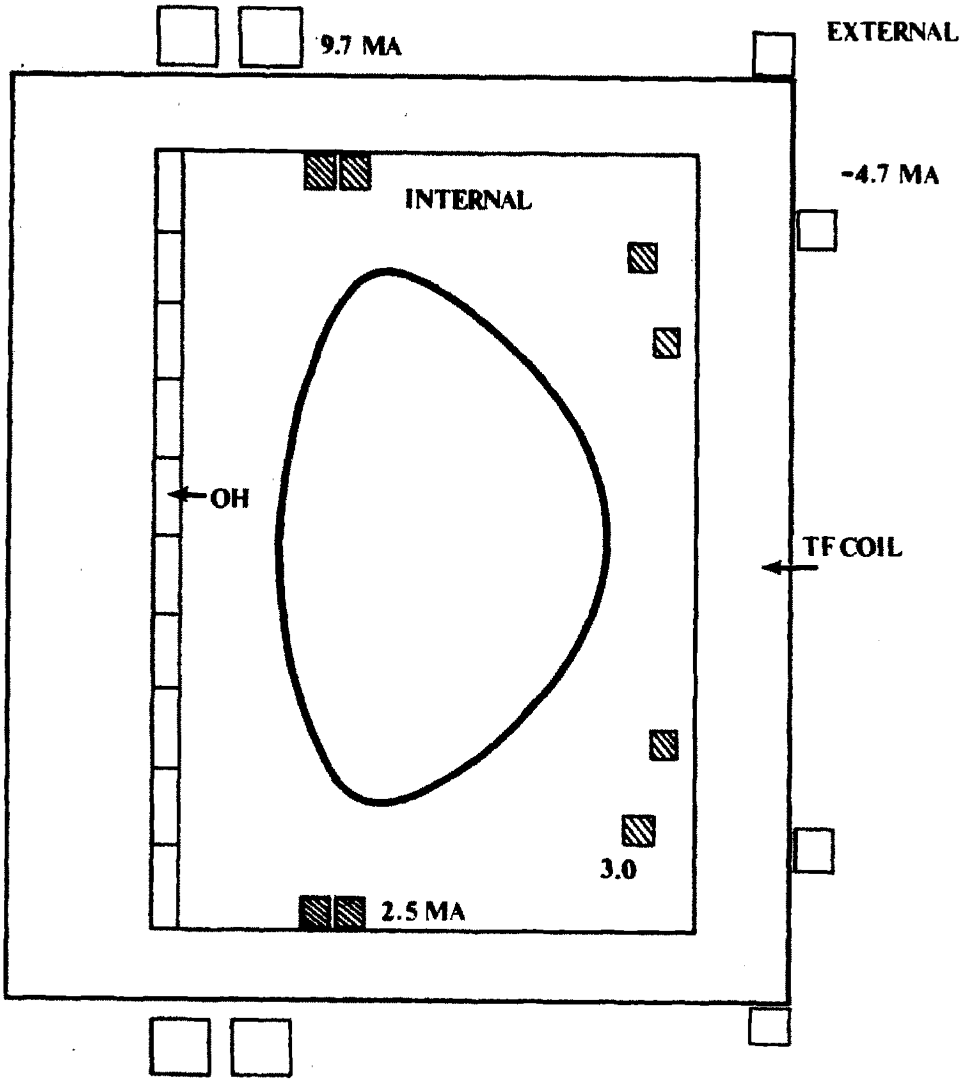

Figure 3.17: Schematic Comparison of Internal and External EF Systems, $P_e = 1200$ MW$_e$, $\beta = 7$ %, $P_w = 4$ MW/m^2, $B_0 = 4.1$ T

EF system results in an overturning force distribution whose centroid is at a significantly smaller radius.

3.7 Summary

A concept for a demountable nuclear island for RCTR has been presented. The concept emphasizes the need for simplicity and maintenance and is integrated with the needs of other systems including PF, blanket/first wall and support structure components. The importance of the impact of the maintenance concept on other systems will receive further treatment in the next chapter which covers the concept and analysis of the blanket/first wall system.

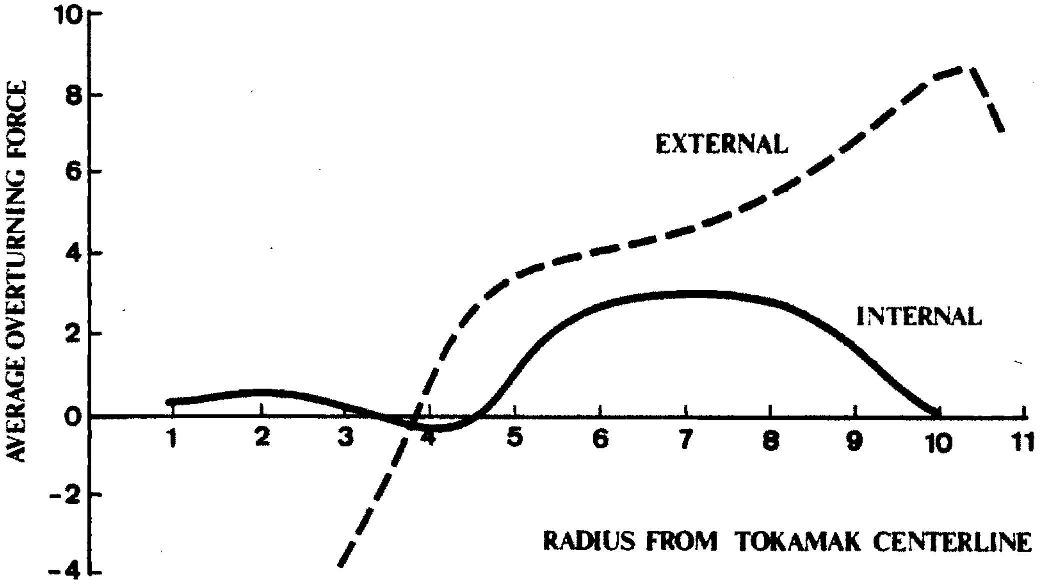

Figure 3.18: Average Overturning Force Per TF Plate

Chapter 4

Blanket/First Wall System

4.1 Introduction

The blanket/first wall system is an integral part of all commercial fusion reactor concepts. The functions of the blanket (heat removal and tritium breeding) and first wall (extraction of heat and survival of first material surface near the plasma) are of central importance to the commercial fusion reactor. The material and configurational details of these components can have a major impact on the complexity, cost and ultimate attractiveness of the commercial fusion device.

The present chapter concerns the choice of materials and configuration for the RCTR blanket/first wall system and presents a reference design for these components. Section 4.2 discusses general issues which led to the choice of materials and configuration for the reference RCTR blanket/first wall concept which is then presented in section 4.3. Supporting work in neutronics using a one-dimensional neutron transport code is discussed in section 4.4. Other supporting work in the areas of MHD pressure drop and stress analysis is covered in section 4.5. Finally, chapter 4 is summarized in section 4.6.

4.2 General Considerations for the Design

The blanket/first wall design was considered in the context of the design philosophy of the entire RCTR concept. Thus, the issues of cost, complexity, high efficiency and demountability were of key importance in settling on a reference design.

Choosing materials for the blanket and first wall system began with the selection of a breeding material consistent with RCTR requirements. This led to the choice of the remaining materials required for the blanket design and a cooling medium and structural material for the first wall. The configuration of the blanket/first wall system was largely driven by the demounting capability of the nuclear island.

4.2.1 Breeding Materials

RCTR will operate on the deuterium-tritium (D-T) fuel cycle and it is required that it be self sufficient in tritium. The tritium is bred in lithium which is contained in the blanket in some form. The major alternatives for the tritium breeding medium are liquid lithium breeders such as lithium (Li) and $^{17}Li^{83}Pb$ (LiPb), solid breeders such as Li_2O and $LiAlO_2$ and the fluoride salt FLIBE (LiF-BeF_2).

Liquid lithium ranks well within each of the major issues of concern identified for RCTR; cost, complexity and high efficiency. The use of lithium can lead to a relatively simple blanket design because it acts as both coolant and breeder and does not require a neutron multiplier or a separate tritium extraction loop. In addition, liquid Li possesses excellent thermo-physical properties allowing the possibility of high temperature operation and operation of the thermal conversion plant with high (greater than 40 %) efficiency. Extraction of the bred tritium is also a relatively simple process. The major disadvantages of Li are its high potential reactivity with air and water and the MHD pressure drop associated with a liquid metal flowing in a magnetic field.

LiPb possesses similar advantages to Li since it also is self-cooled and requires no additional neutron multiplication. However, LiPb has inferior thermo-physical properties in comparison to Li and tritium extraction is more difficult. LiPb also requires special tritium barriers to adequately contain the tritium in the blanket while Li has a high solubility for tritium. LiPb shares MHD pressure drop difficulties with Li but has reduced reactivity problems with water and air.

FLIBE is a liquid breeder which offers chemical stability in water and air environments and is relatively noncorrosive. However, FLIBE has a relatively high melting point ($\approx$ 355 C), a low thermal conductivity, and a low tritium solubility. FLIBE blanket concepts are generally more complex than Li or LiPb, utilizing separate multiplier regions and an additional coolant stream (typically Helium).

Solid breeder concepts lack the problems of MHD pressure drop and reactivity shown by the liquid metal option. However, in general they are considerably more complex than Li or LiPb blankets. All solid breeders require separate channels for both heat and tritium extraction and some require dedicated neutron multipliers. Radiation effects on the properties of the breeder are also a major concern.

Considering the available options, liquid lithium appears to be the most viable choice for the breeding medium in RCTR. It's use provides the potential for a simple yet high performance blanket design. In addition, the problem of MHD pressure drop can be minimized with the low magnetic field designs of resistive magnet commercial reactors. Reactivity problems will preclude the use of water in any component of the nuclear island (see chapter five for TF magnet cooling and impurity control concepts). Also, the use of an inert atmosphere in the reactor building (e.g., nitrogen) will minimize the chance of lithium-air reactions.

4.2.2 Structural Materials

The selection of liquid lithium as the breeding medium greatly simplifies the selection of the remaining materials of the blanket/first wall system. The lithium is self-cooled with excellent thermo-physical properties and a neutron multiplier and helium purge stream are unnecessary. Thus, only a structural material and a reflector/shield composition remain to be selected for the blanket system.

The major candidate material options for structural components are stainless steel (e.g., PCA), ferritic alloys (e.g., HT-9) and vanadium alloys (e.g., V-15Cr-5Ti). Among these options, vanadium alloy is the best choice for the present application. Vanadium is compatible with liquid lithium at relatively high temperature, has excellent thermo-physical properties, possesses excellent high temperature strength and is a low activation material. Irradiation effects and lithium compatibility considerations allow peak metal temperatures greater than 750 C. This high temperature capability is essential to the achievement of high coolant outlet temperatures and the resultant high thermal efficiency. Cost is the only major disadvantage associated with the use of vanadium as the unit cost of vanadium is typically 5 to 7 times that of the steels. This is less of a concern in relatively low-mass applications such as the first wall and some structural components but is a significant problem for high mass applications such as a reflector or shield.

In comparison, ferritics and steels exhibit inferior properties to vanadium in most categories. PCA becomes relatively highly activated and irradiation induced swelling and embrittlement probably limit its use to peak temperatures of ≈ 550 C. Compatibility problems with liquid lithium place an even more severe limit on the use of stainless steel with temperatures limited to 430-460 C. Similar problems with corrosion and mass transfer from liquid lithium will limit the use of HT-9 to 530-570 C [37].

4.2.3 Reflector/Shield Composition

Due to the robust nature of resistive coils, we expect relatively modest shielding requirements for the present concept. In fact, neutronics calculations indicate that adequate coil lifetimes can be achieved without the use of a dedicated neutron shield. However, a reflecting medium must be accounted for in the design to assist in reflecting leakage neutrons back into the blanket volume and to prolong the fluence life of the copper conductor and insulation components in the nuclear island. Although general considerations will be outlined here, specific data on the performance of various reflector options will be presented in section 4.4.

The choice of a reflector material is based largely upon neutronics considerations. Low-Z reflectors are generally better moderators than high-Z materials leading to increased tritium breeding in lithium-6 (which requires a softened spectrum). However, the ability of high-Z materials to absorb secondary gamma radiation is useful for increasing the energy deposition in the blanket region. Generally speaking, the latter capability is more highly valued in liquid lithium blanket systems due to the relative ease of achieving adequate tritium breeding and the importance of attaining high blanket multiplication (see section 4.4.2).

Several high-Z reflector material options were considered for RCTR. The materials analysed include stainless steel (PCA), vanadium, ferritic steel (HT-9) and tungsten. The steels, PCA and HT-9, generally offer the highest energy deposition of these materials but have relatively low temperature limited operation due to compatibility issues associated with liquid lithium. Vanadium offers slightly less energy deposition than the steels but is a low activation material and is significantly less dense than PCA and HT-9. Tungsten is a relatively poor reflector and energy absorber but is an excellent neutron shield.

HT-9 was chosen as the reflecting material for the reference blanket design because of its high energy deposition and acceptable peak temperature limits. The temperature limit from lithium corrosion for PCA is inconsistent with the high performance goals of the RCTR concept while the cost and resource availability of vanadium probably precludes its use as a reflector. Although tungsten offers excellent neutron shielding characteristics, shielding is adequate with the other options available.

4.2.4 First Wall Materials

Subject to issues presented in the next section, the first wall and blanket systems could be either separate or integrated. In the latter case, the materials of the first wall would be the same as for the blanket; vanadium structure cooled by liquid lithium.

If the first wall were separate from the blanket, however, a lithium cooled vanadium structure would still be a superior choice. The first wall receives a high surface heat load and is subject to bombardment from charged particles, neutrals and high energy neutrons from the plasma. This requires a structural material with good radiation resistance and high temperature performance. Vanadium is the best available material in these categories and also is a low activation material.

In addition, the liquid metal lithium is an excellent candidate for removing the large heat loads present at the first wall. The MHD pressure drop problem associated with this coolant can be solved using proper design (see next section).

4.2.5 Blanket/First Wall Configuration

The configuration for the blanket/first wall reference design was driven mainly by compatibility requirements with the demountable TF coil concept and the need to minimize MHD pressure drop.

Following the arguments of section 3.2, the vacuum boundary in the RCTR concept is located either at the first wall or at the outside boundary (with respect to the plasma) of the blanket. Further, this boundary must be intact such that no welding or cutting is needed during the assembly and disassembly of any components in the nuclear island. Using an integrated blanket/first wall design in which the first wall is essentially the inner boundary of the blanket then requires that the entire assembly be removable as a single unit. This scheme is attractive because it is the simplest possible design and the blanket and first wall share the same coolant stream.

The major disadvantage of the integrated concept is its estimated weight of over 2800 tonnes (without Li) for a typical RCTR device. If the reflector were made separate from an integrated blanket/first wall system (and thus be removable separately, in sectors), such a blanket system would still weigh almost twice as much as the first wall. In addition, having a separate reflector region would result in an increase in complexity comparable to that required by the separate first wall option.

Separate blanket and first wall systems will require separate coolant streams but only the first wall ($\approx$ 150 - 200 tonnes) need be removed as a single unit. The blanket system can be broken into sectors which may be removed separately for individual repairs. To help put these weights in perspective, we note that NASA employs a 250 tonne crane to lift the space shuttle ($\approx$ 105 tonnes) from a horizontal to a vertical position.

In light of these considerations, a separate blanket/first wall system has been chosen for the RCTR reference concept. However, assuming the large weight lifts could be handled, the integrated blanket first wall version with separate reflector could be an equally satisfactory option for RCTR. In the latter case, the blanket/first wall assembly would take the form of the poloidal/toroidal flow module reference design from the Blanket Comparison and Selection (BCSS) study [37].

The choice of coolant flow patterns in the blanket and first wall is driven by MHD pressure drop considerations. Toroidal flow is inclined roughly along the field lines and thus suffers little from MHD losses while the opposite is true for poloidal flow. However, as shown in section 4.5, the MHD pressure drop scales with velocity for flow perpendicular to a magnetic field and the MHD losses can be acceptable for sufficiently low velocities.

Due to relatively high flow velocities required at the first wall to remove typical heat fluxes of 0.5 to 1.0 MW/m^2, we are driven to select toroidally directed flow for this component. In contrast, the heat removal problem in the blanket volume is reduced and the volume itself relatively large which suggests low velocity poloidal flow. This arrangement is compatible with the blanket assembly being divided into a number of independent toroidal sectors.

Referring again to the discussion of section 3.2, vertical removal of all nuclear island components has been selected to simplify the design of the overturning structure and to remain compatible with the demountable TF coil system. Thus, the blanket must also be divided along the midplane (horizontal cut at the midsection) to accommodate separate removal of the blanket sectors and the first wall unit. In the absence of radial port space, the blanket and first wall assemblies must be fed through ports at the top and bottom of the device. This space is made available through ports cut into the horizontal sections of the steel wedges.

4.3 Blanket/First Wall Reference Concept

In this section, we present the reference blanket/first wall concept for RCTR subject to the considerations presented to this point and using analysis which will be presented in the remaining sections of this chapter. The scale drawings and calculations are based on reference Case A from the parametrics of chapter 2.

An engineering drawing showing a cross-section of the blanket/first wall system is shown in figure 4.1. A more detailed view of the flow patterns for the lithium coolant is indicated in figure 4.2. A top view of the reference RCTR device (figure 3.7) shows the inlet and outlet port arrangements for this system.

The concept shown is a separate blanket/first wall design using liquid lithium coolant, a vanadium structure and an HT-9 reflector. The concept is designed for relatively simple vertical lift assembly/disassembly operations. The first wall is constructed as a single unit and vacuum tested before assembly. No cutting is required to remove any component within the bore of the TF coil.

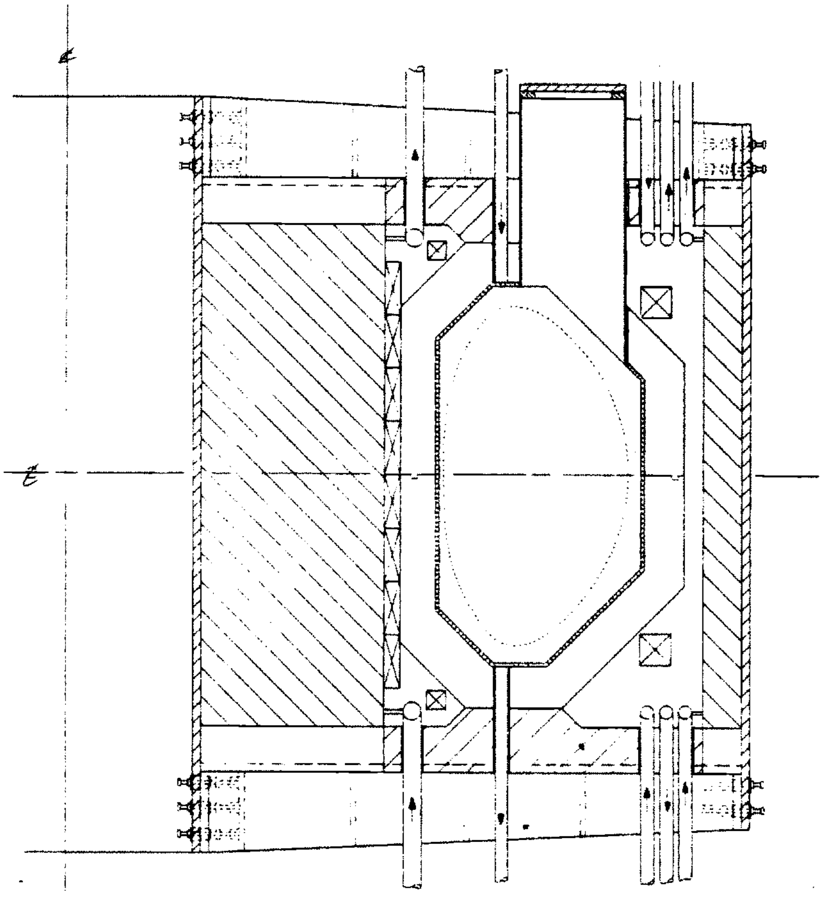

Figure 4.1: Blanket/First Wall Cross-Section

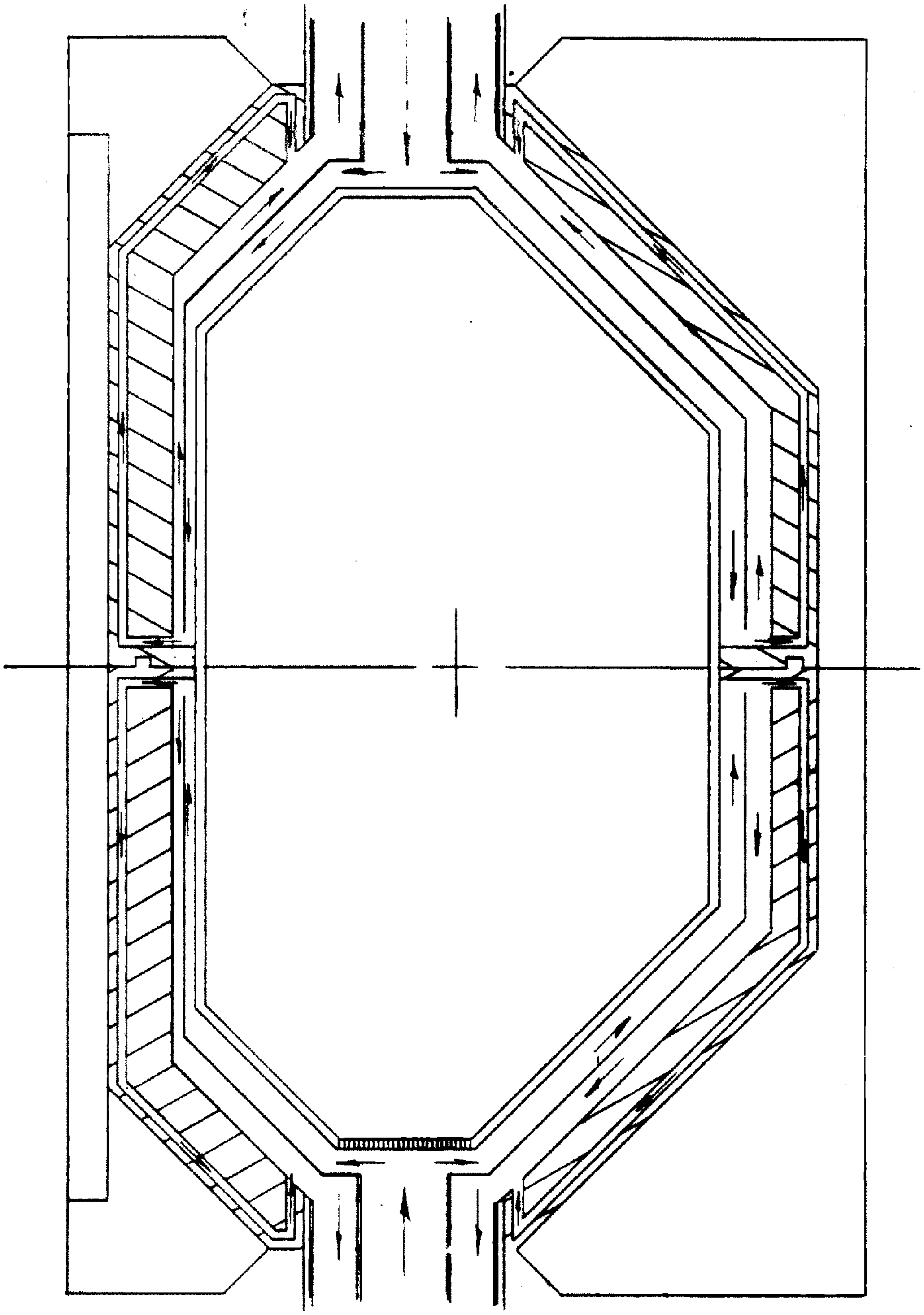

Figure 4.2: Blanket Diagram Showing Flow Patterns

The blanket is divided along the midplane of the device to allow removal of the first wall and is also divided toroidally into six sectors for a total of twelve sectors above and below the midplane. The weight of each sector is 230 tonnes (244 tonnes loaded with lithium). The blanket is fed lithium through ports located in the steel wedges at the top and bottom of the device. In a sector above the midplane, the flow enters through top ports located in each sector and empties into manifolds which form the top area of the blanket sector. From here the flow is channeled poloidally around the device.

The blanket is divided into two main lithium channels and a reflecting region which is located furthest from the plasma. The lithium flows poloidally down the channel closest to the plasma, reverses direction at the midplane of the device and flows back up the remaining channel until it reaches the exit plenum and leaves out the upper port. Some of the lithium flow is also channeled through the reflector on the return leg for heat removal purposes.

A similar flow pattern occurs for sectors below the midplane. These sectors can be drained if needed while the device is not in use simply by letting the lithium flow out the bottom ports. The upper sectors could also be drained through channels at the midplane which exit between the lower blanket sectors.

The major parameters characterizing the reference blanket concept are summarized in table 4.1. These parameters were arrived at using neutronic, MHD flow and stress analyses detailed in the next sections. The inboard blanket system consists of a 35 cm blanket region and a 30 cm reflector. In the outboard sections, the blanket is 45 cm thick with a 45 cm reflector section. The inlet and outlet channels are 70 cm i.d. circular pipes with wall thicknesses of 8 mm (inlet) and 2 mm (outlet). Each blanket sector is divided toroidally into 10 poloidal flow channels. The wall thicknesses of the blanket structure varies, decreasing as the flow progresses through the blanket system from 8 to 2 mm to minimize the MHD pressure drop (see section 4.5).

The total thermal power deposited in the nuclear island at a neutron wall loading of 3 MW/m^2 is 2925 MW. Of this total, 1309 MW are deposited directly in the blanket region with an additional 488 MW deposited in the reflector. The remaining thermal energy is deposited in the first wall (1068 MW) and the coils lying outside the blanket system (60 MW). The corresponding energy multiplication factor is 1.21. The tritium breeding ratio obtained from a one-

Total Thermal Power, MW	2925
Blanket Power, MW	1309
Reflector Power, MW	488
Neutron Wall Loading, MW/m^2	3
Energy Multiplication	1.21
Tritium Breeding Ratio	1.25
Li Mass Flow/Sector, kg/s	144
Mass Flow/Channel, kg/s	14.4
Average Li Velocity, m/s	0.08 - 0.12
Peak Magnetic Field, T	3.51
Pressure Drop/Sector, MPa	1.7
Pumping Power, MW	5.3
Maximum Primary Stress, MPa	83
Exit Li Temperature, C	550
Thermal Efficiency, %	42
Blanket Total Mass, T	281
Reflector Total Mass, T	2643

Table 4.1: Reference Blanket Parameters

dimensional calculation of 1.25 is assumed to be adequate for self-sufficiency in tritium.

Using an inlet lithium temperature of 300 C and a temperature rise through the blanket system of 250 C, the exit lithium temperature is 550 C. With experience from similar lithium blanket systems having the same exit temperature [37], a blanket thermal efficiency of 42 % is assumed. The lithium mass flow rate required per sector is 144 kg/s or 14.4 kg/s per poloidal channel. The velocity of lithium flow through the changing cross-sections of the blanket system varies between and 0.08 and 0.12 m/s.

The moderate lithium velocities and relatively low peak field (3.5 T) of the device results in a moderate pressure drop due to MHD effects of 1.7 MPA. The pumping power required of the system is 5.3 MW. The maximum primary stress of 83 MPa occurs at the first wall side of the blanket near the inlet. The entire blanket system consists of 163 tonnes of lithium (140 in blanket, 23 in reflector), 141 tonnes of vanadium structure including manifolds and inlet/outlet channels and 2620 tonnes of HT-9 reflector material.

The first wall system consists of a 6mm first wall (closest material surface to the plasma), a 3 cm back supporting wall and 4mm thick dividing walls forming

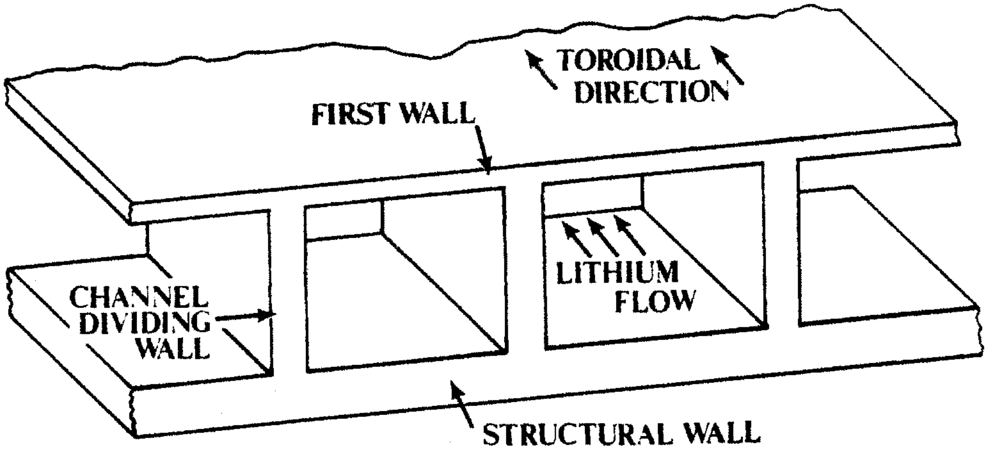

Figure 4.3: First Wall Cross-Section

4 by 5 cm toroidally directed coolant channels. A sketch of the first wall cross-section is shown in figure 4.3. If a thicker first wall is required to maintain structural integrity against erosion from the plasma, a grooved first wall [37] could be employed to retain the peak thermal stress at acceptable levels.

Lithium enters the first wall system through 40 cm diameter inlets located at the top of the device at alternating steel wedges. The inlets feed poloidal manifolds which in turn feed the toroidal channels. The flow travels toroidally for the length of one blanket sector where it empties into another poloidal manifold and exits through an outlet located at the bottom of the device. The poloidal first wall manifolds are kept large to minimize the MHD pressure losses.

Thus, the first wall system resembles a thick toroidal shell with two spare tires (inlet and outlet manifolds) wrapped poloidally around the shell at each intersection of two blanket sectors. These manifolds function as short length (toroidally) blanket sectors and are equal in width to the blanket sections at all locations. The length (toroidally) of each manifold is 50 cm (average) and the wall thicknesses vary from 10 to 2 mm in a similar manner to the blanket system manifolds.

The major parameters characterizing the first wall system are summarized

Thermal Power, MW	1068
Neutron Wall Loading, MW/m^2	3
Surface Heat Flux, MW/m^2	0.75
Li Mass Flow, kg/s	171
Avg. Li Channel Velocity, m/s	0.67
Avg. Li Manifold Velocity, m/s	0.89
Peak Magnetic Field, T	3.51
Pressure Drop, MPa	3.9
Pumping Power, MW	7.5
Maximum Primary Stress, MPa	104
Maximum Thermal Stress, MPa	322
Plasma-Side Vanadium Temp., C	750
Average Vanadium Temp., C	665
Exit Lithium Temperature, C	550
First Wall Mass, T	160

Table 4.2: Reference First Wall Parameters

in table 4.2. For the wall loading of 3 MW/m^2, the entire surface heat flux of charged particles and neutrals of 0.75 MW/m^2 is assumed to be incident on the first wall. Thus, 522 MW from the surface heat load in addition to 546 MW (22.7 percent) of neutron power are deposited in the first wall system (determined from the neutronics analysis). The peak and average temperatures of the vanadium first wall are 750 C and 665 C, respectively. The lithium outlet temperature is 550 C and the maximum thermal stress experienced in the first wall is 322 MPa.

The lithium mass flow rate required for a temperature rise through the system of 250 C is 171 kg/s per sector. This results in an average velocity in the toroidal channels of 0.67 m/s and an average velocity in the poloidal manifolds of 0.61 - 0.85 m/s. The pressure drop due to MHD losses in the system is 3.9 MPa resulting in a pumping power required of 7.5 MW. The maximum primary stress of 104 MPa due to MHD pressure losses occurs on the first wall at the location of the inlet manifolds where the pressure is highest.

4.4 Neutronics Analysis

A one-dimensional neutron transport code, ONEDANT, was used to analyse material and configurational trade-offs for the blanket/first wall design. Issues considered in the analysis include material selection, system configuration, tritium breeding, energy multiplication and component lifetime. The system considered uses a self-cooled liquid lithium breeder with vanadium structure. A number of reflector material options were examined.

4.4.1 Calculational Method

ONEDANT [38] is a ONE-dimensional, Diffusion Accelerated Neutral particle Transport code developed at Los Alamos National Lab (LANL). This modular, fast-running (typical run time for non-fissioning cases is 1 - 2 cpu minutes) code solves the linear Boltzman transport equation using the method of discrete ordinates. The diffusion approximation is used to accelerate covergence of the solution. ONEDANT employs multigroup data for neutron and photon transport using a cross-section library generated with the TRANSX code [39] from MATXS/5 [40] compilations. MATXS/5 is a coupled 30 × 12 neutron-gamma transport cross-section file collapsed from ENDF/B-V pointwise cross-section data.

The first step in the present analysis was to use TRANSX to extract the required cross-sections from MATXS/5 for use with ONEDANT. Cross-section sets already available from previous studies needed to be updated to include data from recently revised Li-7 cross-sections and to include various isotopes such as vanadium. The input used for TRANSX is shown in appendix C.

A sample input file for use with ONEDANT is also presented in appendix C. The RCTR configuration is modeled in cylindrical geometry using a representation like that shown in figure 4.4. The axis of the device is located at $X = 0.0$ with the widths of the inboard and outboard sections represented by their actual dimensions. Regions containing more than one material are homogenized by ONEDANT using designated volumetric fractions.

Previous comparisons of this type of one-dimensional representation with more accurate three-dimensional applications [37] show that accurate values can be obtained for global parameters such as tritium breeding ratio and energy multiplication. Also, pointwise data obtained from homogenized regions for radiation doses to insulation (for example) should be reliable in the absence of strong neutron absorbers.

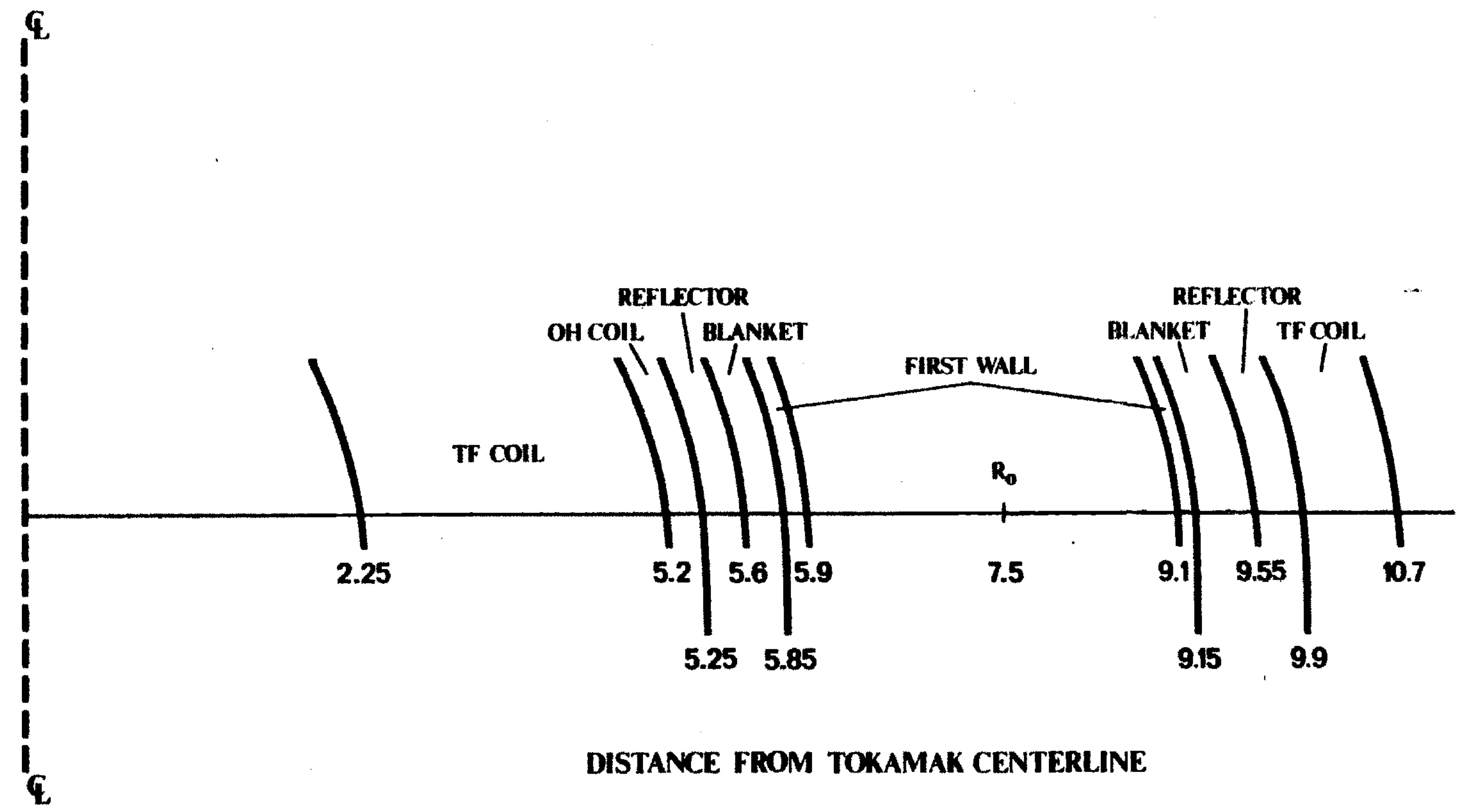

Figure 4.4: ONEDANT Calculational Geometry

The tritium breeding ratio (TBR) can be obtained directly from the reaction rate edits of ONEDANT. Regional edits of the energy deposited per incident fusion neutron determine the energy multiplication factor and the distribution of energy deposition in the RCTR system. Point-wise edits of the neutron and gamma heat deposited at various locations lead to a determination of the local radiation dose to various constituents of the blanket/first wall and coil components. With this information and an assumption for the radiation dose lifetime of various materials, the lifetime of various copper coils can be estimated.

The lifetime of coil components may be limited by either the conductor or the insulation. Polyimide insulators have been tested to 1.4×10^{12} rads at high stress under cyclic conditions [41]. In regions of high radiation fluxes, ceramic insulators should be useful to at least 1×10^{13} rads, limited by swelling [42]. Copper conductor is limited by swelling for temperatures above about 130 C while irradiation embrittlement probably limits their integrity to fluences of $\approx 1 \times 10^{13}$ rads at low temperature. Under RCTR conditions with room temperature magnets at low stress (several kpsi) and low cycles ($\approx$ 50,000 lifetime cycles), both insulation and conductor are assumed to be limited to 1×10^{13} lifetime rads.

Assuming that both conductor and insulation have the same lifetime dose limits, coil component failure is likely to take place first in the conductor where the energy deposition is significantly higher than in the insulation. However, since the neutron flux drops rapidly in the first several centimeters of conductor, early failure will only involve a relatively small volume of the conductor and probably will not compromise the integrity or the function of the coil. This is not the case in the insulation where radiation damage could lead to breakdown of the insulation between adjacent plates. Therefore, the lifetime of coil components is assumed to be limited by the peak radiation dose to their insulation.

4.4.2 Reflector Material Comparison

Stainless steel (PCA), ferritic steel (HT-9), vanadium alloy (V-15Cr-5Ti), and tungsten were compared as options for reflector materials in use with the self-cooled lithium blanket concept for RCTR. The configuration used for the neutronic evaluation is that shown in Figure 4.4. The configuration includes a 5 cm vanadium first wall composed of 50 % natural lithium by volume and a natural

Reflector	TBR	Energy/n (MeV)	Multiplication	Coil Life (Years)
Stainless Steel	1.232	16.961	1.202	20
Vanadium Alloy	1.246	16.934	1.201	24
Ferritic Steel	1.204	16.964	1.203	20
Tungsten	1.066	16.835	1.194	165

Table 4.3: Reflector Material Comparison

lithium blanket with 7.5 % vanadium structure by volume. The blanket region is 20 cm thick inboard and 40 cm thick outboard. The reflector region was 35 cm inboard and outboard.

The resulting TBR, energy multiplication factor (M) and coil lifetime for each of the reflector materials considered in this configuration is shown in table 4.3. PCA, HT-9 and vanadium alloy are each fairly comparable in the categories mentioned. Vanadium yields a slightly higher tritium breeding ratio and longer magnet lifetime than HT-9 or PCA but slightly lower energy deposition in the blanket per fusion neutron. PCA and HT-9 are quite comparable in magnet lifetime and energy deposition but HT-9 yields a slightly lower TBR than PCA. In contrast, the tungsten reflector yields a more significantly decreased TBR and energy deposition in comparison to the other alternatives considered but proves to be an excellent shield for the magnet components.

Other, lower Z materials often considered as reflector materials in fusion blanket design such as carbon, water and aluminum would generally yield higher tritium breeding ratios and lower energy depositions than the materials studied here. These materials were not considered because of the desire to maximize energy deposition in light of adequate tritium breeding already obtainable with the high-Z options.

As a result of this analysis and other considerations to be discussed, HT-9 was chosen as the reference reflector for RCTR. Tungsten was eliminated because of inferior TBR and energy deposition in light of adequate magnet coil protection provided by other options. Neutronically, PCA and vanadium are equally good candidates for reflector materials as HT-9 but considerations of lithium compatibility and cost favor the selection of HT-9. Specifically, vanadium is several times as expensive as HT-9 and is not as readily available and the temperature limit imposed by lithium compatibility on PCA (discussed earlier) is significantly lower than that of HT-9.

4.4.3 Blanket Thickness Trade-offs

Independent trade-offs versus the inboard and outboard blanket thicknesses with fixed reflector thicknesses were performed. In the analysis, the volumetric fraction of vanadium structure in the blanket region was kept constant at 7.5 % and the thickness of the reflector region was 35 cm at all locations. The inboard and outboard reflectors contained 20 % and 10 % lithium by volume, respectively. Only natural lithium was considered in the analysis because Li-6 enrichment generally doesn't pay off unless a neutron multiplier or a large volumetric fraction of structural material are included in the design [37].

The results of parametric scans versus blanket thickness showing TBR and energy multiplication (M) are shown in figure 4.5. TBR generally increases sharply with increasing blanket thickness but eventually levels off at large blanket thicknesses. M exhibits a gradual decline with increasing blanket thickness as the competition for neutrons increasingly favors capture in lithium instead of in the reflector. Decreasing M generally accompanies an increasing TBR due to the higher energy yield reactions occurring in the iron of the HT-9 ($\approx$ 8 MeV) compared to those in Li-6 ($\approx$ 4.8 MeV).

The inboard blanket trade-off reveals that even very thin blankets may provide adequate tritium breeding. TBR is significantly above one ($\approx$ 1.08) even with no inboard breeding region. TBR rises above 1.2 at a blanket thickness of less than 20 cm inboard. Outboard, a blanket thickness of at least 35 - 40 cm is needed to provide a tritium breeding ratio of 1.2 - 1.25. Energy multiplication generally hovers in the vicinity of 1.2.

The lifetime of the inboard and outboard toroidal field coils and the ohmic field coil versus blanket thickness is shown in figure 4.6. The curve of inboard TF lifetime versus inboard blanket thickness shows that a 30 full power year (FPY) lifetime is achieved with a blanket thickness of 20 cm. Without an inboard breeding region, the FPY lifetime of this coil is only 17 years. The lifetime of the ohmic coil versus inboard blanket thickness is considerably shorter than the

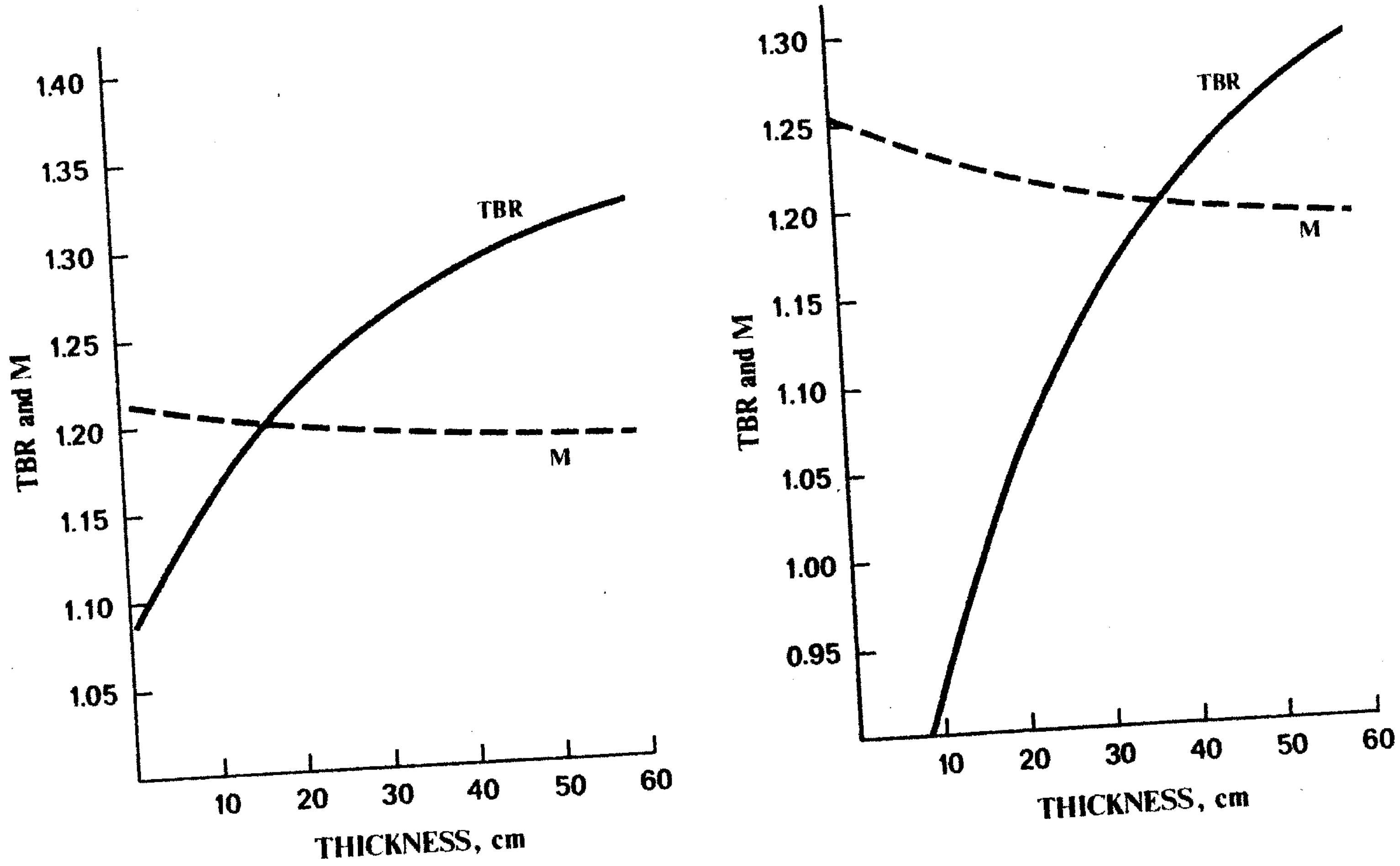

Figure 4.5: Energy Multiplication Factor and Tritium Breeding Ratio versus Blanket Thickness

TF coil due to its proximity between the blanket system and the TF coil. Even so, at a blanket thickness of 20 cm, the OH lifetime is almost ten years.

These facts indicate that the TF coils could be made to last the lifetime of the plant even with very thin blankets but the OH coil will probably require periodic replacement. This should not adversely impact the design, however, since the lifetime of the first wall will likely be less than ten years. (Using the fact that the vanadium first wall structure is estimated to be capable of withstanding up to $\approx$ 220 dpa [43] and that it accumulates about 11 dpa per MW$\cdot$ y/m^2, the first wall lifetime is less than 7 years at a neutron wall loading of 3 MW/m^2.)

The lifetime of the outboard toroidal field coil versus the outboard blanket thickness is also shown in figure 4.6. The adequate survival of this component requires much thicker blanket thicknesses than the inboard case due to the absence of the intervening ohmic coil. Even so, a full power life of 30 years (corresponding to a 40 year plant life at 75 % availability) is achievable with an outboard blanket thickness of 60 cm. However, lithium is relatively transparent to neutrons and increasing the reflector thickness is a more effective method of increasing the coil lifetime.

4.4.4 Reflector Thickness Tradeoffs

Parametric trade-offs for TBR, M and coil lifetime were performed for varying reflector thicknesses both inboard and outboard. Lithium volumetric fractions were kept constant in the reflector at 20 % inboard and 10 % outboard. The blanket thicknesses inboard and outboard were 20 cm and 40 cm, respectively.

The results of the trade-offs for TBR and M are depicted in figure 4.7. The behavior of the curves with increasing reflector thickness is similar to that of those guiding the trade-offs versus blanket thickness. Increased reflector thicknesses result in an increased number of neutrons which are available in the blanket region for capture in Li-6 and thus increase tritium breeding and decrease energy deposition. In contrast to the performance of the blanket trade-offs, the behavior of the reflector is quite comparable for inboard and outboard sections.

Figure 4.8 shows the lifetime of the various coils versus reflector thickness. For the inboard TF coil, 30 cm of HT-9 reflector appears sufficient to provide a 30 FPY life. The same thickness provides only a five year life for the OH coil

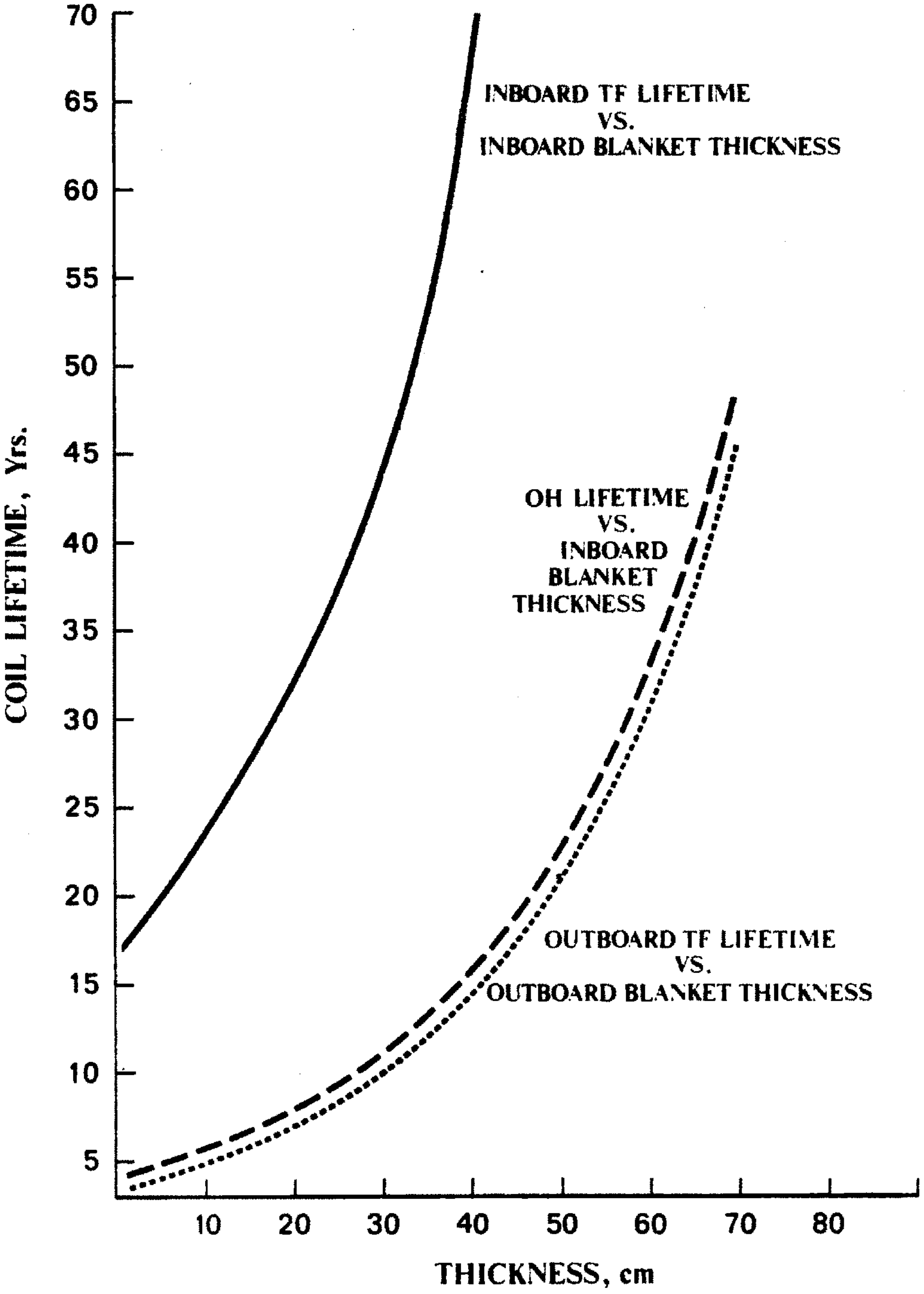

Figure 4.6: Coil Lifetime versus Blanket Thickness

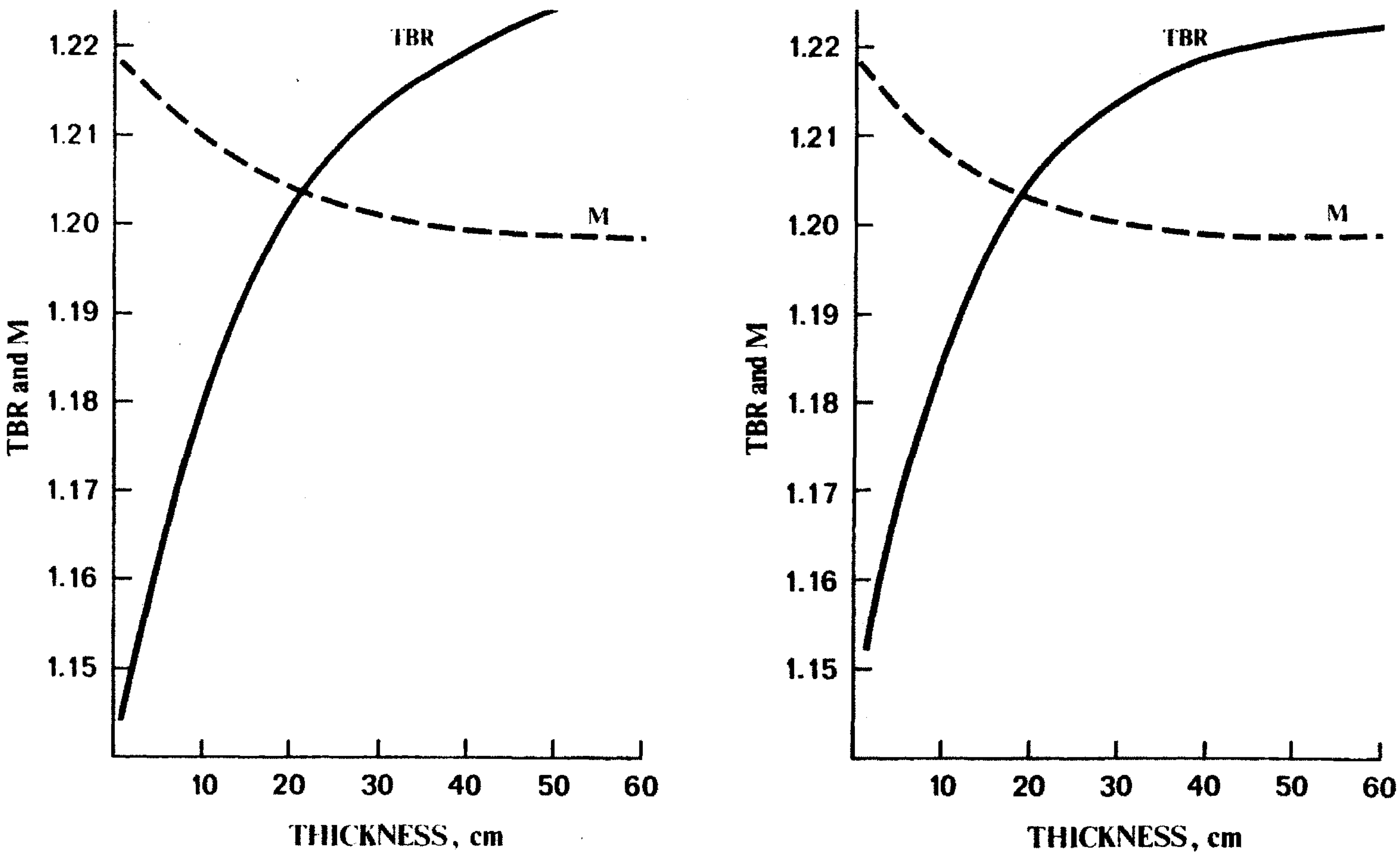

Figure 4.7: Energy Multiplication Factor and Tritium Breeding Ratio versus Reflector Thickness

but another 10 cm will double that lifetime. The curve showing outboard TF coil lifetime versus outboard reflector thickness indicates a somewhat thicker reflector is desirable outboard. A 30 FPY life for this coil is provided by a 45 cm reflector.

4.4.5 Neutronics Summary

A neutronics analysis of the RCTR system with a self-cooled natural liquid lithium blanket and vanadium structure was performed. A number of reflector material options, a lithium cooled, vanadium structure first wall and toroidal and ohmic field coils with copper conductor were considered in the analysis.

The design is substantially driven by the need to protect the coil components from radiation damage. The toroidal field coils can last the lifetime of the power plant without the use of a dedicated shield (using the protection of the reflector) and with a very compact blanket system in comparison to typical superconducting magnet designs. The ohmic coil, located internal to the toroidal field coils, will probably have to be replaced with the first wall every 4 - 8 years.

TBR is not a major driver of the design as adequate tritium breeding is attainable even with very thin breeding regions inboard. The choice of reflector material is driven by the desire for highest energy multiplication in light of adequate tritium breeding with most materials. Of the high-Z materials performing well, HT-9 was chosen as the reference reflector material because of a combination of low cost and favorable compatibility with liquid lithium.

Based on criteria for adequate TBR, M and coil lifetime, a 10 - 20 cm breeding region inboard and 35 - 40 cm breeding region outboard appears adequate. The absence of a breeding region inboard appears to be possible but quite marginal. It will be shown in the next section, however, that the thickness of the inboard blanket may be driven by MHD pumping considerations and not neutronics. The optimum reflector thicknesses are 30 - 35 cm inboard and 40 - 45 cm outboard.

4.5 Supporting Analysis

In addition to the neutronic behavior of the blanket/first wall system, there are other considerations which are important characterizers of the system and are potential drivers of the configuration. These considerations include MHD

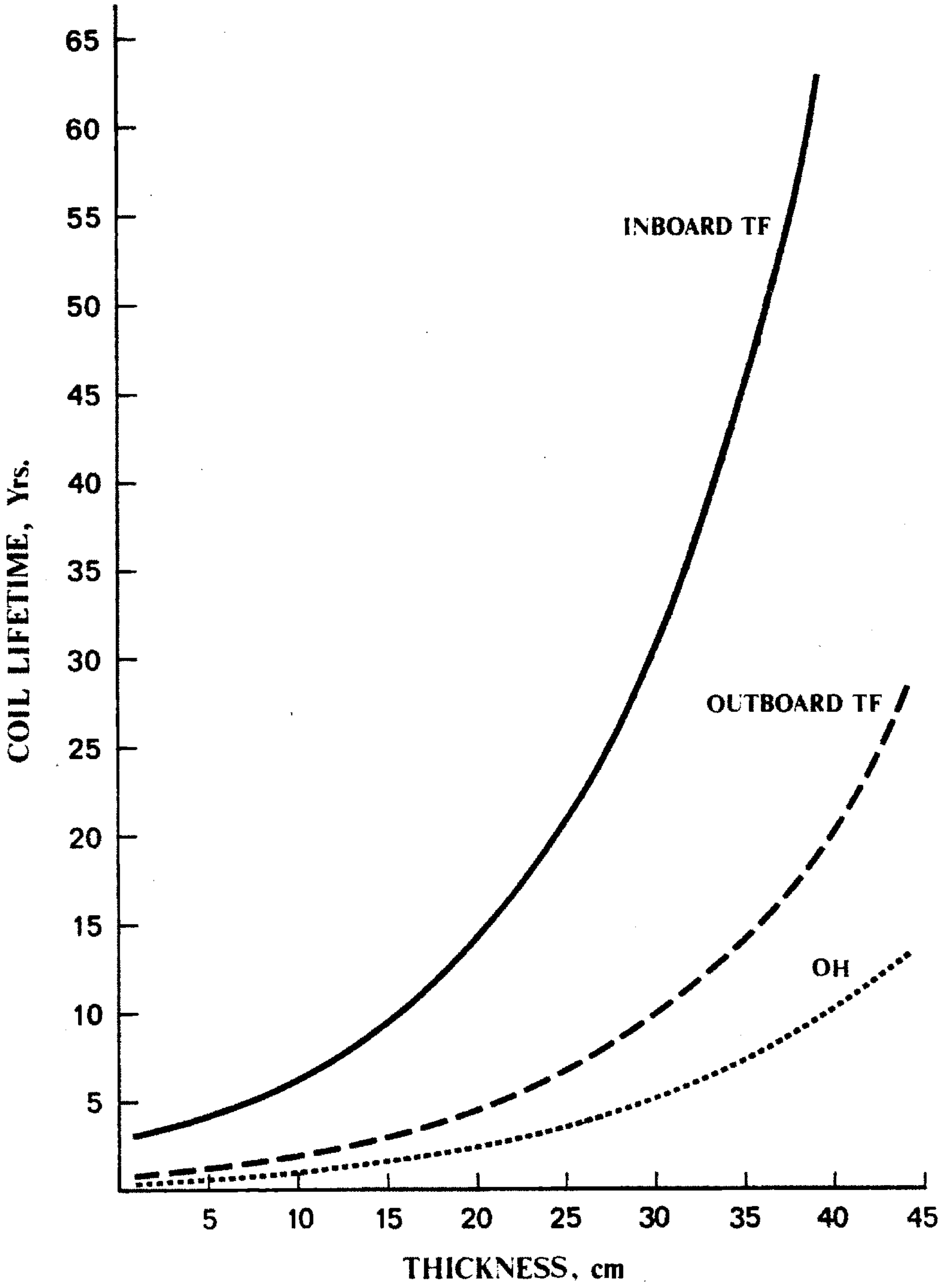

Figure 4.8: Coil Lifetime versus Reflector Thickness

pumping requirements for liquid lithium systems, primary and thermal stresses and weight. MHD pumping and primary stress considerations are closely tied because the pressure drop associated with MHD effects leads to structural requirements on the flow channels and their support. The pumping power required by lithium pumped systems is generally moderate and a minor concern. Weight is an important characteristic for the RCTR system because of the need for regular removal of various components.

In the following sections, the methods used to evaluate the characteristics noted above will be presented. The computer code written to calculate these parameters in a realistic geometry will also be discussed as well as the results of the analysis' and their impact on the blanket/first wall design.

4.5.1 MHD Pumping Losses

The interaction of a flowing liquid metal with a transverse magnetic field results in body forces which influence the liquid metal and require the application of pumping pressure to overcome their retarding effect. This phenomenon, commonly known as the magnetohydrodynamic (MHD) effect, comes about due to the interaction of currents induced in the flowing conducting fluid by the imposed magnetic field with that magnetic field. The result is a force or pressure gradient which scales as the vector product of the current density and the applied magnetic field. This pumping loss is large and generally dominates the total pressure drop in systems of interest for RCTR.

MHD pressure drop is not yet completely understood in the complex geometry of fusion blanket systems. However, the relations used to model the effect in this study, documented in the recent Blanket Comparison and Selection Study (BCSS) [37], are the best available and are estimated to be accurate to within 25 %.

The MHD Pressure gradient in transverse magnetic fields for circular pipes with relatively thin walls is:

$$\frac{dP}{dx} = \sigma V B^2 \frac{\phi}{1+\phi} \tag{4.1}$$

where p is the pressure, x is the dimension along the direction of the flow, σ is the fluid electrical conductivity, V is the average fluid velocity, B is the magnitude of the local magnetic field, and ϕ is:

$$\phi = \frac{\sigma_w t_w}{\sigma a} \tag{4.2}$$

where σ_w is the electrical conductivity of the wall material, t_w is the thickness of the duct wall locally and a is the half width of the duct locally.

The pressure gradient scales with the square of the field so the low field character of RCTR designs is helpful here. For flow transverse to the field, its clear that large ducts are helpful because the gradient scales linearly with flow velocity and inversely with the size of the duct. However, a fundamental difficulty is introduced by the near linear scaling of the pressure drop with duct wall thickness because the hoop (primary) stress created in the duct by this pressure drop scales inversely with wall thickness.

Thus, an increase in thickness of a conducting duct wall will not result in a proportional decrease in the applied stress because of a concurrent increase in the applied pressure. A method of circumventing this problem is to insulate the duct wall either with insulating coatings or a laminated design where the insulator is sandwiched between the structural wall and a thin layer ($\approx$ 0.25 mm) of additional structural material. An investigation of the latter approach in the BCSS study concluded that such laminations are feasible even in regions of high radiation fluxes with the exception of the first wall where the insulator's low thermal conductivity could adversely effect the heat transfer. The use of laminated insulation (an option in this study) decouples the relations for pressure drop and primary hoop stress and results in markedly reduced pressure drops because t_w in the above expression is replaced by the thickness of the thin metal coating (an order of magnitude improvement).

In addition to the basic MHD pressure gradient formulation above, a number of other relations are available for special conditions. For pressure drops associated with abrupt changes in field (such as an inlet) or a bend in the plane normal to B, the pressure drop is:

$$\Delta P = 0.2\ \sigma V a B^2 \sqrt{\phi}. \tag{4.3}$$

For a fluid direction change from that normal to the magnetic field direction to a direction along the field, the pressure drop is:

$$\Delta P = 0.5\ (VB)^{4/3}(\sigma a)^{2/3}\rho^{1/3} \tag{4.4}$$

where ρ is the density of the fluid and a and V are associated with the channel normal to B. The original expression for the pressure gradient in a transverse magnetic field applies to a uniform magnetic field. However, if the magnetic field variations are small enough, the expression can be integrated to find the pressure drop in a field varying inversely with radius. The result is:

$$\Delta P = \sigma V {B_o}^2 {R_o}^2 (\frac{1}{R_1} - \frac{1}{R_2}) \frac{\phi}{1+\phi} \tag{4.5}$$

where B_o and R_o are the magnetic field and radius, respectively, on the axis of the plasma and R_1 and R_2 are the radii at each end of the coolant duct of interest.

These expressions cover the situations encountered in a typical fusion blanket design and are used to estimate the MHD pressure drop for RCTR.

4.5.2 Stress Analysis

Primary stresses set up as a result of the MHD pressure drops in the blanket system and thermal stresses created in the first wall by temperature gradients were considered in the present analysis. As indicated earlier, the primary stresses are closely tied to the MHD pressure gradients and can have a significant impact on the blanket/first wall design. Thermal stresses can limit the thickness of the first wall although this problem tends to be minimized by the excellent thermo-physical characteristics of vanadium. Plasma disruption and earthquake loads were not considered in the present study.

In a series of rectangular ducts under internal pressure, common walls have no pressure gradients normal to their plane but they do experience tensile loads in their own plane equal to the hoop stress:

$$P_h = \frac{Pa}{t_w} \tag{4.6}$$

where P is the internal pressure and 'a' is the duct half width. This expression also governs the hoop stress in cylindrical ducts under internal pressure but with 'a' as the radius of the duct.

The duct walls which are not common to other ducts experience a net pressure normal to their plane. These walls act as plates in bending supported on their edges. The bending stress for rectangular plates is [44]

$$P_b = \frac{1}{2} P \frac{l^2}{{t_w}^2} \tag{4.7}$$

where l is the width of the plate ($= 2a$). For locations at which the first wall becomes the duct wall under pressure such as inside the first wall manifolds and inner blanket channels, an alternate expression for primary bending is applicable. In this case, the first wall acts as a composite beam in bending. This situation was analyzed in detail as part of the BCSS study and the result is given for manifolds directed at arbitrary angles to the vertical. We simplify the result here for the vertical ducts of the RCTR blanket system yielding:

$$P_{b,fw} = \frac{Ez}{(D_x - \nu^2 D_y)} \frac{Pl^2}{12} [1 + \frac{\nu^2}{1-\nu^2} (\frac{D_x - D_y}{D_x})] \tag{4.8}$$

where D_x and D_y are the flexural rigidity in the toroidal and poloidal directions, respectively:

$$D = \frac{El^3}{12(1-\nu^2)} \tag{4.9}$$

E is the elastic modulus of the structural material and z is the distance from the centroidal axis of the first wall system to the plasma side of the first wall itself. We note also that this expression reduces to that of the flat plate solution for $D_x = D_y = D$.

Large temperature gradients set up across the first wall due to a combination of the surface heat flux and neutron energy deposition can lead to significant thermal stresses. The magnitude of the thermal stress can be written [45]:

$$\sigma_{th} = \frac{\alpha E}{1-\nu} \Delta T \tag{4.10}$$

where α is the coefficient of thermal expansion for the structural material, ν is Poisson's ratio and ΔT is the temperature difference between the coolant to structure interface directly behind the first wall and any point in the wall itself. The temperature distribution in the first wall is:

$$T(x_1) = \phi_t \frac{(t_{fw} - x_1)}{k} + q''' \frac{({t_{fw}}^2 - {x_1}^2)}{2k} + T_0 \tag{4.11}$$

where T_0 is the interface temperature at $x_1 = 0.0$, x_1 is the radial depth into the first wall, k is the thermal conductivity of the structural material, ϕ_t is the surface heat flux and q''' is the volumetric heat deposition. The temperature difference, ΔT, is equal to $T(x_1) - T_0$. The maximum temperature, leading to the maximum thermal stress, occurs at $x_1 = t_{fw}$:

$$T_{max} = \frac{\phi\ t_f w}{k} + q''' \frac{t_{fw}{}^2}{2k} + T_0. \tag{4.12}$$

Material properties are evaluated at the average metal temperature which is found by integrating the temperature distribution with the result:

$$T_{avg} = T_{max} - \frac{1}{k}[\frac{\phi\ t_{fw}}{2} + \frac{q'''t_{fw}{}^2}{6}]. \tag{4.13}$$

Each of the stresses discussed must be restricted to some maximum design value to assure the integrity of a given concept. The present analysis incorporates the accepted practice of following guidelines derived from the ASME Boiler Code Case N-47 [36]. Limits are placed on the magnitude of primary and secondary (e.g. thermal) stresses encountered in the design based on the maximum permissible stress intensity S_{mt}, which is defined as the smaller of a primary stress intensity limit, S_m, and an elevated temperature stress intensity limit S_t. S_m is limited by criterion placed on the yield and ultimate strengths of the material while S_t is based on creep-based limits. For vanadium, acceptable irradiated values of S_{mt} are 165 MPa at 100 dpa, 125 MPa at 150 dpa and 105 MPa at 200 dpa in a temperature range of 20 C to 700 C. For temperatures exceeding 700 C up to 750 C, S_{mt} is degraded somewhat to 155 MPa, 115 MPa, and 95 MPa at 100 dpa, 150 dpa and 200 dpa, respectively [37].

4.5.3 Blanket/First Wall System Analysis Code

A code was written to analyse the MHD flow and stress aspects of the RCTR blanket/first wall system. The code models the blanket and first wall systems in a relatively realistic geometry and finds the power deposition distribution, MHD pressure drops, stresses and weights associated with that system. The code, like RTPAC, is written in MACSYMA and runs on a PDP-11.

The geometry of the blanket/first wall system as it is modeled in the code is shown in figure 4.9. The input for the geometry consists of the plasma and

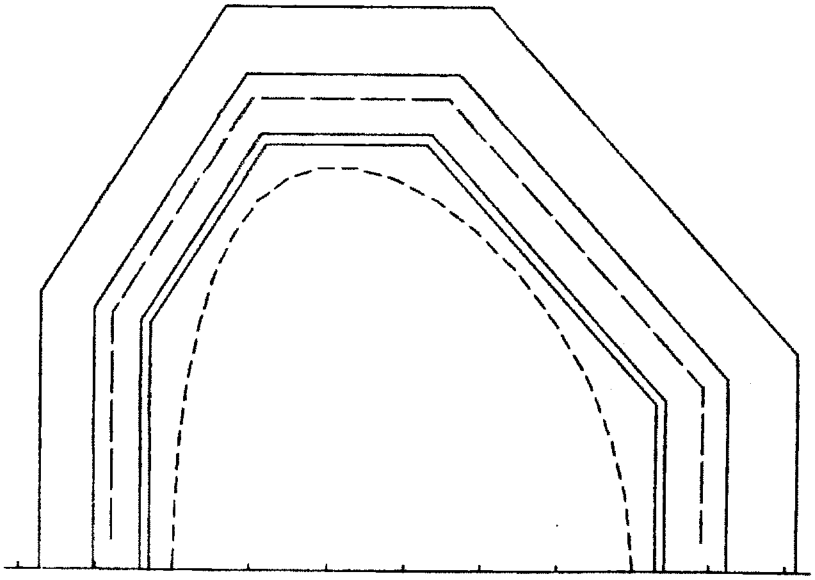

Figure 4.9: Geometry Used by Blanket System Code

scrape-off dimensions as well as the thicknesses of each material region represented. Dimensions of a given component on the inboard, top and outboard sides of the system are variable independently. The code begins by setting up the geometry as shown and calculates volume and mass for all components of interest.

The temperature distribution and thermal stress encountered in the first wall is found according to relations presented in the previous section. Given the surface heat flux and the neutron wall loading, the code calculates the total thermal power in the system as:

$$P_{th} = \phi_t A_w + P_n M A_w f_l \tag{4.14}$$

where A_w is the first wall area, M is the blanket energy multiplication factor obtained from the neutronics and f_l is the fraction of the energy assumed to escape from the system. The power deposited in each of the regions of interest is then found using region-wise energy deposition data from ONEDANT.

The mass flow rate required to remove the heat deposited in a given region is then found from:

$$m_{f,i} = \frac{P_i}{C_p \Delta T_i} \tag{4.15}$$

where P_i is the power deposited in region i, C_p is the specific heat of the coolant and Δ_{T_i} is the temperature rise of the coolant between inlet and outlet of region i. Then the velocity of the coolant in a given channel of a given region is:

$$v = \frac{m_{f,i}}{A_i \rho_c} \tag{4.16}$$

where $m_{f,i}$ and A_i are the mass flow rate and cross-sectional area normal to the flow of the coolant, respectively, in the channel of region i, and ρ_c is the density of the coolant. Applying these relations to the entire system, taking into account changing cross-sectional areas as the coolant proceeds from inlet to outlet, the pressure drop distribution can be found using the results of section 4.5.1.

The code also allows the thickness of the channel walls to vary in different regions. This is a useful design technique for reducing the total pressure drop of a system of uninsulated channels because the local pressure drop decreases as the coolant travels toward the outlet. The decreasing local pressure drop results in thinner wall thicknesses required locally to withstand the applied pressure which in turn decreases the pressure drop itself because ΔP scales almost linearly with wall thickness.

Finally, with all pressure drops determined, the primary tensile and bending stresses created in the first wall, manifolds, and coolant channels can be evaluated. The code also allows three options for the use of insulated channels in the analysis. The first option assumes no insulated channels are used. The second option, termed 'partially insulated', assumes that regions in relatively low radiation fields are insulated which include the inlets, outlets and the reflector channels of the blanket systems. The third option, termed 'full insulation', assumes that all lithium flow channels are insulated except for the first wall channels which are in the region of highest irradiation but do not require insulation because of their direction along the magnetic field lines.

Major Radius, m	7.5
Minor Radius, m	1.5
Elongation	1.8
Field on Axis, T	2.7
Neutron Wall Loading, MW/m^2	3
Surface Heat Flux, MW/m^2	0.75
First Wall Thickness, cm	0.6
First Wall Support Thickness, cm	2
First Wall Channel, cm × cm	4 × 2
First Wall System Thickness, cm	6.6
Inboard Blanket Thickness, cm	25
Outboard Blanket Thickness, cm	45
Inboard Reflector Thickness, cm	35
Outboard Reflector Thickness, cm	35

Table 4.4: Reference Input Parameters for Blanket Analysis

4.5.4 Supporting Analysis Results

The blanket/first wall system analysis code was used to identify the importance of various trade-offs for an RCTR configuration as well as to characterize specific blanket concepts. A set of standard inputs used for the parametric analysis is given in table 4.4.

The impact of incorporating insulated channels in the design is indicated in table 4.5 which shows pressure drops and stresses for the cases of no insulated, partially insulated and fully insulated lithium channels. The standard case of table 4.4 is used for the comparison. Partial insulation doesn't improve the first wall system's pressure drop and pumping power significantly because both the first wall channels and manifolds remain uninsulated. The blanket system pressure drop does decrease significantly, however, due to insulation of the reflector channels. Peak stress due to blanket pressure drops also improves significantly. Marked improvement occurs when the blanket/first wall system becomes 'fully insulated' with the total pressure drop now only 1.2 MPa. In this type of configuration, other contributions to the pressure drop such as friction may become significant. However, pressure drop probably ceases to be a significant design consideration in this case.

The sensitivity of lithium flow related parameters to the thickness of the inboard and outboard breeding regions is shown in figure 4.10. The standard

Parameter	No Insul.	Partial Insul.	Full Insul.
First Wall ΔP, MPa	4.9	4.6	0.9
First Wall Pump Power, MW	9.4	8.7	1.7
First Wall Max. Stress, MPa	139	129	25
Blanket ΔP, MPa	3.7	2.2	0.3
Blanket Pump Power, MW	12.1	7.2	0.9
Blanket Max. Stress, MPa	330	197	26

Table 4.5: Insulated vs Uninsulated Lithium Channels

case of table 4.4 is used except the width of the blanket regions is allowed to vary. Partial insulation is assumed. The curve for the inboard blanket indicates that significant improvements can be made in pressure drop and pumping power even as the thickness increases beyond 30 cm. Thus, lithium pumping appears to have a greater impact on the inboard blanket than the neutronics for partial (and totally absent) insulation. For the fully insulated case, neutronics would again dominate the design. This figure also shows that the first wall pressure drop is generally significantly higher than the blanket ΔP because of relatively high velocities required in the first wall manifolds.

The second curve of figure 4.10 indicates that the outboard blanket is not dominated by pressure drop considerations even with partially insulated channels. Increasing the outboard blanket thickness to 40 cm (the approximate size dictated by the neutronics) achieves most of the benefit for lithium flow associated with increasing blanket width.

One possible remedy for decreasing the impact of lithium flow on the inboard blanket is to increase the lithium flow area in the inboard reflector region. In figure 4.11, the total blanket pressure drop is plotted against the fraction of flow cross-section available to lithium in the inboard reflector. The curve indicates that significant increases in the lithium fraction only have a moderately beneficial impact on lithium pumping. Since an increase in the lithium fraction here will decrease energy deposition and increase tritium breeding, this option does not present a significantly effective method of improving the inboard blanket design.

The impact of increased wall loading on lithium flow for the standard case of table 4.4 is indicated in figure 4.12. Increasing wall loading turns out to be a significant liability for lithium pumping because the higher corresponding fusion

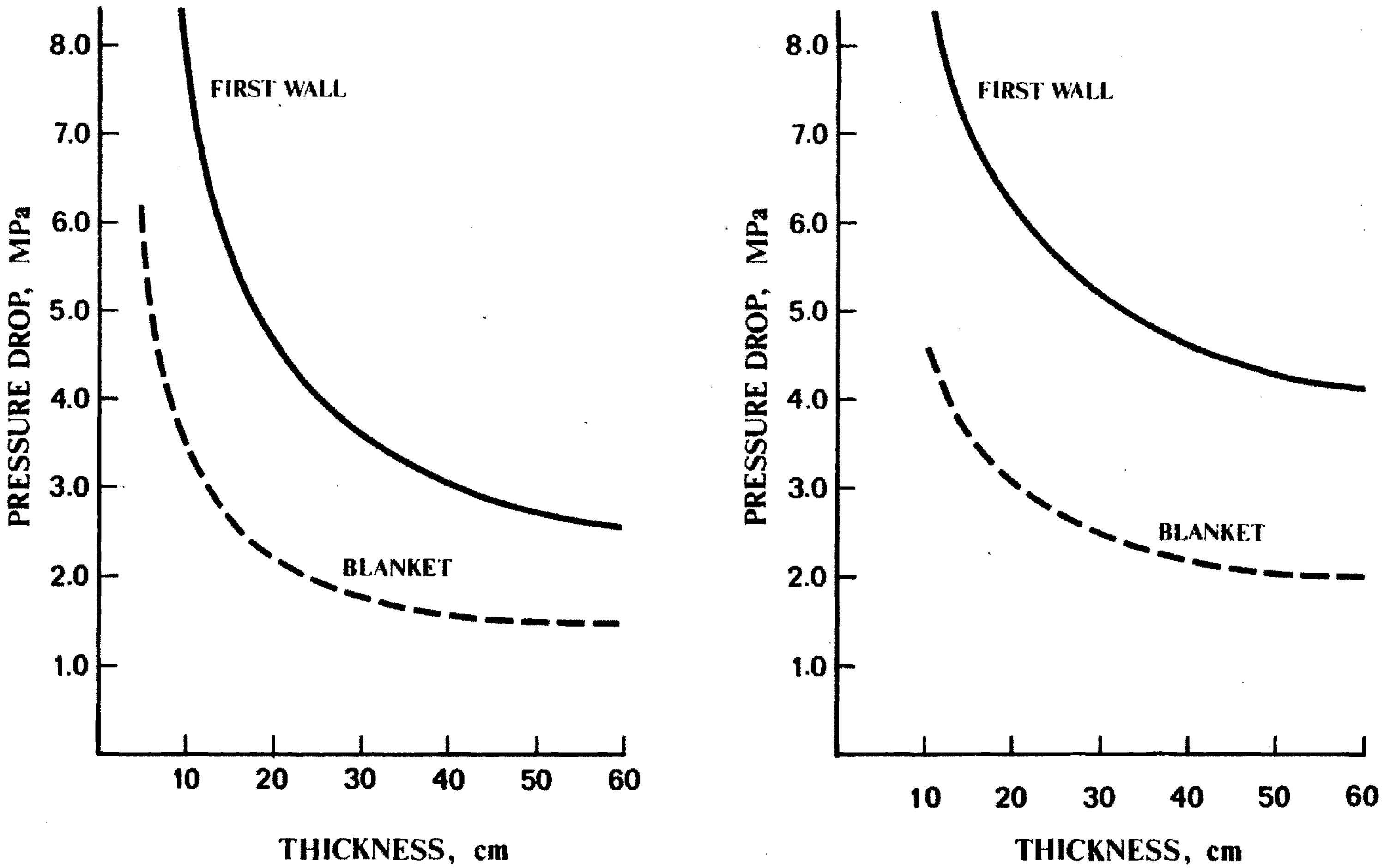

Figure 4.10: Lithium Flow Parameters versus Blanket Thickness

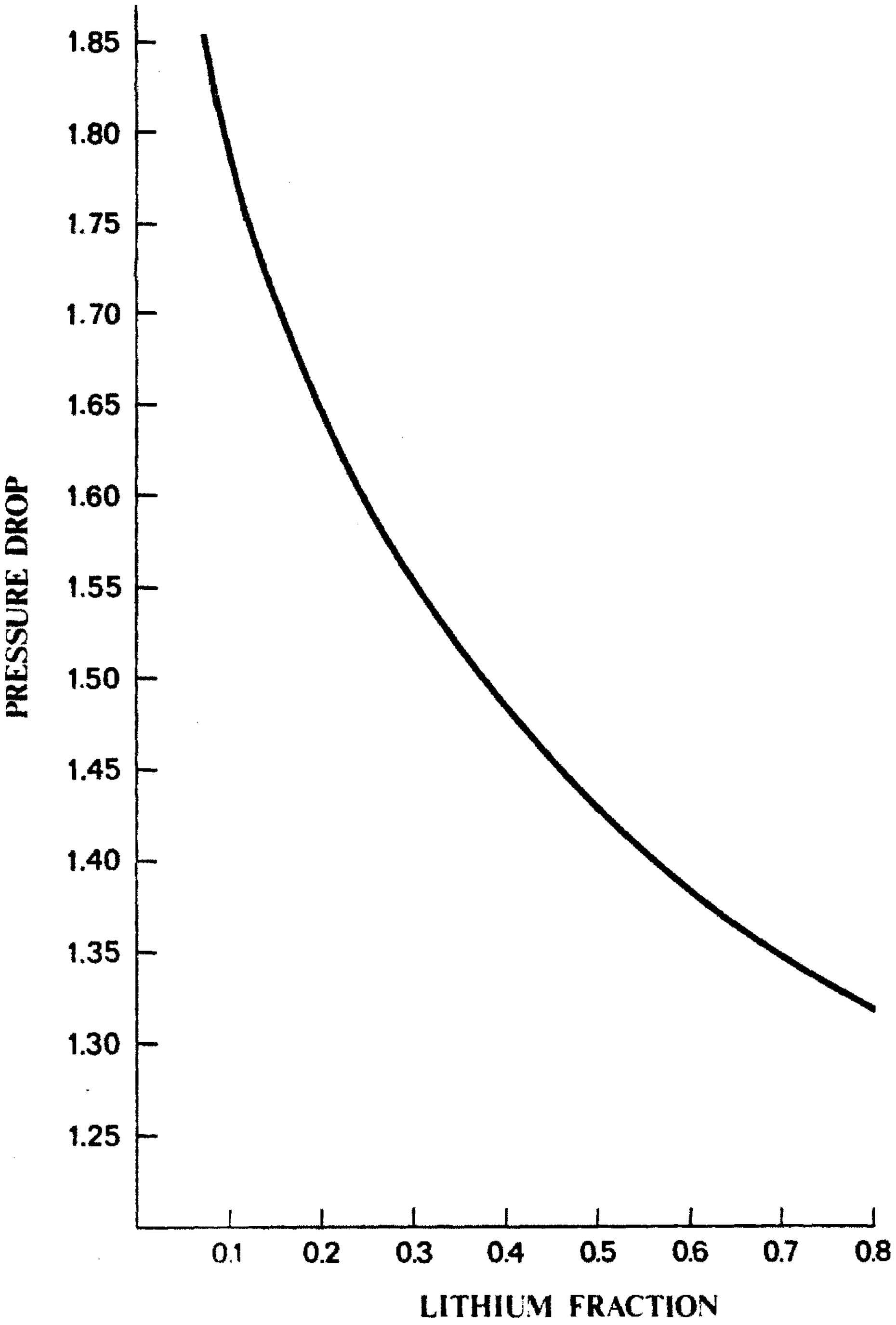

Figure 4.11: Pressure Drop versus Reflector Lithium Flow Cross-Section

power results in more power removal requirements with correspondingly higher flow rates and velocities. This effect is magnified by the increased magnetic field required to deliver the higher fusion power density.

Detailed characteristics of the illustrative case are as shown in table 4.1 and table 4.2. This case was arrived at using the above trade-offs and additional considerations to be discussed in the context of tables 4.1 and 4.2. The example shown is for the 1200 MW_e, 3 MW/m^2, high beta reference case A of chapter 2 (table 2.9). The heat flux at the first wall is assumed to be 0.75 MW/m^2 and no insulated channels are included. The length (toroidally) of the first wall manifold is 50 cm. The length of this manifold is restricted on the low end by the resulting small flow cross-sections and high velocities and on the high end by large bending stresses at the first wall.

The velocity of the lithium in the first wall channels is 0.67 m/s while in the first wall manifold it varies between 0.61 and 0.94 m/s. The peak primary stress intensity is 104 MPa. This stress occurs in the manifold walls and across the first wall near the inlets where the pressure drop is highest. Although the pressure drop in the blanket is half that in the first wall, the width of the inboard blanket is an important parameter because it also governs the width of the first wall manifold (the most critical area).

Note that the inboard blanket (breeding region) width of 35 cm is significantly larger than that dictated by neutronics considerations because of the need to satisfy peak primary stress intensity limits (for a first wall lifetime of 200 dpa, the maximum design stress was 105 MPa). The inboard blanket thickness could be decreased by 5 - 10 cm by either accepting only a 150 dpa lifetime (for an increased stress allowance to 125 MPa) or by insulating the channels in areas of low radiation flux. Only modest benefits accompany this partially insulated case because the peak stress in the first wall remains high even though the total pressure drop decreases significantly. As indicated earlier, full insulation would allow very thin inboard blankets and eliminate lithium flow as a crucial consideration in the design.

No credit has been taken for insulated channels in the reference design. First of all, there are still feasibility issues associated with laminated insulators which need to be examined experimentally. In addition, the use of insulated channels would increase both the complexity and the cost of the RCTR blanket/first

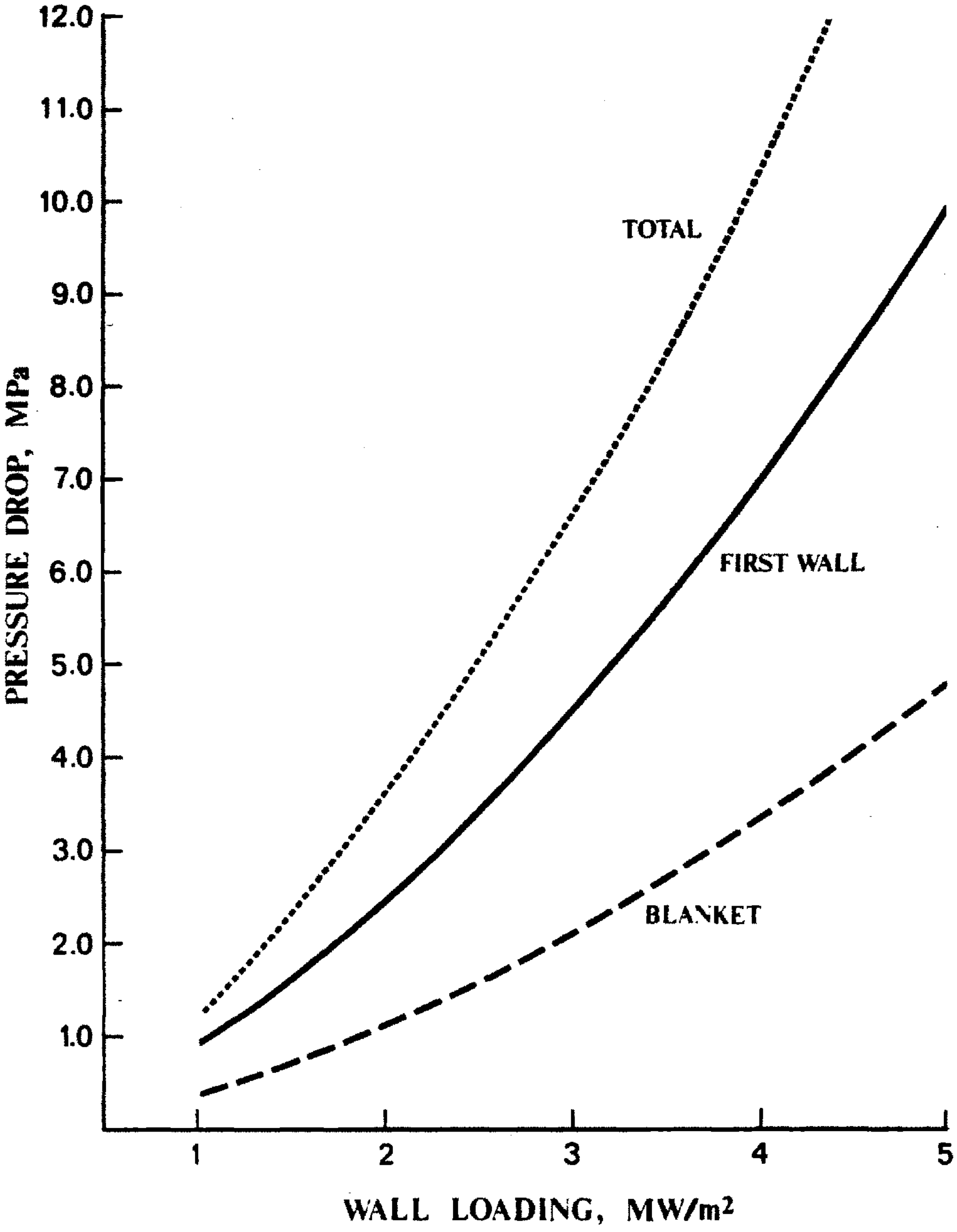

Figure 4.12: Lithium Pressure Drop versus Wall Loading

wall system. Lastly, the design without insulated channels is acceptable and still incorporates a relatively compact system. If issues such as extremely thin inboard blankets or higher wall loading became important, insulated channels would become a more desirable option.

4.6 Summary

A conceptual design for the RCTR blanket/first wall system has been developed based on configurational, neutronic, and lithium flow associated considerations. The design is compatible with the demountable toroidal field coil concept and emphasizes high performance with low complexity. The reference concept uses a self-cooled lithium breeder with vanadium structure and an HT-9 reflector and is relatively compact with no dedicated neutron shield. The blanket system provides sufficient shielding to the magnet coils such that the toroidal field coil can last the life of the plant while the ohmic field coil needs to be replaced periodically with the first wall. Lithium pressure drop considerations are important but manageable with proper design even for uninsulated flow channels.

Chapter 5

Accessible Beta and Tokamak Reactor Design

5.1 Introduction

Toroidal beta is the dimensionless parameter characterizing a tokamak plasma defined as the ratio of plasma pressure to toroidal magnetic field pressure:

$$\beta = \frac{2p}{B^2/2\mu_0} \tag{5.1}$$

where p is the plasma pressure (product of plasma density and temperature) and B is the magnetic field strength. Beta is a fundamentally important parameter in tokamak reactor design because it characterizes plasma confinement limits and provides a key scaling factor in the expression for fusion power density:

$$P_v \propto \beta^2 B^4. \tag{5.2}$$

Thus, increasing beta improves fusion power density significantly for a given magnetic field strength up to some maximum limit on beta which may depend on various other reactor parameters. The exact form of this beta limit is not well known but a number of theories and scaling relations based on experimental data exist and are in use.

In this chapter, we present the major scaling relations presently available which describe beta as a function of plasma parameters and discuss some of their limitations and how they affect tokamak reactor design. Since beta is such an important parameter to the reactor designer, some degree of understanding of the available theory and its limitations is helpful in assuring the proper use of the available beta scalings. At the same time, its the responsibility of the reactor designer to evaluate the potential of beta regimes which certainly lie outside present experimental experience and may not yet be completely described even theoretically.

At this time there is little apparent communication between the tokamak theorist who studies the phenomena limiting beta and the tokamak designer who is interested in how reactors scale with accessible beta. In this chapter we will attempt to briefly review current theory and practice with regard to beta limits as they affect reactor design, evaluate the price of uncertainty with current knowledge and make recommendations on how this information might best be used in reactor design applications.

In section 5.3, conventional or first stability beta relations will be discussed. The possibility of beta existing in the second regime of plasma stability will be discussed in section 5.4. This theory has become popular among reactor designers in recent years because of the promise of the higher beta predicted but a number of uncertainties still exist regarding its viability for practical reactors. First, we present a simplified description of some of the most important terms and parameters used in the discussion of beta limits.

5.2 General Considerations

Major limits on toroidal beta, β, and other parameters affecting the beta limit can be described using the ideal magnetohydrodynamic (MHD) theory of fusion plasmas [14]. Much of the currently available literature on beta limits makes use of MHD theory and a brief discussion of some important concepts from MHD is useful towards understanding the form and region of validity for these formulations.

Beta limits generally come about as a result of various MHD instabilities which arise in a plasma and cause a loss of confinement. These instabilities can be grouped into two categories: current driven modes and pressure driven modes. Current driven modes arise from currents parallel to the magnetic field while pressure driven modes arise from pressure gradients and are driven by perpendicular currents. MHD instabilities may also be classified as either external (plasma boundary moves during unstable perturbation) or internal (plasma boundary fixed during perturbation).

5.2.1 Kink Mode Stability

External kink modes are an important current driven instability in tokamaks that manifest as helical 'kink' perturbations off the magnetic axis. Internal kinks are not as important in tokamak stability and can be stabilized in a manner similar to external kinks. One class of external kink modes (long wavelength oscillations) can be suppressed either by limiting the parallel (toroidal) current at fixed geometry or limiting the major circumference (i.e., the aspect ratio) of the plasma at fixed current. The stability condition for this class of kink modes is the Kruskal-Shafranov condition, $q_a \geq 1$ [14]. The safety factor, q_a, (also known in the literature in various forms q_s, $q(l)$ and q_{mhd}) is the change in the toroidal angle of a magnetic line as it completes a poloidal circuit and can be defined as:

$$q_a = \frac{\epsilon B_0}{2\pi} \int_0^{2\pi} [\frac{d\theta}{B_\theta(a,\theta)}]. \tag{5.3}$$

This q_a is actually the safety factor evaluated at the outer plasma radius, a, derived from the more general form:

$$q_\psi = \frac{1}{2\pi} \int_0^{2\pi} [\frac{rB_t}{RB_\theta}]_s d\theta \tag{5.4}$$

where r is the minor radial dimension, R is the major radial dimension, B_t is the toroidal magnetic field and B_θ is the poloidal magnetic field. The subscript 's' indicates that the integration is done over the flux surface at which the field line is located.

The safety factor should not be confused with a similar expression identified as q^* or q_I in the literature and defined as:

$$q^* = \frac{2\pi a \epsilon B_0}{\mu I_p} F(k) \tag{5.5}$$

where a is the minor plasma radius, B_0 is the toroidal magnetic field on the axis of the plasma and $F(k)$ is a function of elongation which varies depending on the particular definition [16,14]. These two definitions of q are identical as beta approaches zero (or aspect ratio approaches infinity) but can be quite different at higher beta values ($q_a \geq q^*$). The existence of both q's is pointed out here to emphasize the fact that stability criteria based on q-type limits exist in the literature for various maximum beta investigations in a number of forms depending on the q definition and profiles used in the analysis. As seen below, another important stability limit is expressed in terms of q^* and the form of the q's in question should not be confused. The dilemma of multiple q definitions and how they affect the interpretation of available beta scalings will be discussed further in the next section.

Another class of kink modes (shorter wavelength) important for stability limits are more sensitive to the current profile than the magnitude of the current itself [14]. In this case, large current gradients at the plasma surface apply a destabilizing torque on the plasma which is corrected with the use of a more peaked current profile [14]. The existence of a conducting wall at close proximity to the plasma and/or active feedback stabilization of the plasma may be effective in suppressing kink instabilities sensitive to large current gradients [14].

In summary, current driven instabilities tend to drive tokamaks to low aspect ratio, some maximum value of plasma current and peaked current profiles to comply with the desirability of higher beta.

5.2.2 Ballooning Mode Stability

Pressure driven modes also play a major role in beta limitations. In regions where the magnetic field lines are convex to the plasma (as at the outside of a torus), an interchange of adjacent flux tubes at different radii can lead to a system with lower potential energy and an unstable situation [46]. In a tokamak, where the magnetic field lines pass through regions of alternatively bad (field lines convex to the plasma) and good (field lines concave to the plasma) curvature, perturbations concentrating in regions of bad curvature can lead to instability. Modes of this type are known as ballooning modes and they are stabilized most effectively by limiting the plasma pressure and thus limiting the magnitude of beta.

For internal ballooning modes, the maximum current density on the axis of the tokamak is limited to assure that the average curvature as the field lines pass about the torus is favorable. This results in a limit being placed on the safety factor evaluated at the axis of the plasma, q_0, $q_0 \geq 1$ known as the Mercier criterion [47].

Even when the q_0 condition is satisfied, sufficiently high plasma pressure will still drive ballooning modes and lead to instability. The most stable configurations against ballooning modes usually have broad pressure profiles with sharp gradients near the surface of the plasma because large magnetic shear (a quantity proportional to the rate of change of q with plasma radius) is stabilizing. That is, perturbations along the field at one radius encounter field lines at an angle as they grow to another radius in systems having large magnetic shear [14]. Note that this desirability for sharp gradients at the plasma surface is not favorable for certain kink instabilities (see above) and the optimum profile may represent some compromise between kink and ballooning requirements.

Also, allowing another degree of freedom in shaping the plasma through elongation and triangularity can improve the average curvature that a field line sees as it traverses the torus. In this case, the connection length, the distance between regions of bad and good curvature, is shortened by moving regions of bad curvature in a circular plasma to areas possessing favorable curvature. Thus, proper plasma shaping can lead to ballooning mode stability at larger plasma pressures. However, highly shaped plasmas tend to suffer more from vertical stability fluctuations known as axisymmetric modes [14]. Vertical stability may be controlled in this case using feedback coils which compensate for any vertical movement of the plasma.

5.2.3 Beta Limit Mechanisms

Beta limits are often expressed in terms of some restrictions on q which come about from MHD stability conditions. For example, a limit on toroidal beta is reached from restrictions on q^* for a given plasma current because of the formation of a magnetic separatrix on the inside of the torus (the poloidal field and vertical field are opposite in direction here). As the plasma pressure (and beta) are increased, the vertical field required to keep the plasma in equilibrium increases and the separatrix shifts towards the plasma. Note that q_a is freely varying. A beta limit is reached when the separatrix reaches the edge of the plasma (which is then no longer confined). For the simplified case of parabolic pressure and constant current density profiles, this limit takes the form:

$$\beta_{eq} = \frac{\epsilon}{q^{*2}}(\frac{1+3k^2}{4}) \tag{5.6}$$

where k is the elongation [14]. This is known as the MHD equilibrium limit because it is derived from considerations of equilibrium described above.

Alternatively, as β is increased, the plasma current could be increased also, keeping q_a fixed but allowing q^* to vary (decrease). In this case, current and vertical field are increased together to keep the plasma in equilibrium and prevent the separatrix from approaching the plasma and no equilibrium limit exists. However, a beta limit will eventually be reached from stability considerations which place a lower limit on q^*.

In general, instabilities leading to limiting betas in tokamaks are a result of both pressure and current driven phenomena. Theoretical examination of both current and pressure driven stability considerations [14] indicates that MHD limits can be expressed in terms of a limit on q^*, $q^* > 1$, and a limit on the plasma pressure expressed in terms of an upper limit on $\frac{\beta}{\epsilon}$. The lower limit on q^* essentially represents an upper limit on the plasma current while the upper limit on $\frac{\beta}{\epsilon}$ is sensitive to aspects of plasma shaping and external boundary conditions such as the presence of a conducting wall.

5.3 Conventional Beta Limits

5.3.1 Theoretical and Experimental Results

A number of theoretical and experimental studies have been carried out which investigate tokamak beta limits. In this section, some of the most prominent first stability beta scalings are described, indicating their formulation and the criterion which are taken into account (e.g., ballooning and kink modes, data base, etc.). The impact of the scaling choice on reactor design is also indicated.

First we note that if $\beta \propto \frac{\epsilon}{q}$ and $q \propto \frac{a^2B}{RI_p}$ then:

$$\beta \propto \frac{I_p}{aB}. \tag{5.7}$$

Most of the available first stability beta scalings are in this form or can be written in this form with a constant and/or a shaping factor as a multiplier. One of the most conservative of these scalings is the Troyon limit [48]:

$$\beta = 2.7 \frac{I_p}{aB}. \tag{5.8}$$

This formulation is a result of computer aided theoretical studies of plasmas with similar aspect ratio and shape to INTOR [49] and JET [50]. The limits found in the study are based on kink mode stability although ballooning modes are also considered in the analysis. The possibility of wall stabilization of some classes of kink modes is not taken into account. A modest amount of study on the effect of plasma shaping was done but the critical beta for a given current was not found to increase with plasma shaping. However, it is pointed out that plasma shaping may lead to higher allowed currents and thus higher critical betas. It is also suggested that optimization of the pressure profile may be helpful in improving stability at higher beta.

Another theoretical study of beta limits suggesting a more optimistic result was done by Sykes el. al. [16]. The result was presented in the form:

$$\beta = \frac{22k}{Aq_j}, \quad \text{where;} \quad q_j = \frac{2B_0}{R_0 J} \tag{5.9}$$

and J is the plasma current density. Note that q_j is a version of q^* with $F(k) = k$ if $J = I_p/(\pi a^2 k)$. These two expressions can be combined to yield:

$$\beta = 4.4 \frac{I_p}{aB}. \tag{5.10}$$

However, caution should be exercised when re-writing expressions in this way because the point at which the use of the formula is extrapolated outside of the range of interest which applied during the study can become clouded. In this case, it should be noted when values of $\frac{I_p}{aB}$ result in betas much above 10 % then extrapolation outside the parameter space of the study is taking place.

The Sykes formulation is based on ballooning mode limits with optimized pressure profiles. However, it is pointed out that increased triangularity can improve kink stability as well as ease the Mercier criterion. Aspect ratios of 3 and 4.5, elongations of 1 - 2 and triangularities up to 0.5 are considered in the analysis.

A theoretical study of beta limits by Tuda et. al. considered separate beta limits for both ballooning and kink mode instabilities [51]. In the case of ballooning modes, the result was:

$$\beta_b = \frac{30\ k^{1.5}}{Aq_s}[1 + 0.9(k-1)\delta - 0.6\frac{k^{0.75}}{q_s} + 14(k-1)(1.85-k)\frac{\delta^{1.5}}{{q_s}^4}] \tag{5.11}$$

where

$$\frac{1}{q_s} = A\sqrt{1 - 1/A^2}(\frac{2}{1+k^2} - 0.08\delta)\frac{\mu I_p}{2\pi a B_0} - 0.07(1 + (k-1)\delta). \tag{5.12}$$

For the kink mode limit, beta took the form:

$$\beta_k = \frac{C\ k^{1.65}}{Aq_s}(1 + (k-1)\delta) \tag{5.13}$$

where C is a constant equal to 14 for q_s between 2 and 3 and equal to 20 for q_s between 3 and 4. This work systematically varies aspect ratio, elongation and triangularity through an unlisted but presumably relevant range of values. The data is fit to the above curves and plotted for betas up to about 10 %. The above expressions are also rewritten in the work in terms of $\frac{I_p}{aB}$ as:

$$\beta_b = (4.0 \pm 0.45)\frac{I_p}{aB} \tag{5.14}$$

$$\beta_k = (3.2 \pm 0.40)\frac{I_p}{aB}. \tag{5.15}$$

The latter expression gives a similar result to Troyon while the former is closer to the Sykes limit which is consistent with the stability limits being emphasized by each paper. The error bars in the formulas account for variations in shaping factors. It is pointed out also that the expression for β_k approaches that for β_p when wall stabilization is accounted for and the two expressions coincide when the ratio of wall radius to plasma radius is 1.5. In addition, the paper emphasizes that elongation and triangularity can cooperatively increase the beta limit.

Its convenient to re-emphasize here that although Tuda and Sykes may yield similar beta limits for similar values of $\frac{I_p}{aB}$, the q's for constant plasma shaping or the plasma shaping factors for constant q may be quite different. This holds true for comparison's amongst any of the scalings whether the beta limits versus $\frac{I_p}{aB}$ are similar or not.

A beta limit formulation based on experimental data from Doublet III (D-III) has been presented by Bernard et. al. [15]. The result is:

$$\beta = 27{q_s}^{-1.1}\epsilon^{1.3}k^{1.2}(1 + 1.5\delta) \tag{5.16}$$

for q_s greater than 2 where;

$$q_s = \frac{5a^2B}{RI_p}(\frac{1+k^2}{2})[1+\epsilon^2(1+\frac{\Omega^2}{2})][1.24 - 0.54k + 0.3(k^2+\delta^2) + 0.13\delta] \tag{5.17}$$

where;

$$\Omega = \beta_p + \frac{l_i}{2}, \tag{5.18}$$

l_i is the plasma internal inductance and β_p is the poloidal beta, the ratio of plasma pressure to poloidal magnetic field pressure. The formulations are based on data with variations in elongation (0.9 - 1.7), triangularity (-0.05 - 0.3), and plasma minor radius (0.36 - 0.44 m). Peak beta achieved was 4.7 %.

The experimental results were compared with MHD theory predicted limits for ballooning and kink modes. Beta limits predicted from ballooning activity with optimized profiles were not violated by experiment. However, beta limits from kink modes predicted by theory not accounting for wall stabilization *were* exceeded. With wall stabilization assumed, the kink limit proves to be less restrictive than the ballooning limit and is thus not violated by experiment. As indicated in the expression above, triangularity was found to be as important a scaling factor as elongation toward improving the beta limit.

The results hold only when q_s as defined above is greater than 2. Below this point, kink modes become unstable even for walls in close proximity to the plasma. In fact, experimental limits on the value of $\frac{I_p}{aB}$ were observed in Doublet which correlated favorably with increasing distance of the plasma separatrix from the plasma. Kink modes (correlating with a broadening of the current profile) were observed to be the cause of the $\frac{I_p}{aB}$ limits. This will be discussed further in the context of limits on q in the next subsection.

These results suggest, at least in the regime being studied, that wall stabilization is an important consideration and the more favorable ballooning mode limits may be applicable as long as some critical minimum q is satisfied. Although the data is only indicative of up to about 5 % beta, Stambaugh et. al. [52] showed that when written in terms of $\frac{I_p}{aB}$, the D-III result is in good agreement with the ballooning mode studies of Tuda and Sykes. In particular, they found:

$$\beta = 3.5\frac{I_p}{aB} \tag{5.19}$$

from the experimental data and rewrote Bernard's expression as:

$$\beta = 2.9\frac{I_p}{aB}F(k,\delta) \tag{5.20}$$

where $F(k,\delta)$ is a slowly varying function of shape factors equal to 1.27 for k = 1.4 and $\delta = 0.3$. As before, shaping is found to be beneficial for beta because of larger allowed currents for a given a and B. The strong scaling with triangularity present in these results as compared to earlier studies is suggested to be due to a difference in plasma shapes for the same values of A, k and δ (these three do not uniquely define the plasma shape). That is, the D-III plasmas are more strongly non-elliptical with triangularity than other plasmas from previous studies.

The most optimistic beta scaling applicable to the first stability regime to date has been suggested by Yamazaki et. al. [53]. The beta limit in this work is given by:

$$\beta = 4.7\frac{I_p}{aB}(1 - b_2\frac{I_p}{aB}) \tag{5.21}$$

where;

$$b_2 = 0.065\frac{A}{\sqrt{k}}[1 - \frac{(k-1+0.05\delta)}{\sqrt{k}}(\frac{1+1.5\delta}{k})^{2.5}]. \tag{5.22}$$

These results are based on a theoretical ballooning mode examination of critical beta with shaping used to improve the ballooning stability limit. In addition to wide variations in aspect ratio, elongation and triangularity, this work employs indentation of the plasma (resulting in bean-type shapes) and an additional degree of freedom which discriminates between triangulated plasmas with both rounded and pointed ends.

The study indicates that a combination of triangularity and elongation is necessary to achieve a linear scaling with $\frac{I_p}{aB}$ similar to that of Sykes which is consistent with previous work. In fact, the results are quite comparable to the Sykes scaling versus $\frac{I_p}{aB}$ for $\frac{I_p}{aB}$ values up to about 3 and triangularity up to 0.5. However, Yamazaki predicts significantly improved beta limits for a given

$\frac{I_p}{aB}$ with very high triangularities (greater than 0.5) possible with bean shaping. The results also show a saturation of critical beta with increasing $\frac{I_p}{aB}$ above $\frac{I_p}{aB}$ values of 2 - 3 for moderate triangularity and above $\frac{I_p}{aB}$ values of 5 for very strong shaping. Note that for typical RCTR parameters, $\frac{I_p}{aB}$ values of 2 - 3 correspond to plasma currents of 14 - 20 MA. Extrapolation of any of these scalings beyond $\frac{I_p}{aB}$ values of about 3 could possibly present severe technological problems for the equilibrium field system.

The large plasma current regime also emphasizes concerns about kink mode stability which were not explicitly considered in this and other studies. Yamazaki (as well as some of the other papers emphasizing ballooning modes) is optimistic that wall stabilization will be effective in suppressing kink modes which could present beta limits below those given by ballooning theory and points out that various experimental devices have exceeded kink mode limits without wall stabilization. The paper also refers to more recent theoretical studies including kink modes (unpublished) which support the Sykes scaling.

5.3.2 Discussion

In the end, considerations of beta come down to a choice of beta scaling(s) and how they are to be used by the reactor designer. First, it is obvious that a clear picture of the beta limit in tokamaks is not yet available. Not only is the reactor regime extrapolated outside the regimes studied to date but even present experiments are not completely understood. Further, the largest uncertainty (at least on the basis of present theory and experiment) concerns the form of q (I_p,K,δ,a,B,etc.) and what limit needs to be placed on it for stability. There seems to be some agreement with the scaling of beta with $\frac{I_p}{aB}$ even though there is some ambiguity with the 'constant' of proportionality and how it may depend on shaping factors.

Table 5.1 shows a comparison of the various beta scalings versus $\frac{I_p}{aB}$ for $k = 1.8$, $\delta = 0.4$ and $A = 3$. Troyon scaling is the most conservative followed by D-III, Tuda, Sykes and Yamazaki in order of increasing beta. For the most part this ordering is consistent with earlier comparisons from the various authors and remains valid for a given set of shaping factors although the gaps between results can widen, especially with highly shaped plasmas. Troyon scaling is in a class of its own in that it finds kink instabilities as the critical limit for beta.

$I_p/(aB)$	**Troyon**	**D-III**	**Tuda**	**Sykes**	**Yamazaki**
1.0	2.76	2.32	4.31	4.40	4.66
1.2	3.31	3.32	5.45	5.28	5.59
1.4	3.86	4.25	6.49	6.16	6.51
1.6	4.42	5.14	7.41	7.04	7.42
1.8	4.97	6.00	8.23	7.92	8.34
2.0	5.52	6.85	8.94	8.80	9.25
2.2	6.07	7.69	9.56	9.68	10.16
2.4	6.62	8.52	10.07	10.56	11.07
2.6	7.18	9.36	10.5	11.44	11.97
2.8	7.73	10.19	10.85	12.32	12.87
3.0	8.28	11.03	11.12	13.20	13.77

Table 5.1: Beta Scaling Comparison versus $\frac{I_p}{aB}$

The other authors either assume, observe or calculate that these kinks can be stabilized with a conducting wall or a similar mechanism and base their limits on ballooning theory (which generally predicts a more optimistic limit).

However, there seems to be a kink limit which is violated even for close conducting walls which depends on the plasma current. This limit is expressed in terms of q^* and cannot be addressed with the use of an $\frac{I_p}{aB}$ type scaling. The use of $\frac{I_p}{aB}$ masks the behavior of q and could lead to the use of these scalings outside their region of validity. Therefore, it may be useful to keep track of the behavior of q as it is defined for each scaling or fix q to some minimum acceptable value and determine from there what $\frac{I_p}{aB}$ is acceptable.

The use of q^* may be superior to the use of q_a in theoretical beta limit studies because it relates directly to plasma current which is an important factor for kink stability. In addition, there is no clear relationship between q_a and plasma current because of its form as an integral over poloidal field and q_a can vary dramatically with a given plasma current for various shapes. This contention is supported by the experimental data from D-III discussed in the previous subsection. A kink instability was observed to limit the value of $\frac{I_p}{aB}$ attainable which correlated with a broadening of the current profile. In addition, q_a (referred to as q_s in the D-III study) was found to vary significantly at this limit suggesting it is a poor indicator for the onset of this instability. Since q^* is inversely proportional to $\frac{I_p}{aB}$, it likely provides an excellent indicator for the onset of kink modes which limit the largest value of $\frac{I_p}{aB}$.

However, if a minimum q is to be used to determine beta, theory and experiment do not yet provide a limit for q^* even though limiting values of q_a have been found from experiment (D-III) and theory (Tuda). In both cases, the limiting q_a (although in somewhat different form) is found to be about 2.

This result suggests the following use of the beta scalings: Choose a limiting q_a (like 2) and find the corresponding q in the scaling of interest. Then use this result to determine $\frac{I_p}{aB}$ for use in the beta scaling. This method is appealing because it uses the latest available scalings and limits on q to find a self-consistent solution. However, if the correct formulations for both q^* and q_a are not used, not certain, or not available, an assumed value of q_a could lead to a violation of some q^* limit which is actually the relevant q form describing the limit on $\frac{I_p}{aB}$ and beta. In addition, q_a is simply too sensitive a parameter to conditions such as the proximity of the separatrix to be a reliable figure of merit for beta. A more likely approach would be to pick a value for q^* with some awareness (if possible) of its relation to q_a. Even though no clear limit on the latter q is available, sensitivity studies as a function of the limiting q^* would be useful in bracketing the results.

Since the form for q^* is specified and solutions for q_a exist for most of the available scalings, the choice of one q implies a specific choice for its counterpart. Thus, for a given calculation of beta, it doesn't really matter whether q^* or q_a is used as a basis as long as the value for each lies within some range which is deemed acceptable. However, when doing parametric scans, the use of the proper q formulation could be very important because the choice of q form can have a major impact on the results of the scan (because of the different scalings the q's have for the various geometrical parameters). Based on the arguments already presented, keeping q^* fixed during parametric scans is probably the best alternative because it represents some fixed level of uncertainty relevant to the beta limit.

An interesting illustration of the importance of q form to the results of parametric tradeoffs can be made using the D-III beta scalings. Figure 5.1 shows the predicted beta for three different approaches to the use of this beta scaling for a parametric scan versus elongation. The dotted curve shows the resulting beta as a function of elongation on the basis of a fixed q_s of 2.5 using the curve fitting form of D-III (equation 5.16). The result is a strongly increasing function of beta with elongation. The dashed curve shows the same parametric on the basis of a fixed q^* of 1.3 (corresponding to a q_a of 2.5 from eqn. 5.5 with $F(k) = k$ and eqn. 5.17) using the $\frac{I_p}{aB}$ D-III beta scaling form of equation 5.19. In this case, an ever increasing (but weaker) function of beta is found because of the weaker dependence of q^* on k compared to the k dependence of the curve fitting form of the D-III beta scaling. Similar results would be expected from other $\frac{I_p}{aB}$ type scalings such as Troyon and Sykes with a difference in magnitude correlating with the constant of proportionality used.

Finally, the solid line shows this parametric scan on the basis of fixed q^* but in conjunction with the curve fitting form of the D-III scaling (eq. 5.16), using equation 5.5 to scale $\frac{I_p}{aB}$ from the q^* expression with the corresponding q_a obtained from the D-III result (eq. 5.17). For this case, even the shape of the result is quite different because although the beta scaling predicts increasing beta with elongation, increasing $\frac{I_p}{aB}$ at fixed q^* results in an increasing q_a with elongation. Therefore, a maximum in the curve results. This is an interesting result because it predicts a saturation-like behavior as suggested by Yamazaki although there is no apparent connection between the two results. It is clear, however, that the method of incorporating a beta scaling can have as much an impact on the result of a parametric scan as the actual choice of a particular scaling.

Another illustration of the q comparison is given in table 5.2. The table shows the variation of q^*, and q_a according to the D-III scaling versus $\frac{I_p}{aB}$ for $k = 1.8$, $\delta = 0.4$ and $A = 3$. Note that the q_a limit of 2 for D-III (for example) is exceeded at an $\frac{I_p}{aB}$ of 3.2 and higher values of $\frac{I_p}{aB}$ would be unacceptable. This is consistent with other high $\frac{I_p}{aB}$ concerns associated with the equilibrium field system, kink limits, and the saturation of beta limits with that parameter. Its also clear that q^* is well below q_a for a given $\frac{I_p}{aB}$. The difference is something less than a factor of two which is in agreement with a theoretical result from Sykes [16]. Similar behavior is also observed in the D-III data which finds a limit on q^* corresponding to a limiting value of $\frac{I_p}{aB}$. Therefore, the actual q^* limit on $\frac{I_p}{aB}$ which may ultimately limit beta may be significantly less than 2. This should be kept in mind when an assumption for q^* is made in an analysis.

A comparison of the impact of the choice of beta scaling on reactor design is shown in table 5.3. The comparison is on the basis of a limiting q_a of 2.5,

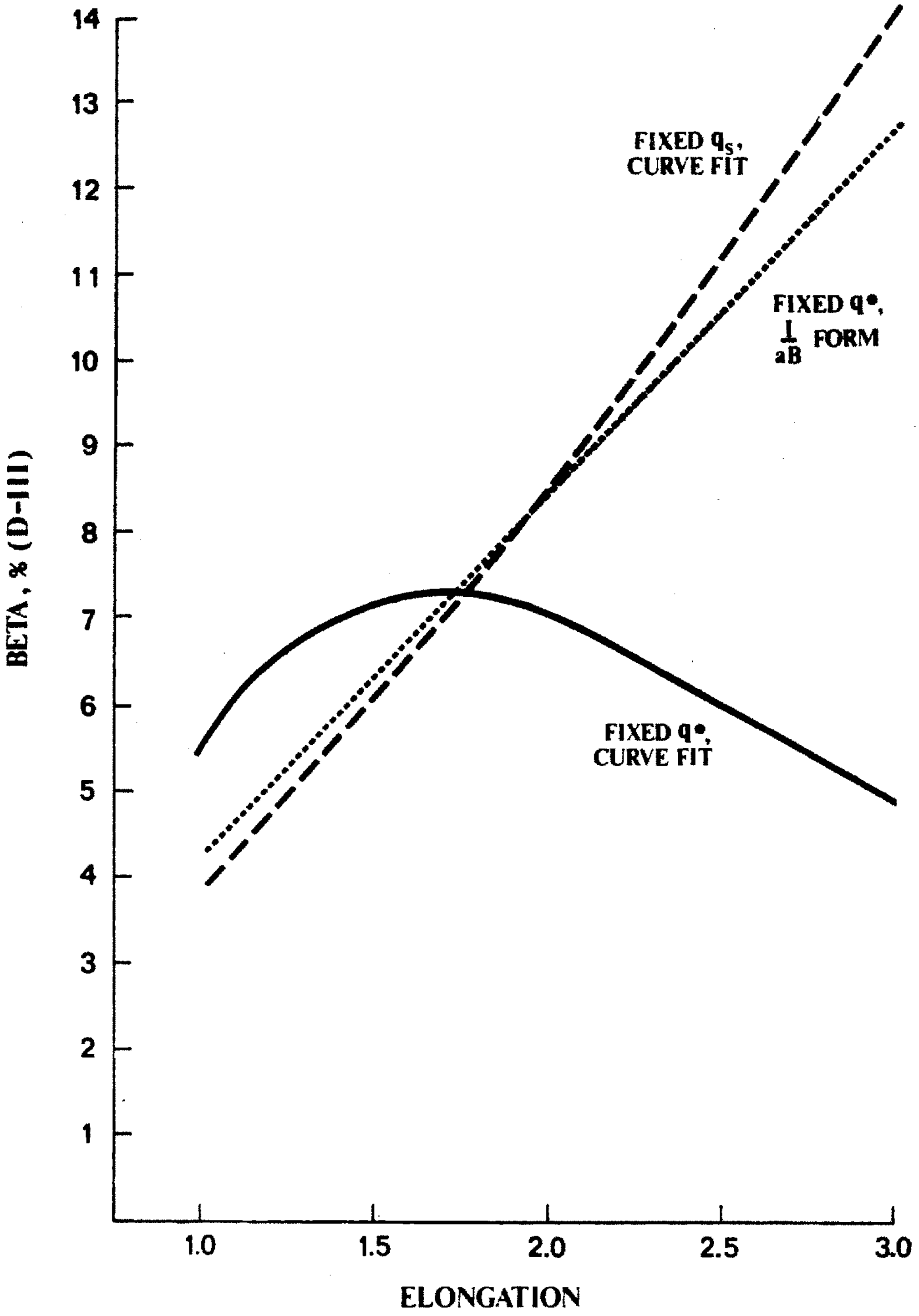

Figure 5.1: Beta vs Elongation for Three Approaches To The Use of the Doublet-III Beta Scaling

$I_p/(aB)$	q^*	q_a
1.0	3.53	7.39
1.2	2.94	5.35
1.4	2.52	4.27
1.6	2.21	3.59
1.8	1.96	3.12
2.0	1.77	2.76
2.2	1.61	2.49
2.4	1.47	2.27
2.6	1.36	2.08
2.8	1.26	1.93
3.0	1.18	1.79

Table 5.2: Numerical Comparison of q^* and q_a (D-III Form)

corresponding to a q^* of 1.3 (or a limiting q^* of 1.3 corresponding to a q_a of 2.5). All of the cases shown are for $P_{net,e} = 1200$, $P_{wall} = 3$ MW/m^2, A = 3, k = 1.8 and $\delta = 0.4$. Of the three scalings compared, Sykes yields the highest beta, lowest plasma current, and lowest recirculating power and cost of electricity. The Yamazaki scaling at high indentation would yield a significantly more optimistic result. The Troyon scaling yields the least optimistic result as expected with the D-III result falling between Troyon and Sykes.

In table 5.4, we base the reactor comparison on the choice of q^*, indicating the sensitivity to this choice. In this case, we have chosen a conservative value for the $\frac{I_p}{aB}$ constant of 3.5, corresponding to D-III. The results indicate that the choice of q^* has an important impact on the reactor characteristics, especially for values of that parameter rising significantly above 1.5 (corresponding to $\frac{I_p}{aB}$ values much less than about 2).

5.3.3 Summary

The following statements are made with regard to beta limits in the conventional or first stability regime:

- There is considerable agreement that the beta limit can be expressed in terms of $\frac{I_p}{aB}$ with a constant (perhaps slowly varying with plasma shaping factors) as a multiplier;

	D-III	**Sykes**	**Troyon**
Major Radius, m	6.30	6.15	6.44
Beta, %	7.3	9.7	6.1
Plasma Current, MA	19.6	16.7	21.8
Field on Axis, T	4.0	3.5	4.4
Burntime, hr	1	1	1
Fusion Power, MW	3061	2916	3187
TF Power, MW_e	283	218	340
Aux. Power, MW_e	463	384	532
Weight, ktonnes	19.4	16.6	21.8
C_{direct}, \$M	2733	2466	2961
C, \$M	4871	4395	5278
COE, mills/kW·hr	59.0	53.1	64.1
Recirc. Power Frac.	0.28	0.24	0.31

Table 5.3: Impact of Beta Scaling Choice on RCTR Parameters, $P_{net,e} = 1200$ MW_e, $P_w = 3$ MW/m^2, $A = 3$, $k = 1.8$

q^*	**1.1**	**1.3**	**1.5**	**1.7**	**1.9**	**2.1**	**2.3**	**2.5**
Major Radius, m	6.24	6.30	6.37	6.45	6.52	6.59	6.67	6.73
Beta, %	8.7	7.3	6.2	5.4	4.8	4.3	3.9	3.5
Plasma Current, MA	21.0	19.6	18.5	17.6	16.9	16.3	15.8	15.3
$\frac{I_p}{aB}$, MA/m·T	2.73	2.31	2.00	1.76	1.58	1.43	1.30	1.20
Field on Axis, T	3.7	4.0	4.4	4.7	4.9	5.2	5.4	5.7
Burntime, hr	1	1	1	1	1	1	1	1
Fusion Power, MW	3002	3061	3124	3199	3263	3336	3409	3476
TF Power, MW_e	257	283	311	342	372	404	437	466
Aux. Power, MW_e	431	463	498	537	572	611	651	687
Weight, ktonnes	18.5	19.4	20.5	21.6	22.8	24.0	25.1	26.4
C_{direct}, \$M	2647	2733	2833	2969	3054	3172	3292	3425
C, \$M	4718	4871	5050	5239	5444	5653	5869	6104
COE, mills/kW·hr	57.5	59.0	61.0	63.0	65.3	67.7	70.1	72.9
Recirc. Power Frac.	0.26	0.28	0.29	0.31	0.32	0.34	0.35	0.36

Table 5.4: Impact of q^* Choice on RCTR Parameters, $P_{net,e} = 1200$ MW_e, $P_w = 3$ MW/m^2, $A = 3$, $k = 1.8$

- Plasma shaping, especially through elongation and triangularity, may allow operation at higher plasma currents resulting in higher achieved beta;
- Up to some limit in $\frac{I_p}{aB}$, kink modes may be stabilized by a conducting wall located a discrete distance from the plasma leaving ballooning modes as the determining limit for beta;
- Even with the use of some stabilization method, there remains a kink limit which is reached at high enough values of $\frac{I_p}{aB}$;
  - This limit is best described theoretically by q^* which is inversely proportional to $\frac{I_p}{aB}$;
- The limiting value of q^* is not well known but can be correlated to and may be significantly less than the limit on q_a from experiment and theory;
- This correlation can be used in conjunction with existing scalings by the reactor designer to choose reactor parameters and beta self-consistently;
  - The choice of q^* and how it is used in conjunction with existing scalings is as important to the results of the parametrics as the choice of beta scaling.

We recommend that the reactor designer incorporate an $\frac{I_p}{aB}$ type scaling using a limiting value input for q^* in the range 1.1 (optimistic) - 1.6 (conservative). An $\frac{I_p}{aB}$ constant of proportionality of 3.5 (conservative) to 4.4 (optimistic) is recommended. Extrapolation of the scalings to values of $\frac{I_p}{aB}$ above about 3 may not be advisable. Note that if we write the beta scaling in terms of q^* directly, this procedure is equivalent to writing beta as $\beta \propto \frac{\epsilon k}{q^*}$ and observing some limit on q^*. Either way, its important that the physics and technology communities work towards a definition of the form and limits for q^* and a uniform approach to setting the beta limit.

5.4 Second Stability Beta

The existence of a second regime of stability to high beta was first suggested by a number of authors in 1978-79 [54,55,56]. The term second stability actually refers to a second stable region against ballooning modes which, as discussed in previous sections, are driven by the interaction of the pressure gradient and the curvature of the field lines. According to second stability theory, as the plasma pressure (and beta) is increased, ballooning modes become unstable at moderate pressure but then become stable again at relatively large pressure.

The theory predicts that as the plasma pressure is increased to moderately high levels, the field lines become sufficiently distorted to reverse the local magnetic shear and stabilize the ballooning. At low pressure, ballooning modes generally occur at local regions of low or zero shear where it is energetically favorable for field lines to interchange. That is, the local shear or the local skewness of the field lines is proportional to the amount of field line stretching or displacement that is allowed due to ballooning activity (lower shear implies the field lines are spending more time in regions of bad curvature). As the plasma pressure is increased from low values the pressure gradient increases and the local shear in regions of bad curvature decreases, leading to instability. However, as the plasma pressure is further increased, the field lines become increasing distorted as the plasma tries to push itself outward in major radius. This distortion can eventually reverse the local shear and re-stabilize ballooning activity.

Stated in another way, the overall or global shear in a tokamak is generally positive and outer lines of magnetic force rotate about the magnetic axis slower than inner ones. Large pressures can alter this situation locally because the increased outward shift of the plasma is balanced by increasing the poloidal field on the outside of the plasma. Where the pressure gradient is large, the increased poloidal field causes field lines to whip around faster which shortens the connection length and reverses the local shear. Thus, the effect of pressure to distort the equilibrium is just as important as its interaction with the field line curvature in determining ballooning mode stability.

For plasmas with standard cross-sections, the second stability regime is only accessible at very high plasma pressures and very high aspect ratio. However, by indenting the plasma on its inboard side and creating 'bean' shapes in the poloidal cross-section, the stabilizing effect of the equilibrium shift can be enhanced leading to second stability at lower values of beta and aspect ratio. As in the first regime of stability, bean shaping can reduce the connection length in regions of bad curvature and increase the connection length in regions of good curvature leading to better ballooning stability. Both high aspect ratio and high q_a enhance the stabilizing effects of high plasma pressure and lead to more accessible second stability regimes.

One of the most complete theoretical studies of second stability ballooning stability has been done by Grimm at. al. [1]. This study shows the effect of aspect ratio, q_a and other parameters on the accessibility of the second stability regime. Figure 5.2 (repeated from [1]) shows accessible beta versus indentation, i, where i is defined as d/a and d and a are as shown in figure 5.3 for a bean-shaped cross-section. The regions in the figure shaped like bell curves oriented sideways enclose the region unstable to ballooning modes. Below these curves is the first (conventional) regime for stability and above is the second regime of stability.

At zero indentation, the second stability regime is completely unaccessible except at an aspect ratio of 10 or higher. At progressively lower aspect ratios, the second stability regime is increasingly less accessible as higher and higher beta and indentation are needed to escape the region of instability. At high enough indentations the region of instability can be completely avoided but very large indentation would likely present significant problems for the equilibrium field system (see below). The influence of q_a (here referred to as $q(l)$) is shown in figure 5.4. Note that the characteristic bell shape occurs only at high values of q_a. The increase of beta in the first regime of stability with increasing indentation at low q_a shown here is consistent with the results of Yamazaki discussed in the previous section.

A number of methods for reaching the second regime applicable to an operating reactor have been proposed. The most obvious solution is to increase the indentation past the 'nose' of the curve representing the unstable region in figure 5.2. However, indentation is produced by a 'bean shaping coil' which is placed as close as possible to the plasma on its inboard side because of the relatively large current requirements of the coil (which increase markedly with indentation). These coils will not be very accessible (especially in superconducting magnet tokamaks) and may experience increased unreliability due to their close proximity to the plasma. Moving through the region of instability during reactor start-up using the stabilizing influence of a hot ion or electron population

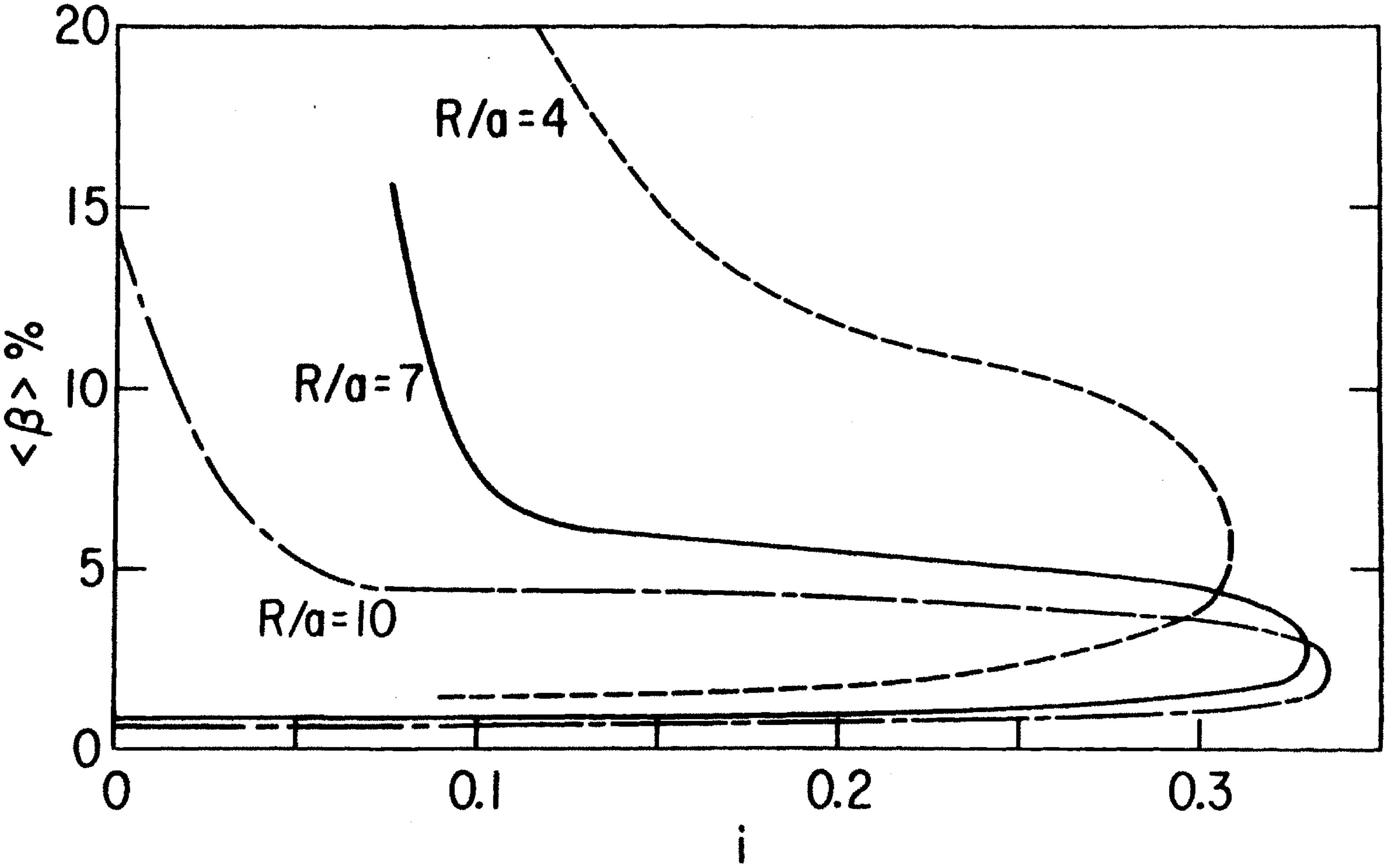

Figure 5.2: Second Stability Beta Accessibility versus Indentation

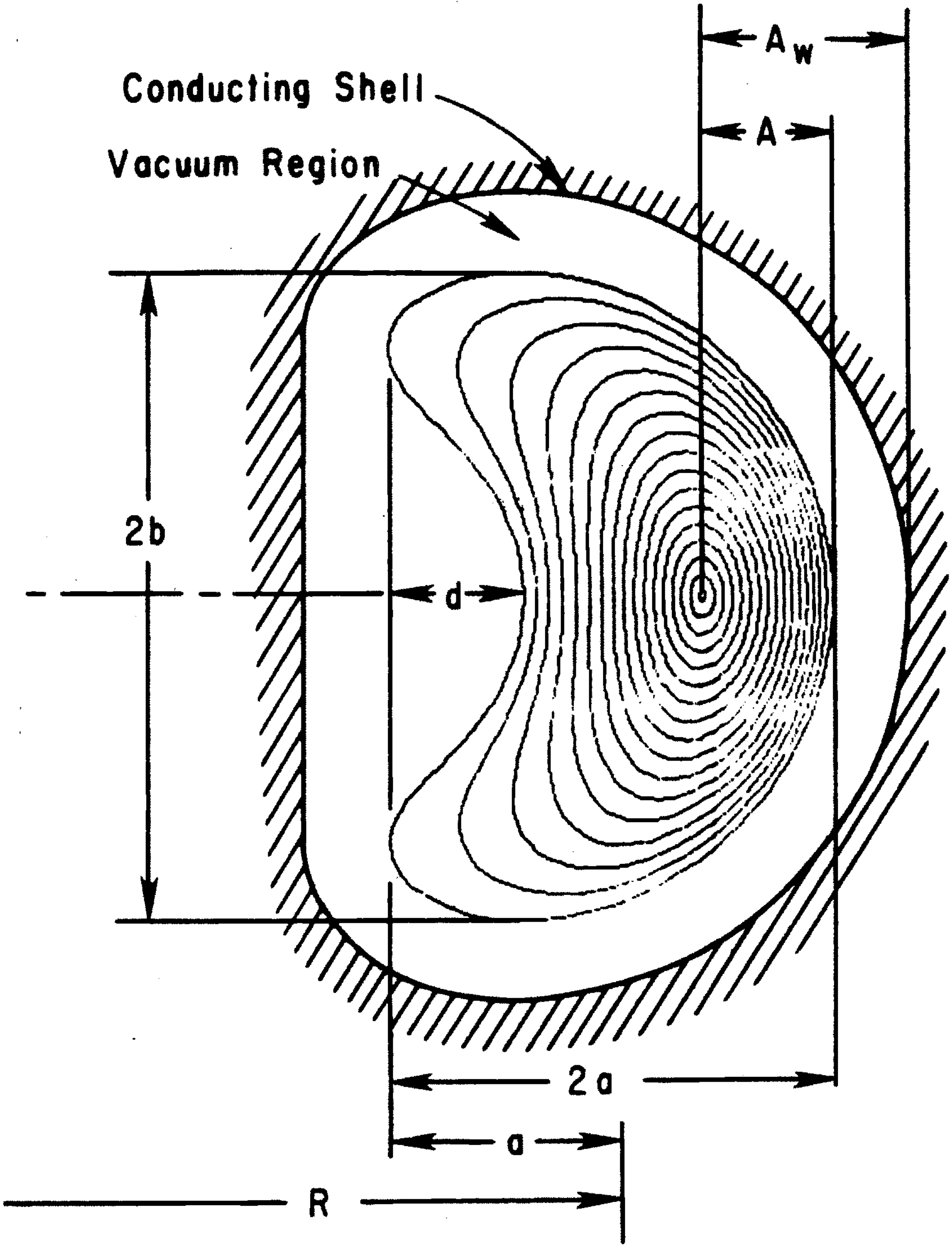

Figure 5.3: Bean Geometry for Second Stability Investigations

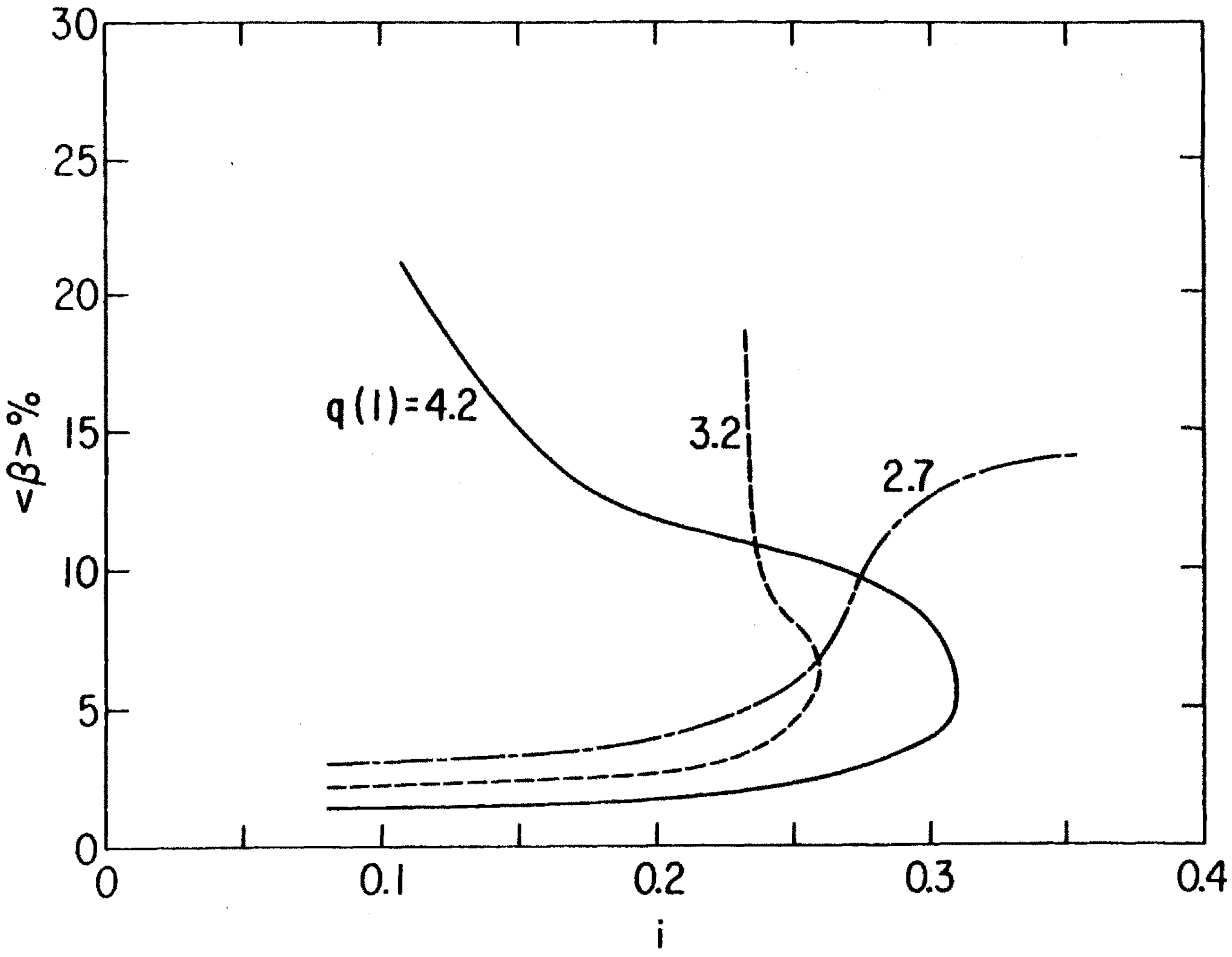

Figure 5.4: Second Stability Beta Accessibility versus Safety Factor

has also been examined but the technological problems appear to be great [57].

Recently, a method of reaching second stability using little or no indentation but using an extremely peaked on edge current profile has been investigated [58]. However, the feasibility of this approach is not clear at present as the work is not sufficiently well developed or published.

The feasibility of second stability beta also depends on other classes of instability in addition to ballooning modes. The achievement of second stability depends on an optimization with respect to ballooning modes which must not be inconsistent with the requirements of stability for other modes. Studies indicate that internal kinks may be stabilized by indentation and the stability of external kinks will depend on wall stabilization [1]. However, it appears that a fair amount of additional work is needed to clarify the stability of external kinks and resistive instabilities such as tearing modes [1], especially in light of the large on-edge current gradients.

Although most of the work to date on second stability has been theoretical, its success has led to an on-going experimental program at Princeton. Bean shaped plasmas have been produced with $\approx 10\%$ indentation in the PBX (Princeton Beta Experiment) device and have yielded relatively high betas of $\approx 5\%$ [59]. At present, however, its not clear whether this performance has been due to higher plasma currents or some second stability effect.

An upper limit on beta relevant to the second stability regime has not yet been identified. However, intuition suggests that as the plasma pressure is pushed higher and higher and the equilibrium becomes extremely distorted with very peaked on-edge current profiles, other mechanisms (such as tearing modes or other kink modes sensitive to sharp gradients in current) will become relevant and limit access to the highest areas of ballooning mode stability. Even if current drive can provide and maintain the required profiles, it doesn't seem reasonable that the plasma would 'want' to stay in a highly non-equilibrium state. Fortunately, as indicated in chapter two, beta achieved in the range of $15 - 20\%$ is sufficient to realize the major benefits of increased beta for commercial tokamak reactors. Therefore, if operation in the second region of ballooning stability was achieved it would not be necessary to push the plasma even further to achieve extremely high beta.

Operation in the second stability regime has the potential of significantly improving commercial tokamak reactor designs. In addition to the direct benefits of high beta (lower required magnetic fields at constant power), the high aspect ratio may be beneficial for access requirements in some designs and leads to lower plasma current requirements. In fact, characteristically low plasma currents could turn out to be the major advantage from second stability (especially for designs incorporating current drive) because of a decreased fusion power density with hollow current profiles [60].

If applicable, the latter result would indicate that the high beta achieved in second stability would not reduce the required field as much for a given fusion power as shown in the comparison of table 5.5. The two cases shown have identical inputs except the constant of proportionality in the expression for fusion power indicating the power density for given temperatures and profiles has been cut in half (this simulates the effect of hollow profiles from [60]). The result is higher required fields, higher recirculating power and higher cost of electricity although the result is still superior to that of a comparable first stability case. Actually, higher required fields may actually be a blessing because it is doubtful that the very low field devices allowed by devices with very high beta and peak profiles could ignite [61]. Thus, second stability physics may simply represent a method for reactors to operate at moderately high aspect ratio without suffering from the effects of low beta predicted by conventional beta scalings.

At present there are no beta scalings describing achievable beta in the second stability region as a function of the relevant parameters. This fact, and the relatively large uncertainties involved with second stability beta make systematic exploration of commercial reactor regimes using this high beta approach difficult. However, using the data provided by reference [1] and similar studies, representative second stability cases can be generated with aspect ratios of 5 - 6, elongations of 1.6 - 1.8, q_a of 4.2 and plasma currents of 5 - 6 MA with betas of 20 - 25 %. A more systematic approach to exploring parameter space is obtained by assuming a value for q^* ($q^* \geq 1$) and operating at the MHD equilibrium limit to determine self-consistent parameters for A, S, I_p, β, and B. This approach yields results in reasonable agreement with the existing data points as long as the calculation is within the regimes of A, S and q_a required by second stability theory. Once second stability operation is assumed, the major uncertainties (in terms of the possible impact on the reactor tradeoffs) are the required magnetic

C_{power}	**0.88**	**0.44**
Net Electric Power, MW_e	1200	1200
Wall Loading, MW/m^2	3	3
Major Radius, m	7.42	7.51
Aspect Ratio	5	5
Elongation	1.8	1.8
Beta, %	24	24
Plasma Current, MA	4.6	5.5
Field on Axis, T	2.4	3.0
Burntime, hr	6	6
Fusion Power, MW	2611	2677
TF Power, MW_e	103	130
Aux. Power, MW_e	218	254
Weight, ktonnes	13.2	14.9
C_{direct}, \$M	1990	2132
C, \$M	3546	3800
COE, mills/kW·hr	42.6	45.7
Recirc. Power Frac.	0.150	0.174

Table 5.5: Impact of Reduced Fusion Power Density with Second Stability Physics on Reactor Parameters

field for a given fusion power output and the requirements of the equilibrium field system.

In summary, the theoretical existence of a second regime of ballooning mode stability has been established and indicates that very high beta $\geq 20\%$ at moderately high aspect ratio, and high q_a may be possible. However, this regime is significantly further displaced from present tokamak physics than the first stability regime and a number of theoretical questions remain. Depending on the answers to some of these questions, second stability operation could lead to a significantly improved reactor concept.

5.5 Summary

The magnitude and formulation for toroidal beta used in reactor studies can have a major impact on the qualitative and quantitative results obtained by those studies. Unfortunately, the beta scaling relevant to commercial fusion reactor studies is not well known at this point in fusion development. In this chapter we have attempted to close the gap between the limits imposed by the theory and the requirements for a meaningfull evaluation of the potential of future reactor designs.

In the first stability regime, the beta limit can be adequately described as $\beta \propto \frac{I_p}{aB}$ with the results relatively sensitive to the selected constant of proportionality. The proper use of these scalings is potentially very sensitive to the limits placed on $\frac{I_p}{aB}$ through the use of a 'q' formulation and limit. The 'q' formulation corresponding to q^* in the literature ($q^* \propto \frac{1}{I_p}$) is probably the best basis upon which beta limits could be scaled.

Significant questions still remain with regard to the accessibility of beta in the second stability regime. However, if achieved, second stability could offer low current, high aspect ratio operation without the degradation in beta found in first stability.

Chapter 6

Summary, Conclusions and Recommendations

6.1 Introduction

The future of the tokamak approach to controlled thermonuclear fusion depends in part on its potential as a commercial electricity producing device. This potential is continually being evaluated in the fusion community using parametric, system and conceptual studies of various approaches to improving tokamak reactor design. The subject of this thesis has been an exploration of the potential of tokamaks using resistive magnets as commercial electricity producing reactors. The study indicates that attractive design space does exist and presents a conceptual design for the Resistive Magnet Commercial Tokamak Reactor (RCTR).

Until recently, resistive magnet tokamaks had only been considered as experimental devices [4], ignition machines [5] or as commercial devices in largely non-electricity producing applications such as the production of copious neutrons and process heat [6,7]. These machines are generally characterized by compact size, high power density and high magnetic field. These characteristics are ideal for such near term applications when low cost and high performance are the primary concerns. The major drawback of resistive magnets, high dissipated power due to joule heating in the conductor, can largely be overlooked in these types of applications.

However, many consider commercial electricity producing applications inappropriate for resistive magnets due to the relatively large recirculating power requirements. This study has shown that high field, high wall loading and large recirculating power need not characterized these designs and identified attractive options for resistive magnet tokamaks. In fact, low toroidal field more naturally charactrizes commercial resistive magnet tokamaks because the minimum dissipated power in the toroidal field (TF) coils is desired. Recirculating power can be further reduced through design by minimizing the distance between the plasma and the TF coil, maximizing the conductor filling fraction, and placing the poloidal field (PF) coils within the bore of the TF coil.

Normal magnets require less shielding than the superconducting variety and thus can be more compact. This can lead to lower costs and higher system power density in the resistive device for the same wall loading. Resistive magnets are less sensitive to neutron streaming and are more tolerant to local hot spots. They are also less sensitive to changing magnetic fields.

Resistive magnets are generally less complex than superconducting magnets, consisting basically of sheets of copper with no requirements for a cryogenic environment. This can lead to a more reliable and available system and perhaps to a lower overall cost. These factors are particularly important in light of the fact that many of the weaknesses of present commercial tokamak designs are associated with either cost or reliability and availability.

A major advantage associated with resistive coils is the possibility of taking apart or demounting the coils with relatively simple designs. Concepts have been proposed for demountable superconducting coils but are not being considered presently in major tokamak studies due to complexities involved with the large number of filaments and the cryogenic environment. In contrast, joints in resistive coils are already being used in a number of devices [8,9] and are being considered even in compact, high field applications [10].

Demountability of the TF coils offers significant advantages to tokamak design. Readily demountable coils may facilitate maintenance with a resulting increase in availability. Furthermore, demountable coils allow the use of various coils inside the TF coil including equilibrium field (EF), ohmic field (OH) and bean shaping coils (for possible high beta application). Placing coils within the TF coil can significantly reduce the resistive power of EF coils, increase the attractiveness of the use of a magnetic divertor, reduce the overturning moment on the TF and allow the achievement of higher elongations.

Thus, despite relatively high recirculating power, resistive magnets may offer significant advantages over superconductors in commercial electricity producing applications from the points of view of complexity, maintenance and availability.

The content of the thesis will be summarized by presenting the results of the parametric studies followed by a conceptual RCTR design including the demountable nuclear island and blanket/first wall reference concepts.

6.2 RCTR Parametric Studies

The first step in the present analysis was to identify the most promising regions of parameter space for resistive magnet commercial tokamaks. A computer code, RTPAC, was developed to model and cost all major systems of the tokamak power plant and used to perform the necessary trade-offs. The sensitivity of parameters such as weight, cost, cost of electricity and recirculating power to net electric output, wall loading, aspect ratio, elongation and beta was examined. The potential of multiplexed power plants [23] and the relative costs of resistive and superconducting magnet tokamaks were also explored.

Special attention was given to the use of presently available toroidal beta scalings in the analysis. Since beta is such an important parameter to the reactor designer, some degree of understanding of the available theory and its limitations is essential. At this time there is little apparent communication between the tokamak theorist who studies the phenomena limiting beta and the tokamak designer who is interested in how reactors scale with accessible beta. We found that the magnitude and formulation for toroidal beta used in reactor studies can have a major impact on the qualitative and quantitative results obtained by those studies.

With regard to the first stability or conventional beta regime, the following conclusions were drawn:

- There is considerable agreement that the beta limit can be expressed in terms of $\frac{I_p}{aB}$ with a constant (perhaps slowly varying with plasma shaping factors) as a multiplier;
- Plasma shaping, especially through elongation and triangularity, may allow operation at higher plasma currents resulting in higher achieved beta;

- Up to some limit in $\frac{I_p}{aB}$, kink modes may be stabilized by a conducting wall located a discrete distance from the plasma leaving ballooning modes as the determining limit for beta;

- Even with the use of some stabilization method, there remains a kink limit which is reached at high enough values of $\frac{I_p}{aB}$;
  - This limit is best described theoretically by q^* which is inversely proportional to $\frac{I_p}{aB}$;

- The limiting value of q^* is not well known but can be correlated to and may be significantly less than the limit on q_a from experiment and theory;

- This correlation can be used in conjunction with existing scalings by the reactor designer to choose reactor parameters and beta self-consistently;
  - The choice of q^* and how it is used in conjunction with existing scalings is as important to the results of the parametrics as the choice of beta scaling.

For the use of conventional beta scalings in reactor design codes, the study recommends that the reactor designer incorporate an $\frac{I_p}{aB}$ type scaling using a limiting value input for q^* in the range 1.1 (optimistic) - 1.6 (conservative). An $\frac{I_p}{aB}$ constant of proportionality of 3.5 (conservative) to 4.4 (optimistic) is recommended. Extrapolation of the scalings to values of $\frac{I_p}{aB}$ above about 3 may not be advisable. Note that if we write the beta scaling in terms of q^* directly, this procedure is equivalent to writing beta as $\beta \propto \frac{\epsilon k}{q^*}$ and observing some limit on q^*. Either way, its important that the physics and technology communities work towards a definition of the form and limits for q^* and a uniform approach to setting the beta limit.

With regard to the second stability beta regime, we found that the theoretical existence of a second regime of ballooning mode stability has been established and indicates that very high beta $\geq 20\%$ at moderately high aspect ratio, and high q_a may be possible. However, this regime is significantly further displaced from present tokamak physics than the first stability regime and a number of theoretical questions remain. Depending on the answers to some of these questions, second stability operation could lead to a significantly improved reactor concept. In effect, second stability could offer low current, high aspect ratio operation without the degradation in beta expected from first stability behavior.

RTPAC was used to perform a large number of trade-offs designed to identify the most promising regions of parameter space for resistive magnet commercial tokamaks. The results of the parametrics may be summarized as follows:

- High beta reactors (assuming second stability physics)
    - Optimum wall loading is ≈ 4 MW/m^2
    - Reactors with $P_{net,e}$ as low as 600 MW$_e$ remain attractive
    - Pulse lengths as long as one day in length can be achieved
    - Lowest aspect ratio allowed by 2nd stability is desirable
    - Optimum elongation is the highest allowed by 2nd stability (≈ 1.8)
- Low beta reactors
    - Optimum wall loading $\approx$ 3 - 4 MW/m^2
    - Decreasing $P_{net,e}$ attractive down to ≈ 800 MW$_e$
    - Pulse lengths of 6 - 12 hours possible
    - Best aspect ratios $\approx$ 2.8 - 3.3
    - Optimum elongation $\approx$ 1.8 - 2.0
- High blanket thermal efficiency is an important asset comparable in impact to high beta in many respects
- High beta operation has advantages of low plasma current and low recirculating power and moderate cost advantages
- Aluminum magnets are attractive for their cost and activation advantages despite high dissipated power
- Multiplexing may significantly reduce the cost of small reactors and could make the application of fusion more attractive for the electric utility
- Low beta devices operate best at relatively high recirculating power fractions ($\approx 25 - 40$ %)

- Increased costs due to recirculating power requirements with RCTR relative to superconducting magnet options might easily be offset by cost savings from simpler technology and reduced shielding requirements

The parametric analysis led to the selection of several illustrative designs. Each illustrative case, summarized in table 6.1, represents an optimized design in the context of a different extrapolated innovation or perception of the most desirable qualities for a fusion reactor.

Selecting a single optimized design would have been extremely difficult. Even after many parametric trade-offs, there is still too much uncertainty surrounding many aspects of fusion reactor design for unique selections to be made for some of the parameters. For example, its difficult to choose the best wall loading because of the complex trade-off between greater compactness and higher system power density for high wall loadings and the corresponding increase in risk and engineering difficulty. Indeed, the impact of going to higher wall loads on the cost of the device is relatively poorly understood. However, some intelligent choices for wall loading and other parameters can be made based on the parametrics and consideration of the goals for RCTR and other factors external to the analysis.

All of the designs shown in table 6.1 have an internal poloidal field system, a lithium-vanadium blanket/first wall system and demountable toroidal field coils. Each possesses the high engineering power density, good mass utilization and decreased complexity characteristic of resistive magnet tokamaks.

Case A shows the potential of RCTR as a tokamak operating in the second regime of plasma stability. The device delivers 1200 MW_ϵ and operates at a wall loading of 3 MW/m^2. 1200 MW_ϵ is comparable in size to the large base-load plants in operation today. The wall loading choice is high enough that the device remains fairly compact but low enough that a relatively simple blanket/first wall and impurity control system is possible. High beta of 24 % contributes to a low recirculating power requirement of 228 MW which is comparable to that of a superconducting tokamak using RF driven current. An aspect ratio of 5 leads to the relatively large major radius of 7.5 m but the compact nature of the nuclear island limits the weight to 14.2 ktonnes.

If the second stability regime does not prove viable, RCTR can still be attractive with only moderate beta as shown in case B. Again, the net electric power and wall loading are 1200 MW_ϵ and 3 MW/m^2, respectively. Recirculat-

Case	**A**	**B**	**C**	**D**	**E**	**F**
Net Electric Power, MW_e	1200	1200	1200	500	1200	800
Wall Loading, MW/m^2	3	3	3	3	6	1.5
TF Material	Cu	Cu	Al	Cu	Cu	Cu
Beta, %	24	9.6	24	24	24	9.6
Major Radius, m	7.5	6.4	7.9	5.0	5.3	7.9
Aspect Ratio	5	3	5	5	5	3
Magnetic Field, T	2.4	3.5	2.4	2.7	3.1	2.8
Plasma Current, MA	4.7	17.2	4.9	3.5	4.3	16.8
Nuclear Island Weight, ktonnes	14.2	17.8	9.3	8.1	8.4	22.5
Thermal Power, MW	3380	3790	3690	1570	3340	2830
TF Dissipated Power, MW_e	108	225	190	80	108	216
Total Recirculating, MW_e	228	400	355	168	212	400
Direct Costs, $M	2065	2590	1740	1380	1850	2660
Capital Cost, $M	3680	4615	3100	2460	3295	4735
Cost of Electricity, mills/kW·hr	45.4	56.7	38.3	73.9	45.1	80.4
Recirculating Power Fraction	0.16	0.25	0.23	0.25	0.15	0.33

Table 6.1: RCTR Illustrative Concepts

ing power requirements (400 MW) and plasma current (17.2 MA) are relatively high but only moderate weight and cost penalties are indicated.

Generally, copper has been considered as the magnet conductor in the analysis. However, despite having twice the resistivity of copper, aluminum can be an attractive alternative to copper. In particular, aluminum has one third the density of copper and may potentially become far less activated under neutron irradiation. A version of RCTR using aluminum magnets is shown as case C. High beta has been assumed which helps to keep recirculating power requirements to 355 MW. The magnets are bulkier than those of case A (the comparable copper version) but are far less massive and costly. In fact, the total cost predicted for the aluminum magnet case is significantly lower than its comparable copper version.

Case D explores the possibility of using fusion plants in small unit sizes. In case D, 600 MW_e is delivered in a high beta version of RCTR using copper magnets. The cost of electricity is higher than in case A but the capital investment required is significantly reduced. Several of these plants could possibly be combined on a single site in a 'multiplex' arrangement.

The final two cases explore two extremes of physics and engineering feasibility. Case E operates at high wall loading (6 MW/m^2) and high beta (24 %). The high wall loading results in a relatively compact device despite the high aspect ratio required by second stability physics. A cost penalty is not indicated in case E. However, the incremental cost of higher wall loads in terms of replacement and loss of availability is difficult to estimate. In any case, the design of the blanket/first wall and impurity control system is significantly more difficult and uncertain at this level of wall loading.

In contrast, case F is a conservative version of RCTR. The low wall loading of 1.5 MW/m^2 results in a large machine (22 ktonnes) but the first wall may only require replacement once during the lifetime of the plant. Consistent with the conservative theme, only moderate beta (8 %) at low aspect ratio is assumed. This contributes to the relatively large recirculating power (400 MW). A significant cost penalty is also indicated.

6.3 Resistive Magnet Commercial Tokamak Reactor (RCTR) Reference Design

6.3.1 General Characteristics

Case A of table 6.1 was used as the basis for more detailed studies of a demountable nuclear island concept and the blanket/first wall system to arrive at an overall conceptual design for RCTR. In most respects, the analysis and the resulting conceptual design will apply to any of the selected cases of table 6.1.

A trimetric view of the reference conceptual design for RCTR is shown in figure 6.1. Recall that Case A is a high beta, copper coil version of RCTR. The aspect ratio of five and choices of net electric power output, $P_{net,e} = 1200$ MW$_e$, and wall loading of $P_{wall} = 3$ MW/m^2 leads to a major radius of 7.5 m. $\beta = 24\%$ is achieved assuming operation in the second stable region.

The high beta results in a very modest magnetic field on the axis of the plasma of 2.4 T. As a result of the use of second stability at high aspect ratio, the plasma current is also modest at 4.7 MA. Very long pulses driven by an OH coil internal to the TF coil are possible. The design is capable of six hour pulses although pulses approaching one day in length are possible with similar machines.

The weight of the nuclear island (all components within the TF boundary including the TF and external support structure) is 14.2 ktonnes including 8.6 ktonnes for the coils. This compares quite favorably with STARFIRE ($\approx$ 26 ktonnes) because of the compact nature of the nuclear island. Also, shielding is not required between the plasma and the coils and the TF coils serve as an effective biological shield.

A major emphasis has been placed on assembly and maintenance in the development of a nuclear island concept for RCTR. The design of all major components has been driven by the importance of maintenance and the decision to use demountable toroidal field coils. The placement of the equilibrium field coils inside the TF bore, the blanket/first wall design, toroidal field coil design and structural components are all subject to maintenance considerations.

The blanket is a self-cooled liquid lithium design using a vanadium structure and a ferritic steel (HT-9) reflector. A separate shield is not necessary. The blanket is divided into twelve sections toroidally and is divided along the mid-

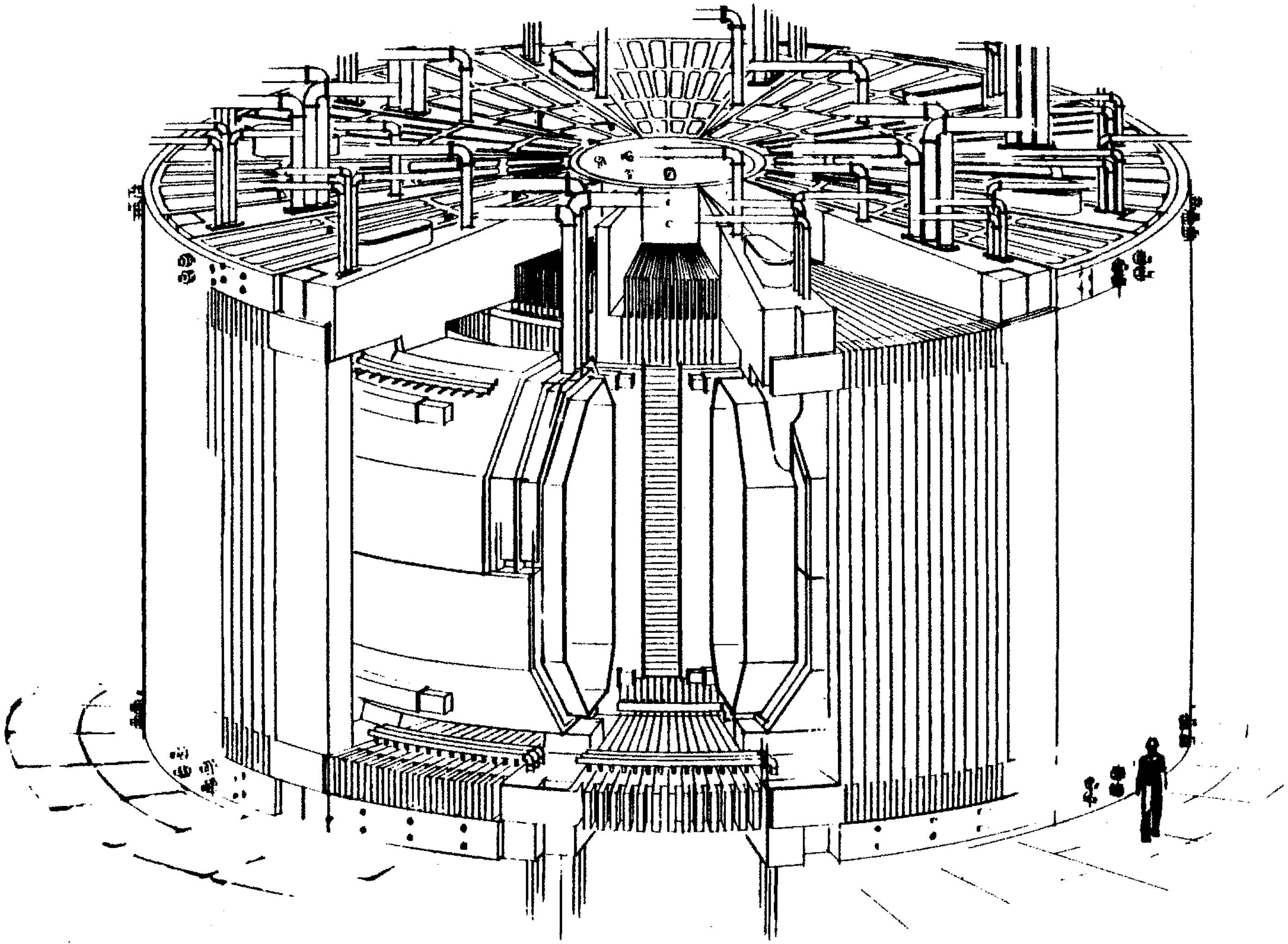

Figure 6.1: Trimetric View of RCTR Conceptual Design

plane, allowing the blanket sectors to be removed independently of the first wall. The first wall is also a vanadium structure with lithium cooling and is designed for assembly and removal as a single, pre-tested unit.

6.3.2 Toroidal Field Coil

The TF coil is optimized for lowest cost by trading off weight against dissipated power. The power required by the TF coil is 108 MW. Combining the power requirements for blanket pumping, balance of plant and other auxiliaries, the total auxiliary power requirement is 228 MW. All magnet coils are constructed of copper and insulated with polyimides. Ceramic insulation may be used in areas of highest radiation dose.

An engineering drawing of the plan view of RCTR is shown in figure 6.2. The TF coil is of frame type and is demountable with lap joints in each of the four corners. Note that the demountability allows placement of the ohmic and equilibrium field coils inside the TF bore. The cooling channel arrangement is also shown. Major parameters characterizing the TF coil are summarized in table 6.2.

Although this case employs a copper conductor, aluminum or hybrid copper/aluminum plates would also be viable. The joints are lap-type and are externally supported against in-plane and out-of-plane loads. The coils are grouped into twelve bunches which are separated by steel wedges. The bunches consist of twelve TF coils, each carrying 477 kA to provide the field of 2.43 T on the plasma axis.

The TF coil has very thick inboard legs (2.1 m) and relatively thin outboard and horizontal legs (0.75 m and 0.80 m, respectively) due to the large contribution of dissipated power and relatively small weight contribution inboard. Despite the relatively low magnetic field, the size of this device results in a vertical force (bursting force from the interaction of the TF current and the toroidal field) of 665 MN. However, the large cross-sectional area available to support this force results in an average membrane stress at the midplane (assuming a continuous, unsegmented coil) of just 6.8 MPA (970 psi). The coil is segmented, however, and the vertical force is transferred through the horizontal TF legs, steel caps and bolts (or plugs) to the support cylinders (section 6.3.3).

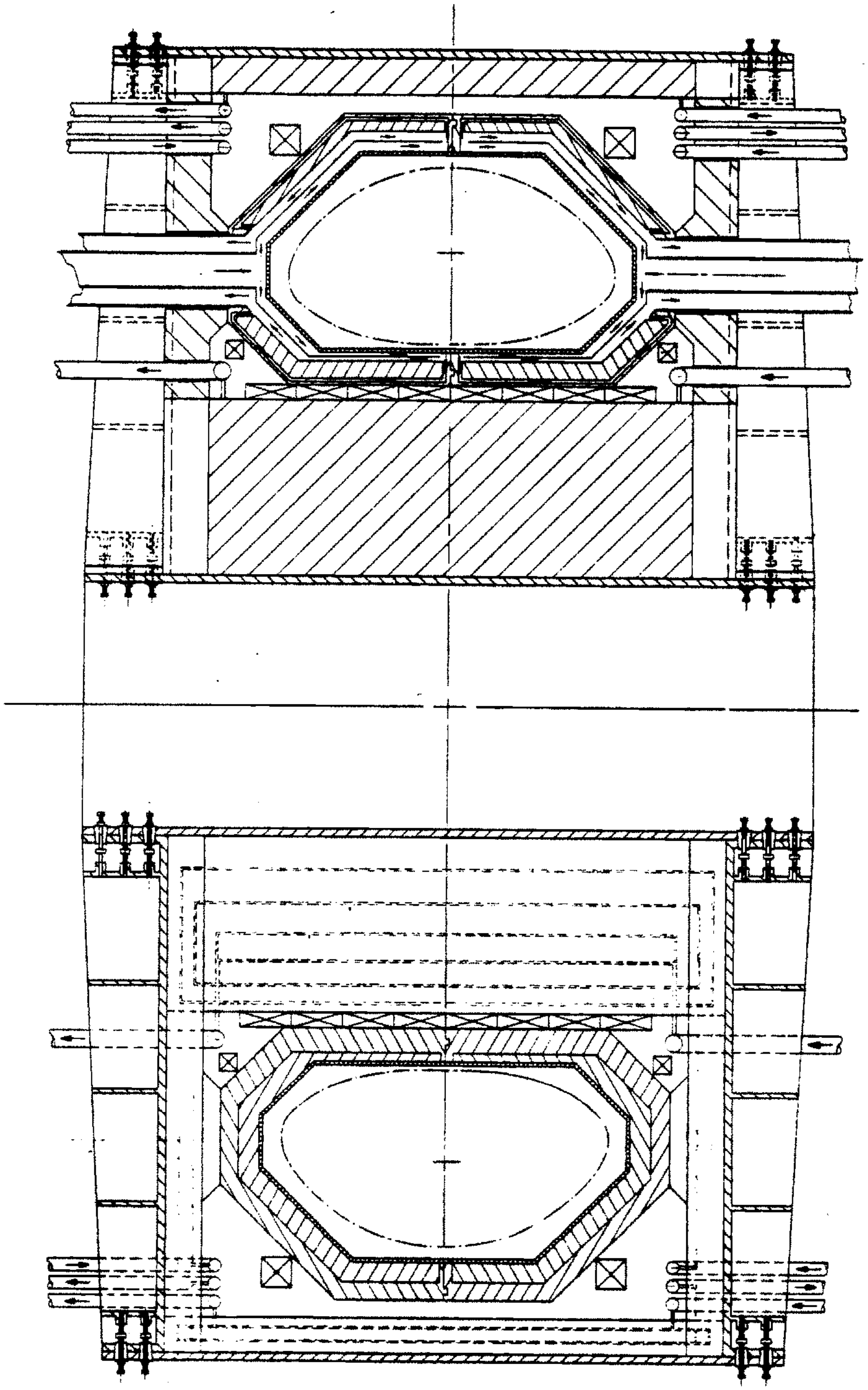

Figure 6.2: Plan View of RCTR Concept

Net Electric Power, MW_e	1200
Wall Loading, MW/m^2	3
Toroidal Beta, %	24
Major Radius, m	7.52
Coil Type	Frame
Conductor Material	Copper
Coil Cooling	Helium
Current Per Turn, kA	477
Field On Axis, T	2.43
Peak Field, T	3.51
Inboard Build, m	2.1
Outboard Build, m	0.75
Horizontal Build, m	0.80
Weight, ktonnes	8.6
Number, TF Coils	12
Number of Turns	192
Turns Per Coil	16
Turn Thickness, inboard, cm	9.2 - 13.6

Table 6.2: Demountable Coil Characteristics

The weights of the TF components are within the capability of present crane technology. For example, the horizontal leg for one of the twelve TF coil bunches weighs approximately 120 tonnes. This is the heaviest TF coil sector although the blanket sectors within the bore of the TF coil are heavier (section 6.3.5).

Current transfer in the joints is facilitated by the low coil current densities and large area available with the lap-type geometry. Average steady state current densities in the inboard and outboard sectors of the TF are only 240 A/cm^2 and 224 A/cm^2, respectively. The area available in the inboard joints is almost 2 m^2 resulting in an average joint current density of 45 A/cm^2. The outer joints have significantly less area available (0.6 m^2) but the current density of 115 A/cm^2 is still within the capability of MULTILAM technology [27].

The toroidal field coils are actively cooled to compensate for both joule and neutron heating. Gaseous helium has been chosen as the reference cooling medium for RCTR. Water cooling is more typical of room temperature resistive magnet designs but water has severe compatibility problems with liquid lithium [28], the coolant/breeder selection for the blanket concept. Helium is also an adequate medium for the heat removal task for typical RCTR toroidal

Net Electric Power, MW_e	1200
Wall Loading, MW/m^2	3
Toroidal Beta, %	24
Cooling medium	Helium
Current Density, Inboard, A/cm^2	240
Joule Heating, MW/m^3	0.06
Neutron Heating, MW/m^3	0.08
Coolant Pressure, MPa	1.5
Mass Flow Rate, kg/s	0.3
Helium Temperature Rise	35
Peak TF Temperature, K	367
Helium Channels per Plate	6
Channel Diameter, cm	1.5 - 3.0
Channel Length, m	8
Exit Velocity, m/s	41.8
Flow Area/Conductor Area, %	5

Table 6.3: Toroidal Field Coil Helium Cooling

field coil current densities. Typical TF cooling parameters for the reference design are shown in table 6.3.

6.3.3 Nuclear Island/Demountability

The major objective of the demountable coil design for RCTR is to provide a means of access to the bore of the toroidal field magnet for maintenance. The design emphasizes the use of the simplest possible joint design and allows for maximum flexibility in the way the coil is disassembled and the internal components exposed. Alternate configurations were investigated in an attempt to minimize the use of bolts and pins and avoid the necessity for the breaking of welds. These requirements are essential for a commercial reactor which cannot afford to be unavailable often or for extended periods. The final requirement is that the maintenance scheme be compatible with support structure and other major components such as the blanket/first wall system.

The nuclear island structure consists of copper coil and steel wedge assemblies which are enclosed by inner and outer support cylinders. The wedges appear as the spokes of a wheel, keyed into the inner and outer cylinders to support the coils against out-of-plane forces. The cylinders and steel wedges extend above (and below) the height of the TF coils. Steel caps are placed on top of the coils within the pocket formed by this extension and are pinned to the cylinders to support the TF coils against in-plane loads. This assembly is illustrated in the engineering drawings of figure 6.3 (top view) and figure 6.2 (plan view).

Vertical access ports are cut into each of the twelve wedge components. Six of these ports provide coolant access to the first wall and blanket assemblies. The remaining six provide direct access to the plasma chamber for vacuum pumping, auxiliary heating and minor repairs. All twelve wedges contain access ports for TF cooling manifolds. These manifolds are located internal to the TF bore in the four corners of the coil.

Note that no radial access has been identified in this concept. A provision for radial access would require a break in the outer support cylinder to allow vertical removal of the vacuum chamber. Such a break would increase the complexity of the concept due to requirements for support structure at the break and would decrease the structural integrity of the outer cylinder. In addition, the access requirements in a commercial device are relatively modest and may be adequately met in this concept with only vertical access ports.

The external structure is designed to support the in-plane vertical bursting forces on the TF coils and the overturning forces created by the interaction of the poloidal field and toroidal current. The vertical forces are transferred from the steel caps to the cylinders by the steel plugs. The plugs are 25 cm in diameter and number 144 each for the top and bottom supports. Each plug carries an average shear stress of 83 MPA. The cylinder thicknesses required to support both in-plane and out-of-plane forces are 25 cm and 10 cm for the inboard and outboard cylinders, respectively. The overturning forces are taken by the continuous structure formed by the steel caps, flanges and inner and outer cylinders.

6.3.4 Assembly and Maintenance

Assembly of the RCTR nuclear island is illustrated in figure 3.9 through figure 3.14 of section 3.4 (page 84). In step 1 shown in figure 3.9, the lower steel wedges separated by the lower steel end caps are assembled around the inner support cylinder. The wedges are keyed into the inner cylinder and the end caps are attached to the inner cylinder via steel plugs. The placement of the lower

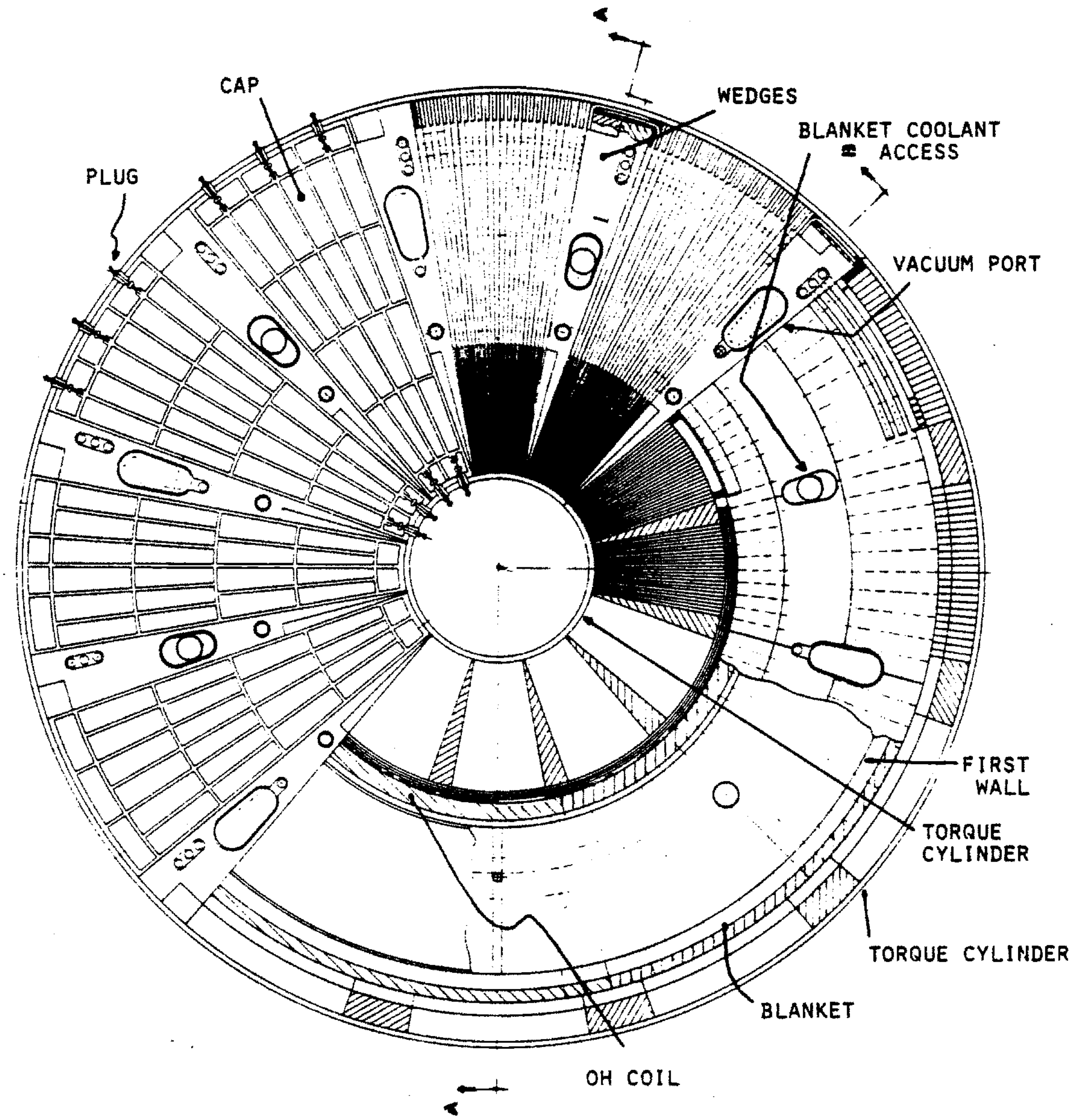

Figure 6.3: Top View of RCTR Nuclear Island

horizontal TF bundles on top of the lower end cap and between the steel wedges is illustrated in step 2. Twelve bunches of 16 one quarter turns of toroidal field coil are assembled in this manner.

The next step involves placement of the inner wedge and TF turns around the inner support cylinder. An inner wedge is dropped into place by matching the two ends of the lap joint from it and the already assembled lower wedge piece and rests up against the inner support cylinder. Insertion of a wedge is followed by the insertion of an inner TF coil bunch in a similar manner. Next, the OH coil (illustrated in step 4 as a solid cylinder) is dropped in around the inner TF/wedge assembly. This is followed by the placement of the lower EF coils. The EF coils are supported from the steel wedges.

In step 5 of figure 3.11, assembly of the lower blanket sectors is illustrated. The blanket is divided along the midplane to allow assembly and removal of the first wall in a single unit. Lower and upper blanket sections are divided into twelve 30 degree sectors. Half of the sectors include cooling ducts for the liquid lithium blanket coolant which are channeled through an equal number of steel wedges. The remaining blanket sectors contain penetrations for the coolant channels of the first wall. Each blanket sector rests on top of protruding areas of the lower steel wedges (visible at previous steps).

The first wall is lowered in next as a single unit. This procedure allows the assembly to be pre-tested for vacuum and coolant integrity before insertion into the nuclear island and avoids the necessity for sealing and breaking of vacuum welds during assembly and maintenance. A similar philosophy could have been applied to the entire blanket/first wall assembly but the weights involved for assembly and maintenance may have been prohibitive (see chapter four). The first wall assembly rests inside the lower blanket assembly. Coolant ducts attached to the first wall fit through penetrations in alternating blanket and steel wedge sectors.

In steps 7 and 8 shown in figure 3.12, the upper blanket and EF coil assemblies are inserted in a complimentary manner to their lower counterparts. Then, in steps 9 and 10 of figure 3.13, the outer section of the nuclear island is assembled. Outer wedge and TF coil sectors are inserted by matching the appropriate lap joints. Then, the outer support cylinder can be dropped in around the entire assembly. The outer support cylinder may not be handled as a single piece due to sheer size and proper fitting constraints. However, the joints required to assemble this component in two or more pieces need not be readily maintainable. At this point, the outer support cylinder can be secured to the lower end caps with steel plugs.

In the final steps, illustrated as steps 11 and 12 in figure 3.14, the upper sectors of the TF coil and wedges are inserted. Wedges fit over upper cooling channels for both blanket and first wall cooling and are joined at lap joints between the inner and outer vertical wedge pieces already in place. The upper TF bundles fit similarly between vertical sections of the TF coil already assembled. The last step is to drop in the upper end caps between protruding sections of the wedges. These may then be pinned to both the inner and outer support cylinders.

Maintenance of the device is accomplished in reverse order of the above procedure depending on the affected component. It may be possible to accomplish minor repairs through the six ports penetrating to the vacuum chamber. Such repairs could involve the application of spray coatings to the first wall surface or the replacement of tiles at the first wall depending on the impurity control scheme.

Major repairs to non-toroidally continuous structures within the nuclear island and above the device midplane may be made by removing selected sectors of the upper end caps. Such repair or replacement operations could involve upper support components such as wedges and end caps, upper or inner and outer vertical sections of the TF coil, and upper sections of the blanket assembly. Removal of upper blanket sectors in this manner would only be possible if the EF system could be designed such that individual coils would not interfere with the vertical removal of these blanket sectors.

Other major repairs could be accomplished with the removal of the upper end caps. Access to all components within the nuclear island is possible with simple vertical lifts without the need for cutting of components or the breaking of welds.

6.3.5 Blanket/First Wall

An engineering drawing showing a cross-section of the blanket/first wall system is shown in figure 6.4. The top view for the reference RCTR device (figure 6.3) shows the inlet and outlet port arrangements for this system.

The concept shown is a separate blanket/first wall design using liquid lithium coolant, a vanadium structure and an HT-9 reflector. The concept is designed for relatively simple vertical lift assembly/disassembly operations. The first wall is constructed as a single unit and vacuum tested before assembly.

The blanket is divided along the midplane of the device to allow removal of the first wall and is also divided toroidally into six sectors for a total of twelve sectors above and below the midplane. The weight of each sector is 230 tonnes (244 tonnes loaded with lithium). The blanket is fed lithium through ports located in the steel wedges at the top and bottom of the device. In a sector above the midplane, the flow enters through top ports located in each sector and empties into manifolds which form the top area of the blanket sector. From here the flow is channeled poloidally around the device.

The blanket is divided into two main lithium channels and a reflecting region which is located furthest from the plasma. The lithium flows poloidally down the channel closest to the plasma, reverses direction at the midplane of the device and flows back up the remaining channel until it reaches the exit plenum and leaves out the upper port. Some of the lithium flow is also channeled through the reflector on the return leg for heat removal purposes.

A similar flow pattern occurs for sectors below the midplane. These sectors can be drained if needed while the device is not in use simply by letting the lithium flow out the bottom ports. The upper sectors could also be drained through channels at the midplane which exit between the lower blanket sectors.

The major parameters characterizing the reference blanket concept are summarized in table 6.4. These parameters were arrived at using neutronic, MHD flow and stress analyses detailed in the thesis. The inboard blanket system consists of a 35 cm blanket region and a 30 cm reflector. In the outboard sections, the blanket is 45 cm thick with a 45 cm reflector section. The inlet and outlet channels are 70 cm i.d. circular pipes with wall thicknesses of 8 mm (inlet) and 2 mm (outlet). Each blanket sector is divided toroidally into 10 poloidal flow channels. The wall thicknesses of the blanket structure varies, decreasing as the flow progresses through the blanket system from 8 to 2 mm to minimize the MHD pressure drop.

The total thermal power deposited in the nuclear island at a neutron wall

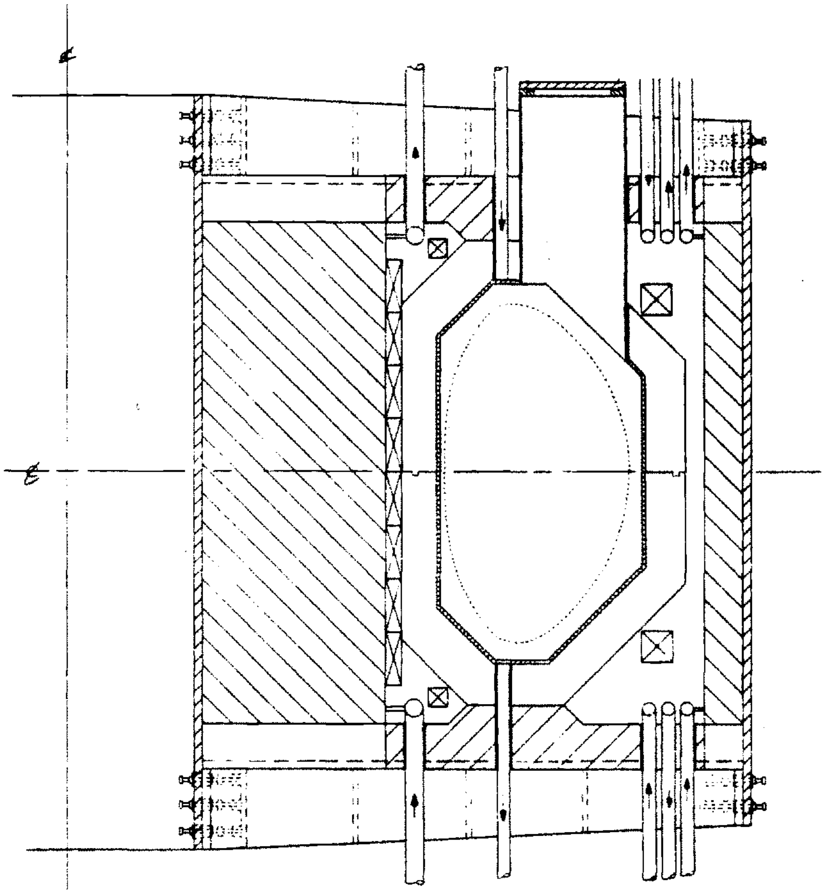

Figure 6.4: Blanket/First Wall Cross-Section

Total Thermal Power, MW	2925
Blanket Power, MW	1309
Reflector Power, MW	488
Neutron Wall Loading, MW/m^2	3
Energy Multiplication	1.21
Tritium Breeding Ratio	1.25
Li Mass Flow/Sector, kg/s	144
Mass Flow/Channel, kg/s	14.4
Average Li Velocity, m/s	0.08 - 0.12
Peak Magnetic Field, T	3.51
Pressure Drop/Sector, MPa	1.7
Pumping Power, MW	5.3
Maximum Primary Stress, MPa	83
Exit Li Temperature, C	550
Thermal Efficiency, %	42
Blanket Total Mass, T	281
Reflector Total Mass, T	2643

Table 6.4: Reference Blanket Parameters

loading of 3 MW/m^2 is 2925 MW. Of this total, 1309 MW are deposited directly in the blanket region with an additional 488 MW deposited in the reflector. The remaining thermal energy is deposited in the first wall (1068 MW) and the coils lying outside the blanket system (60 MW). The corresponding energy multiplication factor is 1.21. The tritium breeding ratio obtained from a one-dimensional calculation of 1.25 is assumed to be adequate for self-sufficiency in tritium.

Using an inlet lithium temperature of 300 C and a temperature rise through the blanket system of 250 C, the exit lithium temperature is 550 C. With experience from similar lithium blanket systems having the same exit temperature [37], a blanket thermal efficiency of 42 % is assumed. The lithium mass flow rate required per sector is 144 kg/s or 14.4 kg/s per poloidal channel. The velocity of lithium flow through the changing cross-sections of the blanket system varies between and 0.08 and 0.12 m/s.

The moderate lithium velocities and relatively low peak field (3.5 T) of the device results in a moderate pressure drop due to MHD effects of 1.7 MPA. The pumping power required of the system is 5.3 MW. The maximum primary stress of 83 MPa occurs at the first wall side of the blanket near the inlet. The entire blanket system consists of 163 tonnes of lithium (140 in blanket, 23 in reflector), 141 tonnes of vanadium structure including manifolds and inlet/outlet channels and 2620 tonnes of HT-9 reflector material.

The first wall system consists of a 6mm first wall (closest material surface to the plasma), a 3 cm back supporting wall and 4mm thick dividing walls forming 4 by 5 cm toroidally directed coolant channels of rectangular cross-section. If a thicker first wall is required to maintain structural integrity against erosion from the plasma, a grooved first wall [37] could be employed to retain the peak thermal stress at acceptable levels.

Lithium enters the first wall system through 40 cm diameter inlets located at the top of the device at alternating steel wedges. The inlets feed poloidal manifolds which in turn feed the toroidal channels. The flow travels toroidally for the length of one blanket sector where it empties into another poloidal manifold and exits through an outlet located at the bottom of the device. The poloidal first wall manifolds are kept large to minimize the MHD pressure losses.

Thus, the first wall system resembles a thick toroidal shell with two spare tires (inlet and outlet manifolds) wrapped poloidally around the shell at each intersection of two blanket sectors. These manifolds function as short length (toroidally) blanket sectors and are equal in width to the blanket sections at all locations. The length (toroidally) of each manifold is 50 cm (average) and the wall thicknesses vary from 10 to 2 mm in a similar manner to the blanket system manifolds.

The major parameters characterizing the first wall system are summarized in table 6.5. For the wall loading of 3 MW/m^2, the entire surface heat flux of charged particles and neutrals of 0.75 MW/m^2 is assumed to be incident on the first wall. Thus, 522 MW from the surface heat load in addition to 546 MW (22.7 percent) of neutron power are deposited in the first wall system. The peak and average temperatures of the vanadium first wall are 750 C and 665 C, respectively. The lithium outlet temperature is 550 C and the maximum thermal stress experienced in the first wall is 322 MPa.

The lithium mass flow rate required for a temperature rise through the system of 250 C is 171 kg/s per sector. This results in an average velocity in the toroidal channels of 0.67 m/s and an average velocity in the poloidal manifolds of 0.61 - 0.85 m/s. The pressure drop due to MHD losses in the system is 3.9

Thermal Power, MW	1068
Neutron Wall Loading, MW/m^2	3
Surface Heat Flux, MW/m^2	0.75
Li Mass Flow, kg/s	171
Avg. Li Channel Velocity, m/s	0.67
Avg. Li Manifold Velocity, m/s	0.89
Peak Magnetic Field, T	3.51
Pressure Drop, MPa	3.9
Pumping Power, MW	7.5
Maximum Primary Stress, MPa	104
Maximum Thermal Stress, MPa	322
Plasma-Side Vanadium Temp., C	750
Average Vanadium Temp., C	665
Exit Lithium Temperature, C	550
First Wall Mass, T	160

Table 6.5: Reference First Wall Parameters

MPa resulting in a pumping power required of 7.5 MW. The maximum primary stress of 104 MPa due to MHD pressure losses occurs on the first wall at the location of the inlet manifolds where the pressure is highest.

6.4 Conclusions

The summary and conclusions of the thesis have been given in section 6.2 with the findings of the parametric study and in section 6.3 in the form of a conceptual design for the Resistive magnet Commercial Tokamak Reactor (RCTR).

We find that resistive magnet tokamaks can be attractive in electricity producing applications and should compete favorably with superconducting magnet options. The cost of the major disadvantage associated with the resistive magnet approach - relatively high recirculating power - appears to be moderate and could be offset by decreased magnet and shielding costs. The advantages of decreased complexity and enhanced maintenance (using demountable coils) associated with resistive magnet tokamaks could ultimately make this approach the preferred option for commercial tokamak applications.

6.5 Recommendations

The major recommendation of this study is that the resistive magnet approach to commercial tokamak design should be considered as a viable option in future design studies. Future work should include a more detailed evaluation of the relationship for specific reactor designs between performance, complexity, maintenance, availability and cost. The ultimate cost and attractiveness of commercial tokamaks will likely have as much to do with their complexity and availability as the weight or capital investment associated with the nuclear island.

With regard to the RCTR conceptual design, additional work is needed to define an impurity control option. In addition, using vanadium structure in the first wall and blanket in conjunction with aluminum magnets could make RCTR very attractive as a low activation design. This option should be explored in more detail. The design should be revised as more information becomes available with regard to beta limits, especially in the second regime of stability. Finally, since demountability is potentially a very important asset for resistive magnet tokamaks, more detailed work in this area may be warranted. Remote maintenance schemes could play an important role in the design of the demountable nuclear island.

Appendix A

Parametric Code RTPAC

A.1 Introduction

In this appendix, a listing of the parametric code used to model commercial resistive magnet tokamaks is given. The methodology used to model RCTR was discussed in some detail in chapter 2. A flow diagram was also given. The costing analysis is detailed in appendix B. Before presenting the parametric code RTPAC itself, a few comments are made regarding the relationship between its programming language (MACSYMA) and FORTRAN.

A.2 Interpreting Macsyma Programming

The programs used in this work were written using the MACSYMA program on the PDP-10 "MC" at MIT. Provided here is the means to interpret the program listings included in these appendices for conversion to the FORTRAN language. The conversion is straight forward since the two languages are quite similar. MACSYMA has advantages over FORTRAN in the form of a completely interactive system and many readily available "canned" routines for plotting, integrating, etc.

The following syntax conversions are applicable:

- MACSYMA colon equivalent to FORTRAN equal sign
- MACSYMA square bracket for arrays equivalent to FORTRAN parenthesis

- MACSYMA carat ($\wedge$) or arrow ($\uparrow$) equivalent to FORTRAN double asterisk (**)

- MACSYMA breaks command lines with a comma

- Columns have no special significance in MACSYMA

- Comment statements begin with "/*" and end with "*/" in MACSYMA

- Variable and array names can be of any size in MACSYMA

A MACSYMA program essentially consists of subroutines which begin with "Function(Variable) := (" and end with ")$". The subroutine can be called by any other routine by specifying "Function(Variable)". No variable need be specified in the function statement. Variables are declared using the MODEDECLARE statement which designates variables as floating point (FLOAT) or integer (FIXNUM). The WRITEFILE and CLOSEFILE statements simply have the program output dumped into a file in the users directory and need not be translated for use in a FORTRAN program.

The equivalent of a do loop in MACSYMA is in the form " For n from k thru l do()" where n is the loop variable, k is the lower limit, l is the upper limit and the looped routines are enclosed in the parenthesis. MACSYMA conditional statements are in the form of "IF ... THEN ... ELSE" statements. There are no GO TO statements in MACSYMA.

Any other unrecognizable symbols or variables in the MACSYMA programs to follow are "canned" routines, the equivalent of which are available on most computer systems with FORTRAN compilers. Note that the intention here is not to teach MACSYMA programming. Following the rules above, however, the reader should be able to translate the enclosed programs into FORTRAN.

A.3 RTPAC Code Listing

```
/*PARAMETRIC CODE FOR THE DESIGN OF COMMERCIAL
RESISTIVE MAGNET TOKAMAKS.....*/
PARAM() := ( /* DOES PARAMETRIC SURVEYS OF THE MAJOR INPUTS */
SUPPRESS : TRUE,
FOR NZ FROM 1 THRU MAXNSAVE DO(
IF PASPECT THEN(
ASPECT : ASPMIN+(NZ-1)*ASPINC),
IF PELONG THEN(
ELONG : ELMIN+(NZ-1)*ELINC),
IF PPNET THEN(
PEBETA : PEMIN+(NZ-1)*PEINC),
IF PPWALL THEN(
PWBETA : PWMIN+(NZ-1)*PWINC),
IF PQI THEN(
QI : QIMIN+(NZ-1)*QIINC),
SAVEWANT : TRUE,
IF BSQAWANT THEN(SOL())ELSE(RUN()) ),
NSAVE : 0, N2 :  N2 + 1, PRINT("N2 = ",N2) )$

PARBSQA() := ( PRINTSOL : FALSE,
MAXNSAVE : 100,
FOR NZ FROM 1 THRU NZMAX DO(
FOR NX FROM 1 THRU NXMAX DO(
IF PELONG THEN (
ELONG : ELMIN+(NZ-1)*ELINC,
IF PASPECT THEN(
ASPECT : ASPMIN+(NX-1)*ASPINC),
IF PPWALL THEN(PWBETA : PWMIN+(NX-1)*PWINC))ELSE(
ASPECT : ASPMIN+(NZ-1)*ASPINC,
PWBETA : PWMIN+(NX-1)*PWINC ),
SAVEWANT : TRUE,
SOL(),
OHSINPUT : 10000.,
IF PWOPT = FALSE THEN(/* INPUT IS PNETE INSTEAD OF PWALL */
PEWANT : PEBETA,
PRBETA : PRSTART,
FOR KZ FROM 1 THRU KZMAX DO( IF PNETE < 10.0 THEN PNETE : 10.0,
IF ABS(PNETE - PEWANT) < PEMARGIN THEN(KZ : KZMAX)ELSE(
IF PNETE < PEWANT THEN(PRBETA:PRBETA+(PEWANT-PNETE),SOL())ELSE(
PRBETA : PRBETA-(PNETE-PEWANT), SOL()) ) ), SOL(),
OHSINPUT : 10000.),
```

```
IF SAVEWANT THEN(NSAVE : NZ, N2 :  NX, TOSAVE(NFILE)) ) ) )$

RUN() := ( PEWANT : PEBETA,
PRBETA : PRSTART,
PRINTSOL : FALSE,
SOL(),
FOR KZ FROM 1 THRU KZMAX DO(
IF PNETE < 10.0 THEN PNETE : 10.0,
IF ABS(PNETE - PEWANT) < PEMARGIN THEN(KZ : KZMAX)ELSE(
IF PNETE < PEWANT THEN(PRBETA:PRBETA+(PEWANT-PNETE), SOL())ELSE(
PRBETA : PRBETA-(PNETE-PEWANT), SOL()) ) ),
IF SUPPRESS = FALSE THEN PRINTSOL : TRUE,
SOL(),
OHSINPUT : 10000.,
IF SAVEWANT THEN(NSAVE:NSAVE+NSAVEINC, TOSAVE(NFILE)) )$

SOL():= BLOCK(
BETALIMIT(),
OHSYSTEM(DOUBLESWING),
IF INNEROH THEN(RA : RF - A - DELTAF - OHTHICKNESS)
ELSE(RA : RF - A - DELTAF),
IF RA < 2.  THEN RA : 2.,
RB : RF + A + DELTAI,
RT : A*ELONG + DELTAT,
IF INNEROH THEN(R1OPT(), R1 :  OPTR1),
IF OPTWANT THEN(TFOPT(), THICKOUT : OUTOPT, TOPTHICK : TOPOPT),
RO : RF+A+DELTAI+THICKOUT,
HEIGHT : A*ELONG+DELTAT+TOPTHICK,
IF INNEROH THEN(MGIN : RMI - R1)ELSE(MGIN : RF - A - DELTAF - R1),
CONSTR : STRVER(RF),
ENERGYINBORE : MAGENERELON(),
PWALL : 0.4*MYPOWERCONST*(CBETA)**2*(A/100.)**3*BF**4
/(RF/100.)**2*ELONG*SQRT(2./(1.+ELONG**2)),
PWALLWALL : PWALL*A/(A+TSO*100.),
PFUSION : 4.*3.1416**2*A/100.*RF/100.*PWALL*
SQRT((1.+ELONG**2)/2.)*1.25,
PERF : (CBETA/RF*A*A*BF*BF/100.)**2,
IF PRINTSOL THEN(
PRINT("**************** INPUT *******************"),
PRINT("POWERCONST = ", POWERCONST,
" ELONG = ", ELONG),
IF BETAMODELWANT THEN(
PRINT("SECOND STABILITY BETA (MHD EQUIL. LIMIT)"),
```

```
PRINT("QI = ", QI, "QPSI = ", QPSI) ),
IF DTHREEWANT THEN (PRINT("D-III DATA FIT USED FOR BETA"),
PRINT("QS = ", QS, "TRIANGULARITY = ", TRIANG) ),
IF TRYONWANT THEN (PRINT("TRYON BETA LIMIT USED FOR BETA"),
PRINT("QIFIRST = ", QIFIRST) ),
IF SYKESWANT THEN (PRINT("SYKES BETA LIMIT USED FOR BETA"),
PRINT("QIFIRST = ", QIFIRST) ),
IF SIMPLEBETA THEN (PRINT("SIMPLE BETA SCALING USED"),
PRINT("CBETA = ", CBETA) ),
PRINT("INPUTQS = ", INPUTQS, " BSQAWANT = ", BSQAWANT,
" PWOPT = ", PWOPT) ),
WALLAREA : PFUSION/1.25/PWALLWALL,
PBLANK : PFUSION*(MULTIPLICATION-1.),
SOLSQUARE(),
TFRESISPOWER : PTOT*FLANGEFUDGE/1.E6,
RESISPOWER : TFRESISPOWER+PEXTRA,
ENERGYMAG : ENERGYSQ+ENERGYINBORE,
IF PRINTSOL THEN(
PRINT("***************** GEOMETRY ********************"),
IF COPPERTF = O THEN PRINT("THIS IS A COPPER TF MAGNET")ELSE(
PRINT("THIS IS AN ALUMINUM TF MAGNET")),
PRINT("RMI =", RMI, "R1 =", R1, "THKIN =", MGIN, "DTIN =", DELTAF),
PRINT("MINR =", A, "MAJR =", RF, "THKOUT = ", THICKOUT,
"DTOUT =", DELTAI, "RO =", RO),
PRINT("PLASMAHEIGHT = ", ELONG*A, "THKTOP = ",
TOPTHICK, "DELTATOP = ", DELTAT),
PRINT("MAGHALFHEIGHT = ", HEIGHT, " ASPECT RATIO =", ASPECT),
PRINT("***************** CHARACTERISTICS ********************"),
PRINT("B SQUARED A = ", BSQA, " PLASMA VOL = ",
4.*PI**2*RF*A**2*ELONG),
PRINT("B =", BF, "BPK =", BF*RF/(R1+MGIN), "IPLASMA =", IP,
"BETA = ", CBETA*A/RF) ),
IF INCLUDEEF THEN(VERTICALCURRENT(),
EFM : MASSOFEFCOILS,
EFRESIS : TOTRES*EFRESISFUDGE) ELSE(EFM : 0.,
EFRESIS : 0.),
POWERBALANCE(),
FEDCST(),
PLANTEFF : PNETE/(PFUSION+PBLANK),
QELEC : PGE/AUX,
RECIRC : 1./QELEC,
MASSUTIL : TOTALMASS/1.E3/(PFUSION+PBLANK),
```

```
SPECDENS : (PFUSION+PBLANK)/VOLNUCL,
IF PRINTSOL THEN(
PRINT("PFUSION = ", PFUSION, "PWALL (NEUTRON, AT WALL) = ",
PWALLWALL, "WALL AREA = ", WALLAREA),
PRINT("PBLANKET (M = 1.2) = ",
PFUSION*MULTIPLICATION, "PGROSSELEC (EFFIC = 0.35) = ", PGE),
PRINT("PNETELEC = ", PNETE, "PLANTEFF = ", PLANTEFF),
PRINT("TF POWER = ", PTOT/1.E6, "TOTAL AUX = ", AUX),
PRINT("TEMPE = ", TEMPE, "FCUIN = ", FCUIN, "FCUOUT = ", FCUOUT,
"ENERGYMAG = ", ENERGYMAG),
PRINT("PPUMP = ", AUX5, "QELEC = ", QELEC,
"RECIRC FRAC = ", RECIRC),
PRINT("WEIGHT = ", TOTALMASS, "TENSTRESS = ", CONSTR, "(",
CONSTR*6895., ")"),
PRINT("MASSUTIL(T/MWtH)=", MASSUTIL, "VOLISLAND(M**3)=", VOLNUCL),
PRINT("SPECDENS(MWTH/M**3)=", SPECDENS, "NUCLISLCSTDOLPERWE=",
(CC221+CC222)/PNETE, "DIRCSTDOLPERWE=", CDIR/PNETE),
PRINT("PERF= ", PERF, "MARGIN OF IGNITION =", PERF/1.305,
"MI*ELONG =", PERF/1.305*ELONG ) ),
IF PRINTSOL THEN(
PRINT("******************* OHMIC COIL *********************"),
IF INNEROH THEN(PRINT("OH COIL IS INSIDE THE TF COIL")),
PRINT("OH COIL THICKNESS = ", OHTHICKNESS),
PRINT("BURNTIME = ", BURNTIME, "TELECTRON = ", TELECTRON,
"DOUBLESWING = ", DOUBLESWING),
PRINT("OHS =", OHSI/6895., "(", OHSI, ")", "INITIAL OHEN
(FINAL) =", ENOHI, "(", ENOHF, ")"),
PRINT("INITIAL OHDISP (FINAL) =", RESTOHI,
"(", RESTOHF, ")" ),
PRINT("INITIAL CURRENT (FINAL) = ", IOHI, "(", IOHF, ")"),
PRINT("INITIAL OHFIELD (FINAL) = ", BOHI, "(", BOHF, ")"),
PRINT("INITIAL SWING (FINAL) = ", SWINGI, "(", SWINGF, ")"),
PRINT("******************* EF COILS ***********************"),
PRINT(" COIL 1 COIL 2"),
PRINT("LOCATION - RADII", RFIL1, RFIL2),
PRINT("LOCATION - HEIGHT", HEI1, HEI2),
PRINT("COIL RADII ", COILRAD1, COILRAD2),
PRINT("CURRENTS ", IFIT1, IFIT2),
PRINT("CURRENT DENSITY", CURDEN1, CURDEN2),
PRINT("ENERGY = ", ENERCOIL/1.E9, " RES POW = ", EFRESIS/1.E6,
" MASS = ", MASSOFEFCOILS),
PRINT("****************** COSTING *********************"),
```

```
PRINT("ACCT 21 ACCT 22 ACCT 23 ACCT 24 ACCT 25 ACCT 26"),
PRINT(CC21, CC22, CC23, CC24, CC25, CC26),
PRINT("C221 (NUCLEAR ISLAND XCEPT MAGNETS) = ",
CC221, "MAGNET COST = ", CC222),
PRINT("TOTAL DIRECT COST = ", CDIR,
"CAPITAL COST = ", TCC),
PRINT("COST OF ELECTRICITY = ", LRR
) ) )$

TOSAVE(NFILE) := (
N : NSAVE,
RFARRAY[N, N2] :  RF/100.,
INBARRAY[N, N2] :  DELTAF/100.,
OUTBARRAY[N, N2] :  DELTAI/100.,
R1ARRAY[N, N2] :  R1/100.,
ROARRAY[N, N2] :  RO/100.,
HEIGHTARRAY[N, N2] :  HEIGHT/100.,
OHTHICKARRAY[N, N2] :  OHTHICKNESS/100.,
TFTHICKARRAY[N, N2] :  MGIN/100.,
PLASMAIARRAY[N, N2] :  IP/1.E6,
ENERGYARRAY [N, N2] :  ENERGYMAG/1.E9,
WEIGHTARRAY[N, N2] :  WEIGHT/1.E6,
BETAARRAY[N, N2] :  BETAEQ,
BFARRAY[N, N2] :  BF,
ELONGARRAY[N, N2] :  ELONG,
WALLARRAY[N, N2] :  PWALLWALL,
TFSTRESSARRAY[N, N2] :  CONSTR*6895./1.E6,
ASPECTARRAY[N, N2] :  RF/A,
PFUSIONARRAY[N, N2] :  PFUSION,
BURNARRAY[N, N2] :  BURNTIME,
NETELECARRAY[N, N2] :  PNETE,
TFPOWERARRAY[N, N2] :  PTOT/1.E6,
TOTALAUXARRAY[N, N2] :  AUX,
CAPCOSTARRAY[N, N2] :  TCC,
COEARRAY[N, N2] :  LRR,
QARRAY[N, N2] :  QI,
MASSUTILARRAY[N, N2] :  MASSUTIL,
NUCLISLDOLPERWE[N, N2] :  (CC221+CC222)/PNETE,
SPECDENSARRAY[N, N2] :  SPECDENS,
RECIRCARRAY[N, N2] :  RECIRC,
APPLY(APPENDFILE, FILE),
APPLY(CLOSEFILE, FILE) )$
```

```
/* INPUTS AND CONSTANTS ************** */ ( PEXTRA : 0.,
NSAVEINC : 1,
PRINTSOL : TRUE,
TEMPE : 25., /* TEMPERATURE OF CU IN C */
MU : 4.*3.14159E-7,
COPPERTF : 0, /* IF 0 THEN COPPER, OTHERWISE ALUMINUM */
N2 :  1,
QI2 :  2.5,
RMISMALLEST : 2.5,
RFSTARTUP : FALSE,
R1SMALLEST : 1.,
PTHMARGIN : 0.02,
STRUCFRAC : 0.1,
FLANGEFUDGE : 1.05,
INCLUDEEF : TRUE,
SAVEWANT : FALSE,
INNEROH : TRUE,
INNEREF : TRUE,
OHSINC : 200.,
OHSINPUT : 10000.,
PO :  200.E6,
VO :  1200.,
DDOMIN : 0.1,
CONSTANTFORRMI : 0.5,
DDOMAX : 5.0,
RTAPMINUS : 0.0,
NUSTRESS : 0.3,
A1 :  1.,
A2 :  1.,
MAXNSAVE : 12,
NFILE : 1,
ASPMIN : 2.,
ASPINC : 0.5,
ELMIN : 1.0,
ELINC : 0.25,
PEMIN : 200.,
PEINC : 100.,
PWMIN : 1.0,
PWINC : 1.0,
QIMIN : 1.0,
QIINC : 0.1,
SUPPRESS : FALSE,
```

```
PASPECT : FALSE,
PELONG : FALSE,
NZMAX : 10,
NXMAX : 10,
PPNET : FALSE,
NEWWAY : TRUE,
PPWALL : TRUE,
PQI : FALSE,
FCUIN : 0.9,
FCUOUT : 0.9,
NSAVE : 0,
TEINIT : 2.,
TELECTRON : 20.0,
INTPOLERROR:-10.,
FILLING : .90,
MAXNCONSTR : 100,
CONSTRINC : 50.,
DELTAF : 65.,
DELTAI : 100.,
DELTAT : 80.,
PRSTART : 350.,
MULTIPLICATION : 1.2,
FLOATFORMAT:’F,
FLOATFRAC : 3,
HELPUMP : 5.,
LITHPUMP : 15.,
KZMAX : 10,
PEMARGIN : 2.,
THICKOUT : 100.,
TOPTHICK : 100.,
RMAMINUS : 0.1,
RAMINUS : 0.5,
R1STEP : 5.,
R1STEP1 :  0.5,
KR1MAX : 500.,
OPTWANT : TRUE,
ZEFF:1.,
EFRESISFUDGE : 1.5,
NOHMAX : 100,
ELONG : 1.8,
CURDEN1 :  5.E6,
CURDEN2 :  5.E6,
```

```
RFILFACTOR : 1.1,
DOUBLESWING : -0.3,
BURNTIME : 3600.,
THEAT : 4.,
FRACTIONOFCONTR : 0.8,
ARRAYWANT: FALSE,
TESTFIRSTOH : TRUE,
COMPGRIND : TRUE,
OHSTRESSFIXED : TRUE,
MU2:2.*4.*3.14159E-7,
PI:3.14159,
PISQ : PI**2,
PI2:PI/2.  )$

/* INPUT FOR BETALIMIT SECTION */
(POWERCONST : 2.21/2.5,
ASPECT : 3.,
BETAMODELWANT : FALSE,
DTHREEWANT : TRUE,
TRYONWANT : FALSE,
BSQAWANT : FALSE,
SIMPLEBETA : FALSE,
PWOPT : TRUE,
SYKESWANT : FALSE,
DTHREE2 :  FALSE,
BETPOL : 1.,
LI : 0.8,
QS : 2.5,
QIFIRST : 1.5,
INPUTQS : TRUE,
TRIANG : 0.4,
QPSI : 4.2,
QI : 1.4,
BETAFRAC : 0.95,
PWBETA : 3.,
PEBETA : 1200.,
PRBETA : 400.,
M : 1.2,
EFF : 0.42 )$

(/* INPUT FOR COSTING AND BALANCE OF PLANT */
COMPOSITE : FALSE, /* TELLS IF TF IS COMPOSITE OF AL AND C */
SWITCHTHETA : 3.1416*5./16., /* THETA WHERE COIL TURNS
```

```
FROM COPPERTF TO AL */
NSAVE : 0,
CONSTRUCTIONTIME : 8.,
CONSTRUCTIONTIMENP : 6.,
MWYRPERM2 :  20., /* FOR VANADIUM */
ONETURBINE : FALSE, /* ALLOWS CALC OF MULTIPLEX COST
FOR A SINGLE OR N TURBINES */
LPLANTS:40., /* TOTAL PLANT LIFE FOR STARFIRE IN YEARS */
LPLANT : 40., /* TOTAL PLANT LIFE IN YEARS */
TREPLACES : 2./12., /* TIME TO REPLACE BLKT/FW SECTION FOR
STARFIRE IN YEARS */
TREPLACE : 2./12., /* TIME TO REPLACE BLKT/FW SECTION IN YEARS */
PWALLS : 3.6, /* STARFIRE WALL LOAD */
MWYRPERM2S : 20., /* FLUENCE LIFE OF STARFIRE BLKT/FW */
AVAILNPFACTOR : 0.07, /* AVAIL OF MULTIPLEX PLANT IS HIGHER
THAN SINGLE LARGE PLANT */
UL : 0.1, /* EXPONENTS FOR AVAILABILITY SCALING FUDGE */
UR : 0.1,
UPW : 0.10,
UMW : 0.1,
DLITHE : 450.,
CPLI : 4200.,
PDTLI : 250.,
KSAVE : 0,
NUMBERPLANTS : 3.,
CDRIVEWANT : FALSE, /* ADD CURRENT DRIVE IN COST? */
ETA : 0.42, /* THERMAL EFFICIENCY */
TSO : 0.15, /* SCRAPEOFF */
TSHI : 0.35, /* INNER REFLECTOR THICKNESS */
TSHO : 0.55,
SHAPEFAC : 1.10, /* INCREASE IN VOLUME DUE TO SQUARED-OFF
SHAPE OF BLKT/FW */
SHCOST : 15.0, /* THIS FOR STEEL REFLECTOR */
TMULT : 0.0, /* MULTIPLIER THICKNESS */
TFWALL : 0.06, /* FIRST WALL THICKNESS */
FWDENSITY : 6100., /* VANADIUM */
COVERAGEFACTOR : 0.8, /* FRACTION OF OUTER TORUS WHERE THE PLASMA
SEES THE BLANKET */
INFLATION : 0.,
DWELL : 100., /* DWELL TIME BETWEEN PULSES IF ONLY OH DRIVEN */
FWCOST : 200., /* UNIT COST OF FIRST WALL MATERIAL, $/KG */
MULTDENSITY : 1850., /* BERYLLIUM */
```

```
PINO :  3000.,
EXPSTOR : 0.0,
PSCOST : 0.04,
MAGCOOLCOST : 0.004,
MULTCOST : 50.,
BRDENSITY : 6100., /* VANADIUM BLANKET STRUCTURE */
BRCOST : 200.,
TFCOST : 30.,
CUCOST : TFCOST,
ALFUDGE : .75,
OHCOST : 30.,
COOLANTFRACTION : 0.92, /* FRACTION OF BLANKET
THAT IS COOLANT BY VOLUME */
COOLDENSITY : 450., /* LIQUID LITHIUM */
COOLCOST : 30.0,
ETACD : 0.65, /* EFFICIENCY OF CURRENT DRIVE */
CPCOOLANT : 4200.,
TEMPRISECOOLANT : 250.,
TBR : 1.1,
AVAIL : 0.75,
PMULT : 4670.,
OUTFRACTION : 0.6, /* FRACTION OF BLANKET WHICH IS COUNTED AS
OUTER BLANKET FOR VOLUME CALCULATION */
SHDENSITY : 8030.  )$ (/* STARFIRE PARAMETERS TO SCALE FROM */
/* RF HEATING POWER (MWE) */
PHTS : 90.,
/* BLANKET THERMAL POWER */
PTS : 4065.,
/* TOROIDAL FIELD COIL VOLUME (M**3) */
VTFCS : 781.,
/* PRIMARY POWER (MW) */
PRIMS : 3800.4,
/* LIMITER HEATING (MW) */
PLIMS : 199.6,
/* TURBINE REJECT HEAT (MW) */
PWASTS : 2593.2,
/* FIRST WALL AREA (M**2) */
AREAWS : 754.976,
/* INBOARD BLANKET THICKNESS (M) */
DELBIS : .28,
/* OUTBOARD BLANKET THICKNESS (M) */
DELBOS : .46,
```

```
/* WALL MINOR RADIUS AT MIDPLANE (M) */
RWALLS : 2.14444,
/* INBOARD BLANKET/SHIELD THICKNESS (M) */
DLBSIS : 1.2,
/* OUTBOARD BLANKET/SHIELD THICKNESS (M) */
DLBSOS : 2.60,
DELSIS : DLBSIS-DELBIS,
DELSOS : DLBSOS-DELBOS,
/* PLASMA VOLUME (M**3) */
VOLS : 781.36,
/* PLASMA CURRENT (AMPS) */
PCURS : 10.0752E6,
/* PLASMA MAJOR RADIUS (M) */
RFS : 7.00,
/* PLASMA E-SHAPEDNESS */
DEITYS : .5,
/* AVERAGE ELECTRON DENSITY (1/M**3) */
XNES : 1.1774E20,
/* AVERAGE ELECTRON TEMPERATURE (KEV) */
TES : 17.3,
/* OHMIC HEATING OF PLASMA (MW) */
POHMS : .193,
/* PLASMA HEIGHTPL (M) */
HEIGTS : 6.22,
/* PLASMA MINOR RADIUS AT MIDPLANE (M) */
AS : 1.94444,
/* TOROIDAL FIELD AT R : RO (T) */
BPLASS : 5.80,
/* TURBINE INPUT POWER (MW) */
PINS : 4033.,
/* TOTAL REJECT HEAT (MW) */
PREJS : 2620.2,
/* GROSS ELECTRIC POWER (MWE) */
PGES : 1439.8,
/* FIRST WALL/BLANKET LIFETIME (Y) */
BLIFES : 6.,
/* FUEL BURNUP (G/DAY) */
DBURNS : 539.5,
/* PLANT AVAILABILITY */
AVAILS : .75,


/* WILDCAT PARAMETERS TO SCALE FROM */
```

```
PHTW : 107.,
PGEW : 1017.,
PTW : 2915.,
BMAXW : 14.35,
BPLASW : 8.23,
RFW : 8.58,
ASPW : 3.25,
AW : RFW/ASPW,
PRFW : 107.,
DBSIW : .82,
RMW : 4.92,
PCURW : 29.9E6,
DEITYW : .2,
XNEW : 2.55E20,
TEW : 30.,
AVAILW : .75,
THRUW : 1.,
VSPDW : 1.,
/* DEMO PARAMETERS TO SCALE FROM */
POHMD : .520 )$

( /* STARFIRE POWER FLOW PARAMETERS FOR COMPARISON */
/* STARFIRE VALUES FOR COMPARISON */
SPF : 3608.,
SPBKT : 457.,
SPHT : 90.,
SPLIM : 200.,
SPSCHL : 65.,
SPRIM : 3800.,
SPIN : 4033.,
SPGE : 1440.,
SPWAST : 2593.,
SPREJ : 2620.,
SPREJH : 0.0,
SAUX1 :  13.,
SAUX2 :  5.,
SAUX3 :  152.5,
SAUX4 :  7.,
SAUX5 :  33.,
SAUX6 :  27.,
SPT : 4065.,
SAUX : 237.5,
SREJEC : 2685.,
```

```
SPNETE : 1202.  )$ /* INITIALIZE ARRAYS *********** */
(ARRAY(XBUTTCOIL2ARRAY, 11, 11),
ARRAY(COILCLEARANCE1ARRAY, 11, 11),
ARRAY(ENERGYINEFCOIL, 11, 11),
ARRAY(RESTOTINEFCOIL, 11, 11),
ARRAY(AMPTURNINEFCOIL, 11, 11),
ARRAY(MASSINEFCOIL, 11, 11) )$ ( ARRAY(AARRAY, FLOAT, 12, 12),
ARRAY(RFARRAY, FLOAT, 12, 12),
ARRAY(WALLARRAY, FLOAT, 12, 12),
ARRAY(INBARRAY, FLOAT, 12, 12),
ARRAY(OUTBARRAY, FLOAT, 12, 12),
ARRAY(R1ARRAY, FLOAT, 12, 12),
ARRAY(ROARRAY, FLOAT, 12, 12),
ARRAY(HEIGHTARRAY, FLOAT, 12, 12),
ARRAY(OHTHICKARRAY, FLOAT, 12, 12),
ARRAY(ENERGYARRAY, FLOAT, 12, 12),
ARRAY(TFSTRESSARRAY, FLOAT, 12, 12),
ARRAY(WEIGHTARRAY, FLOAT, 12, 12),
ARRAY(BETAARRAY, FLOAT, 12, 12),
ARRAY(BFARRAY, FLOAT, 12, 12),
ARRAY(ELONGARRAY, FLOAT, 12, 12),
ARRAY(WALLARRAY, FLOAT, 12, 12),
ARRAY(PFUSIONARRAY, FLOAT, 12, 12),
ARRAY(TFPOWERARRAY, FLOAT, 12, 12),
ARRAY(TOTALAUXARRAY, FLOAT, 12, 12),
ARRAY(NETELECARRAY, FLOAT, 12, 12),
ARRAY(QELECARRAY, FLOAT, 12, 12),
ARRAY(RECIRCARRAY, FLOAT, 12, 12),
ARRAY(COSTARRAY, FLOAT, 12, 12),
ARRAY(COSTNPARRAY, FLOAT, 12, 12),
ARRAY(COEARRAY, FLOAT, 12, 12),
ARRAY(COENPARRAY, FLOAT, 12, 12),
ARRAY(OHSARRAY, FLOAT, 12, 12),
ARRAY(BURNARRAY, FLOAT, 12, 12),
ARRAY(PLANTARRAY, FLOAT, 12, 12),
ARRAY(MARGINARRAY, FLOAT, 12, 12),
ARRAY(ITIMESAARRAY, FLOAT, 12, 12) )$

/* COLLECTION OF SUBROUTINES FOR USE IN PARAMETRIC CODE *RCTR* */
/* ALLOWS YOU TO RUN SOL() ON THE BASIS OF A GIVEN QSUBI AND
GEOMETRY. ROUTINE WILL RUN SOL AT BETAFRAC TIMES THE
CRITICAL BETA EITHER USING TRYON, D III OR DIFFUSE CURRENT
MODEL. IT ALSO FINDS IP, B AND A, R FOR INPUT TO SOL() WITH
```

```
A STIPULATED PW, PE, AND RECIRCULATING POWER */
BETALIMIT() :=( MYPOWERCONST : POWERCONST*5./2.,
/* DEFINED DIFFERENTLY FROM LESLIE'S */
EPS : 1./ASPECT,
LAMBDA : BETPOL+LI/2.,
IF BETAMODELWANT THEN(INPUTQS : FALSE, QIFIRST : QI),
IF INPUTQS THEN( /* BASE Q'S ON D-III QS */
IAB : 5./2./QS*EPS*(1.+ELONG**2)*(1.+EPS**2*(1.+LAMBDA**2/2.))*
(1.24-0.54*ELONG+0.3*(ELONG**2+TRIANG**2)+0.13*TRIANG),
QIFIRST : 5.*ELONG*EPS/IAB)ELSE( /* BASE Q'S ON SYKES QI */
IAB : 5.*ELONG*EPS/QIFIRST,
QS : 5./2./IAB*EPS*(1.+ELONG**2)*(1.+EPS**2*(1.+LAMBDA**2/2.))*
(1.24-0.54*ELONG+0.3*(ELONG**2+TRIANG**2)+0.13*TRIANG)),
BETAMODEL : 100.*(EPS/QI**2*(1.+3.*ELONG**2)/4.*
SQRT(1.-QI**2/QPSI**2)),
DTHREE : 27.*EPS**1.3*ELONG**1.2*(1.+1.5*TRIANG)/QS**1.1,
IF DTHREE2 THEN(DTHREE : 3.5*IAB),
SYKES : 22.*ELONG/(ASPECT*QIFIRST),
TRYON : SYKES*2.76/4.40,
SIMPBETA : 100.*0.148*(ELONG/1.6)/ASPECT,
IF BETAMODELWANT THEN BETAEQ:BETAMODEL*BETAFRAC,
IF DTHREEWANT THEN BETAEQ:DTHREE*BETAFRAC,
IF SYKESWANT THEN BETAEQ : SYKES*BETAFRAC,
IF TRYONWANT THEN BETAEQ:TRYON*BETAFRAC,
IF SIMPLEBETA THEN BETAEQ : SIMPBETA,
IF BSQAWANT THEN(IF PWOPT THEN(/* IF BSQA AND PWALL
ARE THE INPUTS */
ABETA : BSQA**2*MYPOWERCONST*(BETAEQ/100.)**2*ELONG/
(PWBETA*2.5*SQRT((1.+ELONG**2)/2.))  - TSO)ELSE(
/* IF BSQA AND PNETE ARE INPUTS */
PFBETA:(PEBETA+PRBETA)/M/EFF,
RMAJ : PFBETA/(BSQA**2*2.*PI**2*ELONG*(BETAEQ/100.)**2*
MYPOWERCONST),
ABETA : RMAJ/ASPECT,
PWBETA : BSQA**2*MYPOWERCONST*(BETAEQ/100.)**2*ELONG/
(2.5*SQRT((1.+ELONG**2)/2.)*(ABETA+TSO))) )
ELSE( /* IF PWALL AND PNETE ARE INPUT */
PFBETA:(PEBETA+PRBETA)/M/EFF,
THEC:PFBETA/PWBETA*EPS/(5.*PI**2*SQRT((1.+ELONG**2)/2.)),
ABETA:-TSO/2.+SQRT(TSO**2/4.+THEC)),
RMAJ : ABETA/EPS,
PWPLASMA:PWBETA*(ABETA+TSO)/ABETA,
```

```
BFBETA : SQRT(SQRT(5./2.*PWPLASMA/MYPOWERCONST/(BETAEQ/100.)**2*
SQRT((1.+ELONG**2)/2.)/ELONG/ABETA)),
CURR : ABETA*BFBETA*IAB*1.E6,
BF :BFBETA,
IP : CURR,
RF : RMAJ*100.,
A : ABETA*100.,
BSQA : BF**2*A/100.,
CBETA:BETAEQ/100.*RF/A )$

OHSYSTEM(DELTASWING):= BLOCK(
ESE : SQRT((1.+ELONG**2)/2.),
CBETAAQ2BASE : .2/1.5*(3.18)**2,
CBETAAQ2 :  CBETA/ELONG*QI**2,
BP:2.E-7*IP/(A/100.)/ESE,
/* BETP:2.68E-16*NC*TELECTRON/BP**2,
LI/2 = .7 FOR ENERGY
BZVERF:1.E-7*(IP/(RF/100.))*(LOG(8.*RF/A/ELONG)+BETP-1.5+.7),
FLUXF:BZVERF*3.1416*(RF)*(RF)/10000., */
/* LI/2 = 1 FOR INDUCTANCE */
IF RFSTARTUP THEN DELTASWING : -1.,
RESTOT(),
AIDATF : RESTIVITY,
CELON : 1.0 + 0.283*(ELONG-1.), /* GOOD FOR S = 1 - 4 */
LIF:4.*3.1416E-7*(1 + (A/RF)**2.8)*RF/100.*IP*
(LOG(8.*RF/A/CELON) - 2.+ ELONG/(1.+ELONG**2)),
IF RFSTARTUP THEN LIF : 0.0,
RESVOLSTARTUP : LIF*.1,
FORRESVOLFLATTOP(),
RESVOLHEAT : RESVOLFLATTOP/BURNTIME*(THEAT*7.31*
(TEINIT/TELECTRON/.05)**(-0.63)),
FLUXF :FRACTIONOFCONTR*18.*(1.   + 1.43*(1.5/(3.3*(3.2)**2))
(CBETAAQ2-CBETAAQ2BASE))*
EXP(0.28*(1.   + (ELONG-1.5))*(ELONG-1.5))*
(RF/A/3.36)**(-1.69)* (QI/3.2)**(-1.16*(1.   + .25*(QI-3.2)))*
(BF/6.7)* (RF/300.)**1.9,
SWING : LIF-FLUXF+RESVOLFLATTOP+RESVOLSTARTUP+RESVOLHEAT,
SWINGI : SWING/(1.-DELTASWING),
SWINGF : SWING*DELTASWING/(1.-DELTASWING),
SWING : SWINGI,
RMA : R1-1.,
RMI : R1*CONSTANTFORRMI,
IF INNEROH THEN(OHCOIL()),
```

```
IF INNEROH THEN(HOH:2.*(A*ELONG+DELTAT))ELSE(HOH :
2.*(A*ELONG+DELTAT+TOPTHICK)),
IF INNEROH THEN(OHS : OHSINPUT*6895.)ELSE(OHS : OHM() ),
IF FLAGOH = 1 THEN(IF PRINTSOL THEN
PRINT("PROBLEM NOT CONVERGED...RMA < .25")),
OHTHICKNESS : RMA-RMI,
OHSI : OHS,
BOHI : BOH,
VOLOHI : HOH*(RMA*RMA-RMI*RMI)*3.1415*FILLING,
IOHI : BOH*HOH/100./4./3.1415E-7,
RESTOHI : AIDATF*100.*3.1415/HOH*(RMA+RMI)/(RMA-RMI)/
FILLING*IOHI**2,
POWOHI : (IOHI)**2*RESTOHI/VOLOHI,
ROHAVEI : (RMA+RMI)/2.,
LOHI : 4.*3.1415E-7*3.1415*ROHAVEI**2/100./(HOH)*0.88,
ENOHI : 0.5*LOHI*IOHI*IOHI,
SWING : SWINGF,
IF INNEROH THEN(OHS : OHSINPUT*6895.)ELSE(OHS : OHM() ),
OHSF : OHS,
BOHF : BOH,
IOHF : BOHF*HOH/100./4./3.1415E-7,
RESTOHF : AIDATF*100.*3.1415/HOH*(RMA+RMI)/(RMA-RMI)/
FILLING*IOHF**2,
POWOHF : (IOHF)**2*RESTOHF/VOLOHF,
ENOHF : 0.5*LOHI*IOHF*IOHF )$

FORRESVOLFLATTOP() := (
RESVOLFLATTOPOLD : 5.E-9*(RF/100.)/(ELONG*(A/100.0)**2)*
(15./TELECTRON)**1.5*
BURNTIME*IP,
DENSITY :1.89E14*CBETA*(A/100.)/(RF/100.)*(A/100.)*
BF**2/SQRT(3.94)/(A/100.),
LOGLAMBDA : 25.3 -1.15*LOG(DENSITY)/LOG(10.)
+ 2.3*LOG(TELECTRON*1000.)/LOG(10.),
RESVOLFLATTOP : 5.E3*BF*LOGLAMBDA/10*ZEFF/(
TELECTRON*1000.)**1.5*BURNTIME )$

RESTOT() := (
IF COPPERTF = 0 THEN(
RESTIVITY : 1.57067E-8+0.545491E-10*TEMPE-0.165573E-12*TEMPE**2-
0.449932E-15*TEMPE**3)ELSE(
RESTIVITY: 3.9E-8) )$

OHCOIL() := ( RMA : RF - A - DELTAF,
```

```
IF RMA < 3.  THEN(RMA : 3., RMI : 2.5, FLAGOH : 1)ELSE(
RMI : INTERPOLATE(OHM(), RMI, 2., RMA - RMAMINUS),
FOR N FROM 1 THRU NOHMAX DO(
IF RMI = -10.  THEN (OHSINPUT : OHSINPUT+OHSINC,
OHCOIL2() )ELSE(N:NOHMAX) ),
IF OHSINPUT > 25000.  THEN RMI : RMISMALLEST,
IF RMI < RMISMALLEST THEN RMI : RMISMALLEST) )$

OHCOIL2() :=(
RMI : INTERPOLATE(OHM(), RMI, 2., RMA - RMAMINUS) )$

OHM():= (
CONSTOH:(RMA*(RMA**2-RMI**2)/2.  -
(RMA**3-RMI**3)/3.)/(RMA-RMI)**3,
CONST2OH:3.1415*(RMI**2/1.E4)*(1.+(2.*RMI-3.*RMA+RMA**2*
RMA/RMI**2)/3./(RMA-RMI)),
BOH:(SWING)/CONST2OH,
OHSMOD : OHSINPUT,
PRESS:BOH**2/(4.*3.1415E-7)*CONSTOH/FILLING,
IF INNEROH THEN (PRESS/6895.  - OHSMOD)
ELSE( PRESS) )$

R1OPT() := ( R1 :  RA - RAMINUS,
ATH:PI*(RA**2-R1**2)/1.E4,
JTH:2.*PI*RF*BF/100./(MU*ATH*FCUIN),
PTHOLD:AIDATF*JTH**2*ATH*FCUIN*2.*RT/100.,
R1 :  R1 - R1STEP1,
FOR K FROM 1 THRU KR1MAX DO(
ATH:PI*(RA**2-R1**2)/1.E4,
JTH:2.*PI*RF*BF/100./(MU*ATH*FCUIN),
PTH:AIDATF*JTH**2*ATH*FCUIN*2.*RT/100.,
IF R1 <= R1SMALLEST THEN (PTHOLD : PTH, R1 :  R1SMALLEST),
IF R1 > RA THEN R1 :  RA - 2.,
IF (ABS((PTHOLD-PTH)/PTH)) < PTHMARGIN
THEN(OPTR1 :  R1, K : KR1MAX)
ELSE(R1 :  R1 - R1STEP,
PTHOLD : PTH) ) )$


TFOPT() := ( FP : (RA-R1)/RA,
RTAP : (RF - RTAPMINUS)/100.,
RA : RA/100.,
RB : RB/100.,
RT : RT/100.,
```

```
Z : AIDATF*BF**2*RF**2/1.E4/MU**2,
CC1 :  4.*PI*Z*RT/(RTAP*FCUOUT),
CC2 :  4.*PI*Z/(RTAP*FCUOUT),
CC3 :  8.*PI*Z*RT/(RA**2*(2.*FP-FP**2)*FCUIN),
CC4 :  8.*PI*Z/(RA**2*(2.*FP-FP**2)*FCUIN),
CC5 :  (4.*PI*Z*(RB-RTAP)/(RTAP*FCUOUT) +
4.*PI*Z*LOG(RTAP/RA)/FCUIN),
CC6 :  4.*PI*FCUOUT*RTAP*RT,
CC7 :  4.*PI*FCUOUT*RTAP,
CC8 :  2.*PI*FCUIN*RA**2*(2.*FP-FP**2)*RT,
CC9 :  (2.*PI*FCUIN*RA**2*(2.*FP-FP**2) +
4.*PI*FCUOUT*RTAP*(RB-RTAP)
+ 2.*PI*(RTAP**2-RA**2)*FCUIN),
CC9P : 4.*PI*FCUOUT*RTAP*(RB-RTAP)+2.*PI*(RTAP**2-RA**2)*FCUIN,
IF NEWWAY THEN(BIGX : A1*VO/(A2*PO),
OUTOPT : SQRT(BIGX*CC1/CC6)*100.,
TOPOPT : SQRT(BIGX*CC5/CC9P)*100.  )ELSE(
OUTOPT : INTERPOLATE(SOLDDO(), DDO, DDOMIN, DDOMAX)*100.,
TOPOPT : SQRT(BIGX*CC5/(CC7*OUTOPT/100.+BIGX*CC2/OUTOPT/100.+
BIGX*CC4+CC9))*100.),
RTAP : RTAP*100.,
RB : RB*100.,
RA : RA*100.,
RT : RT*100.  )$

SOLDDO() := ( BIGX : A1*VO/(A2*PO),
CC6*DDO**2+(-BIGX*CC2+CC7*DDO**2)*SQRT(
BIGX*CC5/(CC7*DDO+BIGX*CC2/DDO+BIGX*CC4+CC9)) - BIGX*CC1)$

STRVER(RF) := ( IF INNEROH THEN( OHT : OHTHICKNESS)ELSE(OHT : 0.0),
BFRF:BF*RF/100.,
RA:RA/100.,
RB:RB/100.,
RO:RO/100.,
MAG:BFRF*BFRF/MU2*2.*3.14159,
R1 :  R1/100.,
FT:MAG*(LOG(RB/RA)+ ((RA-R1)**2/4.+(RA-R1)*R1/3.)/RA/RA),
FTNEW1:MAG*(LOG(RB/RA)),
FTNEW2 :  MAG*((RA-R1)**2/4.+(RA-R1)*R1/3.)/RA/RA,
FTNEW3 :  MAG*(RO*(RO-RB)/3.  - (RO-RB)**2/4.)/RB**2,
FTNEW:FTNEW1+FTNEW2+FTNEW3,
MT:MAG*(RB-RA +(RA-R1)/RA/RA*((RA-R1)**2/5.+2.*R1*
(RA-R1)/4.+R1**2/3.)  ),
```

```
MTNEW1:MAG*(RB-RA),
MTNEW2:  MAG*(RA-R1)/RA/RA*((RA-R1)**2/5.+2.*R1*
(RA-R1)/4.+R1**2/3.),
MTNEW3:  MAG*(R0-RB)/RB**2*((R0-RB)**2/5.+R0**2/3.-
R0*(R0-RB)/2.),
MTNEW:MTNEW1+MTNEW2+MTNEW3,
S1:(MT*3./2./3.1415 - ((R0**3-RB**3)/(R0**2-RB**2)*FT/3.1415))/
((RA**3-R1**3) - (R0**3-RB**3)*(RA**2-R1**2)/(R0**2-RB**2) ),
S1NEW:(MTNEW*3./2./3.1415 - ((R0**3-RB**3)/(R0**2-RB**2)*
FTNEW/3.1415))/
((RA**3-R1**3) - (R0**3-RB**3)*(RA**2-R1**2)/(R0**2-RB**2) ),
S2 :  3.*MTNEW/2./3.1416/(R0**3-RB**3) - (FTNEW/3.1416 - 3.*
MTNEW/2./3.1416
(R0**2-RB**2)/(R0**3-RB**3) )/((RA**2-R1**2)*(R0**3-RB**3)/(
RA**3-R1**3) - (R0**2-RB**2) ),
BC1 :  RF*BF/MGIN,
SIGMARAD : -BC1**2/2./MU*((3.+NUSTRESS)/2.*
(1.- (R1+MGIN/200.)**2/(MGIN/100.)**2)),
SIGMATH : -BC1**2/2./MU*((3.+NUSTRESS)/2.- (3.*NUSTRESS+1.)/2.*
(R1+MGIN/200.)**2/(MGIN/100.)**2),
FORCEIN : S1NEW*PI*(RA**2-R1**2),
FORCEOUT : S2*PI*(R0**2-RB**2),
CIRCSTRESS:5.*(RF/100.)**2*BF**2*140./(4.*3.1415*
((RF/100.)-(A/100.)-(DELTAF/100.)-R1)*((RF/100.)
-(A/100.)-(DELTAF/100.))  ),
IF INNEROH THEN(CIRCSTRESS:5.*(RF/100.)**2*BF**2*140./(4.*3.1415*
(RMI-R1)*(RMI)/1.E4 ) ),
CIRC : CIRCSTRESS*2.,
VMS : SQRT(CONSTR**2+CONSTR*CIRC+CIRC**2),
R1 :  R1*100.,
R0 : R0*100.,
RA : RA*100.,
RB : RB*100.,
S1NEW/6895.  )$

MAGENERELON() := ( ROMBERGTOL:1.E-2,
RA1 :  RF - A - DELTAF,
MAGEQW : ROMBERG(MAGELON(R), R , RA1*1.0001, RB*.9999),
ROMBERGTOL:1.E-4,
MAGEQW : MAGEQW*BF**2*RF**2/(2.*4.*3.1415E-7)*2.*3.1415*2.,
MAGEQW*1.E-6)$

MAGELON(R) := ( MODEDECLARE([R, FUNCTION(HT)], FLOAT),
```

```
HBORE : IF R <= RF THEN
(A*ELONG+DELTAT)*SQRT(1.-((R-RF)/(A+DELTAF))**2) ELSE
(A*ELONG+DELTAT)*SQRT(1.-((R-RF)/(A+DELTAI))**2),
HBORE/R ) )$

SOLSQUARE() := ( TFTHICK: MGIN,
HH:HEIGHT,
BFRC:BF,
AOL:2.*PI*RTAP*THICKOUT/1.E4, /* OUTER LEG */
JOL:2.*PI*RF*BF/100./(MU*AOL*FCUOUT),
POL:AIDATF*JOL**2*AOL*FCUOUT*2.*(HH-TOPTHICK)/100.,
VOLOL:AOL*FCUOUT*2.*(HH-TOPTHICK)/100.,
ATH:PI*((R1+TFTHICK)**2-R1**2)/1.E4, /* THROAT */
JTH:2.*PI*RF*BF/100./(MU*ATH*FCUIN),
PTH:AIDATF*JTH**2*ATH*FCUIN*2.*(HH-TOPTHICK)/100.,
VOLTH:ATH*FCUIN*2.*(HH-TOPTHICK)/100.,
AH:2.*PI*(RTAP)*TOPTHICK/1.E4, /* HORIZ. LEGS PAST RTAP */
JH:2.*PI*RF*BF/100./(MU*AH*FCUOUT),
PH:AIDATF*JH**2*2.*AH*(RO-THICKOUT-RTAP)/100.*FCUOUT,
VOLH:2.*AH*(RO-THICKOUT-RTAP)/100.*FCUOUT,
/* HORIZ. SECTION FROM CORNER TO RTAP */
PTAP:4.*PI*AIDATF*RF2̂/1.E4*BF2̂/(MU2̂*FCUIN*TOPTHICK/100.)
LOG(RTAP/(R1+TFTHICK)),
VOLTAP:2.*PI*(RTAP2̂-(R1+TFTHICK)2̂)*TOPTHICK/1.E6,
/* INSIDE CORNERS */
ACORNERI:PI*((R1+TFTHICK)2̂/1.E4+R12̂/1.E4+SQRT(TOPTHICK2̂/1.E4
+TFTHICK2̂/1.E4)*(2.*R1+TFTHICK)/100.),
JMINI:2.*PI*RF*BF/100./(MU*ACORNERI*FCUIN),
JCORNERI:.5*(JMINI+JH),
PCORNERI:AIDATF*JCORNERI2̂*2.*TOPTHICK/100.*PI*((R1+TFTHICK)2̂
-R12̂)/1.E4*FCUIN,
VOLCORNERI:2.*PI*((R1+TFTHICK)2̂-R12̂)*TOPTHICK/1.E6,
/* OUTSIDE CORNERS */
ACORNERO:PI*((RO-THICKOUT)2̂/1.E4+RO2̂/1.E4+SQRT(TOPTHICK2̂/1.E4
+TFTHICK2̂/1.E4)*(2.*RO-THICKOUT)/100.),
JMINO:2.*PI*RF*BF/100./(MU*ACORNERO*FCUOUT),
JCORNERO:.5*(JMINO+JH),
PCORNERO:AIDATF*JCORNERO2̂*2.*TOPTHICK*PI*((RO2̂)-
(RO-THICKOUT)2̂)/1.E6*FCUOUT,
VOLCORNERO:2.*PI*RTAP*TOPTHICK*THICKOUT*2./1.E6,
IF INNEROH THEN(VOLNUCL:3.1416*(RO2̂-R12̂)/1.E4*2.*HH/100.)ELSE(
VOLNUCL:3.1416*(RO2̂-RMI2̂)/1.E4*2.*HH/100.),
PTOT:PTH+POL+PH+PTAP+PCORNERI+PCORNERO,
```

```
VOLTOT:VOLTH+VOLOL+VOLH+VOLTAP+VOLCORNERI+VOLCORNERO,
IF COPPERTF=0 THEN(ENSITY:8900.)ELSE(ENSITY:2700.),
WEIGHTSQ:VOLTOT*ENSITY,
ENERGYSQ : 2.*PI*BF2̂*(RF/100.)2̂/MU*(HH/100.*LOG((R1+TFTHICK)/R1)
+HH*RTAP/1.E4*(100./(RO-THICKOUT)-100./RO)+TOPTHICK/100.*
LOG(RTAP/(R1+TFTHICK))+TOPTHICK*RTAP/1.E4*(100./RTAP-
100./(RO-THICKOUT))) )$
```

Appendix B

Costing Code

B.1 Introduction

The costing routine used in the parametric studies is given in this appendix. Cost scalings not explicitly referenced in the code are scaled from STARFIRE [62]. Discussion of the basic methodology used is given in chapter 2. The first section of the code calculates the reactor power balance and weights of the components of the nuclear island. The second section finds direct cost, capital cost and cost of electricity for single and multiplexed plants with variable construction time, inflation rate and availability.

B.2 Costing Code Listing

```
/* COSTING ROUTINE FOR RTPAC BASED ON FEDC GUIDELINES FOR
TPSS STUDIES AND USING STARFIRE TYPE SCALINGS. 1985 DOLLARS
USED WITH VARIOUS INFLATION RATES AND CONSTRUCTION
TIMES POSSIBLE */
POWERBALANCE() := ( ETA : EFF,
HEIGHT : HEIGHT/100.,
RO : RO/100.,
RMI : RMI/100.,
HOH : HOH/100.,
RMA : RMA/100.,
RF : RF/100.,
DELTAI : DELTAI/100.,
DELTAF : DELTAF/100.,
MGIN : MGIN/100.,
R1 :  R1/100.,
```

```
A : A/100.,
/* BLANKET/SHIELD THICKNESS (M)
-DISTANCE BETWEEN OH AND FW/SCRAPE INTERFACE*/,
DELBSI : DELTAF-TSO,
DELBSO : DELTAI-TSO,
/* BLANKET THICKNESS (M) -
BLANKET PLUS FIRST WALL MINUS REFLECTOR THICKNESS */ ,
DELBI : DELBSI-TSHI,
DELBO : DELBSO-TSHO,
/* BREEDER THICKNESS (M) - JUST BLANKET, NO FW OR MULT. */
DELBRI : DELBI-TMULT-TFWALL,
DELBRO : DELBO-TMULT-TFWALL,
/* CALCULATE FIRST WALL */
RWALL1 :  A+TSO,
RWALL2 :  A*ELONG+TSO,
AREAW : WALLAREA,
VOLF1 :  2.*PISQ*RWALL1*RWALL2*RF,
VOLF2 :  2.*PISQ*(RWALL1+TFWALL)*(RWALL2+TFWALL)*RF,
VOLFW : VOLF2*SHAPEFAC-VOLF1*SHAPEFAC,
FWM : VOLFW*FWDENSITY*0.5+VOLFW*COOLDENSITY*0.5,
/* CALCULATE VOLUME OF PLASMA (M**3) */
VOLPL : 2.*PISQ*A*A*ELONG*RF,
/* CALCULATE VOLUME OF SCRAPE OFF REGION (M**3) */
RSO1 :  A+TSO,
RSO2 :  A*ELONG+TSO,
VSO : (2.*PISQ*RSO1*RSO2*RF)*SHAPEFAC-VOLPL,
/* CALCULATE VOLUME OF BLANKET (M**3) */
RBL1OUT : RSO1+DELBO,
RBL2OUT : RSO2+DELBO,
RBL1IN : RSO1 + DELBI,
RBL2IN : RSO2 + DELBI,
OUTFRACBLKT : OUTFRACTION*(RF+DELTAI-TSHO-DELBRO/2.)/
(RF-DELTAF+TSHI+DELBRI/2.),
VBLOUT : (2.*PISQ*RBL1OUT*RBL2OUT*RF*SHAPEFAC-VOLFW-VSO-VOLPL)
COVERAGEFACTOR*OUTFRACBLKT,
VBLIN : (2.*PISQ*RBL1IN*RBL2IN*RF*SHAPEFAC-VOLFW-VSO-VOLPL)*
(1.-OUTFRACBLKT),
VBL : (VBLOUT + VBLIN),
/* CALCULATE VOLUME OF MULTIPLIER */
RMULT1 :  RSO1+TMULT+TFWALL,
RMULT2 :  RSO2+TMULT+TFWALL,
VMULT : (2.*PISQ*RMULT1*RMULT2*RF)*SHAPEFAC-VOLFW-VSO-VOLPL,
```

```
/* CALCULATE VOLUME OF BREEDER */
VBR : VBL-VMULT,
/* CALCULATE COST OF FIRST WALL AND BLANKET */
/* BREEDER REFERRED TO IS REALLY BLANKET STRUCTURE
(VAN) - REAL BREEDER IS THE COOLANT */
CFW : (VOLFW*FWDENSITY*FWCOST*0.5+VOLFW*
COOLDENSITY*COOLCOST*0.5)/1000000.,
CMULT : VMULT*MULTDENSITY*MULTCOST/1000000.,
CBREEDER : VBR*BRDENSITY*BRCOST/1000000.*(1.  - COOLANTFRACTION),
VOLCOOL : VBR*COOLANTFRACTION,
CCOOLANT : VOLCOOL*COOLDENSITY*COOLCOST/1000000.,
CBKT : CFW+CMULT+CBREEDER+CCOOLANT,
BLM : FWM+VMULT*MULTDENSITY+VBR*BRDENSITY+VOLCOOL*COOLDENSITY,
/* CALCULATE VOLUME OF SHIELD (M**3) -
SHIELD IS REALLY A REFLECTOR */
RSH1IN : RBL1IN+TSHI,
RSH2IN : RBL2IN+TSHI,
RSH1OUT : RBL1OUT+TSHO,
RSH2OUT : RBL2OUT+TSHO,
OUTFRACSHLD : OUTFRACTION*(RF+DELTAI-TSHO/2.)/(RF-DELTAF+TSHO/2.),
VSHIN : (2.*PISQ*RSH1IN*RSH2IN*RF*SHAPEFAC-VBLIN/(1.-OUTFRACBLKT)
-VOLFW-VSO-VOLPL)*(1.-OUTFRACSHLD),
VSHOUT : (2.*PISQ*RSH1OUT*RSH2OUT*RF*SHAPEFAC-
VBLOUT/OUTFRACBLKT/COVERAGEFACTOR
-VOLFW-VSO-VOLPL)*OUTFRACSHLD*COVERAGEFACTOR,
VSH : VSHIN + VSHOUT,
SHM : VSH*SHDENSITY*0.80+VSH*COOLDENSITY*0.20,
TFM : WEIGHTSQ,
/* CALCULATE VOLUME OF OHMIC HEATING COIL (M**3) */
VOHC : PI*(R1**2.-RMI**2.)*HEIGHT*2.,
IF INNEROH THEN VOHC : PI*(RMA**2-RMI**2)*HOH*2.,
OHM : VOHC*8900.,
/* CALCULATE THE TOTAL MASS OF NUCLEAR ISLAND */
STRUCMASS : (TFM+BLM+SHM+EFM+OHM)*STRUCFRAC,
TOTALMASS : OHM+TFM+SHM+BLM+EFM+STRUCMASS,
HEIGHTPL : 2.*A*ELONG,
/* POWER BALANCE MODEL */
PLIM : .10*WALLAREA*1.25*.25*PWALLWALL,
/* SHIELD REJECT HEAT */
/* PSCHLD : 65.*PT/PTS, */
PSCHLD : 0.0,
PRIM : PFUSION+PBLANK-PSCHLD-PLIM,
```

```
/* RF HEATING OF THE PLASMA AS BYPRODUCT OF CURRENT DRIVE */
/* LOWER HYBRID */
IF CDRIVEWANT THEN(
PHT : PHTS*(IP*DENSITY*1.E6/TELECTRON)/
(PCURS*XNES/TES) ) ELSE( PHT : 0.0),
/* BOP AUXILIARIES */
AUX1 :  13.,
AUX2 :  RESISPOWER + RESTOHI/1.E6/3.,
IF INCLUDEEF THEN(AUX2 :  RESISPOWER + RESTOHI/1.E6/3.
+ EFRESIS/1.E6),
/* RF SYSTEM */
AUX3 :  PHT/ETACD,
/* CRYOGENICS */
/* AUX4 :  7.*VTFC/VTFCS, */
/* NO SUPERCONDUCTING MAGNETS */
AUX4 :  0.0,
/* PUMPING POWERS */
AUX5 :  HELPUMP + LITHPUMP,
/* INPUT POWER TO TURBINE */
PIN : PRIM+AUX5+PLIM,
PGE : ETA*PIN,
PWAST : (1.-ETA)*PIN,
/* HEAT TRANSPORT AND CONDENSATION */
AUX6 :  27.*PWAST/PWASTS,
AUX : AUX1+AUX2+AUX3+AUX4+AUX5+AUX6,
PNETE : PGE-AUX,
PREJ : PWAST+AUX6,
/* HEAT REJECTED FROM RF SYSTEM */
PREJH : AUX3-PHT,
REJECT : PSCHLD+PREJ+PREJH,
HEIGHT:HEIGHT*100.,
RO : RO*100.,
RF : RF*100.,
DELTAI:DELTAI*100.,
DELTAF:DELTAF*100.,
MGIN : MGIN*100.,
R1:R1*100.,
RMI : RMI*100.,
HOH : HOH*100.,
RMA : RMA*100.,
A : A*100.  )$

FEDCST() :=( RMI : RMI/100.,
```

```
RF : RF/100.,
DELTAI : DELTAI/100.,
DELTAF : DELTAF/100.,
MGIN : MGIN/100.,
R1 :  R1/100.,
A : A/100.,
ALCOST : TFCOST*ALFUDGE,
IF COPPERTF > 0 THEN (TFCOST : ALCOST, OHCOST : ALCOST),
T085 :  (1.+0.06)**(1985.-1979.),
/* ACCT 20 */
/* LAND AND LAND RIGHTS */
CC20 :  3.3*T085,
/* ACCT 21 */
/* STRUCTURES AND SITE FACILITIES */
/* SITE IMPROVEMENTS AND FACILITIES */
CC211 :  11.15*((PFUSION*MULTIPLICATION)/4000.)**0.5*T085,
CC211NP : CC211*NUMBERPLANTS**0.5,
/* REACTOR BUILDING */
CC212 :  157.44*(VOLNUCL/24000.)**0.5*T085,
CC212NP : CC212*NUMBERPLANTS,
/* TURBINE BUILDING */
CC213 :  35.92*(PGE/1440.)**0.5*T085,
IF ONETURBINE THEN (EXPT1:0.5) ELSE(EXPT1:1.0),
CC213NP : 35.92*NUMBERPLANTS**EXPT1*(PGE/1440.)**0.5*T085,
/* REACTOR MAINTENANCE BUILDING */
CC214 :  55.57*(VOLNUCL/24000.)**0.5*T085,
CC214NP : CC214*NUMBERPLANTS**0.5,
/* TRITIUM BUILDING */
CC215 :  8.63*((PFUSION*MULTIPLICATION)/4000.)**0.5*T085,
CC215NP : CC215*NUMBERPLANTS**0.5,
/* ELECTRICAL EQUIPMENT BUILDING */
CC216 :  9.16*(PGE/1440.)**0.5*T085,
CC216NP : CC216*NUMBERPLANTS**0.5,
/* OTHER BUILDINGS AND STRUCTURES */
CC217 :  20.0*((PFUSION*MULTIPLICATION)/4000.)**0.5*T085 +
3.26*(AUX/240.)**0.5*T085,
CC217NP : CC217*NUMBERPLANTS**0.5,
/* ACCT 21 TOTAL */
CC21 :  CC211+CC212+CC213+CC214+CC215+CC216+CC217,
CC21NP : CC211NP+CC212NP+CC213NP+CC214NP+CC215NP+CC216NP+CC217NP,
/* ACCT 22 */
/* REACTOR PLANT EQUIPMENT */
```

```
/* ACCT 221 */
/* REACTOR SYSTEM */
/* REACTOR VACUUM/IMPURITY CONTROL */
CC2211 :  (4.86+2.45)*VOLPL/VOLS*T085,
/* BLANKET AND FIRST WALL */
CC2212 :  CBKT*T085,
/* SHIELD AND STRUCTURE */
/* VACUUM DUCT, RF AND ECRH SHIELD */
CC2213A : 77.29*VOLPL/VOLS*0.5*T085,
/* MAGNET SHIELD - THIS IS REALLY REFLECTOR,
MAGNET IS THE SHIELD */
CC2213B : SHM*SHCOST/1.E6,
/* PRIMARY STRUCTURE AND SUPPORT */
CC2214 :  STRUCMASS*20./1000000.*T085,
CC221 :  CC2211 + CC2212 + CC2213A + CC2213B + CC2214,
/* MAGNETS */
CEF : EFM*2.*TFCOST/1.E6*T085,
COH : OHM*OHCOST/1000000.*T085,
CC2221 :  CEF+COH,
CTF : TFM*TFCOST/1000000.*T085,
IF COMPOSITE THEN(CTF:PARTIALMASSCU*CUCOST/1000000.*T085 +
(TFM-PARTIALMASSCU)*ALCOST/1000000.*T085),
CC2222 :  CTF,
CC222 :  CC2221+CC2222,
/* RF HEATING AND CURRENT DRIVE */
/* USE THIS TO ACCOUNT FOR COST OF HEATING POWER (LHRF)
ADDITION TO POWER BALANCE (IN OTHER SUB.)
IS SMALL FOR LONG PULSE SO NEGLECT..*/
CC223A : 33.49*(IP*DENSITY*1.E6/TELECTRON)/(PCURS*XNES/TES)*T085,
/* ECRH PLASMA BREAKDOWN */
CC223B : 2.82*RF/RFS*HEIGHTPL/HEIGTS*(BF/BPLASS)**2.*T085,
CC223 :  CC223A + CC223B,
CC223NP : CC223*NUMBERPLANTS**0.666,
/* VACUUM PUMPING SYSTEMS */
CC224 :  4.89*(2.*PI**2*A**2*RF*ELONG/950.)**0.67*T085,
CC224NP : CC224*NUMBERPLANTS**0.5,
/* POWER CONDITIONING */
/* MAGNET POWER SUPPLIES */
PSTF : RESISPOWER*PSCOST*T085,
PSPF : 27.2*IP/PCURS*1.5*T085, /* SOME ALLOWANCE HERE */
PSOH : RESTOHI/1.E6/3.*PSCOST*T085,
CC2251 :  PSTF+PSPF+PSOH,
```

```
/* ENERGY STORAGE FOR MAGNET SYSTEMS (FROM OHTE/DIII)
INCL. ALLOWANCE FOR PF*/
CC2252 :  2600.*(ENERGYMAG/1.E6)*1.E-6*(1.06)**(1985.-1976.)*1.5,
CC225 :  CC2251+CC2252,
CC225NP : CC225*NUMBERPLANTS**0.666,
/* MAIN HEAT TRANSFER AND TRANSPORT SYSTEMS */
/* PRIMARY COOLANT SYSTEM (INCL. BLANKET, SHIELD, LIMITER) */
/* MASS FLOW LITHIUM (KG/HR) - BLKT, SHIELD, LIMITER AND
WALL ALL LITHIUM COOLED */
/* ASSUME 4 PERCENT OF POWER GOES INTO MAGNETS */
PMFLI:1000000.*(PFUSION+PBLANK)*0.96/(CPLI*PDTLI)*3600.,
/* COST OF PUMPS AND MOTOR DRIVES */
CPPUMP:(PMFLI)*2./10000000.*T085,
/* 100M OF PIPING */
CPPIPE:100.*0.15*T085,
/* PRIMARY HEAT EXCHANGER */
CPHX:PRIM*0.025*T085,
/* TANKS */
VOLLIE:(VBL*0.8)*1.1,
CPTANK:(VOLLIE)*0.0011*T085,
/* CLEANUP SYSTEM */
CPCLEN:(VOLLIE*DLITHE)*1.2E-5*T085,
/* TOTAL COST FOR PRIMARY COOLANT SYSTEM */
CC2261:CPPUMP+CPPIPE+CPHX+CPTANK+CPCLEN,

/* INTERMEDIATE COOLANT SYSTEM
SECONDARY MASS FLOW OF LITHIUM (KG/HR) */
/* $300,000 PER 100000 KG/HR */
CPUMP:PMFLI/100000.*0.3*T085,
/* $15 PER KWTH - LI TO STEAM */
CSG:15.*PRIM*0.001*T085,
CC2262:CPUMP+CSG,
CC2262NP : CC2262*NUMBERPLANTS**0.666,
/* MAGNET COOLING $4/KWTH */
CC2263:((AUX2+PEXTRA)+0.04*(PFUSION+PBLANK))*MAGCOOLCOST*T085,
/* RESIDUAL HEAT REMOVAL SYSTEM
USE 2.5CC2264:0.025*CC2261,
CC2264NP : CC2264*NUMBERPLANTS**0.666,
/* HEAT TRANSPORT TOTAL */
CC226 :  CC2261+CC2262+CC2263+CC2264,
CC226NP : (CC2261+CC2263)*NUMBERPLANTS+CC2262NP+CC2264NP,
/* FUEL HANDLING */
```

```
/* RADIOACTIVE WASTE TREATMENT AND DISPOSAL */
CC2271 :  4.8*((PFUSION+PBLANK)/4000.)**0.7*T085,
/* FUEL HANDLING AND STORAGE SYSTEMS */
CC2272 :  (33.2*((PFUSION+PBLANK)/4000.)**0.7 + 5.4*TBR)*T085,
CC227 :  CC2271 + CC2272,
CC227NP : CC227*NUMBERPLANTS**0.5,
/* INSTRUMENTATION AND CONTROL */
CC228 :  23.41*T085,
/* MAINTENANCE EQUIPMENT */
CC229 :  50.69 + 0.02*(CC221+CC222+CC223+CC224+
CC225+CC226+CC227+CC228),
CC229NP : CC229*NUMBERPLANTS**0.5,
/* ACCT 22 TOTAL */
CC22 :  CC221+CC222+CC223+CC224+CC225+CC226+CC227+CC228+CC229,
CC22NP : NUMBERPLANTS*(CC221+CC222+CC228)+CC223NP+CC224NP+CC225NP+
CC226NP+CC227NP+CC229NP,
/* ACCT 23 */
/* TURBINE PLANT EQUIPMENT */
/* TURBINE-GENERATORS */
EXPN : NUMBERPLANTS/(1+NUMBERPLANTS),
CC231 :  77.33*SQRT(PIN/PINS)*T085,
IF ONETURBINE THEN(EXPT2:0.5)ELSE(EXPT2:1.0),
CC231NP : 77.33*SQRT(PIN/PINS)*NUMBERPLANTS**EXPT2*T085,
/* MAIN STEAM (OR OTHER FLUID) SYSTEM */
CC232 :  4.37*SQRT(PIN/PINS)*T085,
CC232NP : 4.37*SQRT(PIN/PINS)*NUMBERPLANTS**EXPT2*T085,
/* CONDENSING SYSTEMS */
CC233 :  19.18*PWAST/PWASTS*T085,
CC233NP : CC233*NUMBERPLANTS**EXPN,
/* FEED HEATING SYSTEM */
CC234 :  9.39*PLIM/PLIMS*T085,
CC234NP : CC234*NUMBERPLANTS**EXPN,
/* OTHER TURBINE PLANT EQUIPMENT */
CC235 :  50.84*PIN/PINS*T085,
CC235NP : CC235*NUMBERPLANTS**EXPN,
/* INSTUMENTATION AND CONTROL EQUIPMENT */
CC236 :  8.70*T085,
CC236NP : CC236*NUMBERPLANTS**EXPN,
/* ACCT 23 TOTAL */
CC23 :  CC231+CC232+CC233+CC234+CC235+CC236,
CC23NP : CC231NP+CC232NP+CC233NP+CC234NP+CC235NP+CC236NP,
/* ACCT 24 */
```

```
/* ELECTRIC PLANT EQUIPMENT */
/* SWITCHGEAR */
CC241 :  12.39*(PGE/1440.)**0.5*T085,
/* STATION SERVICE EQUIPMENT */
CC242 :  17.04*(PGE/1440.)**0.5*T085,
/* SWITCHBOARDS (INCLUDING HEAT TRACING) */
CC243 :  7.8*(PGE/1440.)**0.5*T085,
/* PROTECTIVE EQUIPMENT (GENERAL STATION GROUNDING SYSTEMS */
/* AND CATHODIC PROTECTION) */
CC244 :  2.11*(PGE/1440.)**0.5*T085,
/* ELECTRICAL STRUCTURES AND WIRING CONTAINERS */
CC245 :  (11.12+6.28*PGE/PGES)*T085,
CC245NP : (11.12+6.28*PGE*NUMBERPLANTS/PGES)*T085,
/* POWER AND CONTROL WIRING */
CC246 :  (23.0+13.0*PGE/PGES)*T085,
CC246NP : (23.0+13.0*PGE*NUMBERPLANTS/PGES)*T085,
/* ELECTRICAL LIGHTING */
CC247 :  8.20*(PGE/1440.)**0.5*T085,
/* ACCT 24 TOTAL */
CC24 :  CC241+CC242+CC243+CC244+CC245+CC246+CC247,
CC24NP : (CC241+CC242+CC243+CC244+CC247)*
NUMBERPLANTS**0.5+CC245NP+CC246NP,
/* ACCT 25 */
/* MISCELLANEOUS PLANT EQUIPMENT - INCLUDE ENERGY STORAGE
FOR PULSED SYSTEMS HERE */
/* GENERAL MISCELANEOUS */
CC25A : 40.77*(PIN/PINS)**0.5*T085,
CC25ANP : CC25*NUMBERPLANTS*0.5,
/* ENERGY STORAGE */
CC25B : (32.0 + 1.9*DWELL)*(1.+0.06)**(1985-1983),
/* FROM ANL PULSED VS SS STUDY (SODIUM SYSTEM) */
CC25B : CC25B*(PIN/PINO)**EXPSTOR,
IF CDRIVEWANT = TRUE THEN CC25B : 0.0,
/* TOTAL MISCELANEOUS */
CC25 :  CC25A + CC25B,
CC25NP : CC25ANP + CC25B,
/* ACCT 26 */
/* HEAT REJECTION SYSTEM */
CC26 :  44.34*PREJ/PREJS*T085,
CC26NP : CC26*NUMBERPLANTS**0.666,
/* TOTAL DIRECT COST */
CDIR : CC20+CC21+CC22+CC23+CC24+CC25+CC26,
```

```
CDIRNP : CC20+CC21NP+CC22NP+CC23NP+CC24NP+CC25NP+CC26NP,
/* INDIRECT COST - 35CINDIR : 0.35*CDIR,
CINDIRNP : 0.35*CDIRNP,
/* GENERAL SYSTEM CONTINGENCY - 15CONTIN : (CDIR+CINDIR)*0.15,
CONTINNP : (CDIRNP+CINDIRNP)*0.15,
/* THE SUM OF DIRECT, INDIRECT, AND CONTINGENCY
IS THE TOTAL CONSTRUCTED COST*/
/* FINANCIAL PARAMETERS AS FUNCTION OF INFLATION RATE
AND CONSTRUCTION TIME */
IF INFLATION = 0.  THEN(MONEYCOST : 4.2, /* (% PER YEAR) */
LAFCR : 8.3, /* PERCENT PER YEAR */ LN30 :  1.00,
/* LAFCR = LEVELIZED ANNUAL FIXED CHARGE RATE */
/* LN30 = 30 YEAR LEVELIZING FACTOR - NO REAL ESCALATION */
IF CONSTRUCTIONTIME = 4. THEN(PCF : 1.070),
/*PLANT COST FACTOR */
IF CONSTRUCTIONTIME = 6. THEN(PCF : 1.109),
IF CONSTRUCTIONTIME = 8. THEN(PCF : 1.148),
IF CONSTRUCTIONTIME = 10. THEN(PCF : 1.188),
IF CONSTRUCTIONTIMENP = 4. THEN(PCFNP : 1.070),
IF CONSTRUCTIONTIMENP = 6. THEN(PCFNP : 1.109),
IF CONSTRUCTIONTIMENP = 8. THEN(PCFNP : 1.148),
IF CONSTRUCTIONTIMENP = 10. THEN(PCFNP : 1.188) ),
IF INFLATION = 6. THEN(MONEYCOST : 9.0, LAFCR : 14.4,
LN30 :  1.95,
IF CONSTRUCTIONTIME = 4. THEN(PCF : 1.324),
IF CONSTRUCTIONTIME = 6. THEN(PCF : 1.523),
IF CONSTRUCTIONTIME = 8. THEN(PCF : 1.751),
IF CONSTRUCTIONTIME = 10. THEN(PCF : 2.014),
IF CONSTRUCTIONTIMENP = 4. THEN(PCFNP : 1.324),
IF CONSTRUCTIONTIMENP = 6. THEN(PCFNP : 1.523),
IF CONSTRUCTIONTIMENP = 8. THEN(PCFNP : 1.751),
IF CONSTRUCTIONTIMENP = 10. THEN(PCFNP : 2.014) ),
IF INFLATION = 10. THEN(MONEYCOST : 12.2, LAFCR : 19.1,
LN30 :  2.822,
IF CONSTRUCTIONTIME = 4. THEN(PCF : 1.517),
IF CONSTRUCTIONTIME = 6. THEN(PCF : 1.866),
IF CONSTRUCTIONTIME = 8. THEN(PCF : 2.296),
IF CONSTRUCTIONTIME = 10. THEN(PCF : 2.824),
IF CONSTRUCTIONTIMENP = 4. THEN(PCFNP : 1.517),
IF CONSTRUCTIONTIMENP = 6. THEN(PCFNP : 1.866),
IF CONSTRUCTIONTIMENP = 8. THEN(PCFNP : 2.296),
IF CONSTRUCTIONTIMENP = 10. THEN(PCFNP : 2.824) ),
```

```
/* TOTAL CAPITAL COST - PCF ACCOUNTS FOR INTEREST AND INFLATION
DURING CONSTRUCTION */
TCC : (CDIR+CINDIR+CONTIN)*PCF,
TCCNP : (CDIRNP+CINDIRNP+CONTINNP)*PCFNP,
/* OPERATIONS AND MAINTENANCE COSTS */
/* OPERATIONS COST - SALARIES, MISC. SUPPLIES AND SUPPORT */
COP : 0.015*(CDIR+CINDIR),
COPNP : 0.015*(CDIRNP+CINDIRNP),
/* AVAILABILITY CALCULATION...TRYING TO MODEL THE EFFECT....
NO BASIS IN HARD FACT */
/* IMPACT OF HIGHER WALL LOAD, ETC CAN BE AFFECTED BY
ADJUSTING THE EXPONENTS */
WALLLIFE : MWYRPERM2/PWALLWALL,
AVAIL : AVAILS*(LPLANTS/LPLANT)**UL*(TREPLACES/TREPLACE)**UR*
(PWALLS/PWALL)**UPW*(MWYRPERM2/MWYRPERM2S)**UMW,
AVAILNP : AVAIL*(1.+AVAILNPFACTOR), /* AVAIL OF MULTIPLEX
IS BETTER THAN FOR LARGE PLANT OF EQUIVELENT SIZE */
/* ANNUAL SCHEDULED COMPONENT REPLACEMENT COST */
/* REPLACE THE BLANKET AND REFLECTOR AND OH COIL
EVERY FIRST WALL LIFETIME */
CSRC : (CBKT+CC2213B+COH)/(WALLLIFE/AVAIL),
CSRCNP : ((CBKT+CC2213B+COH)/(WALLLIFE/AVAILNP))*NUMBERPLANTS,
/* TOTAL OPERATIONS AND MAINTENANCE COST */
COM : COP + CSRC,
COMNP : COPNP + CSRCNP,
/* FUEL COST */
CF : .333*PF/SPF*AVAIL/AVAILS*T085,
CFNP : .333*PF/SPF*AVAILNP/AVAILS*NUMBERPLANTS*T085,
/* COST OF ELECTRICITY (LEVELIZED REVENUE REQUIREMENT
OR LEVELIZED BUSBAR COST OF ELECTRICITY) */
LRR : (LAFCR/100.*TCC + (COM + CF)*LN30)/(0.00876*PNETE*AVAIL),
LRRNP : (LAFCR/100.*TCCNP + (COMNP + CFNP)*LN30)/
(0.00876*PNETE*NUMBERPLANTS*AVAILNP),
RF : RF*100.,
DELTAI:DELTAI*100.,
DELTAF:DELTAF*100.,
MGIN:MGIN*100.,
R1:R1*100.,
RMI:RMI*100.,
A:A*100.  )$
```

Appendix C

Blanket Analysis Codes

C.1 Introduction

In this appendix, input files for TRANSX [39] and ONEDANT [38] and a code listing for the blanket analysis code are given. The code is written in the MACSYMA language which is discussed in Appendix A. The methodology used in the blanket analysis code as well as comments on the use of TRANSX and ONEDANT are described in chapter 3.

C.2 Sample Input File for TRANSX

```
/*filem read 5006 .ctransx matxs5 x7
*file name=input
46hcross-section library for leclaire thesis 1985 /
*matxs5* *tape3c* /
0 3 0 3 1 1 1 3 0 0
30 12 4 53 0 27 1 60 8 42
*h*
*he*
*li6*
*li7*
*li7a*
*f*
*na*
*mg*
*al*
*ti*
*cu*
```

```
*be*
*b10*
*b11*
*c*
*o*
*si*
*p*
*s*
*v*
*cr*
*mn*
*fe*
*ni*
*mo*
*pb*
*w* /
* * 0 0 0 0 /
1 1 *h1* 1.0 1e10 0 /
2 1 *he4* 1.0 1e10 0 /
3 1 *li6* 1.0 1e10 0 /
4 1 *li7* 1.0 1e10 0 /
5 1 *li7a* 1.0 1e10 0 /
6 1 *f19* 1.0 1e10 0 /
7 1 *na23* 1.0 1e10 0 /
8 1 *mgnat* 1.0 1e10 0 /
9 1 *al27* 1.0 1e10 0 /
10 1 *tinat* 1.0 1e10 0 /
11 1 *cunat* 1.0 1e10 0 /
12 1 *be9* 1.0 1e10 0 /
13 1 *b10* 1.0 1e10 0 /
14 1 *b11* 1.0 1e10 0 /
15 1 *cnat* 1.0 1e10 0 /
16 1 *o16* 1.0 1e10 0 /
17 1 *sinat* 1.0 1e10 0 /
18 1 *p31* 1.0 1e10 0 /
19 1 *s32* 1.0 1e10 0 /
20 1 *vnat* 1.0 1e10 0 /
21 1 *crnat* 1.0 1e10 0 /
22 1 *mn55* 1.0 1e10 0 /
23 1 *fenat* 1.0 1e10 0 /
24 1 *ninat* 1.0 1e10 0 /
25 1 *monat* 1.0 1e10 0 /
```

```
26 1 *pbnat* 1.0 1e10 0 /
27 1 *w182l* .2634 1e10 0 /
27 1 *w183l* .1433 1e10 0 /
27 1 *w184l* .3070 1e10 0 /
27 1 *w186l* .2863 1e10 0 /
1 1 *h* 1.0 1e10 0 /
2 1 *he* 1.0 1e10 0 /
3 1 *li* 1.0 1e10 0 /
4 1 *li* 1.0 1e10 0 /
5 1 *li* 1.0 1e10 0 /
6 1 *f* 1.0 1e10 0 /
7 1 *na* 1.0 1e10 0 /
8 1 *mg* 1.0 1e10 0 /
9 1 *al* 1.0 1e10 0 /
10 1 *ti* 1.0 1e10 0 /
11 1 *cu* 1.0 1e10 0 /
12 1 *be* 1.0 1e10 0 /
13 1 *b* 1.0 1e10 0 /
14 1 *b* 1.0 1e10 0 /
15 1 *c* 1.0 1e10 0 /
16 1 *o* 1.0 1e10 0 /
17 1 *si* 1.0 1e10 0 /
18 1 *p* 1.0 1e10 0 /
19 1 *s* 1.0 1e10 0 /
20 1 *v* 1.0 1e10 0 /
21 1 *cr* 1.0 1e10 0 /
22 1 *mn* 1.0 1e10 0 /
23 1 *fe* 1.0 1e10 0 /
24 1 *ni* 1.0 1e10 0 /
25 1 *mo* 1.0 1e10 0 /
26 1 *pb* 1.0 1e10 0 /
27 1 *w* .2634 1e10 0 /
27 1 *w* .1433 1e10 0 /
27 1 *w* .3070 1e10 0 /
27 1 *w* .2863 1e10 0 /
*nheat*
*n2n*
*ntold*
*ntnew*
*ntchk*
*gheat*
*ngam*
```

```
*dmgen*
1 *nheat* 1.0 /
2 *n2n* 1.0 * *
2 *n2na* 1.0 * *
2 *n2n1* 1.0 * *
2 *n2n2* 1.0 * *
2 *n2n3* 1.0 * *
2 *n2n4* 1.0 * *
3 *nt* 1.0 *li6*
3 *ncnt* 1.0 *li7*
3 *nt2a* 1.0 * *
4 *nt* 1.0 *li6* /
4 *n52t* 1.0 *li7a* /
4 *n53t* 1.0 *li7a* /
4 *n54t* 1.0 *li7a* /
4 *n55t* 1.0 *li7a* /
4 *n56t* 1.0 *li7a* /
4 *n57t* 1.0 *li7a* /
4 *n58t* 1.0 *li7a* /
4 *n59t* 1.0 *li7a* /
4 *n60t* 1.0 *li7a* /
4 *n61t* 1.0 *li7a* /
4 *n62t* 1.0 *li7a* /
4 *n63t* 1.0 *li7a* /
4 *n64t* 1.0 *li7a* /
4 *n65t* 1.0 *li7a* /
4 *n66t* 1.0 *li7a* /
4 *n67t* 1.0 *li7a* /
4 *n68t* 1.0 *li7a* /
4 *n69t* 1.0 *li7a* /
4 *n70t* 1.0 *li7a* /
4 *n71t* 1.0 *li7a* /
4 *n72t* 1.0 *li7a* /
4 *n73t* 1.0 *li7a* /
4 *n74t* 1.0 *li7a* /
4 *n75t* 1.0 *li7a* /
4 *n76t* 1.0 *li7a* /
4 *n77t* 1.0 *li7a* /
5 *nt* 1.0 *li6* /
5 *n51* 1.0 *li7a* /
6 *gheat* 1.0 /
7 *ng* 1.0 /
```

```
8 *ndame* 1.0 * * /
*stop* /
*x7
*netout output
*allout fr80 input output box m18 011033
```

C.3 Sample Input File for ONEDANT

```
3
rctr copper high beta case 1
lithium blanket
helium cooled TF coil
igeom=2 ngroup=42 isn=8 niso=27 mt=8
nzone=9 im=15 it=464
maxscm=33000 maxlcm=260000
t
xmesh= 0.0 185.  495.  509.  510.  545.  595.  600.
610.  890.  900.  905.  945.  980.  981.  1060.
xints= 1 150 25 1 50 50 15 1 4 1 15 50 50 1 50
zones= 0 1 2 0 3 4 5 0 0 0 6 7 8 0 9
t
lib=bxslib lng=30
/ savbxs=1
maxord=3 ihm=53 iht=11 ifido=1 ititl=1 lng=30
names= h he li6 li7 li7a f na mg al ti cu be b10 b11
c o si p s v cr mn fe ni mo pb w
edname= nheat n2n ntold ntnew ntchk gheat ngam dmgen
t
matls= ss ni 1.29e-2 cr 1.274e-2 fe 5.499e-2 c 1.971e-4 ;
ht9 fe 7.2264e-2 cr 1.0202e-2 mo 8.501e-4 w 4.25e-4 v 2.55e-4 ;
van v 5.762e-2 cr 1.08e-2 ti 3.6e-3 ;
copr cu 8.49e-2 ;
natli li6 3.45e-3 li7a 4.255e-2 ;
tung w 6.32e-2 ;
/ tih2 ti 4.707e-2 h 9.414e-2 ;
b4c b10 2.084e-2 b11 8.336e-2 c 2.605e-2 ;
insul h 2.902e-2 c 3.809e-2 o 2.616e-2 si 5.712e-3 al 4.394e-3
mg 8.878e-4
assign= ibtf copr 0.90 insul 0.05 ;
oh copr 0.80 ss 0.05 insul 0.05 ;
ibrefl ht9 0.80 natli 0.20 ;
```

```
ibblkt van 0.075 natli 0.925 ;
ibfw van 0.50 natli 0.50 ;
obfw van 0.50 natli 0.50 ;
obblkt van 0.075 natli 0.925 ;
obrefl ht9 0.90 natli 0.10 ;
obtf copr 0.80 ss 0.05 insul 0.05 ;
t
ievt=0 isct=3 fluxp=0 sourcp=0 geomp=0
iquad=4 iitm=40 iitl=60 norm=1.0
source= 0.0 1.0 28r 0.0 f 0.0
sourcx= 293r 0.0 2.0 8.0 8.0 2.0 f 0.0
t
pted=1
points= 2 151 176 227 277 292 299 314 364 415 464
zned=1
edxs= nheat ntnew ngam gheat
edmats= ss copr natli insul van
edisos= fe v ti mo w si al mg h c o cr ni cu li6 li7a
edcons= fe v ti mo w si al mg h c o cr ni cu li6 li7a
micsum= fe,v,ti,mo,w,si,al,mg,h,c,o,cr,ni,cu,li6,li7a,0,nheat,0,
fe,v,ti,mo,w,si,al,mg,h,c,o,cr,ni,cu,li6,li7a,0,gheat,0,
li6,li7a,0,ntnew,0
t
```

C.4 Blanket Analysis Code

```
sol() := ( /* set up first wall boundary to plasma */
x1 :  rf-a-scri,
y1 :  fy1*a,
x2 :  rf-fx2*a,
y2 :  a*elong+scrt,
x3 :  rf+fx3*a,
y3 :  y2,
x4 :  rf+a+scro,
y4 :  fy4*a,
mp :  (y2-y1)/(x2-x1), /* slopes of corner segments */
mpp :  (y4-y3)/(x4-x3),
l12 :  sqrt((y2-y1)**2+(x2-x1)**2),
/* length of corner segments */
l34 :  sqrt((y4-y3)**2+(x4-x3)**2),
tdivi :  fudge*tbli,
```

```
tdivo :  fudge*tblo,
tbltp :  tblo,
tdivt :  tdivo,
treflt :  treflo,
/* find areas of inner and outer sectors */
afw1 :  2.*pi*(x1*y1+(x1+x2)/2.*l12+(x3+x2)/
2.*(x3-x2)+(x3+x4)/2.*l34+x4*y4)*2.,
afw1in :  2.*pi*(x1*y1+(x1+x2)/2.*l12)*2.,
afw1out :  2.*pi*((x3+x2)/2.*(x3-x2)+(x3+x4)/2.*l34+x4*y4)*2.,
/* find volumes enclosed by inner and outer sectors */
vfw1 :  2.*pi*((x2+x1)/2.*(x2-x1)*y1+(x1+(x2-x1)*2./3.)
*0.5*(x2-x1)*(y2-y1)+(x3+x2)/2.*(x3-x2)*y2+
(x3+(x4-x3)/3.)*0.5*(x4-x3)*(y3-y4)+(x4+x3)/2.*
(x4-x3)*y4)*2.,
vfw1in :  2.*pi*((x2+x1)/2.*(x2-x1)*y1+(x1+(x2-x1)
*2./3.)*0.5*(x2-x1)*(y2-y1))*2.,
tfw :  w1+w2+b1, /* total first wall thickness */
/* draw the plasma and the inner first wall boundary */
if drawwish then(drawplasma(),
drawboundary(x1, y1, x2, y2, x3, y3, x4, y4))
else(printwish :  true),
/* find coordinates of corners for next region's boundary */
/* then draw boundary and repeat volume calculations */
findcorners(x1, y1, x2, y2, x3, y3, x4, y4,
tfw, tfw, tfw, l12, l34),
if drawwish then(drawboundary(xc1, yc1, xc2,
yc2, xc3, yc3, xc4, yc4)),
l12c :  sqrt((yc2-yc1)**2+(xc2-xc1)**2),
l34c :  sqrt((yc4-yc3)**2+(xc4-xc3)**2),
afw2 :  2.*pi*(xc1*yc1+(xc1+xc2)/2.*l12c+(xc3+xc2)/2.
*(xc3-xc2)+(xc3+xc4)/2.*l34c+xc4*yc4)*2.,
afw2in :  2.*pi*(xc1*yc1+(xc1+xc2)/2.*l12c)*2.,
afw2out :  2.*pi*((xc3+xc2)/2.*(xc3-xc2)+(xc3+xc4)/2.
*l34c+xc4*yc4)*2.,
vfw2 :  2.*pi*((xc2+xc1)/2.*(xc2-xc1)*yc1+(xc1+(xc2-xc1)
*2./3.)*0.5*(xc2-xc1)*(yc2-yc1)+(xc3+xc2)/2.
*(xc3-xc2)*yc2+(xc3+(xc4-xc3)/3.)*0.5*(xc4-xc3)*(yc3-yc4)
+(xc4+xc3)/2.*(xc4-xc3)*yc4)*2.,
vfw2in :  2.*pi*((xc2+xc1)/2.*(xc2-xc1)*yc1+(xc1+(xc2-xc1)
*2./3.)*0.5*(xc2-xc1)*(yc2-yc1))*2.,
vfw :  vfw2-vfw1, /* volume of first wall region */
vfwin :  vfw2in-vfw1in,
```

```
vfwout :  vfw-vfwin,
fcool :  b1*b2/(tfw*(b2+w3)), /* fraction of first wall
x-s area that is coolant */
vmanfw1 :  2.*((yc1+l12c)*tbli+(xc3-xc2+l34c+yc4)*tblo)*tmanfw,
vmanfw2 :  2.*((yc1+l12c)*hmanifw+(xc3-xc2+l34c+yc4)
*hmanofw)*tmanfw,
massmanfw :  (vmanfw1*nsecfw*4.+vmanfw2*nsecfw+pi*dinlfw
*tinlfw*linlfw*nsecfw*2.)*strucdens,
massfwmain :  vfw*fcool*cooldens+vfw*(1.-fcool)*strucdens,
massfwc :  vfw*fcool*cooldens,
massfw :  massfwmain+massmanfw,
/* find the average q''' in each of the regions of the
blanket/first wall system */
qbarfw :  q0/(aq*tfw)*(1.-exp(-aq*tfw)),
qbardivin :  q0/(aq*tdivi)*(exp(-aq*tfw)-exp(-aq*(tfw+tdivi))),
qbardivout :  q0/(aq*tdivo)*(exp(-aq*tfw)-exp(-aq*(tfw+tdivo))),
qbarblin :  q0/(aq*(tbli-tdivi))*(exp(-aq*(tfw+tdivi))-
exp(-aq*(tfw+tbli))),
qbarblout :  q0/(aq*(tblo-tdivo))*(exp(-aq*(tfw+tdivo))-
exp(-aq*(tfw+tblo))),
qbarreflin :  q0/(aq*trefli)*(exp(-aq*(tfw+tbli))-
exp(-aq*(tfw+tbli+trefli))),
qbarreflout :  q0/(aq*treflo)*(exp(-aq*(tfw+tblo))-
exp(-aq*(tfw+tblo+treflo))),
/* find the temperature distribution in first wall */
tm :  tmax+273.15,
tinlet :  texit-deltat,
const1 :  g1*tm+g1*g2-g3,
z :  flux*w1/2.+q0*w1**2/3.,
tbarfw :  (const1+sqrt(const1**2-4.*g1*(g1*g2*tm-g3*tm+z)))/
(2.*g1)-273.15,
prop(tbarfw),
t0 :  tmax-flux*w1/kvan+q0*w1**2/2./kvan, /* t at inner
surface of front first wall */
sigthtor :  0.055*kvan*(deltatfw+flux*w1/kvan+q0*w1**2/2./kvan),
psur :  flux*afw1, /* total power from surface heat
(non-neutron) load */
pneut :  pwall*m*leak*afw1, /* total (multiplied) neutron
power deposited in system */
power :  psur+pneut, /* total thermal power deposited in system */
powerin :  afw1in/afw1*power,
powerout :  afw1out/afw1*power,
```

```
powfw :  psur+pneut*ffw,
powbl :  pneut*fbl,
powrefl :  pneut*frefl,
plost :  power-powfw-powbl-powrefl,
/* now find flows necessary to carry power for each cooled
first wall sector */
prop(texit),
aflowfw :  vfw/(2.*pi*rf)*fcool,
mdotfwin :  (psur+pneut*ffw)*powerin/power/nsecfw/
(cpli*deltat), /* kg/s */
mdotfwout :  (psur+pneut*ffw)*powerout/power/nsecfw
/(cpli*deltat), /* kg/s */
mdotfw :  mdotfwin+mdotfwout,
vcoolfw :  mdotfw/(aflowfw*densli), /* flow velocity in toroidal
first wall channels */
vinletfw :  mdotfw/(pi*dinlfw**2/4.*densli), /* other vel.
associated w/ first wall */
vmanfwi :  mdotfwin/(tbli*hmanifw*densli),
vmanfwo :  mdotfwout/(tblo*hmanofw*densli),
/* first wall cooling pressure drops */
/* uses variable manifold wall thickness.

eg.  '35' indicates the sector and a or b refers to above
or below the midplane */
if partins then (partialinsulation()), /* makes low radiation
area channels insulated */
if fullins then (insulated()), /* makes all channels except
first wall insulated */
dpfwin :  0.2*sigli*vinletfw*b0**2*dinlfw/2.*sqrt(2.*sigv
*tinlfw/(sigli*dinlfw)), /* inlet */
dpfwout :  0.2*sigli*vinletfw*b0**2*dinlfw/2.
*sqrt(2.*sigv*toutlfw/(sigli*dinlfw)), /* outlet */
dpfw2a :  sigli*vmanfwo*b0**2*rf**2*abs(1./xc2-1./xc3)*
phi(tfw2a,hmanifw)/(1.+phi(tfw2a,hmanifw)),
dpfw2b :  sigli*vmanfwo*b0**2*rf**2*abs(1./rf-1./xc2)*
phi(tfw2b,hmanifw)/(1.+phi(tfw2b,hmanifw)),
dpfw3a :  sigli*vmanfwi*b0**2*rf**2*abs(1./xc2-1./xc1)
*l12c/(xc2-xc1)*phi(tfw35a,hmanifw)/(1.+phi(tfw35a,hmanifw)),
dpfw3b :  sigli*vmanfwi*b0**2*rf**2*abs(1./xc2-1./xc1)
*l12c/(xc2-xc1)*phi(tfw35b,hmanifw)/(1.+phi(tfw35b,hmanifw)),
dpfw4a :  sigli*vmanfwi*(b0*rf/xc2)**2*yc1*
phi(tfw46a,hmanifw)/(1.+phi(tfw46a,hmanifw)),
```

```
dpfw4b :  sigli*vmanfwi*(b0*rf/xc2)**2*yc1*
phi(tfw46b,hmanifw)/(1.+phi(tfw46b,hmanifw)),
dpfw5a :  sigli*vmanfwo*b0**2*rf**2*abs(1./xc3-1./xc4)
*l34c/(xc4-xc3)*phi(tfw35a,hmanofw)/(1.+phi(tfw35a,hmanofw)),
dpfw5b :  sigli*vmanfwo*b0**2*rf**2*abs(1./xc3-1./xc4)
*l34c/(xc4-xc3)*phi(tfw35b,hmanofw)/(1.+phi(tfw35b,hmanofw)),
dpfw6a :  sigli*vmanfwo*b0**2*rf**2/xc4**2*yc4*
phi(tfw46a,hmanofw)/(1.+phi(tfw46a,hmanofw)),
dpfw6b :  sigli*vmanfwo*b0**2*rf**2/xc4**2*yc4*
phi(tfw46b,hmanofw)/(1.+phi(tfw46b,hmanofw)),
dpfw7 :  4.*0.5*((vmanfwi+vmanfwo)/2.)**1.33*b0**1.33
*sigli**0.66*densli**0.33*((hmanofw/2.+hmanifw/2.)/2.)**0.66,
/* for the bend into toroidal channels */
dptotfw :  dpfwin+dpfw2a+dpfw2b+dpfw3a+dpfw3b+dpfw4a+dpfw4b
+dpfw5a+dpfw5b+dpfw6a+dpfw6b+dpfw7+dpfwout,
ppumpfw :  mdotfw*dptotfw/densli*nsecfw,
/* calculate the region of the blanket up to the flow divider */
findcorners(xc1, yc1, xc2, yc2, xc3, yc3, xc4, yc4,
tdivi, tdivt, tdivo, l12c, l34c),
if drawwish then(drawdiv(xc1, yc1, xc2, yc2, xc3, yc3, xc4, yc4)),
l12c :  sqrt((yc2-yc1)**2+(xc2-xc1)**2),
l34c :  sqrt((yc4-yc3)**2+(xc4-xc3)**2),
adiv :  2.*pi*(xc1*yc1+(xc1+xc2)/2.*l12c+(xc3+xc2)/2.
*(xc3-xc2)+(xc3+xc4)/2.*l34c+xc4*yc4)*2.,
adivin :  2.*pi*(xc1*yc1+(xc1+xc2)/2.*l12c)*2.,
adivout :  2.*pi*((xc3+xc2)/2.*(xc3-xc2)+(xc3+xc4)/2.
*l34c+xc4*yc4)*2.,
vdiv :  2.*pi*((xc2+xc1)/2.*(xc2-xc1)*yc1+(xc1+(xc2-xc1)
*2./3.)*0.5*(xc2-xc1)*(yc2-yc1)+
(xc3+xc2)/2.*(xc3-xc2)*yc2+(xc3+(xc4-xc3)/3.)*0.5
*(xc4-xc3)*(yc3-yc4) +(xc4+xc3)/2.*(xc4-xc3)*yc4)*2.,
vdivin :  2.*pi*((xc2+xc1)/2.*(xc2-xc1)*yc1+
(xc1+(xc2-xc1)*2./3.)*0.5*(xc2-xc1)*(yc2-yc1))*2.,
vdivide :  vdiv-vfw2,
vdividein :  vdivin-vfw2in,
vdivideout :  vdivide-vdividein,
/* now find flows necessary to carry power for each cooled
inner blanket sector */
distfwi :  rf-a-scri-tfw,
distfwo :  rf+a+scro+tfw,
hblt :  (2.*pi*rf-nsecfw*2.*hmanifw)/(nsecbl*nchan),
/* widths of blanket channels */
```

```
hsli :  (2.*pi*(distfwi+rf)/2.-nsecfw*2.*hmanifw)/(nsecbl*nchan),
hslo :  (2.*pi*(distfwo+rf)/2.-nsecfw*2.*hmanofw)/(nsecbl*nchan),
hbli :  (2.*pi*(distfwi-tbli/2.)-nsecfw*2.*hmanifw)/(nsecbl*nchan),
hblo :  (2.*pi*(distfwo+tblo/2.)-nsecfw*2.*hmanofw)/(nsecbl*nchan),
mdotblin :  (pneut*(fbl+frefl))*powerin/power/(nsecbl*2.)
/(cpli*deltat), /* kg/s per sector */
mdotblout :  (pneut*(fbl+frefl))*powerout/power/(nsecbl*2.)
/(cpli*deltat), /* kg/s per sector */
mdotbl :  mdotblin+mdotblout,
mdotperchin :  mdotblin/nchan, /* mass flow in each channel */
mdotperchout :  mdotblout/nchan, /* mass flow in each channel */
vinletbl :  mdotbl/(pi*dinlbl**2/4.*densli),
/* inlet to blanket velocity */
vblt :  mdotperchout/((tdivo)*hblt*densli),
/* flow velocities in inner blkt */
vsli :  mdotperchin/((tdivi)*hsli*densli),
vslo :  mdotperchout/((tdivo)*hslo*densli),
vbli :  mdotperchin/((tdivi)*hbli*densli),
vblo :  mdotperchout/((tdivo)*hblo*densli),
/* inner blanket pressure drops */
dpinlet :  0.2*sigli*vinletbl*b0**2*dinlbl/2.*
sqrt(2.*sigv*tinlbl/(sigli*dinlbl)), /* inlet */
dpt :  sigli*vblt*b0**2*rf**2*abs(1./xc3-1./xc2)*
phi(tblt,hblt)/(1.+phi(tblt,hblt)),
dpsli :  sigli*vsli*b0**2*rf**2*abs(1./xc2-1./xc1)*l12c/(xc3-xc2)*
phi(tsli,hsli)/(1.+phi(tsli,hsli)),
dpslo :  sigli*vslo*b0**2*rf**2*abs(1./xc3-1./xc4)*l34c/(xc4-xc3)*
phi(tslo,hslo)/(1.+phi(tslo,hslo)),
dpbli :  sigli*vbli*(b0*rf/xc2)**2*yc1*
phi(twbli,hbli)/(1.+phi(twbli,hbli)),
dpblo :  sigli*vblo*b0**2*rf**2/xc4**2*yc4*
phi(twblo,hblo)/(1.+phi(twblo,hblo)),
dpturni :  0.2*sigli*vbli*b0**2*rf**2/xc2**2*hbli/2.
*sqrt(2.*sigv*twbli/(sigli*hbli)),
dpturno :  0.2*sigli*vblo*b0**2*rf**2/xc4**2*hblo/2.
*sqrt(2.*sigv*twblo/(sigli*hblo)),
dptotinch :  nchan*(dpt+dpsli+dpslo+dpbli+dpblo+dpturni+dpturno),
dptotinner :  dpinlet+dptotinch,
/* find mass of dividers and inlets/outlets for blanket */
vmanbl :  2.*((yc1+l12c)*tbli+(xc3-xc2+l34c+yc4)*tblo)*tmanbl,
massmanbl :  (vmanbl*nsecbl*(nchan-2.)+pi*dinlbl*linlfw
*(tinlbl+toutlbl)*2.*nsecfw)*strucdens,
```

```
/* find the region of the remainder of the blanket */
findcorners(xc1, yc1, xc2, yc2, xc3, yc3, xc4,
yc4, tbli-tdivi, tbltp-tdivt, tblo-tdivo, l12c, l34c),
if drawwish then(drawboundary(xc1, yc1, xc2, yc2, xc3, yc3,
xc4, yc4)),
l12c :  sqrt((yc2-yc1)**2+(xc2-xc1)**2),
l34c :  sqrt((yc4-yc3)**2+(xc4-xc3)**2),
abl :  2.*pi*(xc1*yc1+(xc1+xc2)/2.*l12c+(xc3+xc2)/2.
*(xc3-xc2)+(xc3+xc4)/2.*l34c+xc4*yc4)*2.,
ablin :  2.*pi*(xc1*yc1+(xc1+xc2)/2.*l12c)*2.,
ablout :  2.*pi*((xc3+xc2)/2.*(xc3-xc2)+(xc3+xc4)/2.
*l34c+xc4*yc4)*2.,
vbl :  2.*pi*((xc2+xc1)/2.*(xc2-xc1)*yc1+(xc1+(xc2-xc1)
*2./3.)*0.5*(xc2-xc1)*(yc2-yc1)+(xc3+xc2)/2.*(xc3-xc2)
*yc2+(xc3+(xc4-xc3)/3.)*0.5*(xc4-xc3)*(yc3-yc4)
+(xc4+xc3)/2.*(xc4-xc3)*yc4)*2.,
vblin :  2.*pi*((xc2+xc1)/2.*(xc2-xc1)*yc1+(xc1+(xc2-xc1)
*2./3.)*0.5*(xc2-xc1)*(yc2-yc1))*2.,
vblkt :  vbl-vfw2, /* total blanket volume */
vblktin :  vblin-vfw2in,
vblktout :  vblkt-vblktin,

massblktmain :  vblkt*fblktvol*cooldens+vblkt
*(1.-fblktvol)*strucdens,
massblktc :  vblkt*fblktvol*cooldens,
massblkt :  massblktmain+massmanbl,
/* find the region of the reflector */
findcorners(xc1, yc1, xc2, yc2, xc3, yc3, xc4, yc4,
trefli, treflt, treflo, l12c, l34c),
if drawwish then(drawboundarylast(xc1, yc1, xc2, yc2, xc3,
yc3, xc4, yc4)),
l12c :  sqrt((yc2-yc1)**2+(xc2-xc1)**2),
l34c :  sqrt((yc4-yc3)**2+(xc4-xc3)**2),
arf :  2.*pi*(xc1*yc1+(xc1+xc2)/2.*l12c+(xc3+xc2)/2.
*(xc3-xc2)+(xc3+xc4)/2.*l34c+xc4*yc4)*2.,
arfin :  2.*pi*(xc1*yc1+(xc1+xc2)/2.*l12c)*2.,
arfout :  2.*pi*((xc3+xc2)/2.*(xc3-xc2)+(xc3+xc4)/2.
*l34c+xc4*yc4)*2.,
vrf :  2.*pi*((xc2+xc1)/2.*(xc2-xc1)*yc1+(xc1+(xc2-xc1)
*2./3.)*0.5*(xc2-xc1)*(yc2-yc1)+
(xc3+xc2)/2.*(xc3-xc2)*yc2+(xc3+(xc4-xc3)/3.)
*0.5*(xc4-xc3)*(yc3-yc4)+(xc4+xc3)/2.*(xc4-xc3)*yc4)*2.,
```

```
vrfin :  2.*pi*((xc2+xc1)/2.*(xc2-xc1)*yc1+(xc1+(xc2-xc1)
*2./3.)*0.5*(xc2-xc1)*(yc2-yc1))*2.,
vrefl :  vrf-vbl,
vreflin :  vrfin-vblin,
vreflout :  vrefl-vreflin,
massrefl :  vreflin*fracrfi*cooldens+vreflin*(1.-fracrfi)*refldens+
vreflout*fracrfo*cooldens+vreflout*(1.-fracrfo)*refldens,
massreflc :  vreflin*fracrfi*cooldens+vreflout*fracrfo*cooldens,
/* now find flows necessary to carry power for each cooled inner
blanket sector */
hbltr :  (2.*pi*rf-nsecfw*2.*hmanifw)/(nsecbl*nchan),
/* widths of blanket channels */
hslir :  (2.*pi*(distfwi-tbli+rf)/2.-nsecfw*2.*hmanifw)/
(nsecbl*nchan),
hslor :  (2.*pi*(distfwo+tblo+rf)/2.-nsecfw*2.*hmanofw)/
(nsecbl*nchan),
hblir :  (2.*pi*(distfwi-tbli)-nsecfw*2.*hmanifw)/
(nsecbl*nchan),
hblor :  (2.*pi*(distfwo+tblo)-nsecfw*2.*hmanofw)/
(nsecbl*nchan),
vbltr :  mdotperchout/(((tblo-tdivo)*hbltr+fracrfo*hbltr
*treflo)*densli),
vslir :  mdotperchin/(((tbli-tdivi)*hslir+fracrfi*hslir
*trefli)*densli),
vslor :  mdotperchout/(((tblo-tdivo)*hslor+fracrfo*hslor
*treflo)*densli),
vblir :  mdotperchin/(((tbli-tdivi)*hblir+fracrfi*hblir
*trefli)*densli),
vblor :  mdotperchout/(((tblo-tdivo)*hblor+fracrfo*hblor
*treflo)*densli),
/* outer blanket (nearest to and including reflector)
pressure drops */
dpoutlet :  0.2*sigli*vinletbl*b0**2*dinlbl/2.*
sqrt(2.*sigv*toutlbl/(sigli*dinlbl)), /* outlet */
dptr :  sigli*vbltr*b0**2*rf**2*abs(1./xc3-1./xc2)*
phi(tbltr,hbltr)/(1.+phi(tbltr,hbltr)),
dpslir :  sigli*vslir*b0**2*rf**2*abs(1./xc2-1./xc1)*l12c/
(xc2-xc1)*phi(tslir,hslir)/(1.+phi(tslir,hslir)),
dpslor :  sigli*vslor*b0**2*rf**2*abs(1./xc3-1./xc4)*l34c/
(xc4-xc3)*phi(tslor,hslor)/(1.+phi(tslor,hslor)),
dpblir :  sigli*vblir*(b0*rf/xc1)**2*yc1*
phi(twblir,hblir)/(1.+phi(twblir,hblir)),
```

```
dpblor :  sigli*vblor*b0**2*rf**2/xc4**2*yc4*
phi(twblor,hblor)/(1.+phi(twblor,hblor)),
dptotoutch :  nchan*(dptr+dpslir+dpslor+dpblir+dpblor),
dptotouter :  dptotoutch+dpoutlet,
dptotbl :  dptotinner + dptotouter,
ppumpbl :  mdotbl*dptotbl/densli*2.*nsecbl,
ppumpli :  ppumpfw+ppumpbl,
resett(),
/* find the stresses due to pressure drops in first wall*/
sigfwtor :  0.5*(dptotfw-dpfwin)*(b2/2.)**2/w1**2,
siginfw :  dptotfw*dinlfw/2./tinlfw,
sigoutfw :  dpfwout*dinlfw/2./toutlfw,
sigfw2a :  (dptotfw-dpfwin)*hmanifw/2./tfw2a,
sigfw2b :  (dpfwout+dpfw2b+dpfw7)*hmanifw/2./tfw2b,
sigfw3a :  (dptotfw-dpfwin-dpfw2a)*hmanifw/2./tfw35a,
sigfw3b :  (dpfwout+dpfw2b+dpfw3b+dpfw5b)*hmanifw/2./tfw35b,
sigfw4a :  (dptotfw-dpfwin-dpfw2a-dpfw3a-dpfw5a)*hmanifw/2./tfw46a,
sigfw4b :  (dpfwout+dpfw2b+dpfw3b+dpfw5b+dpfw4b+dpfw6b)
*hmanifw/2./tfw46b,
sigfw5a :  (dptotfw-dpfwin-dpfw2a)*hmanofw/2./tfw35a,
sigfw5b :  (dpfwout+dpfw2b+dpfw3b+dpfw5b)*hmanofw/2./tfw35b,
sigfw6a :  (dptotfw-dpfwin-dpfw2a-dpfw3a-dpfw5a)*hmanofw/2./tfw46a,
sigfw6b :  (dpfwout+dpfw2b+dpfw3b+dpfw5b+dpfw4b+dpfw6b)
*hmanofw/2./tfw46b,


/* bending at first wall, /* treating it as a composite beam */
iy :  1./12.*((b2+w3)**3-b2**3),
ix :  1./12.*(tfw**3-b1**3),
dy :  evan*iy/(1.-nu**2),
dx :  evan*ix/(1.-nu**2),
zb :  tfw-(w2**2/2.*(b2+w3)+(w2+b1/2.)*w3*b1+(w2+b1+w1/2.)
*w1*(b2+w3))/(w2*(b2+w3)+w3*b1+w1*(b2+w3)),
pbendfwman :  evan*zb/(dx-nu**2*dy)*dptotfw*hmanifw**2/12.*
(1.+nu**2/(1.-nu**2)*(dx-dy)/dx),
pbendblman :  evan*zb/(dx-nu**2*dy)*dptotbl*hbltr**2/12.*
(1.+nu**2/(1.-nu**2)*(dx-dy)/dx),
/* find the other stresses due to pressure drops in the blanket */
siginlbl :  dptotbl*dinlbl/2./tinlbl,
sigt :  ((dptotinch+dptotoutch)/nchan)*hblt/2./tblt,
sigsli :  ((dptotinch+dptotoutch+dpoutlet)/nchan-dpt)*hsli/2./tsli,
sigslo :  ((dptotinch+dptotoutch+dpoutlet)/nchan-dpt)*hslo/2./tslo,
```

```
sigbli :  ((dptotinch+dptotoutch+dpoutlet)/nchan-dpt-dpsli-dpslo)
hbli/2./twbli,
sigblo :  ((dptotinch+dptotoutch+dpoutlet)/nchan-dpt-dpsli-dpslo)
hblo/2./twblo,
sigblor :  ((dptotoutch+dpoutlet)/nchan)*hblor/2./twblor,
sigblir :  ((dptotoutch+dpoutlet)/nchan)*hblir/2./twblir,
sigslor :  ((dptotoutch+dpoutlet)/nchan-dpblir-dpblor)
hslor/2./tslor,
sigslir :  ((dptotoutch+dpoutlet)/nchan-dpblir-dpblor)
hslir/2./tslir,
sigtr :  (dptr+dpoutlet/nchan)*hbltr/2./tbltr,
sigoutlbl :  (dpoutlet)*dinlbl/2./toutlbl,
if printwish then printout() )$

q(x) := (/* q''' distribution */
q0/1.e6*exp(-aq*x) )$

phi(tz,hz) := ( 2.*sigv*tz/(sigli*hz))$

findcorners(u1, v1, u2, v2, u3, v3, u4, v4, i, t, o, lp, lpp) := (
thp :  acos((v2-v1)/lp),
phip :  pi/2.-thp,
sp :  ti/sin(phip),
yp :  v2,
xp :  u2-sp,
mp :  (v2-v1)/(u2-u1),
xc1 :  u1-ti,
yc1 :  mp*(u1-ti-xp)+yp,
xc2 :  (v2+tt-yp+mp*xp)/mp,
yc2 :  v2+tt,
thpp :  acos((u4-u3)/lpp),
phipp :  pi/2.-thpp,
spp :  to/cos(phipp),
ypp :  v3,
xpp :  u3+spp,
mpp :  (v4-v3)/(u4-u3),
xc3 :  (v3+tt-ypp+mpp*xpp)/mpp,
yc3 :  v3+tt,
xc4 :  u4+to,
yc4 :  mpp*(u4+to-xpp)+ypp )$

drawplasma() := ( ymax :  a*elong+1.5,
ymin :  0.,
xmax :  rf+a+1.5,
```

```
xmin :  rf-a-2.5,
equalscale :  true,
paramplot2(rf+a*cos(th+d*sin(th)), elong*a*sin(th), h,
0., pi, [2], first) )$

drawboundary(xx1, yy1, xx2, yy2,
xx3, yy3, xx4, yy4) := (
graph2([xx1, xx1, xx2, xx3, xx4, xx4],
[0., yy1, yy2, yy3, yy4, 0.])  )$

drawdiv(xx1, yy1, xx2, yy2, xx3,
yy3, xx4, yy4) := (
graph2([xx1,xx1,xx2,xx3,xx4,xx4],
[0.2, yy1, yy2, yy3, yy4, 0.2], [1]) )$

drawboundarylast(xx1, yy1, xx2, yy2, xx3,
yy3, xx4, yy4) := (
graph2([xx1, xx1, xx2, xx3, xx4, xx4],
[0., yy1, yy2, yy3, yy4, 0.], last) )$

prop(t) := ( /* t is in degrees c */
tk :  t+273.,
a1 :  4.1609,
a2 :  1.3603,
a3 :  3.7757e-4,
cpli :  a1*a2**(a3*t/1000.)*1000.,
kli :  40.1246+1.9037e-2*(tk-273.),
densli :  535.2-0.101e-4*t,
kvan :  g1*(tk-g2)+g3 )$

tfw(xx) := (/* first wall temperature distribution */
t0+flux*(w1-xx)/kvan+q0*(w1**2-xx**2)/(2.*kvan))$

(pi :  3.1415926,
strucdens :  6160.,
cooldens :  535.,
refldens :  7800.,
nu :  0.36,
rf :  7.5,
a :  1.5,
elong :  1.8,
d :  0.3, /*triangularity of plasma */
ffw :  0.227, /* fractions of total NEUTRON power going
to various regions (from neutronics)*/
fbl :  0.545,
```

```
frefl :  0.203,
tbli :  0.2, /* thicknesses of blanket and reflector regions */
tblo :  0.4,
fudge :  0.6, /* determines thickness of channels in blanket */
trefli :  0.35,
treflo :  0.35,
fblktvol :  0.92, /* fraction of blanket region that is coolant */
partins :  false,
fullins :  false,
drawwish :  false,
printwish :  false,
leak :  0.95, /* fraction of energy leakage from blanket system */
pwall :  3.e6, /* neutron wall loading */
m :  1.21,
flux :  0.75e6, /* surface heat flux at first wall */
deltat :  250., /* temperature rise of coolant,
/* inlet to outlet */
texit :  550., /* coolant outlet temperature */
nsecfw :  6, /* number of first wall cooling sectors */
nsecbl :  6, /* number of blanket cooling sectors */
nchan :  10., /* number of poloidal channels per blanket sector */
dinlfw :  0.4, /* diameter of inlet channel to first wall */
linlfw :  1.0, /* length of inlet channel to first wall */
hmanifw :  0.4, /* width of manifold for first wall */
hmanofw :  0.6,
tmanbl :  0.004,
tmanfw :  0.003,
sigli :  3.2e6,
sigv :  1.43e6,
evan :  118.e9, /* elastic modulus of vanadium in Pa */
b0 :  2.7,
deltatfw :  30.,
fracrfi :  0.2, /* fraction of reflector x-s that is coolant */
fracrfo :  0.1,
tinlfw :  0.01, /* thickness of wall for inlet
first wall channel */
toutlfw :  0.002, /* thickness of wall for outlet
first wall channel */
tfw2a :  0.007, /* thickness of first wall manifold walls */
tfw2b :  0.002,
tfw35a :  0.006,
tfw35b :  0.003,
```

```
tfw46a :  0.005,
tfw46b :  0.004,
w1 :  0.006, /* thickness, front edge of first wall */
w2 :  0.02, /* thickness, back edge of first wall */
w3 :  0.005, /* thickness, inner walls of first wall */
b1 :  0.04, /* radial thickness of first wall coolant channel */
b2 :  0.02, /* poloidal thickness of first wall coolant channel */
scri :  0.15, /* scrapeoff distances */
scrt :  0.15,
scro :  0.15,
dinlbl :  0.8,
tinlbl :  0.008, /* thickness of walls for inlet and
outlet to blanket/refl */
toutlbl :  0.002,
tblt :  0.003, /* thicknesses of walls for inner blanket */
twbli :  0.0015,
twblo :  0.0015,
tsli :  0.002,
tslo :  0.002,
tbltr :  0.0015,
twblir :  0.003,
twblor :  0.003,
tslir :  0.002,
tslor :  0.002,
tmax :  750., /* max first wall structural temperature in C */
q0 :  25.e6, /* average volumetric heat load at front of blanket */
aq :  4., /* exponent constant for shape of volumetric
heat load distribution */
g1 :  0.01342, /* constants for thermal conductivity of vanadium */
g2 :  900.,
g3 :  29.75,
fy1 :  1.1, /* fudges to determine first wall boundary to plasma */
fx2 :  0.6,
fx3 :  0.1,
fy4 :  0.75)$

resett():=(
tinlfw :  0.008, /* thickness of wall for inlet
first wall channel */
toutlfw :  0.002, /* thickness of wall for outlet
first wall channel */
tfw2a :  0.007, /* thickness of first wall manifold walls */
tfw2b :  0.002,
```

```
tfw35a :  0.006,
tfw35b :  0.003,
tfw46a :  0.005,
tfw46b :  0.004,
tinlbl :  0.008,
/* thickness of walls for inlet and outlet to blanket/refl */
toutlbl :  0.002,
tblt :  0.003,
/* thicknesses of walls for inner blanket */
twbli :  0.0015,
twblo :  0.0015,
tsli :  0.002,
tslo :  0.002,
tbltr :  0.0015,
/* thicknesses of walls for outer blanket and reflector */
twblir :  0.003,
twblor :  0.003,
tslir :  0.0015,
tslor :  0.0015 )$

partialinsulation():=(
tinlfw :  0.00025,
/* thickness of wall for inlet first wall channel */
toutlfw :  0.00025,
/* thickness of wall for outlet first wall channel */
tinlbl :  0.00025,
/* thickness of walls for inlet and outlet to blanket/refl */
toutlbl :  0.00025,
tbltr :  0.00025,
/* thicknesses of walls for outer blanket and reflector */
twblir :  0.00025,
twblor :  0.00025,
tslir :  0.00025,
tslor :  0.00025 )$

insulated():=( tinlfw :  0.00025,
/* thickness of wall for inlet first wall channel */
toutlfw :  0.00025,
/* thickness of wall for outlet first wall channel */
tfw2a :  0.00025,
/* thickness of first wall manifold walls */
tfw2b :  0.00025,
tfw35a :  0.00025,
```

```
tfw35b :  0.00025,
tfw46a :  0.00025,
tfw46b :  0.00025,
tinlbl :  0.00025,
/* thickness of walls for inlet and outlet to blanket/refl */
toutlbl :  0.00025,
tblt :  0.00025,
/* thicknesses of walls for inner blanket */
twbli :  0.00025,
twblo :  0.00025,
tsli :  0.00025,
tslo :  0.00025,
tbltr :  0.00025,
/* thicknesses of walls for outer blanket and reflector */
twblir :  0.00025,
twblor :  0.00025,
tslir :  0.00025,
tslor :  0.00025 )$
```

Bibliography

[1] R. C. Grimm, M. S. Chance, et al. *MHD Stability Properties of Bean-Shaped Tokamaks.* Technical Report PPPL-2090, Princeton Plasma Physics Laboratory, March 1984.

[2] Massachusetts Institute of Technology. *Tokamak Power Systems Studies (TPSS)*, August 1985.

[3] C. C. Baker et al. *STARFIRE, A Commercial Tokamak Power Plant Study.* Technical Report ANL/FPP/82-1, Argonne National Laboratory, 1982.

[4] C. Weggel, W. Hamburger, B. Montgomery, and N. Pierce. Alcator-C Tokamak. In *Proceedings of the Seventh Symposium on Engineering Problems of Fusion Research*, 1977.

[5] L. Bromberg, D.R. Cohn, et al. Engineering Aspects of LITE (Long Pulse Ignition Experiment) Devices. In *Proceedings of the Tenth Symposium on Fusion Engineering*, Philadelphia, PA, December 1983.

[6] D. L. Jassby. *TORFA - Toroidal Reactor for Fusion Applications.* Technical Report PPPL-1700, Princeton Plasma Physics Laboratory, October 1980.

[7] J. Stephen Herring. *The Design of a Small Normally Conducting Tokamak Reactor.* PhD thesis, Massachusetts Institute of Technology, September 1979.

[8] D. C. Lousteau, T. C. Jernigan, et al. Engineering Features of ISX. In *Sixth Symposium on Engineering Problems of Fusion Research*, November 1975.

[9] F. A. Puhn, R. W. Callis, et al. Design of Demountable Joint for Doublet III Toroidal Field Coil. In *Sixth Symposium on Engineering Porblems of Fusion Research*, November 1975.

[10] Princeton Plasma Physics Laboratory. *Workshop on High Current Electrical Joints for Tokamaks*, March 1985.

[11] J. N. Brooks et al. Engineering Design of Self Pumped Limiters. In *Tokamak Power System Studies*, August 1985.

[12] J. E. C. Williams, L. Bromberg, D. R. Cohn, et al. *Conceptual Design of a Bitter Magnet Toroidal Field System for the ZEPHYR Ignition Test Reactor.* Technical Report PFC/RR-81-24, Massachusetts Institute of Technology, May 1981.

[13] W. R. Hamilton, D. C. Keeton, and S. L. Thomson. *Cost Accounting System for Fusion Studies.* Technical Report, Fusion Engineering Design Center, 1985.

[14] J. P. Freidberg. Ideal Magnetohydrodynamic Theory of Magnetic Fusion Systems. *Reviews of Modern Physics*, 1982.

[15] L. C. Bernard, F. J. Helton, and R. W. Moore. MHD Beta Limits: Scaling Laws and Comparison with Doublet III Data. *Nuclear Fusion*, 23(11), 1983.

[16] A. Sykes, M. F. Turner, and S. Patel. Beta Limits in Tokamaks Due to High-N Ballooning Modes. In *Proceedings on the Eleventh European Conference on Controlled Fusion and Plasma Physics*, 1983.

[17] M. Murakami et al. Confinement Studies of Neutral Beam Heated Discharges in TFTR. In *Proceedings of the Twelfth European Conference on Controlled Fusion and Plasma Physics*, 1985.

[18] W. A. Houlberg. Plasma Engineering Assessments of Compact Ignition Experiments. In *Proceedings of the Eleventh Symposium on Fusion Engineering*, 1985.

[19] J. E. C. Williams, H. Becker, D. Blackfield, et al. *FED-R2: Concept and Magnet Design of a Low Cost FED.* Technical Report PFC/RR-82-23, Massachusetts Institute of Technology, December 1982.

[20] D. J. Strickler, J. B. Miller, K. E. Rothe, and T-K.M. Peng. *Equilibrium Modeling of the TFCX Poloidal Field Coil System.* Technical Report ORNL/FEDC-83-10, Oak Ridge National Laboratory, 1983.

[21] E. Bobrov, L. Bromberg, D. R. Cohn, et al. *High Field Tokamaks with DD-DT Operation and Reduced Tritium Breeding Requirements.* Technical Report PFC/RR-83-5, Massachusetts Institute of Technology, 1983.

[22] D. A. Ehst et al. *Tokamak Burn Cycle Study: A Data Base for Comparing Long Pulse and Steady State Power Reactors.* Technical Report ANL/FPP/TM-178, Argonne National Laboratory, 1983.

[23] *Workshop on Reactor Multiplexing*, Rockville, Marchyland, July 1985.

[24] R. H. Whitley, G. R. Lutz, S. A. Freije, D. H. Berwald, and J. D. Gordon. *An Assessment of Multiplexed Plant Deployment of Commercial Tokamaks.* Technical Report, TRW Inc., 1985.

[25] D. L. Jassby et al. *Resistive Demountable Toroidal Field Coils for Tokamak Reactors.* Technical Report PPPL-1809, Princeton Plasma Physics Laboratory, July 1981.

[26] F. Puhn et al. Mechanical Design of a High Beta TFCX Tokamak with a Demountable Toroidal Field Coil. In *Thirteenth Symposium on Fusion Technology*, 1984.

[27] F. Puhn and J. Strohmayer. Design and Testing of a Sliding Joint for a High Performance Toroidal Field Coil. In *IEEE Eleventh Symposium on Fusion Engineering*, 1985.

[28] S. J. Piet. *Potential Consequences of Tokamak Fusion Reactor Accidents: The Materials Impact.* PhD thesis, Massachusetts Institute of Technology, 1982.

[29] P. J. Gierszewski, A. S. Wan, and T. F. Yang. *CCAN and TCAN* - $1\frac{1}{2}$*-D Compressible Flow and Time Dependent Codes for Conductor Analysis.* Technical Report PFC/RR-83-1, Massachusetts Institute of Technology, January 1983.

[30] R. J. Roark and W. C. Young. *Formulas for Stress and Strain.* McGraw-Hill Book Company, 1975.

[31] J. Kalnavarns and D. L. Jassby. *Resistive Toroidal Field Coils for Tokamak Reactors.* Technical Report PPPL-1685, Princeton Plasma Physics Laboratory, October 1980.

[32] A. Kleinlogel. *Rigid Frame Formulas.* Frederick Ungar Publishing Company, New York, NY, 1958.

[33] S. Timoshenko. *Elements of Strength of Materials.* D. Van Nostrand Company, New York, NY, 1949.

[34] E. S. Bobrov. Structural Response of Tokamak TF Magnet Systems to In-Plane and Out-of-Plane Electromagnetic Loads. *Nuclear Engineering and Design/Fusion*, 1(1), January 1984.

[35] Stephen H. Crandall, Norman C. Dahl, and Thomas J. Lardner. *An Introduction to the Mechanics of Solids.* McGraw-Hill Book Company, 1978.

[36] *Class I Components in Elevated Temperature Service.* 1979. Cases of ASME Boiler and Pressure Vessel Code N-47-17.

[37] D. L. Smith, G. D. Morgan, et al. *Blanket Comparison and Selection Study Final Report.* Technical Report ANL/FPP-84-1, Argonne National Laboratory, September 1984.

[38] R. D. O'Dell et al. *User's Manual for ONEDANT: A Code Package for One-Dimensional Diffusion Accelerated Neutral Particle Transport.* Technical Report LA-9184-M, Los Alamos National Laboratory, February 1982.

[39] R. E. MacFarlane and R. J. Barrett. *TRANSX.* Technical Report T-2-L-2923, Los Alamos National Laboratory, August 1978.

[40] C. I. Baxman and P. G. Young. *Applied Nuclear Data Research and Development Januaryuary 1 - Marchch 31, 1977.* Technical Report LA-6893-PR, Los Alamos National Laboratory, July 1977.

[41] R. E. Shmunck and H. Becker. Extension of the Irradiation and Testing of SPAULRAD-S for Fusion Magnet Application. In *Proceedings of the Sixth Topical Meeting on the Technology of Fusion Energy*, 1985.

[42] Joel H. Schultz. Design Practice and Operational Experience of Highly Irradiated, High Performance Normal Magnets. *Journal of Fusion Energy*, 3(2), March 1983.

[43] M. A . Abdou et al. *Blanket Comparison and Selection Study.* Technical Report ANL/FPP/82-1, Argonne National Laboratory, 1982.

[44] J. T. A. Roberts. *Structural Materials in Nuclear Power Systems.* Plenum Press, New York and London, 1981.

[45] B. A . Boley and J. H. Weiner. *Theory of Thermal Stresses.* John Wiley and Sons, 1960.

[46] Francis F. Chen. *Introduction to Plasma Physics.* Plenum Press, New York and London, 1974.

[47] C. Mercier. A Necessary Condition for Hydromagnetic Stability of Plasma with Axisymmetry. *Nuclear Fusion*, 1, 1960.

[48] F. Troyon, R. Gruber, et al. MHD Limits to Plasma Confinement. In *Proceedings on the Eleventh European Conference on Controlled Fusion and Plasma Physics*, 1983.

[49] W. M. Stacey, M. A. Abdou, J. A. Schmidt, T. E. Shannon, and J. K. Griffith, editors. *The U.S. Contribution to the International Tokamak Reactor Phase-I Workshop*, June 1981.

[50] H-O Wuster. JET: Programme and Results. In *Sixth Topical Meeting on the Technology of Fusion Energy*, San Francisco, CA, March 1985.

[51] T. Tuda, M. Azumi, K. Itoh, et al. Accessible Beta Value of Tokamaks. In *Proceedings on the Tenth International Conference on Controlled Fusion and Plasma Physics*, 1984.

[52] R. D. StambAugusth, R. W. Moore, L. C. Bernard, et al. Tests of Beta Limits as a Function of Plasma Shape in Doublet III. In *Proceedings on the Tenth International Conference on Controlled Fusion and Plasma Physics*, 1984.

[53] K. Yamazaki, T. Amano, H. Naitou, and Y. Hamada. Ballooning Beta Limits of Dee- and Bean-Shaped Tokamaks. *Nuclear Fusion*, 25(11), 1985.

[54] R. L. Miller and R. W. Moore. Shape Optimization of Tokamak Plasmas to Localized Magnetohydrodynamic Modes. *Physical Review Letters*, 43(11), 1979.

[55] B. Coppi, A. Ferreira, J. W.-K. Marchk, and J. J. Ramos. Ideal-MHD Stability of Finite-Beta Plasmas. *Nuclear Fusion*, 19(6), 1979.

[56] J. M. Greene and M. S. Chance. The Second Regime of Stability Against Ballooning Modes. *Nuclear Fusion*, 21(4), 1981.

[57] R. J. LeClaire, R. E. Potok, et al. System Studies of Commercial Tokamak Reactors with Resistive Magnets. In *Sixth Topical Meeting on the Technology of Fusion Energy*, San Francisco, CA, March 1985.

[58] D. A. Ehst et al. High Beta Stability Without Indentation, Minimum Current FW Current Drive, and Profile Control. In *Tokamak Power System Studies*, August 1985.

[59] M. Okabayashi et al. Studies of Bean-Shaped Tokamaks and Beta Limits for Reactor Design. In *Proceedings of the Tenth Conference on Plasma Physics and Controlled Nuclear Fusion Research*, London, England, September 1984.

[60] R. E. Potok, L. Bromberg, R. J. LeClaire, and D. R. Cohn. Trade-offs for Tokamak Power Reactors in the First and Second Stability Regimes. In *Tokamak Power System Studies*, August 1985.

[61] D. R. Cohn and L. Bromberg. *Advantages of High Field Tokamaks for Fusion Reactor Development.* Technical Report PFC/JA-85-39, Massachusetts Institute of Technology, December 1985.

[62] K. Evans, Jr. *A Tokamak Reactor Cost Model Based on STARFIRE and WILDCAT Costing.* Technical Report ANL/FPP/TM-168, Argonne National Laboratory, March 1983.